Hydrogels derived from decellularised tissues for nerve repair

Simon Christopher Kellaway

Thesis submitted in fulfilment of the requirements for the degree of

Doctor of Philosophy

School of Pharmacy

University College London

February 2021

Declaration

I, Simon Kellaway, confirm that the work presented in this thesis is my own. Where information has been derived from other sources, I confirm that this has been indicated in the thesis.

Signed: ███████████

Date: _____22/07/2021_____

For Joyce and Ray

Acknowledgements

This PhD thesis is dedicated to all of the wonderful people I have been fortunate enough to share a Friday beer or bottle of red wine with over the course of my academic career.

First and foremost, I would like to thank my two supervisors Lisa White and James Phillips for their expert academic guidance and support outside of the lab. The past four years have been indescribably challenging, and they have both shown levels of patience and understanding that I have rarely experienced in my entire life that was both humbling and motivating.

I have been incredibly privileged to have spent time in the research groups at Nottingham and UCL and feel I have gained a really unique PhD experience. Teresa Marshall and Anne Williams were always a pleasure to work with at the University of Nottingham, providing crucial support to all of the research staff. I would also like to thank all of the fellow PhD students who made me feel welcome in Nottingham. Harry Sherman, Rabea Loczenski, Jasmine Stenning, Mat Hollingworth, Joshua Jones, Gordon Bruce, and Andrea Torchi; our pub trips and game nights kept me going more than you know! Additionally, I would like to thank Niels Klaver and Sean Dixon at Midtown Hostel for keeping me sane through the seemingly endless year away from my friends and family.

This thesis would never have been completed without the guidance and support from some people in the Phillips' group. Papon Muangsanit for his valued insight and assistance from the very first day when I started my mini project, to his continued remote help even in the last days of my PhD. Victoria Roberton for her guidance, support, and knowledge (as well as the occasional stress cigarette). Rachael Evans and Mariann Angola for our pub trips and tips on thesis writing (also for helping make my CV make sense). Kulraj Bhangra for his patience and assistance with our trips to the butchers. "The dream team" Becca Powell and Depsoina Eleftheriadou for putting up with my shenanigans, as well as the rest of the lab for putting up with my music! Whilst late to the party, Owein Guillemot-Legris has been a huge help in the final months of this PhD and has given valuable insight to myself and the whole group. Being part of the CDT in Nanomedicines and Advanced Therapeutics was a wild ride and I would like to thank Alex Keeley, Raphael Egbu, Sean Askin, and everyone else that shared some long nights and even longer mornings with me at the colloquia.

Last, but certainly not least, I would like to thank my immediate support bubble (apt vernacular for the current times). My family and friends have supported me through some dire times over the past four years; especially my two brothers Paddy and Francis, and my flatmate Matt. This last year has been immensely tough for everyone, and I would like to thank Alice de Dumast for managing to simultaneously be on the frontline of healthcare and also attend to an incredibly stressed, incredibly erratic PhD student. I would never have dreamed I would have been capable of completing a PhD, but there are two people that have never

doubted me. So, Mum and Dad I hope I have finally proven you right; thank you for (quite literally) everything!

Abstract

Peripheral nerve injury poses a serious clinical problem, with sensory and motor deficits resulting in significant reductions in patient quality of life. Nerve guidance conduits aim to overcome issues with the current gold standard for repair, the autograft. Recent advances in the field of tissue engineering have allowed for the devlopment of biochemically and physically complex constructs that aim to bridge the injury site to provide an environment that favours regeneration.

This thesis explores the possibility of extracellualr matrix (ECM) hydrogels derived from decellularised tissues (dECM-h) and their potential for the maintenance of Schwann cells, ability to form anisotropic cellular tissue, and their subsequent ability to promote *in vitro* and *in vivo* neurite extension. A number of tissues were decellularised, biochemical properties assessed, and formed into hydrogels that were mechanically characterised. *In vitro* screening was then performed to assess Schwann cell metabolic activity, contraction, and alignment within three selected dECM-h. Additionally, stabilised dECM-h seeded with Schwann cells were formed and seeded with dorsal root ganglia to assess their *in vitro* capabilities to promote neurite extension. Hydrogels derived from decellularised cancellous bone (B-ECM) were found to be appropriate to be taken forward into a rat sciatic nerve transection model to be compared to the currently used purified collagen I derived from rat tails. *In vivo* axonal regeneration was found to be comparable between the two groups, however did not match that observed in nerve autografts.

This study brought a portfolio of decellularised materials from generation, through characterisation and *in vitro* screening, to selction of one candidate that was taken forward into an *in vivo* model. This has shown, for the first time, that alternatives to the currently used collagen I hydrogels may be employed in the production and utilisation of engineered neural tissue (EngNT).

Impact Statement

Peripheral nerve injury (PNI) poses a serious clinical problem. Reduced motility, chronic pain, and unemployment can result in dramatic loss in patient quality of life whilst surgical, rehabilitation as well as social costs are excessive. Surgical intervention is often required, and for long gap repairs the gold standard remains the autograft; autologous nerve tissue from a second site is implanted into the lesion site. This causes donor site morbidity, is limited in availability, and requires a second surgical site. Insufficient functional recovery and the presentation of neuropathic pain has led to the development of tissue engineered nerve guidance conduits (NGC) to find a solution.

The work presented in this thesis involves the utilisation and modification of the previously established engineered neural tissue (EngNT); a type of artificial living tissue that can facilitate nerve regeneration. Currently a material derived from purified rat tail type I collagen is used to produce EngNT. This work investigated a range of materials derived from decellularised animal tissues that were produced, characterised, and tested for the potential to be incorporated into EngNT. For the first time, it has been shown that EngNT may be produced to an acceptable standard from an alternative material to the currently used collagen I.

As a whole, this thesis has advanced the field of nerve tissue engineering via the incorporation of biologically active materials into a currently used NGC to improve its capacity for nerve regeneration. The work further paves a path for the possibilities in the use of a variety of decellularised materials and their potential for improving cell-matrix interactions in nerve tissue engineering.

Contents

List of Figures

List of Tables

Abbreviations

BDNF	**Brain derived neurotrophic factor**
B-ECM	**Bone derived extracellular matrix**
BL	**Basal lamina**
BM	**Basement membrane**
CNS	**Central nervous system**
CS	**Chondroitin sulphate**
dECM	**Decellularised extracellular matrix**
dECM-h	**Hydrogel derived from decellularised ECM**
dH$_2$O	**Deionised water**
DMEM	**Dulbecco's modified Eagle's medium**
DRG	**Dorsal root ganglion**
dsDNA	**Double stranded deoxyribonucleic acid**
ECM	**Extracellular matrix**
EDTA	**Ethylenediaminetetraacetic acid**
EngNT	**Engineered neural tissue**
FBS	**Foetal bovine serum**

GDNF	Glial cell-line derived neurotrophic factor
HCl	Hydrochloric acid
LIV-ECM	Liver derived extracellular matrix
NaOH	Sodium hydroxide
NF	Neurofilament
NGC	Nerve guidance conduit
NGF	Nerve growth factor
NGS	Normal goat serum
NHS	Normal horse serum
PBS	Phosphate buffered saline
PCL	Polycaprolactone
PDL	Poly-d-lysine
PNI	Peripheral nerve injury
PNS	Peripheral nervous system
SC-ECM	Spinal cord derived extracellular matrix
SDC	Sodium deoxycholate
SDS	Sodium docecyl sulphate
sGAG	Sulphated glycosaminoglycan

SIS	**Small intestinal submucosa**
SIS-ECM	**Small intestinal submucosa derived extracellular matrix**
UBM	**Urinary bladder matrix**
UBM-ECM	**Urinary bladder matrix derived extracellular matrix**

Chapter 1 Introduction

1.1. The peripheral nervous system

The PNS relays information from the rest of the body to the CNS, thus acting as the interface with our environment; transforming sensory information into electrrochemical impulses to be sent to the brain and enabling complex, rapid responses to various external stimuli (Cuevas, 2007). Additionally, the PNS is responsible for the relay of information to the muscles for voluntary motor function as well as the modulation of involuntary bodily functions such as heart rate, digestion and urination (Jänig, 1989).
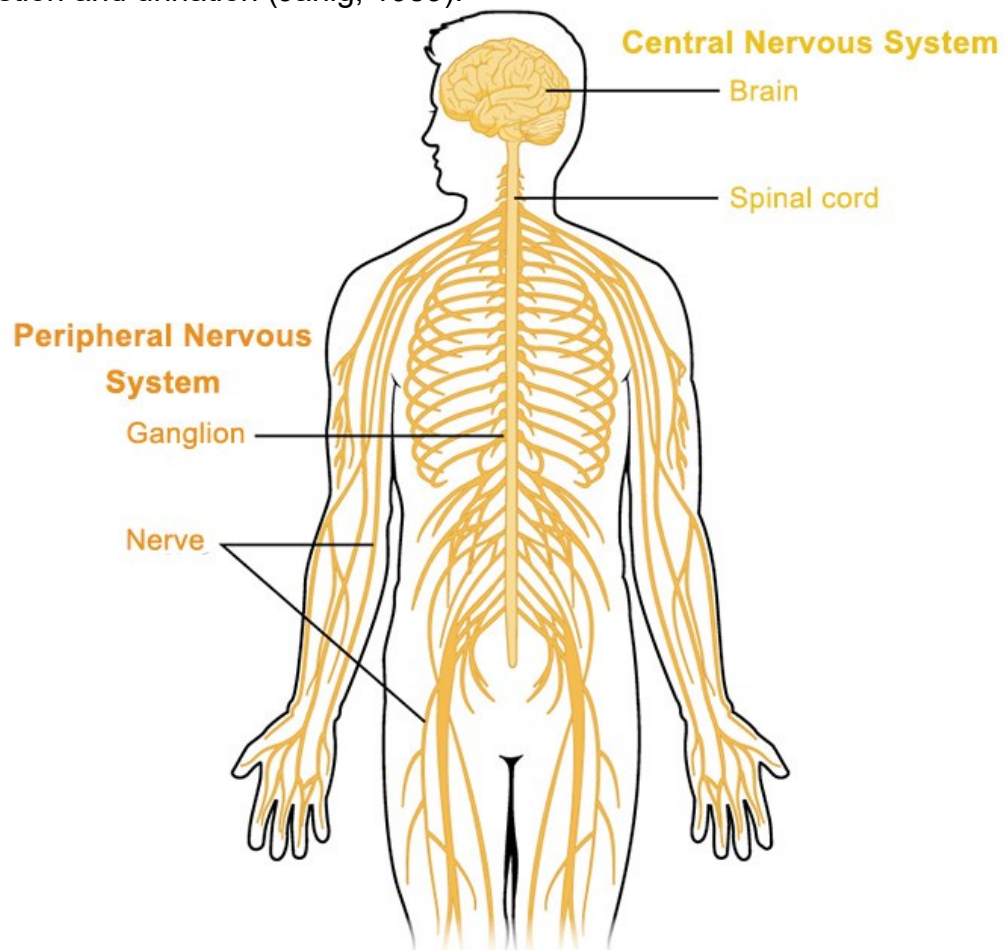
Figure 1.1 The nervous system. The central and peripheral nervous systems in the human body. Peripheral nerves extend out from the spinal cord to innervate the rest of the body. Figure reproduced from (OpenStax, 2016).

Neuronal cell bodies of the PNS reside in the dorsal root ganglia (sensory neurons) and the spinal cord, brain stem or motor cortex (Motor neurons) (Figure 1.2).
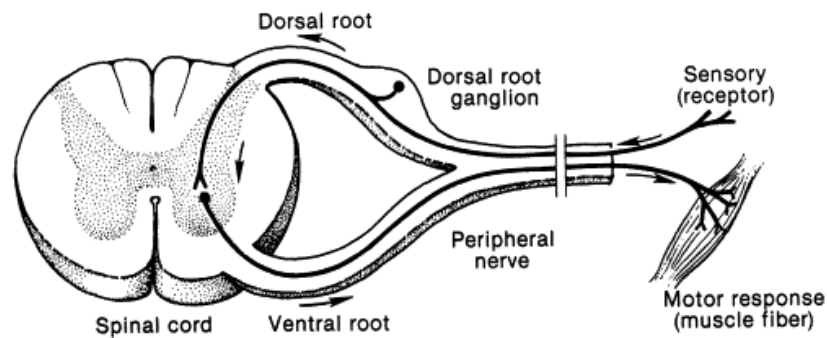
Figure 1.2 Connection between central and peripheral nervous systems. Dorsal roots relay sensory information, whilst ventral roots innervate the body. Figure reproduced from (Krassioukov, 2002).

1.1.1. Anatomy of the peripheral nerve

Axons may be myelinated or unmyelinated and are bundled into fascicles, in the loose connective tissue of the endoneurium (Figure 1.3), and are closely associated with Schwann cells, further accompanied by lymphocytes, fibroblasts, mast cells, as well as blood vessels and interstitial fluid (Dubový et al., 2002, Lorimier et al., 1992, Poduslo et al., 1985). In the endoneurium axon-Schwann cell groupings exist within a secreted fibrillar collagenous ECM whilst the Schwann cells either form the multilamellar myelin sheath surrounding the axon as seen in Figure 1.3 (Peltonen et al., 2013), or exist as Remak Schwann cells that wrap around the axon without producing myelin (Harty and Monk, 2017). The Schwann cell basement membrane is largely comprised of collagen IV, fibronectin and laminin whereas collagen I and III dominate the fibrillar ECM of the endoneural space (Lorimier et al., 1992).

21
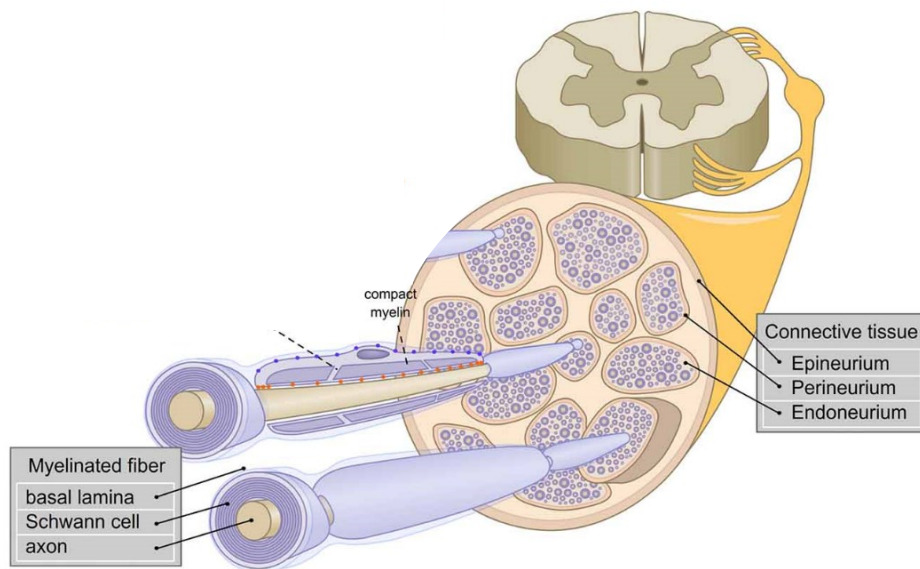
Figure 1.3 Macroscopic and microscopic anatomy of the peripheral nervous system. Peripheral nerves are comprised of cable like structures of grouped myelinated and unmyelinated axons bundled into fascicles, sheathed in the epineurium. Figure reproduced from (Belin et al., 2017).

The fascicular bundles of nerve fibres and blood vessels of the endoneurium are enveloped in a tubular sheath known as the perineurium (Figure 1.3); comprised of alternating layers of connective tissue, predominantly comprised of collagen I, and a type of fibroblast that secrete a basement membrane rich in type III and IV collagen, and fibronectin (Lorimier et al., 1992, Peltonen et al., 2013). Perineurial cells are held together via tight junctions that prevent diffusion of molecules into the endoneurium and, further ensure homeostatic pressure within the endoneurium (Peltonen et al., 2013). Multiple fascicular bundles are further encompassed in the epineurium (Figure 1.3): a loose layer of connective tissue, predominantly comprised of longitudinally aligned collagen I in a "wavy" pattern that allows for extension during normal movement (Stolinski, 1995).

22

1.1.2. Peripheral nerve injury

Peripheral nerve injury (PNI) can be debilitating and cause devastating loss in patient quality of life (Rasulic et al., 2017), and further carries hidden socioeconomical costs as patients are more often of working age (Wojtkiewicz et al., 2015). PNI may arise from surgical procedures, metabolic diseases such as diabetes, autoimmune disorders, cancer, neuromas and exposure to toxins, although is most commonly due to physical trauma (Burnett and Zager, 2004). The intrinsic ability for the PNS to regenerate distinguishes it from the CNS; following injury, a molecular and physiological cascade of events occurs to provide a regenerative environment that promotes axonal regrowth toward the denervated target organ. Dependent on the severity of the injury this regeneration may occur spontaneously and unaided. Sunderland (1951) introduced a grading system, improving on the previous Seddon scale (Seddon et al., 1943) to classify the severity of PNI (Table 1.1), with which prediction of regenerative potential and the requirement for surgical intervention may be assessed. The Sunderland grading scale is explained further in Figure 1.4.

Table 1.1 Seddon and Sunderland scales for nerve injury with associated intervention.

Seddon scale	Sunderland Grade	Outcome
Neurapraxia	I	Damage to myelin sheath, nerve uncompromised
Axonotmesis	II	Axonal damage, endoneurium uncompromised
Axonotmesis	III	Axon and endoneurium damage, perineurium uncompromised
Axonotmesis	IV	Axon, endoneurium and perineurium damaged, epineurium uncompromised
Neurotmesis	V	Nerve and nerve sheath damaged. Complete recovery impossible without intervention
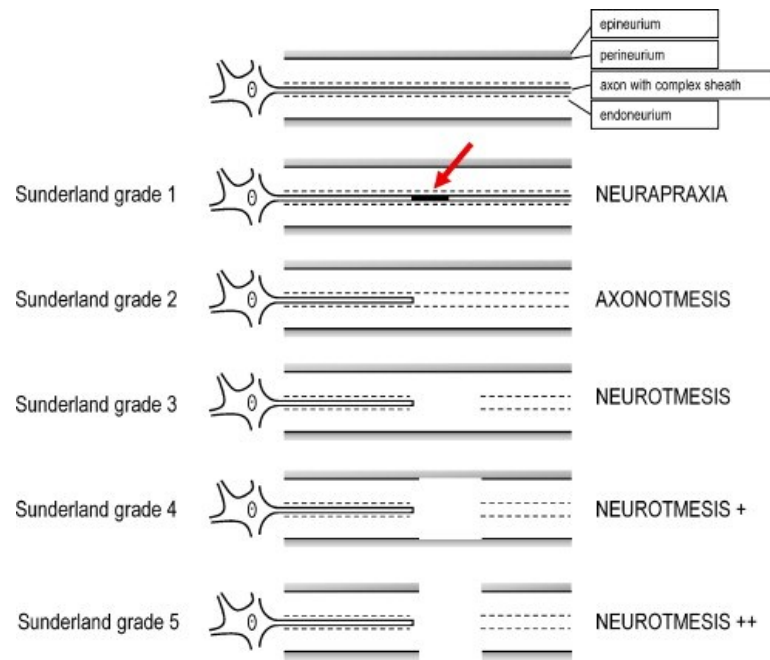
Figure 1.4 Visual representation of the Seddon and Sunderland grading scales for nerve injury. Figure reproduced from (Deumens et al., 2010).

Following laceration of an axon and subsequent interruption of the action potential (Figure 1.5 A) the nerve and surrounding tissue undergo morphological and biochemical changes to promote regeneration. The proximal and distal axonal segments endure for around 48 hours following injury whilst also retaining some of their electrophysiological capabilities. The degeneration of the distal stump, known as Wallerian degeneration, can begin within a few hours after injury and commences with disintegration of the axon, causing the sequential rupturing of the blood-nerve barrier along the distal stump (Fu and Gordon, 1997, Seitz et al., 1989). Schwann cells sense nearby axotomy around the distal stump via ligation of toll-like receptors with aberrant extracellular debris (Figure 1.5 B), instigating reprogramming immediately after axonal degeneration. SC therefore exhibit both a sensory, sentinel like function in the PNS as well as acting as first

24

responders. These Schwann cells alter their gene expression and halt myelin production, increase expression of neural cell adhesion molecule (NCAM) and neurotrophic factors (nerve growth factor, brain derived nerve factor) whilst also increasing proliferation (Chen et al., 2007, Goethals et al., 2010, Jessen and Mirsky, 2016). Moreover, infiltration of nearby macrophages and other immune cells to the lesion site occurs to clear cellular and extracellular debris, phagocytosing the fragments of myelin and debris not eliminated by the Schwann cells (Perry and Brown, 1992). Macrophages not only play a pivotal role in Wallerian degeneration, but also in the consequential axonal regrowth. They have been implicated in the modulation of Schwann cell phenotype via release of the mitogens, platelet-derived growth factor, fibroblast growth factor and the secretion of pro-regenerative ECM components (Davis and Stroobant, 1990, Perry and Brown, 1992, Stratton et al., 2018). Moreover, macrophage-derived VEGF-A is responsible for the formation of novel vasculature that further act as directional cues for migratory Schwann cells (Cattin et al., 2015).The now proliferating Schwann cells adopt an elongated morphology and align themselves longitudinally inside the endoneurial tubes of the basal lamina and form the Bands of Büngner (Figure 1.5 C), providing multiple channels and upregulating cell adhesion molecules (CAMs) that provide optimum conditions for axonal

regeneration (Fu and Gordon, 1997). Axons will typically extend through the

bands of Büngner at a rate of 1-3mm a day (Seddon et al., 1943)..
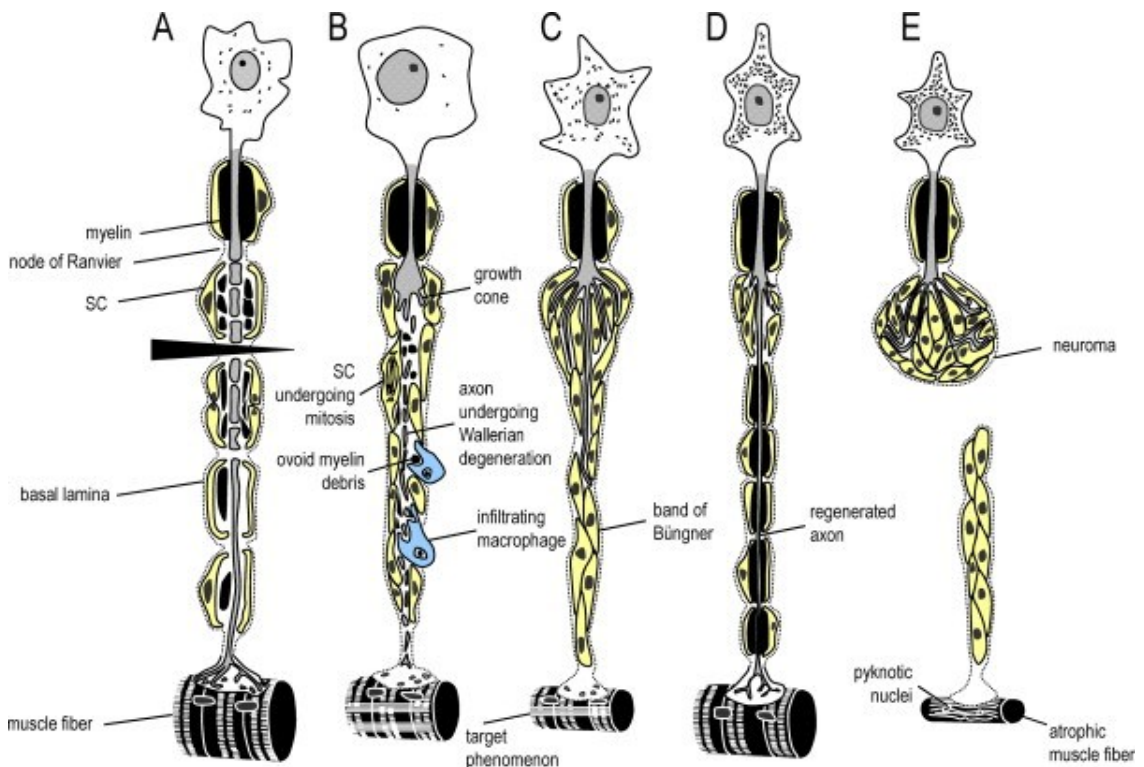
Figure 1.5 Peripheral nerve injury and regeneration process. Laceration causes distal degeneration, basal lamina persists [A]. Schwann cells and macrophages clear axonal cell debris [B]. Schwann cells dedifferentiate and proliferate to form the bands of Büngner [C] that promotes directional neurite outgrowth [D]. Neuroma formation an muscule atrophy in large gaps where trophic and structural support is absent [E]. Figure reproduced from (Deumens et al., 2010)

When the laceration is severe and the gap between proximal and distal stumps

is larger than around 10 mm, spontaneous regeneration does not occur, as

depicted in Sunderland grade V (Table 1.1). Rupture of the perineurium or

complete transection of the nerve trunk results in connective tissue formed via

fibroblast and Schwann cell proliferation in an attempt to bridge the gap

(Parrinello et al., 2010). The regenerated neural tissue is often abridged in

function due to improper remyelination and a reduction in number of distal axons

as a result of their inability to traverse the aberrant scar tissue. Excessive scar tissue may also cause sporadic axonal sprouting leading to neuroma formation (Fig 1.5 E), preventing regeneration with the consequential chronic denervation of the target organ (Tos et al., 2015, Sumner, 1990). Delayed re-innervation of the target organ can lead to dramatic loss in function, for example muscular atrophy, and a critical decline in patient quality of life.

1.2. Strategies for peripheral nerve repair

For small gap PNI (up to ≈ 9mm), immediate suturing of either the epineurium or fascicles of the proximal and distal stumps (Figure 1.6) is sufficient to allow axonal regeneration and functional regeneration, providing a critical tension threshold of 0.41-0.51 N is not reached (Sunderland et al., 2004). For larger defects (> 10 mm), the current "gold standard" of care for PNI remains an autologous transplantation of nervous tissue; a technique developed in 1967 whereby neural tissue is taken from a sacrificial region of the patients' body (often the sural nerve) and transplanted to the injury site (Ray and Mackinnon, 2010).
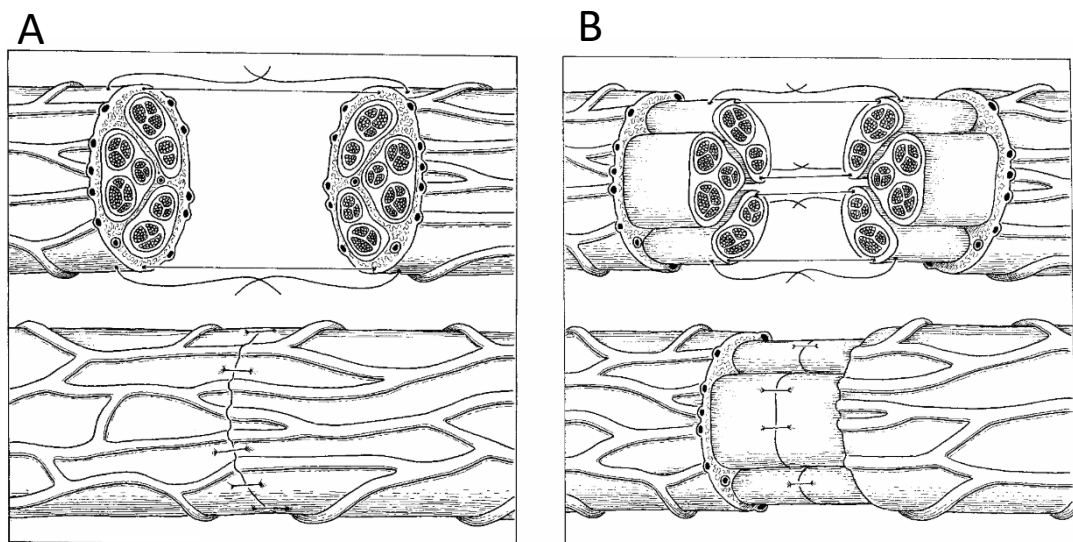
Figure 1.6 Primary nerve repair. Epineural repair [A]. Fascicular repair [B]. Figure reproduced from (Lee and Wolfe, 2000).

1.2.1. The autograft

Nerve autografts are easily sutured and provide a nonimmunogenic environment that promotes directional nerve regeneration across the gap toward the distal stump of the injury site. The transplanted tissue undergoes Wallerian degeneration, as described previously, and so the autografts' principal mode of action may be viewed as the extension of the supportive channels of neurotrophic repair Schwann cells and ECM residing in the Bands of Büngner (Lassner et al., 1995, Ray and Mackinnon, 2010).

Complications arise from donor site morbidity (loss of function in the donor site), limits of available donor material, the requirement for two surgeries, and with only around 50% of patients achieving complete functional recovery at the lesion site, there is clear clinical need for alternatives (Ray and Mackinnon, 2010). Allogeneic transplantation can be as effective in functional recovery, however, the requirement for chronic immunosuppression is suboptimal (Sergeyenko et al., 2018).

1.2.2. Nerve guidance conduits

The concept of tubulisation for the repair of peripheral nerves is thought to have originated in the late 19th century (IJpma et al., 2008), whilst modern advances in tissue engineering and the necessity for an alternative to the autograft have given rise to the development of complex nerve guidance conduits (NGC). Superficially, this appears to be a straightforward clinical problem for tissue engineering to solve, i.e. design and fabricate a device that is easily sutured, nonimmunogenic and, in mimicry of the autograft, often contains channels of support cells embedded in an ECM. Various approaches have been developed, drawing from

techniques in engineering, biochemistry, biology and physics in order to design the ideal NGC (Figure 1.7).
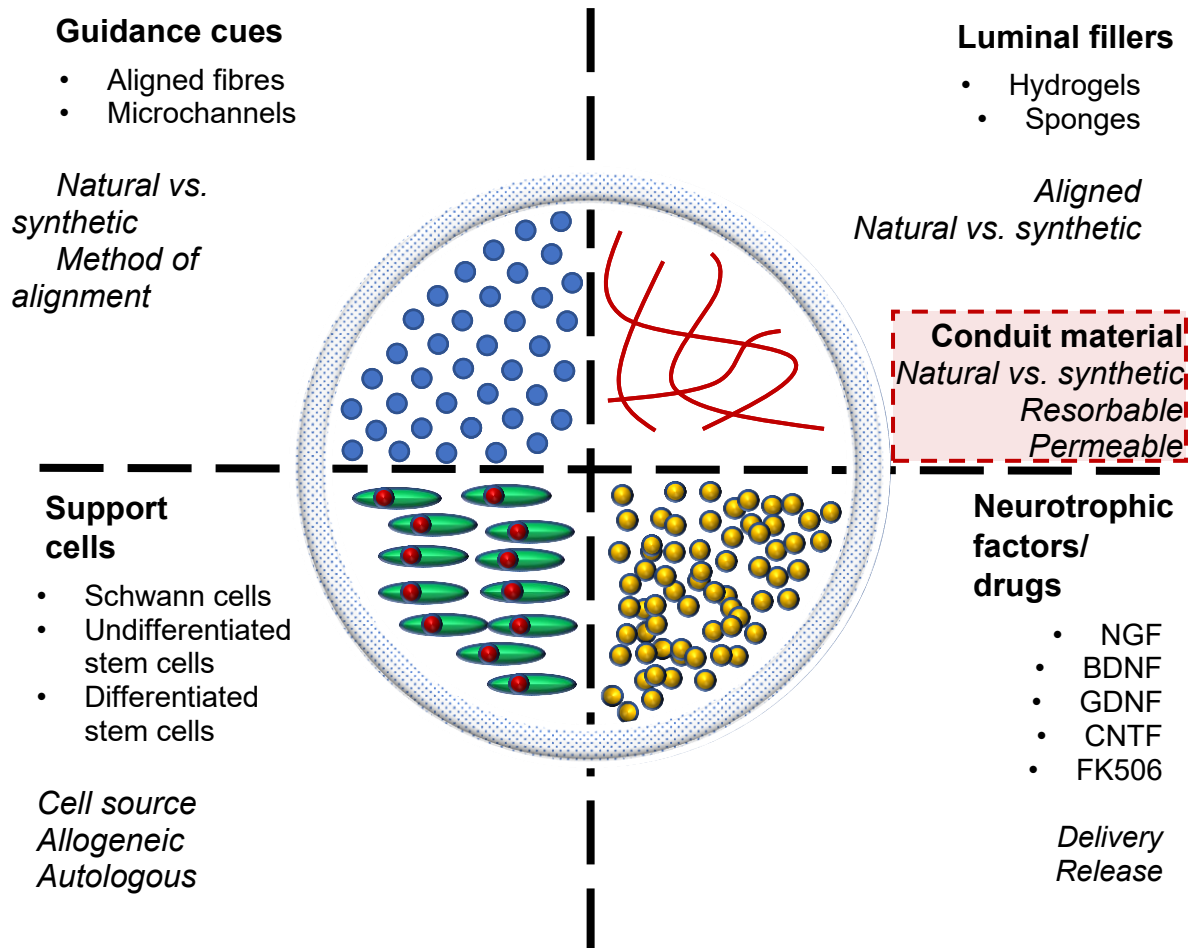
Figure 1.7 Targeting the ideal nerve guidance conduit. Components and modifications for incorporating into the design and fabrication of NGCs. Italicised text outlines key considerations for their application. Red box highlights considerations for conduit material properties.

Criteria to consider are as follows:

- *Permeability* – techniques should be employed to allow the diffusion of oxygen and nutrients into the conduit, particularly when using support cells to maintain viability.

- *Biodegradability* – the conduit and supportive environment should be present for sufficient time to provide support for the axons to traverse the conduit but also degrade in time to prevent adverse tissue reaction.

- *Flexibility and strength* – the biomechanics of the NGC should be tuned so as to allow for flexing and bending to prevent scarring of the surrounding tissue, during normal movement, whilst protecting the cells and axons contained within the conduit.

- *Directional growth* – microchannel or polymer fibre and cellular alignment techniques should be utilised to ensure directional regrowth of axons.

- *Neurotropism* – cues should be provided that encourage axonal regeneration.

1.2.2.1.   Guidance cues

Directional axonal regeneration is desired. Non-directional axonal regeneration is associated with poor functional recovery (Sumner, 1990) and may lead to the formation of neuroma, and subsequent chronic denervation, causing muscle atrophy (Deumens et al., 2010, Wall et al., 1979). Incorporation of physical structures that provide anisotropic support for the outgrowth of axons toward the distal device of the NGC is therefore frequently carried out (Bellamkonda, 2006). Microchannels (Shahriari et al., 2017, Ding et al., 2010), aligned filaments (Saeki et al., 2018), or micropatterning (Kim et al., 2018b) may be employed to achieve anisotropy in NGCs.

1.2.2.2.   Support cells

The benefits of the supplementation of NGC with a cellular component is well documented (Gao et al., 2014a, Gulati, 1988, Hoben et al., 2015). Schwann cells are essential to the regeneration process, releasing neurotrophic factors

(Fontana et al., 2012), secretion of supportive ECM (Doyu et al., 1993), and remyelinating the sprouting axons (Grove et al., 2020, Kim et al., 2018a). It is therefore unsurprising that many studies opt to develop strategies for the incorporation and implantation of Schwann cells within NGC (Salehi et al., 2018b, Salehi et al., 2018a, Smith and Stevenson, 1988, Mosahebi et al., 2002b, Kim et al., 2007, Gonzalez-Perez et al., 2018, Georgiou et al., 2013). However, difficulties arise when considering Schwann cell source and effective application; culture periods take at least two weeks (Dilwali et al., 2014), whilst the implantation of xenogeneic or allogeneic cells requires immunosuppression (Mosahebi et al., 2002a). As such, the application of stem cells for nerve repair has been a focus of recent research (Bhangra et al., 2016) due to their ability to differentiate into neural lineage specific cells to release neurotrophic factors, whilst overcoming issues surrounding allogeneic and xenogeneic cell sources (Georgiou et al., 2015, Reid et al., 2011, Scholz et al., 2011, Zhang et al., 2010).

1.2.2.3. *Neurotrophic factors*

Nerve regeneration may be accentuated via the incorporation, or functionalisation, of NGC with neurotrophic factors. These may be administered directly such as in protein delivery, or indirectly via cell and gene therapies (Hu et al., 2010, Eggers et al., 2020). Effects may be improved by devising methods for sustained release as this can maintain their neurotrophic effect over the, often months long, regeneration period (Fadia et al., 2020). There are many ways to achieve this: incorporation into electrospun conduit sheaths (Liu et al., 2021), bound to ECM molecules within the NGC lumen (McKay Hart et al., 2003, Terris et al., 2001), microsphere encapsulation (Wang et al., 2014, Fadia et al., 2020), and covalent binding to molecules in the conduit (Ho et al., 1998).

1.2.2.4.   *Natural materials*

Natural biomaterials are inherently biocompatible and possess binding motifs for cell adhesion (Theocharis et al., 2016, Madri and Basson, 1992, Petreaca and Martins-Green, 2020). Moreover, their degradation products are non-cytotoxic, can promote progenitor cell infiltration (Agrawal et al., 2011c), and often may be metabolised by cells in the local environment, stimulating the synthesis of novel and supportive ECM (Telejko et al., 1992, Laurent, 1987, Lu et al., 2011). Intrinsic biological variability leads to the possibility of batch to batch variation in mechanical and biochemical properties (Malafaya et al., 2007), whilst purification methods to overcome this can result in accelerated degradation rates *in vivo* (Ulery et al., 2011).

Due to its abundance in the mammalian ECM and tensile strength (Kadler et al., 2007), collagen type I is widely used within the field of neural tissue engineering (Boni et al., 2018). Moreover, high evolutionary conservation across species (Stover and Verrelli, 2011) allows extraction from xenogeneic sources for implantation without significant aberrant immune responses (Bayrak et al., 2013). Hollow collagen-based NGC have proven efficacious in promotion of axonal regeneration and functional recovery across short and long gap repairs (Archibald et al., 1991, Jeon et al., 2018b, Saltzman et al., 2019), whilst devices such as NeuraGen® have been approved for clinical use in humans (Kehoe et al., 2012). Moreover, due to its presence in the endoneurium (Luque et al., 1983, Nath et al., 1997) and role in the native peripheral nerve regeneration response (Siironen et al., 1992a, Siironen et al., 1996), collagen I has been frequently employed as a luminal filler as a hydrogel, either acellular (Yoo et al., 2020) or as a support cell delivery system, or as aligned fibres to provide adhesive guidance

cues for axonal regeneration (Saeki et al., 2018, Kazuya et al., 2000, Toba et al., 2002, Zhou et al., 2017).

Convincing arguments may be made for the utilisation of other ECM components as luminal fillers such as laminin, fibronectin, hyaluronic acid, and sulphated glycosaminoglycans due to their modulation of neurite and glial cell behaviour *in vitro* (Bailey et al., 1993, Wrobel and Sundararaghavan, 2018, McKee et al., 2012, Cornbrooks et al., 1983, Chernousov et al., 2008, Suri and Schmidt, 2010, Deister et al., 2007). However, mechanical properties such as degradation time can be suboptimal (Stern et al., 2007), whilst synergistic effects have further been observed in co-delivery of ECM components (Schense et al., 2000). Therefore *in vivo* applications are often expanded to a combinative delivery approach of these with either collagen or synthetic polymers (Lee et al., 2012, Toba et al., 2002, Kazuya et al., 2000, Mottaghitalab et al., 2013, Bailey et al., 1993, Labrador et al., 1998). Hydrogels derived from decellularised matrices for the introduction of nerve-appropriate ECM within NGC may provide an elegant solution, and recent studies have shown positive outcomes *in vivo* (Qiu et al., 2020b, Prest et al., 2017).

Other natural materials that have been explored include fibrin (Pettersson et al., 2010), silk (Alessandrino et al., 2019), chitosan (Gonzalez-Perez et al., 2017, Guo et al., 2018), and chitin (Jiang et al., 2019). The fibrin bridge is essential for Schwann cell organisation and subsequent axonal regeneration, and so, by introducing aligned fibrin nanofibers Du et al. (2017) achieved robust regeneration following a 10 mm sciatic laceration. Chitosan, a polysaccharide acquired through purification processes from shellfish (de Queiroz Antonino et al., 2017) degrades *in vivo* to produce chitooligosaccharides that encourage

macrophage polarisation towards an M2 phenotype associated with improvements in sciatic nerve repair (Zhao et al., 2017a).

Decellularised allogeneic nerve grafts have been employed to some success (Hudson et al., 2004, Whitlock et al., 2009). Antigenic material is removed during the decellularisation process and so, unlike allogeneic nerve grafts, immunosuppression is not required (Hudson et al., 2004). Decellularised nerve preparations providing site specific ECM components that maintain the appropriate topographical and structural architecture of the native nerve have been reported (Prest et al., 2017, Hundepool et al., 2017). Moreover, these materials contain neurotrophic factors bound to these ECM components that aid axonal regeneration (Pollins et al., 2018). However, these acellular grafts are limited to use across small gaps of 10 mm and under as, in longer gap models, migratory Schwann cells begin to exhibit signs of stress, resulting in senescence and a poor functional recovery (Saheb-Al-Zamani et al., 2013). Poor outcomesmay be improved via the seeding of support cells with a number of studies reporting improved outcomes, similar to those of an autograft, after the incorporation of Schwann cells within the acellular grafts for longer gap repairs (Jesuraj et al., 2014, Hoben et al., 2015).

1.2.2.5.   *Synthetic materials*

In contrast to natural materials. synthetic polymers are easily manufactured to precision with predictable and tuneable mechanical and biochemical properties (Gunatillake et al., 2006) . Lundborg et al. (1981) used empty silicone tubes to repair a 10 mm sciatic nerve gap in rats. At this distance, axonal regeneration was observed and successful reconnection to the distal nerve achieved with the authors suggesting that chemotactic cues secreted from the distal stump and the

infiltration of fibroblasts were responsible for the organisation and regeneration of the axons across the empty lumen. Further studies found minimal immune rejection of the construct; a finding validated in smaller gap (3-5 mm) repairs in humans (Lundborg et al., 1994). Since, conduits have been fabricated and filled with a plethora of synthetic polymers and materials, yielding a variety of results. Biodegradable polymers such as polycaprolactone (PCL) and polyethylene glycol (PEG) often outperform empty silicone tubes over short gap repairs, however, still do not possess the regenerative capacity of the autograft (Niu et al., 2014, Potas et al., 2015). Zhang et al. (2020a) report an improved outcome for PCL conduits loaded with methylcobalamin when compared to PCL alone, however, do not use an autograft comparator and so it is unclear as to the extent of its effect. Permeable polyurethane films fashioned into conduits proved to achieve far more robust regeneration and functional recovery when compared to an empty Neurotube® although, histological analysis showed that it was still incomplete in comparison to native nerve (Hsu et al., 2017). Conductive polymeric materials also may be employed to potentiate neural cell responses *in vivo* through electrical stimulation, such as polypyrrole (Zhang et al., 2007), carbon nanotubes (Lee et al., 2018), and poly(3,4-ethylenedioxythiophene) (Abidian et al., 2012).

1.2.3. Engineered neural tissue

Developed as an alternative to the autograft, EngNT is a type of living artificial tissue comprised of a highly aligned cellular component embedded in a purified collagen I hydrogel (Georgiou et al., 2013, Georgiou et al., 2015, Muangsanit et al., 2020, O'Rourke et al., 2018). Utilising simple notions of cell-ECM biomechanics it is possible to encourage cellular self-alignment within the collagen I hydrogel. Cells are seeded into the hydrogel placed within a rectangular mould tethered at either end, therefore forcing cellular contraction to occur exclusively in the lateral plane and subsequently resulting in a highly aligned cellular construct (Figure 1.8). Following removal of the interstitial fluid via plastic compression with the utilisation of a RAFT™ absorber, a stabilised sheet is formed that may then be rolled and placed in a nerve sheath or silicone tube to be sutured into the injury site.

To date investigations have been mostly focused on the cellular component of EngNT. Robust *in vivo* axonal regeneration has been observed in EngNT derived from rat Schwann cells (Georgiou et al., 2013), differentiated adipose derived stem cells (dASC) (Georgiou et al., 2015), dental pulp stem cells (DPSC) (Sanen et al., 2017), human endothelial cells (Muangsanit, 2020) and clinical grade human neural stem cells (O'Rourke et al., 2018).
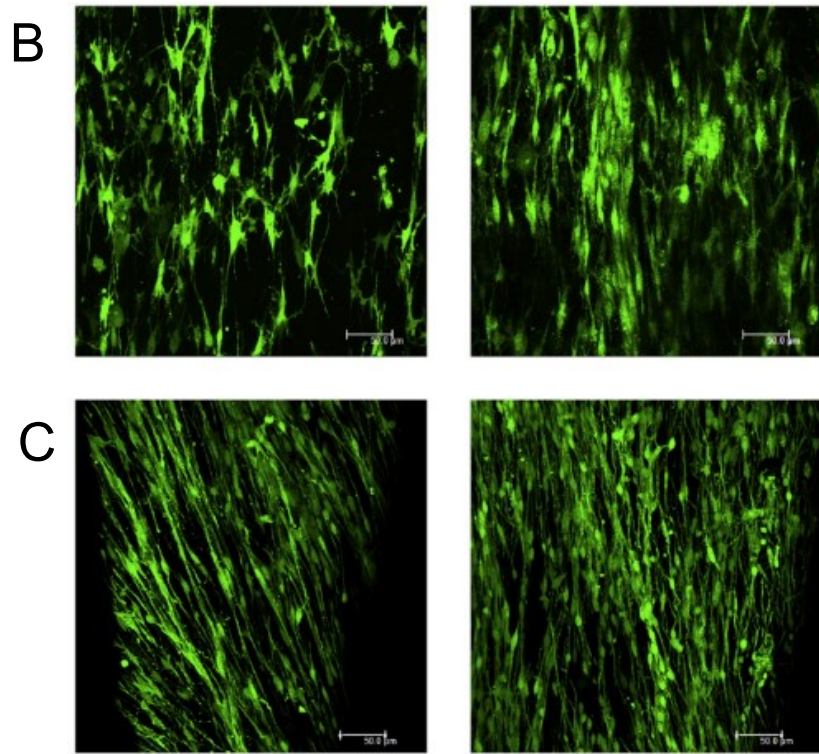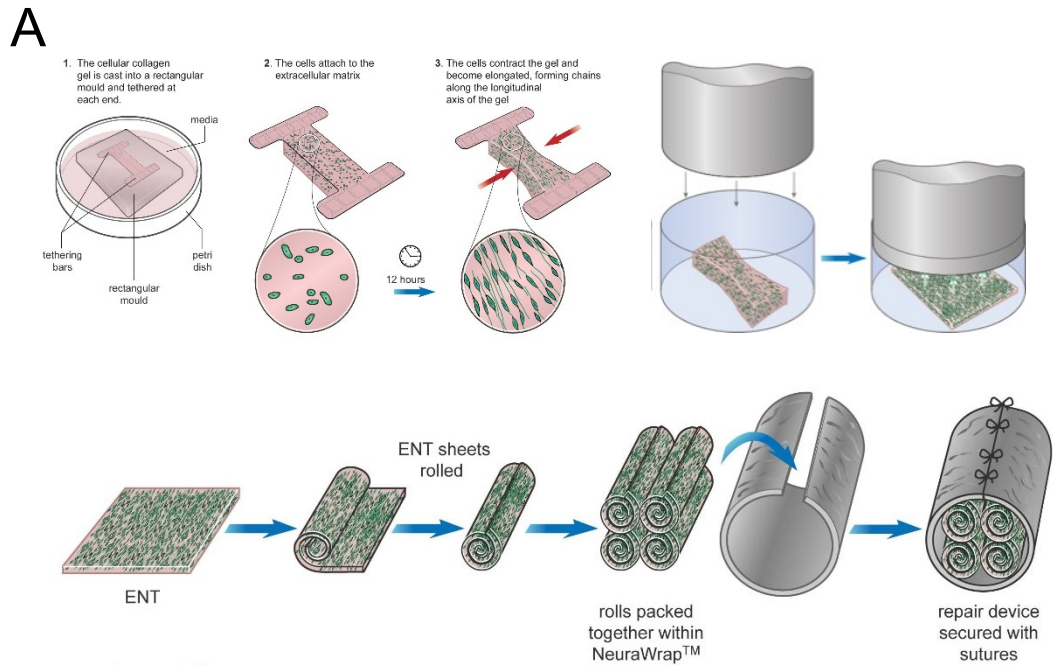
Figure 1.8 Engineered neural tissue for peripheral nerve repair. Schematic of the process for the production of engineered neural tissue sheets. Gels are seeded with cells in a tethered mould so as to enforce unilateral tension. Plastic compression is then utilised to remove interstitial fluid and a sheet of highly aligned cells is formed Figure reproduced from jamesphillips.org [A]. Fully hydrated constructs containing collagen I hydrogels embedded with Schwann cells [B]. Following plastic compression, the resultant stabilised cellular constructs are more densely populated with aligned cells that promote *in vitro* directional neurite extension [C]. Figures B and C reproduced from (Georgiou et al., 2013).

1.3. ECM

The ECM is the secreted functional and dynamic component of biological tissue, providing its structural architecture whilst further maintaining tissue specific function via influencing cell phenotype, proliferation, differentiation, gene expression and modulation of intracellular signalling (Bissell, Hall, & Parry, 1982; Flanagan et al., 2002; Gospodatowicz, Delgado & Vlodavsky, 1980; Lin & Bissell, 1993; Wells, 2008). In mammals it is comprised of collagens, laminin, fibronectin, elastin, proteoglycans, and glycosaminoglycans (GAGs) and forms a complex macromolecular network that provides its surrounding cells with structural and biochemical cues that shape their microenvironment.

Figure 1.9 outlines the key processes with which ECM influences cell behaviour. Cell-ECM interactions occur via cell surface receptors, such as integrins, resulting in downstream intracellular signalling that affects nuclear transcription. At the same time, the ECM is broken down by matrix metalloproteases (MMPs) releasing the embedded growth factors and matrix bound vesicles (MBV) and revealing cryptic peptides within the ECM. The ECMdegradation products are in turn taken up by the cell and further affect intracellular signalling and transcription.
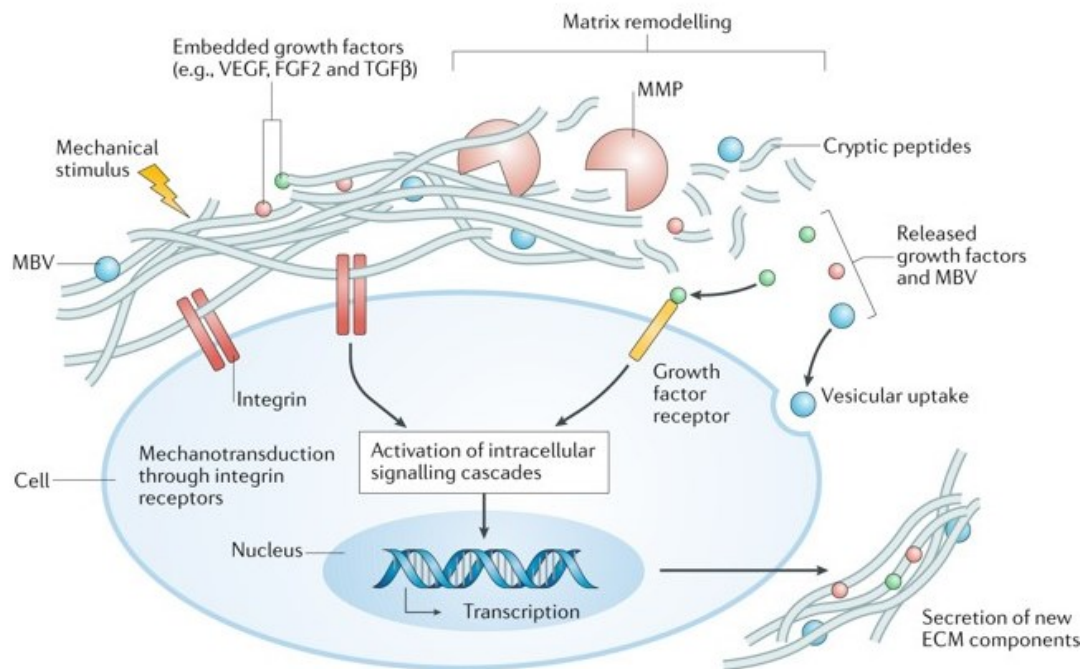
Figure 1.9 Dynamic reciprocity between ECM and cellular components of tissue. Extracellular components influence gene expression via cell surface receptors and, following degradation by matrix metalloproteases (MMPs), the release of matrix bound vesicles (MBV), growth factors, and cryptic peptides. New ECM components are subsequently synthesised and formed on and near the cell surface. As such, cells and ECM exist in constant feedback loop of recognition and remodelling. Figure reproduced from (Hussey et al., 2018).

1.3.1. Collagen

Collagens contribute to 30 % of the total protein mass in mammals, making them the most abundant protein (Ricard-Blum, 2011). All collagens share a common triple helical tertiary structure and are synthesised as procollagen, an intermediary protein that undergoes extensive posttranslational modification to give rise to a family of at least 28 subtypes of collagen with diverse supramolecular structure and function (Ricard-Blum, 2011, Kadler et al., 2007). Initially considered to exclusively perform a structural function within the ECM, collagens have been shown to be modulators of cell adhesion, proliferation (Pickering, 2001), and migration (Schor, 1980).

The triple helical structure is ubiquitous across all subtypes and is comprised of three polypeptide chains, held together via hydrogen bonds, and each containing a repeating amino acid (aa) motif: Gly-Xaa-Yaa, where X is often proline and Y often hydroxyproline (Yamada et al., 1980).

1.3.1.1.   Fibril forming

Fibrillar forming collagens form tight cable supramolecular structures and possess implicit roles in maintenance of tissue architecture and mechanical stability (Bella and Hulmes, 2017). Fibrillogenesis involves specific binding of their telopeptides into fibrils, mediated by cell surface receptors and ECM molecules such as fibronectin and other collagens (Milan et al., 2005, Brightman et al., 2000b, Birk and Silver, 1984). Collagen fibrillogenesis is a spontaneous, self-assembly process (Birk and Silver, 1984). Initiated by three single chain procollagen C-terminal propeptides nucleation (Doege and Fessler, 1986) and subsequent cleavage of the N and C-terminal propeptides, fibrillogenesis is mediated by fibronectin, collagen V (Wenstrup et al., 2004), and cell surface integrins (Li et al., 2003). A schematic of the process may be seen in Figure 1.11. Collagen I may be seen as the archetypical fibril forming collagen; other collagens contain interruptions in their triple helix, collagen I however, does not (Kadler et al., 2007).
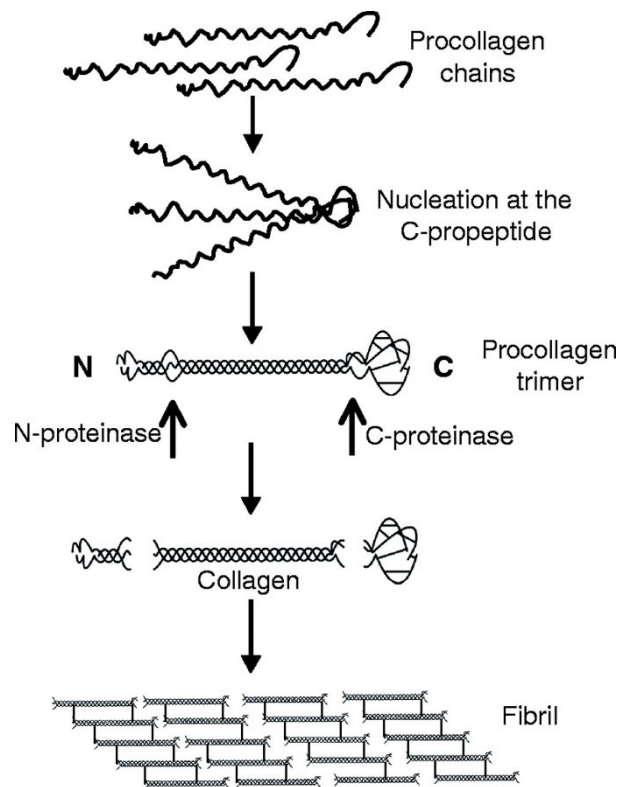
Figure 1.10 Collagen fibrilliogenesis. Procollagen C-terminal nucleation and triple helical formation. N and C terminal propeptide cleavage results in collagen fibrillogenesis. Figure reproduced from (Canty and Kadler, 2005).

1.3.1.2. Network forming

Collagen IV forms a supramolecular network. Four collagen protomers assemble at their amino terminals as a tetramer whilst their carboxy (NC1) terminals form dimers (Yurchenco and Ruben, 1987). Collagen IV acts as a scaffold and its binding to integrin on the cell-surface membrane provides a nucleation site for the assembly of proteoglycans, glycoproteins, and proteins that constitute basement membranes (Fleischmajer et al., 1998, Tsilibary et al., 1988)

1.3.2. Laminin

Laminin is a structural glycoprotein of the ECM, existing as a heterotrimer of α, β, and γ chain subunits (Aumailley et al., 2005). Following translation these three monomers self-assemble and typically form a cross shape with three short arms and one long helical domain (Figure 1.11) (Engel et al., 1981). These domains contain multiple binding sites for various integrins (Nishiuchi et al., 2006), as well as dystroglycan and syndecans (Hozumi et al., 2006). An integral component of the basal lamina, laminin interactions drive basement membrane formation (Li et al., 2005) and are therefore critical in the development and homeostasis of many organs including the kidneys, lungs (Willem et al., 2002), brain (Halfter et al., 2002), and peripheral nerves (Patton, 2000). Some laminin-integrin interactions have been implicated with improved cell survival from mediation of apoptotic pathways (Esco et al., 2001, Gu et al., 2002) whilst further modulating cell proliferation, differentiation, and migration (Paulsson, 1992).
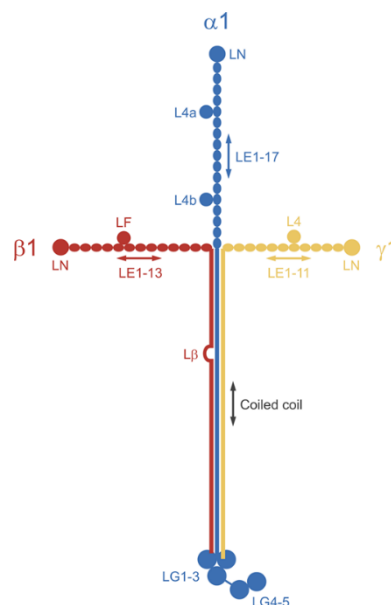
Figure 1.11. The archetypical laminin (laminin-111) with its cross shaped structure. Reproduced from (Hohenester, 2019).

1.3.3. Fibronectin

Fibronectin is the second most abundant protein of the ECM (Pankov, 2002). Existing as hetereodimers, fibronectins are highly conserved large molecular weight (up to 250 kDa) glycoproteins that appear as soluble molecules in plasma and as fibrillar structures in the ECM (Pankov, 2002). Fibronectin monomers are modular and are comprised of three subunits; type I, type II and type III, encoded by a single gene (Figure 1.12) (Pankov, 2002). Fibrillar, cellular fibronectin contains the alternatively spliced exons EIIIA and EIIIB and is critical in development and regeneration, regulating cell adhesion, migration and proliferation via their binding sites to multiple integrins and further associates with other ECM components such as heparin and denatured collagenous materials/gelatin (Liao et al., 2002, Mostafavi-Pour et al., 2001, Pankov, 2002). Akin to laminin, cellular adhesion to fibronectin has been associated with mediation of apoptosis and promotion of cell survival (Gu et al., 2002).
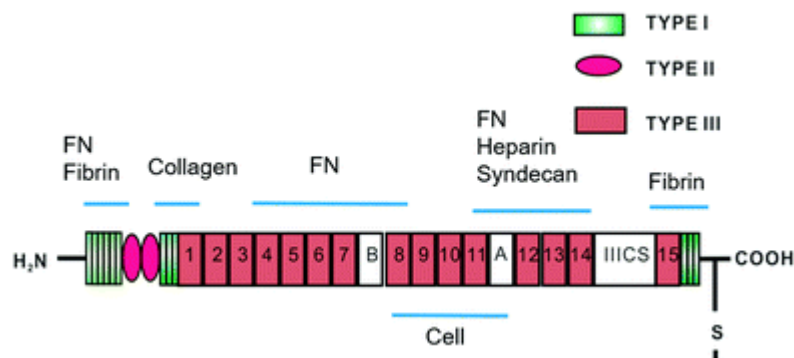
Figure 1.12 Modular structure of fibronectin monomer with its subunits and binding domains. Reproduced from (Han and Lu, 2017).

1.3.4. Glycosaminoglycans

Glycosaminoglycans (GAGs) are a family of unbranched polysaccharides comprised of basic repeating disaccharide units; D-glucuronic acid or L-iduronic

acid with a D-galactosamine or D-glucosamine. GAGs contribute to the physical

integrity of the ECM via their interconnectivity with proteins in the interstitial space

Four classes of GAG exist. Three of which are sulphated GAG (sGAG):

heparin/heparan sulphate, chondroitin/dermatan sulphate and keratin sulphate

that are all often found as part of proteoglycans. Hyaluronan/ hyaluronic acid (HA)

is the fourth class and is unsulphated (Yamada, Sugahara & Özbek, 2011).

Although essentially a basic motif of repeating disaccharide units, GAGs display

structural heterogeneity and therefore function through variations in chain length

and addition of sulphate groups (Victor et al., 2009). GAG functions vary from

increasing tensile strength and resistance to compression (Pfeiffer et al., 2008),

binding of growth factors and inflammatory cytokines (Evanko et al., 2012, Wight

et al., 2014), influencing fluid flow within tissues (Mow et al., 1980), naturally

cross-linking various components of the ECM, and bone mineralization (Grynpas

& Hunter, 1988).

1.3.5. Matrix-bound vesicles

Recently it was discovered that matrix bound vesicles (MBV) exist within

decellularised tissues (Huleihel et al., 2016). These MBV are a distinct class of

extracellular vesicles (EV), containing distinct nucleic and protein cargo

associated with cell cycle regulation and differentiation (van der Merwe et al.,

2017, Huleihel et al., 2017). MBV have been proven to modulate macrophage

phenotype (Hussey et al., 2019, Huleihel et al., 2017) and increase neurite

outgrowth in hippocampal neurons (Faust et al., 2017).

1.4. ECM of the peripheral nerve

Composition of the ECM within the peripheral nerve is dependent on its function and location. The perineurium is composed of multiple compact lamellae of fascicular orientated collagen I and II with flattened perineurial cells (Gamble and Eames, 1964, Thomas, 1963). These perineurial cells further contain a partial basal lamina rich in laminin, fibronectin, and collagen IV (Hill and Williams, 2002, Schiff and Rosenbluth, 1986). Alongside the epineurium, the perineurium is responsible for the majority of a nerves' tensile strength and elasticity (Rydevik et al., 1990) whilst further protecting the nerve fascicles from shear forces and maintaining homeostatic pressure within the endoneurium (Pina-Oviedo and Ortiz-Hidalgo, 2008, Ask et al., 1983). In the endoneurium, Schwann cells reside within their basal lamina containing collagen IV, laminin, fibronectin (Court et al., 2006, Ide et al., 1983, Mehta, 1985). Highly aligned collagen I fibrils dominate the endoneurial space, often in close contact with the Schwann cell basal lamina (Friede and Bischhausen, 1978). The sheathing epineurium is a loose double layer of connective tissue. The outer layer of the epineurium is predominantly composed of a ripple like pattern of collagen I and III fibres longitudinally orientated with the direction of the fascicle, aiding the elastic extension and spatial displacement of the nerve fibre that is necessary during natural movement (Luque et al., 1983, Stolinski, 1995).

Specific ECM components that may be of interest with respect to peripheral nerve engineering are summarised in Table 1.2. Biological roles as well as considerations for how each component may relate to peripheral nerve repair are shown.

Table 1.2 ECM components, their broad biological roles, and their prospective for peripheral nerve repair.

ECM component	General biological role	Biological role with respect to peripheral nerve injury and regeneration	References
COLLAGEN			
COLLAGEN-I	Fibril-forming, most abundant collagen. Provides structural and mechanical support.	90% of peripheral nerve ECM. Provides mechanical support, elasticity, and tensile strength	(Craig et al., 1989, Fujii et al., 1986, Koopmans et al., 2009)
COLLAGEN-III	Fibril forming, regulate collagen-I fibrillogenesis.	Elevated gene expression in basement membrane of proximal stump. Provides mechanical support for axonal regeneration.	(Koopmans et al., 2009, Liu et al., 1997, Siironen et al., 1992a)
COLLAGEN-IV	Network-forming. Main collagenous component of basement membrane.	Maintains the Schwann cell basal lamina.	(Siironen et al., 1992b, Timpl et al., 2000)
COLLAGEN-V	Fibril forming. Regulates collagen-I fibrillogenesis. Co-localises with collagen-I and –III.	Found in Schwann cell basal lamina. Modulates Schwann cell myelination.	(Chernousov et al., 2006, Sun et al., 2011)
COLLAGEN-VI	Microfilament forming.	Modulation of Schwann cell myelination and macrophage phenotype.	(Chen et al., 2013, Chen et al., 2015)
FIBRONECTIN			
FIBRONECTIN	Involved in wound healing. Modulates collagen fibrillogenesis.	Present in Schwann cell basal lamina and perineurium. Upregulated following nerve injury. Promotes Schwann cell migration *in vitro*	(Lefcort et al., 1992, Lorimier et al., 1992, Milner et al., 1997)

GLYCOSAMINOGLYCANS			
HEPARAN SULPHATE	Regulation of cell adhesion. Growth factor reservoir.	Found in the Schwann cell basal lamina. Binding and temporal release of neurotrophic factors.	(Eldridge et al., 1986, Gorio et al., 1997)
CHONDROITIN SULPHATE	Present in chondroitin sulphate proteoglycan families such as aggrecan, versican, and neurocan in a variety of tissues.	Inhibits neurite extension. Associated with glial scar. Modulates Schwann cell behaviour *in vitro*.	(Monnier et al., 2003, Wrobel and Sundararaghavan, 2018, Kuffler et al., 2009)
LAMININ			
LAMININ-111	Epithelial development/ polarisation. Highly expressed in embryonic development.	Abundant in the endoneurium. Schwann cell radial sorting. Modulation of Schwann cell myelination. Promotes neurite extension in vitro.	(Plantman et al., 2008, McKee et al., 2012)
LAMININ-211	Mesh-like formations in Schwann cell basal lamina.	Principal component of Schwann basal lamina. Schwann cell radial sorting. Modulation of Schwann cell myelination.	(Ghidinelli et al., 2017, Leivo and Engvall, 1988)
LAMININ-511	Found in basement membrane of variety of organs.	Abundant in perineurium. Improves neuronal cell viability and neurite extension in vitro.	(Hyysalo et al., 2017, Patton et al., 1997, Plantman et al., 2008)
LAMININ-521	Found in basement membrane of variety of organs.	Abundant in perineurium. Improves neuronal cell viability and neurite extension in vitro.	(Hyysalo et al., 2017, Patton et al., 1997, Plantman et al., 2008)
NIDOGEN			
NIDOGEN-1	Found in the basement membrane of a variety of organs	Regulates Schwann cell proliferation and migration in vitro. Promotes axonal outgrowth in vitro.	(Lee et al., 2009, Lee et al., 2007)

1.5. ECM components as substrates for nerve engineering

ECM components have been employed as substrates in general tissue engineering applications for decades (Kim et al., 2016, Kleinman et al., 1987). Innate features promote cell adhesion and modulate behaviour (Theocharis et al., 2016, Madri and Basson, 1992, Petreaca and Martins-Green, 2020), making ECM components ideal for *in vitro* cell culture that is biochemically representative of native environments (Kleinman et al., 1987).

1.5.1. Schwann cell response to ECM components

In vitro data into the effect of ECM components on Schwann cell behaviour has been extensive. Armstrong et al. (2007) showed that Schwann cell proliferation is higher on coatings of laminin and fibronectin with respect to collagen. Wrobel and Sundararaghavan (2018) investigated Schwann cell behaviour when interacting with a spinal cord ECM coating, aligned hyaluronic acid fibres, or soluble chondroitin sulphate substrates. Spinal cord ECM had no effect on morphology, however, appeared to promote a myelinating Schwann cell phenotype whilst the aligned hyaluronic acid had the greatest effect on Schwann cell elongation. Chondroitin sulphate, in contrast, had no significant effects on Schwann cell proliferation, morphology, and gene expression. Xu et al. (2020) compared the effect of varying stiffnesses of polydimethylsiloxane stamps coated with collagen I, fibronectin, and laminin on Schwann cell morphology, proliferation, and gene expression. Cell spreading was highest on fibronectin whilst laminin displayed the greatest increase in cell proliferation. All substrates increased c-Jun expression compared to the uncoated control, however the effect was most prominent on collagen I and laminin. c-Jun expression was further elevated when elongated Schwann cell phenotype was produced (Xu et al.,

2020). On one hand Milner et al. (1997) observed increased Schwann cell adhesion and migration on laminin as opposed to collagen I. In contrast, (Klein et al., 2016a) showed that Schwann cell viability was highest on collagen I and that Schwann cell migration was greater on both collagen I and fibronectin when compared to laminin. Chafik et al. (2003) presented findings suggesting Schwann cells favourably adhere to laminin and fibronectin when compared to collagen IV and that fibronectin bound Schwann cells displayed the highest levels of proliferation. Schwann cell-laminin contact (Fernandez-Valle et al., 1994), and maintenance of ECM structural integrity (Podratz et al., 2001) are essential for Schwann cell myelination.

1.5.2. *Neuronal cell response to ECM components*

ECM composition and mechanical properties influence neurite elongation (Swindle-Reilly et al., 2012, Bixby and Jhabvala, 1990, Heidemann et al., 1995). Retinal neurons showed greater neurite extensions when seeded on a collagen I coated surface than any other collagen subtype (Carri et al., 1992). Zander et al. (2010) found that laminin significantly increased PC12 neurite growth when compared to PCL and collagen. Armstrong et al. (2007) showed that NG-108 neurite extension was greater when grown on coatings of laminin or fibronectin when compared to collagen I and poly-d-lysine (PDL). Moreover, a synergistic effect on neurite length was observed between ECM and Schwann cells. Fibronectin was found to increase neurite extension in polyethylene glycol (PEG) gels, however in collagen gels of lower concentration it was inhibitory (Zhou et al., 2013). Wrobel and Sundararaghavan (2017) reported DRG neurites grew favourably on a coating of spinal cord ECM when compared to laminin, with inhibitory effects seen following the inclusion of chondroitin sulphate.

1.5.3. *Macrophage response to ECM components*

Phenotypic changes in macrophages are central to the correct repair, reorganisation and subsequent regeneration of peripheral nerves (Liu et al., 2019a, La Fleur et al., 1996). ECM components have shown to be a potent modulator of macrophage phenotype (Sikkema et al., 2018, Simon and Bromberg, 2017, Sridharan et al., 2019, Sapudom et al., 2020). Wrobel and Sundararaghavan (2018) reduced iNOS expression in macrophages, both when seeded on aligned HA fibres and on spinal cord ECM coatings. Moreover, aligned HA fibres promoted a more elongated morphology compared to spinal cord ECM, chondroitin sulphate, and tissue culture plastic.

1.6. Decellularisation

Decellularisation may be defined as the removal of cellular material, including inflammation inducing antigens, from biological tissues to produce acellular scaffolds that are rich in biochemical complexity, containing structural ECM components, native ECM micro- and ultrastructure (Fernández-Pérez and Ahearne, 2019, Freytes et al., 2008, Hussey et al., 2018, Nagao et al., 2011, Ren et al., 2013), cell-ECM binding motifs, sGAG (Hodde et al., 1996, Loneker et al., 2016, Prest et al., 2017), matrix-bound vesicles and growth factors (Voytik-Harbin et al., 1997, van der Merwe et al., 2017). These materials provide chemotactic and mechanical cues, affecting cell differentiation (Alom et al., 2017, Lin and Bissell, 1993, Paulsson, 1992) migration and mitogenesis (Kočí et al., 2017, Muncie and Weaver, 2018). The result of these biochemical and mechanical stimuli is, when implanted *in vivo*, there are macrophage phenotypic changes within the injury site as well as matrix remodelling resulting in the secretion of new and site appropriate ECM in the local environment (Brown et al., 2009,

McWhorter et al., 2015, Meng et al., 2015, Petrosyan et al., 2017, Slivka et al., 2014) and the recruitment of stem cells (Gattazzo et al., 2014, Agrawal et al., 2011b), causing a positive tissue remodelling response at the site of implantation.

The process of cellular removal often requires the utilisation of agents that can cause detrimental effects to the resultant material. A balance should ideally be struck between removing antigenic material and the preservation of biologically active soluble factors and the ECM architecture. Chemical, physical, and biological methods are used, often in combination, to decellularise tissues. The choice of method is dependent on the tissue that is being decellularised; cell density and variations in ECM components present have an impact on which treatments will be effective in removal of cellular material (Crapo et al., 2011).
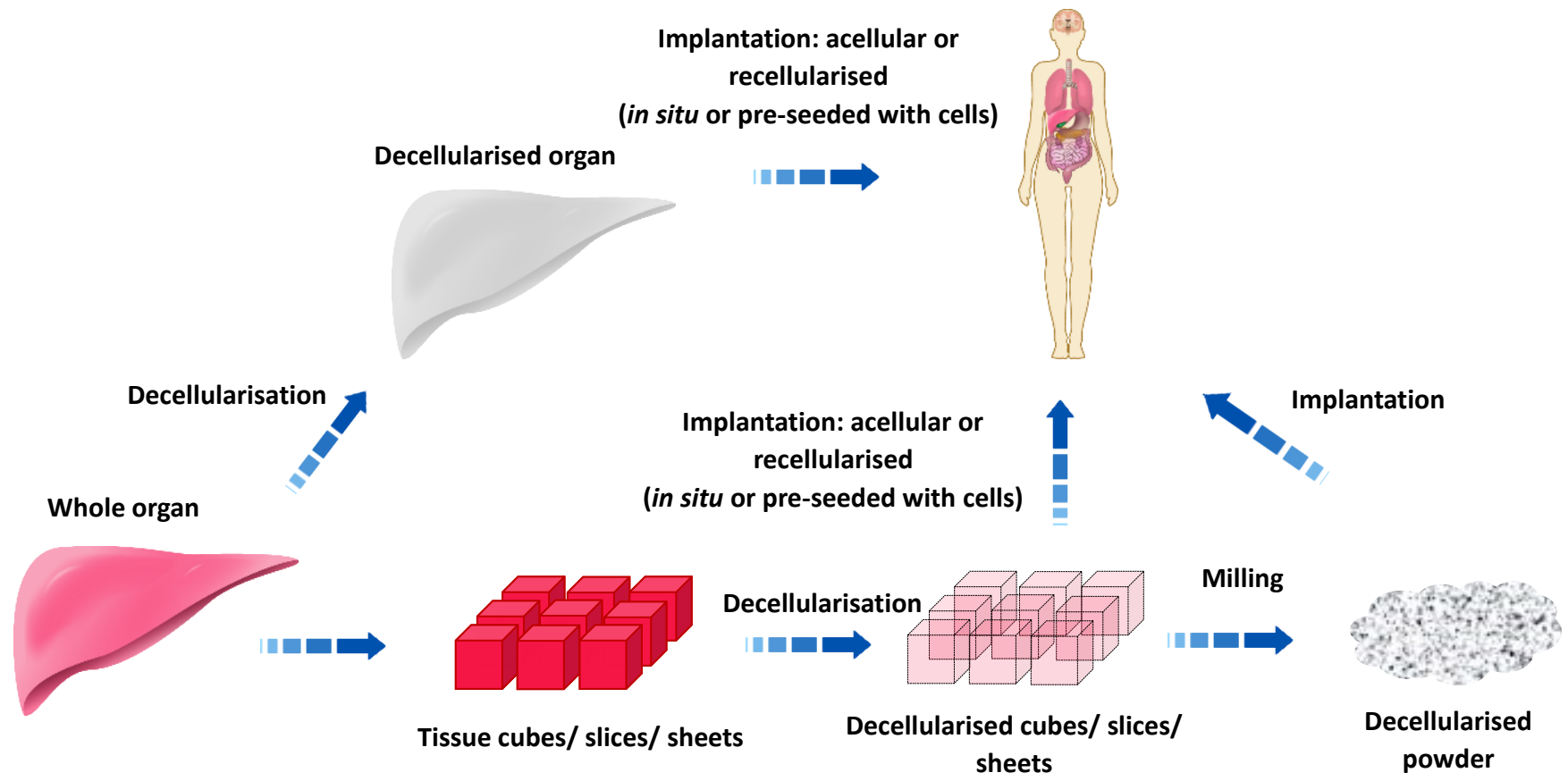
Figure 1.13 Decellularisation of tissues and their applications *in vivo*. Whole organs may be decellularised and either implanted as an acellular scaffold for *in situ* recellularisation or pre-seeded with site-appropriate cells. Alternatively, tissue may be sliced into cubes/ slices/ sheets to undergo decellularisation. These decellularised pieces may then either be implanted *in vivo* or lyophilised and milled into a powder.

1.6.1. Methods for decellularisation

1.6.1.1   Detergents

Cell membranes become solubilised when exposed to detergents in an aquesus environment. Ionic detergents such as sodium dodecyl sulphate (SDS) and sodium deoxycholate (SDC) denature proteins whereas non-ionic detergents such as Triton X-100 affect interactions between DNA and lipids, largely retaining protein structure (Yeagle, 2016). Zwitterionic detergents such as 3-[(3-cholamidopropyl)dimethylammonio]-1-propanesulfonate (CHAPS) possess the ability to behave as both ionic and non-ionic detergents, however have only shown to be efficacious for very thin tissue (Petersen et al., 2010). SDS is a commonly used detergent for decellularisation and has been shown to be efficient in cellular removal from liver (Ren et al., 2013), heart (Ferng et al., 2017), small intestine (Syed et al., 2014), and lung (Gilpin et al., 2014). Widely utilised in the decellularisation of whole organs, SDS has been proven to consistently remove over 90% of genetic material (Crapo et al., 2011). SDS cell removal is more effective than enzymatic methods such as trypsin, however, this is often at the expense of the quality of the resultant material due to residual detergent fragments embedded in the ECM (Vavken et al., 2009, White et al., 2017). In some cases, SDS significantly more damaging to the ultrastructure of the collagen network when compared to non-ionic detergents methods (Triton X-100), whilst further altering the materials biomechanical properties, often reducing its elastic modulus and toughness (Kasimir et al., 2003, Ren et al., 2013, Vavken et al., 2009, Xu et al., 2014). Xu et al. (2014) reported a lower GAG content in SDS treated tissue in contrast to trypsin, SDC or Triton X-100 treated and Kasimir et al. (2003) showed how a combination of Triton X-100 and sodium

deoxycholate (SDC) achieved complete cellular removal whilst retaining ECM structure in heart valve decellularisation. Moreover, regardless of extensive material washing, residual SDS often remains within the dECM, causing aberrant cellular responses when attempting to recellularise the scaffold; in comparison, higher metabolic activity is displayed in matrices treated with SDC (Rieder et al., 2004, Syed et al., 2014, White et al., 2017).

1.6.1.2   Acids and bases

Hydrochloric acid (HCl) has been used in the demineralization stage, removing most of the DNA and cellular material prior to bone decellularisation (Sawkins et al., 2013). The oxidizing agent peracetic acid (PAA) is commonly used as a disinfectant following decellularisation and has been shown to inactivate bacteria and viruses (Hodde and Hiles, 2002). Small intestinal submucosa (SIS) and urinary bladder matrix (UBM) may be prepared into thin sheets via delaminiation of the muscularis layers (Lindberg and Badylak, 2001, Massensini et al., 2015). Furthermore, agitation of these tissues in PAA is performed to disinfect these materials, but can additionally remove cellular material (Yamanaka et al., 2020), whilst retaining sGAG content, and actually induce biochemical changes that promote cell adhesion (Matuska and McFetridge, 2015). Reversible alkaline swelling (RAS), using a regimen of calcium oxide followed by ammonium salt, has been used to decellularise bovine pericardial tissue (Mendoza-Novelo et al., 2011). However, the authors proved that this technique was not as effective as Triton X-100 in removing cellular material and further resulted in detrimental effects to the ECM including damage to the ultrastructure, reduced mechanical properties and a significantly lower sGAG content. These effects from alkaline solutions can be attributed to the cleavage of crosslinks in the collagen network

(Crapo et al., 2011). The weak base ammonium hydroxide has been typically employed as a supplementary treatment in conjunction with detergents or freeze-shock methods (Lu et al., 2012, Perea-Gil et al., 2015), whilst Coronado et al. (2017) have shown that a treatment of ammonium hydroxide is more effective at cellular removal than sodium deoxycholate in the decellularisation of liver segments.

1.6.1.3   Biological agents

Various enzymatic agents have been used for decellularisation, although it is difficult to achieve complete decellularisation with enzymatic methods alone, especially without causing major disruption to the ECM architecture (Crapo et al., 2011). Enzymatic methods include trypsin, collagenase, nucleases and lipases. Trypsin is a serine protease that cleaves polypeptides at the arginine or lysine residues (Olsen, Ong & Mann, 2004). Trypsinisation should be performed with care as collagen has a limited resistance to the enzyme's activity (Keech, 1954; Waldrop, Puchtler, Meloan & Younker, 1980). Usually used in conjunction with EDTA, trypsin has been used to decellularise a variety of tissues including the trachea (Giraldo-Gomez et al., 2016), cartilage (Rahman et al., 2018), liver (Mazza et al., 2015b), heart valves (Schenke-Layland et al., 2003), and cancellous bone (Sawkins et al., 2013). There are inconsistencies in the literature surrounding GAG content retention as a function of trypsinisation; some reporting greater retention (Grauss et al., 2005; Kasimir et al., 2003), whereas others report a loss of GAGs when compared to detergent based methods (Xu et al., 2014). Bader and colleagues (2000) showed that, alone, trypsin displays insufficient cellular removal and so most decellularisation regimens use trypsin in parallel with detergents such as Triton X-100, SDS or SDC. Denser tissues can prove

harder to decellularise and so, trypsin is often used in the initial treatment stage, to disturb the peripheral tissue, and to provide the following treatments with a greater penetration potential (Crapo et al., 2011). Collagenase has been frequently used to isolate cells from tissues, however due to its specificity for collagen it can severely disrupt the ECM when compared to trypsin (Keech, 1954).

1.6.1.4 Physical methods

Although chemical and enzymatic methods of decellularisation have been proven to be efficient in cellular removal, there is apprehension to apply them as the toxicity of residual decellularisation agents in the scaffolds as well as there are concerns that these agents may affect the ECM structural integrity (White et al., 2017). Therefore, non-chemical decellularisation techniques may be desirable. Mechanical dissociation of surface cellular material from basement membranes has been reported for urinary bladder and small intestine (Syed et al., 2014). Supercritical carbon dioxide (scCO2) has been employed in conjunction with a detergent treatment for the decellularisation of heart valves to reduce ECM exposure to destructive and toxic agents (Casali et al., 2018).

1.6.2. Hydrogels derived from decellularised ECM

Hydrogels are hydrated networks of hydrophilic polymers held together via crosslinks that maintain the networks structural integrity (Hoffman, 2001). Their biomechanical mimicry of soft tissues make hydrogels attractive tools in the field of tissue engineering and as such have been used for applications such as *in vitro* disease models (Liaw et al., 2018), cell and controlled drug delivery (Marusina et al., 2020, Rao et al., 2017), and as injectable materials for tissue repair and regeneration (Rederstorff et al., 2011, Liu et al., 2017).
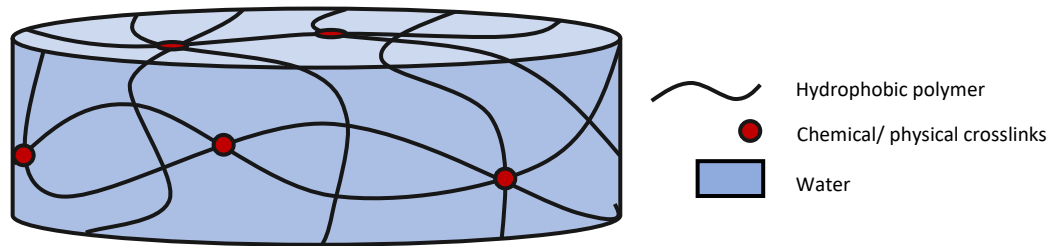
Figure 1.14 Schematic of a typical hydrogel. Hydrophilic polymers suspended in a water-based solution. Structural integrity is maintained via chemical or physical crosslinks of the poiymer.

The potential applications of decellularised ECM (dECM) were therefore diversified through the development of processes to generate hydrogels derived from decellularised ECM (dECM-h). Freytes et al. (2008) presented a process for production of a dECM-h; urinary bladder matrix ECM (UBM-ECM) was produced and lyophilised into powder form. This powder was then partially digested with pepsin in acidic solution to solubilise it into a temperature and pH sensitive pre-gel solution to be later neutralised to form stable hydrogels; allowing the material to remain in liquid form until reaching physiological conditions. Since this paper was published in 2008, dECM-h have been produced from a range of decellularised tissues such as dermis (Wolf et al., 2013), cancellous bone (Sawkins et al., 2013), small intestinal submucosa ECM (SIS-ECM) (Liang et al., 2015), liver (Ijima et al., 2019, Loneker et al., 2016), peripheral nerve (Prest et al., 2017, Qiu et al., 2020b), spinal cord (Medberry et al., 2013), brain (Wu et al., 2017) and pancreas (Sackett et al., 2018). The most common application of dECM-h is as injectable materials that retain the immunomodulatory and pro-regenerative properties of dECM, (Singelyn et al., 2009, Wang et al., 2017b) however, other uses include the improvement of *in vitro* disease models (Zhang et al., 2019), improving immunomodulatory effects and differentiation of stem

cells *in vitro* (Paduano et al., 2017, Tatic et al., 2019, Yuan et al., 2017, Zhang et al., 2017) and their delivery *in vivo* (Kim and Kim, 2016, Zhou et al., 2018, Kargar-Abarghouei et al., 2018).

1.6.2.1   *dECM hydrogels for nervous system repair*

As described above in Section 1.2 repair and the restoration of function in the nervous system following injury remains a challenge. Key challenges arise due to chronic inflammation (Buttner et al., 2018, Jin et al., 2010, Schimmel et al., 2017) and the formation of scar tissue resulting in tissue degeneration and loss of function (Yuan and He, 2013, McKee and Daneshvar, 2015, Li et al., 1997). Hydrogels derived from synthetic and natural materials can match the soft biomechanics of the CNS (Bartlett et al., 2020) and PNS (Madhusudanan et al., 2020), whilst the inherent immunomodulatory (Lin et al., 2018), angiogenic (Dew et al., 2016, Fercana et al., 2017), and reconstructive properties of dECM may prove beneficial in improving the regenerative capacity of the nervous system.

dECM-h have been employed in treatments for stroke (Ghuman et al., 2017, Ghuman et al., 2016, Koči et al., 2017, Massensini et al., 2015, Výborný et al., 2019), traumatic brain injury (TBI) (Wang et al., 2013, Zhang et al., 2013), spinal cord injury (SCI) (Cornelison et al., 2018, Hong et al., 2020, Tukmachev et al., 2016, Xu et al., 2016, Xu et al., 2018), and PNI (Lin et al., 2018, Qiu et al., 2020b). Novelty of the materials and the possibility of incomplete decellularisation drives the requirement for sufficient characterisation of their biochemical components. Moreover, hydrogel mechanics are of interest. The viscoelastic properties of an ECM hydrogel are dependent on the decellularisation methods employed and, due to their differences in biochemical makeup and this subsequent effect on mechanical behaviour, the source tissue; for example, GAG content has been

shown to affect gelation and storage moduli of materials (Brightman et al., 2000a). dECM-h functionality is therefore multifaceted; differences in biochemical composition result in diverse and complex cellular responses (Wolf et al., 2013), whilst biomechanical properties such as matrix elasticity, ultrastructure, and topography have the potential to affect cell differentiation, migration, and mitogenesis (Sun et al., 2018). Table 1.3 summarises the methods of dECM hydrogel production, biochemical and physical characterisation, and key *in vivo* findings.

ECM proteins are highly conserved across species, and as such effects of dECM are not necessarily tissue nor species specific. Indeed, materials derived from porcine SIS have been fashioned into nerve conduits (Yi et al., 2013), oesophageal wraps (Syed et al., 2014), and in cardiovascular patches (Mosala Nezhad et al., 2016a). As such, it is unsurprising that porcine UBM, a clinically used dECM, has been investigated in its hydrogel form for the treatments of stroke (Massensini et al., 2015) and TBI (Zhang et al., 2013). Similarly, Cornelison et al. (2018) employ a dECM-h derived from nerve tissue for use in SCI, reasoning that, due to its relative regenerative capacity to the CNS, the ECM of the PNS may improve the local environment following SCI. On the other hand, Kočí et al. (2017) use a material derived from umbilical cord (UC) for SCI as reports show that neonatal and foetal ECM sources improve the regenerative capacity of dECM (Kurtz and Oh, 2012).

Removal of antigenic material is essential in avoiding aberrant reactions *in vivo,* such as inflammation, and so assessment of residual cellular debris is desired (Londono et al., 2017, Keane et al., 2012). This may be done qualitatively via H&E staining or quantitatively via measurement of dsDNA (Gilbert et al., 2009).

Ideally, these are complementary data sets, however, as can be seen in Table 1.3 the quantitation of dsDNA is occasionally circumvented, and a lack of visible nuclei is proclaimed as appropriate acceptance criteria for complete decellularisation (Ghuman et al., 2016, Wang et al., 2013, Xu et al., 2016, Xu et al., 2018, Zhang et al., 2013). Moreover, if dsDNA is present, it should be ideally cleaved to below 200 bp to reduce immunogenicity associated with apoptotic pathways (Crapo et al., 2013, Nagata et al., 2010b). Of the studies that quantified dsDNA content, the nerve tissue presented in Lin et al. (2018) and Qiu et al. (2020b) was the most completely decellularised with a removal of around 98 % of the dsDNA from the native (3600 ± 315 ng/mg dry tissue weight) to the resultant dECM (60 ± 4 ng/mg). In contrast, the peripheral nerve ECM (PN-ECM) produced in Prest et al. (2017) removed approximately 85 % of the nucleic material; 1043.6 ± 291.2 ng/mg dry tissue weight (native) to 158.1 ± 34.5 ng/mg (decellularised). However, electrophoresis data showed that the dsDNA was mostly under 100 bp, whilst whole nuclei were absent in the H&E and DAPI staining. Prest et al. (2017) argue that this material is therefore decellularised. Differences in animal source may be cause for the variations in native dsDNA content between the two studies whereas the disparities in decellularisation efficiency are likely a result of the employment of different decellularisation agents and procedures: The peripheral nerves processed in Prest et al. (2017) were subjected to the decellularisation agents 3 % TX-100 and 4 % SDC for one hour treatments each, whereas Lin et al. (2018) and Qiu et al. (2020b) opt for a twelve hour 3 % TX-100 treatment and a 24 hour 4 % SDC treatment.

Due to their ability to modulate cell behaviour (Kliemt et al., 2013, Kuang et al., 2007, Evanko et al., 2012), binding of growth factors (Rother et al., 2019), and

effects on fibrillogenesis (Munakata et al., 1999, Milan et al., 2005) and mechanical properties of the resultant hydrogel (Daamen et al., 2003), sGAG are often quantified in dECM. In fact, Table 1.3 shows that they are the most frequently quantified biochemical component of dECM. The two studies that neglected sGAG quantification, opted for a qualitative analysis using a periodic acid-Schiff stain of the dECM (Xu et al., 2018, Xu et al., 2016). By far, the PN-ECM produced by Prest et al. (2017) has the highest sGAG content of roughly 50 μg/ mg dry tissue weight, whereas Hong et al. (2020) measured the lowest at just 0.7 ± 0.1 μg/mg in their brain ECM.

Possibly a more powerful qualitative method of biochemical characterisation in comparison to histology, is immunohistochemistry (IHC) as it allows for characterisation of specific ECM component isoforms (Lattouf et al., 2014). For example Prest et al. (2017) identified the preservation of collagen IV, within the basal lamina, and the removal of collagen I in the endoneurium during the decellularisation of peripheral nerve. Collagen IV was also visualised in resultant SC-ECM (Xu et al., 2016). Other components of basal laminae residing in the decellularised materials, such as laminin and fibronectin, may be assessed using IHC (Kočí et al., 2017, Xu et al., 2016, Výborný et al., 2019), whilst, Lin et al. (2018) opted to characterise collagen I, IV, and fibronectin with a western blot.

Growth factor content was one of the least utilised biochemical characterisation methods in Table 1.3. Hong et al. (2020) quantified an array of growth factors and cytokines present in the native and acellular brain tissue, reporting significant reductions in every molecule and even the complete depletion of fibroblast growth factor 2 (FGF-2) chemokine (C-X3-C motif) (CX3CL1), and insulin-like growth factor-binding protein (IGFBP) -3 and -9. Xu et al. (2021) and Li et al. (2020) were

the only studies to characterise dECM with mass spectroscopy. Becoming increasingly prevalent, mass spectroscopy allows for fast and thorough analysis of the entire matrisome (Bi et al., 2020, Henning et al., 2019, Li et al., 2016b). For example, (Xu et al., 2021) show that SC-ECM is comprised of a diverse compilation of glycoproteins, collagens, proteoglycans, ECM regulators, and secreted factors that are shared with PN-ECM by approximately 60 %. This was shown to be useful when elucidating *in vitro* tissue specific effects such as neural cell differentiation and nerve regeneration *in vivo*.

Table 1.3 Hydrogels derived from decellularised extracellular matrix, their characterisation, and their *in vivo* applications for nervous system repair.
Search string: "decell*" AND "hydrogel" AND (nerve*) OR (brain) OR (peripheral nerv*) OR (central nerv*)
Exclusion criteria: No *in vivo*, no hydrogel

Application	Tissue	Source	Mods	Characterisation												Model	Outcome	References
				Biochemical								Mechanical			Topographical			
				DNA	GAG	Collagen	GF	Histology	IHC	Western blot	MS	Turbidimetric	Rheology	Compression	SEM			
PNI	Nerve	*Porcine*	AC	✓	✓	✓				✓			✓		✓	Rat sciatic transection 15 mm (12 weeks)	Conduits filled with dECM-h outperformed empty conduits in SFI, CMAP, myelin thickness and muscle fibre regeneration. Not comparable to dNerve	(Lin et al., 2018)
		Porcine	VEGF/NGF	✓	✓	✓				✓	✓		✓		✓	Rat sciatic crush	Combination of NGF and VEGF with dECM-h resulted in increased neovascularisation, higher axon counts, and superior CMAP recovery.	(Li et al., 2020)
		Porcine	GDNF	✓	✓	✓				✓	✓		✓		✓	Canine sciatic 50 mm (6 months)	dNerve modified with ECM-h-GDNF far superior to dNerve in number of axons, walking track analysis, myelin thickness and muscle fibre regeneration. Not comparable to autograft.	(Qiu et al., 2020b)
		Porcine	NGF	✓	✓	✓				✓			✓		✓	Rat sciatic transection 15 mm (4, 12 weeks)	Aligned microchannels, dECM-h, NGF group showed comparable results to autograft in CMAP recovery and axon counts.	(Rao et al., 2021)
		Porcine	PLLA	✓	✓	✓				✓			✓		✓	Rat sciatic transection 5 mm (8 weeks)	PLLA with 0.25% dECM-h showed improved orientated outgrowth to 1 % dECM-h *in vitro* resulting in improved functional outcomes *in vivo*.	(Zheng et al., 2021)
		Canine	AC	✓	✓			✓							✓	Rat sciatic 8 mm (16 weeks)	M2:M1 phenotype higher than that of empty conduit with greater Schwann cell infiltration and a higher perioneal functional index	(Prest et al., 2017)

Application	Tissue	Source	Mods	DNA	GAG	Collagen	GF	Histology	IHC	Western blot	MS	Turbidimetric	Rheology	Compression	SEM	Model	Outcome	References
SCI	**Brain**	*Porcine*	AC	✓		✓								✓	✓	Rat T9/10 contusion (8 weeks)	M2:M1 phenotype was higher in 5 mg/ml dECM gels than both 8 mg/ml dECM and collagen gels. Significant differences were also observed in BBB and ladder scores.	(Hong et al., 2020)
	Nerve	*Rat*	AC		✓							✓	✓	✓	✓	Rat C3/4 contusion (8 weeks)	M2:M1 phenotype increased compared to saline controls but no significant increase in functional outcome	(Cornelison et al., 2018)
	Spinal cord	*Rat*	bFGF/ HP					✓					✓		✓	Rat T9/10 hemi-section (4 weeks)	dECM-h with bFGF increased neuronal survival, footprint and BBB scores when compared to bFGF and dECM-h alone implying a synergistic effect of having bFGF immobilised in the ECM-h.	(Xu et al., 2016)
		Rat	FGF2/ HP					✓					✓		✓	Rat T9/10 hemi-section (4 weeks)	dECM-h with FGF2 increased neuronal survival, neural regeneration and BBB scores when compared to FGF2 and dECM-h alone.	(Xu et al., 2018)
		Rat	MSC		✓							✓	✓	✓	✓	Rat T8 hemi-section (8 weeks)	dECM-h promoted cell infiltration into the lesion and at 2 weeks showed immunomodulation. At 4 weeks, no difference was seen between dECM-h and negative control implying the gel had degraded.	(Tukmachev et al., 2016)
		Porcine	AC	✓		✓		✓		✓					✓	Rat T9/10 hemi-section (8 weeks)	Tissue specific effects observed *in vitro* and *in vivo*. SC-ECM and PN-ECM promoted specific neural differentiation *in vitro*. SC-ECM promoted repair in favour of PN-ECM. Both were superior to collagen I.	(Xu et al., 2021)

Application	Tissue	Source	Mods	DNA	GAG	Collagen	GF	Histology	IHC	Western blot	MS	Turbidimetric	Rheology	Compression	SEM	Model	Outcome	References
Stroke	**UBM**	*Porcine*	AC		■	■		■				■	■		■	Rat MCAO (12 days)	Higher dECM-h concentrations were retained within the lesion site when compared with lower concentrations	(Massensini et al., 2015)
		Porcine	AC		■			■				■	■		■	Rat MCAO (24 hrs)	The highest concentration (8 mg/ml) resulted in higher progenitor cell infiltration and a higher M2:M1 phenotype.	(Ghuman et al., 2016)
		Porcine	AC		■			■				■	■		■	Rat MCAO (90 days)	dECM-h significantly reduced lesion volume however most microglia co-expressed M1 and M2 markers	(Ghuman et al., 2017)
	UC	*Human*	AC	■	■	■		■	■			■			■	Rat CPL (24 hrs)	After 24 hours the implanted UC-ECM hydrogels were densely populated with microglia	(Kočí et al., 2017)
		Human	Genipin	■	■	■						■			■	Rat CPL (2 weeks)	Genipin crosslinking decreased the *in vivo* degradation of the dECM-h without adverse inflammatory repercussions.	(Výborný et al., 2019)
TBI	**UBM**	*Porcine*	AC		■			■				■			■	Rat CCI (21 days)	dECM-h injection alleviated the white matter degradation and improved walking performance.	(Zhang et al., 2013)
		Porcine	NSC		■			■				■			■	Rat CCI (28 days)	NSCs combined with dECM-h improved on white matter preservation seen in Zhang et al., (2013) as well as showed significant improvements in long term cognitive abilities	(Wang et al., 2013)

AC – Acellular, CCI – controlled cortical impact, CPL- cortical photothrombotic lesion, dECM – decellularised ECM, dNerve – decellularised nerve graft, dECM-h – hydrogel derived from decellularised ECM, FGF2 – fibroblast growth factor 2, GAG –

glycosaminoglycan, GDNF – glial derived nerve factor, GF – growth factor, HP - heparin modified poloxamer, IHC – immunohistochemistry, M1 – classically activated macrophage, M2 – alternatively activated macrophage, MCAO – middle cerebral artery occlusion, Mods – Modifications, MS – mass spectrometry, MSC – mesenchymal stem cells, NSC – neural stem cell, PNI – peripheral nerve injury, SCI – spinal cord injury, TBI – traumatic brain injury, UBM – urinary bladder matrix, UC – umbilical cord

As with their biochemical characterisation, approaches to characterise dECM hydrogel mechanical properties are varied. The most frequent method among the studies reviewed in Table 1.3 is rheology. Storage and loss moduli were often measured (Cornelison et al., 2018, Ghuman et al., 2017, Ghuman et al., 2016, Kočí et al., 2017, Lin et al., 2018, Massensini et al., 2015, Qiu et al., 2020b, Tukmachev et al., 2016, Výborný et al., 2019, Wang et al., 2013, Zhang et al., 2013). Examples of how different decellularisation protocols or animal source may affect mechanical properties of the resultant dECM hydrogels can be seen within the studies that processed peripheral nerve tissue. Cornelison et al. (2018) reported a storage modulus of 31.3 Pa for a rat derived PN-ECM hydrogel at 9.5 mg/ ml whereas at a similar concentration of 10 mg/ ml, Lin et al. (2018) reported a storage modulus of 280 Pa in a PN-ECM from a porcine source. This may be further explained by the additional treatment of chondroitinase ABC by Cornelison et al. (2018) to remove possible inhibitory proteoglycans for nerve grafting. Kočí et al. (2017) used rheology to comparatively assess the storage moduli of umbilical cord (UC-ECM), brain (BN-ECM), SC-ECM, and UBM-ECM, further highlighting the differences in dECM hydrogel stiffness as a result of varying source tissue; BN-ECM was the softest and UBM-ECM the stiffest.

The considerable majority of the studies presented in Table 1.3 employ dECM hydrogels in their unaltered acellular form. Qiu et al. (2020b), however, postulated that due to its biochemical composition, the PN-ECM (produced and characterised previously in Lin et al. (2018) to treat PNI) would be able to bind, retain, and release GDNF into the injury site to improve nerve regeneration. PN-ECM hydrogels were either left unaltered or mixed with 0.05 ml of 800 μg/ ml GDNF and injected into a decellularised nerve graft (dNerve) for implantation into

a 50 mm sciatic nerve transection dog model for 6 months. Whilst inferior to the autograft, the group treated with GDNF loaded PN-ECM hydrogels presented a significantly improved functional recovery, greater axonal and Schwann cell positive areas, and an increased number and thickness of myelinated axons. It is unclear, however, whether the effect observed can be attributed to the combination of PN-ECM and GDNF as the authors neglected to include an experimental group in which a decellularised nerve graft supplemented with GDNF was used without the PN-ECM hydrogel. Similarly, Xu et al. (2018) utilised a spinal cord ECM (SC-ECM) derived hydrogel to functionalise a heparin-poloxamer (HP) to immobilise fibroblast growth factor-2 (FGF-2) for the treatment of spinal cord injury (SCI). Xu et al. (2018) present an improved, slower *in vitro* and *in vivo* release of FGF-2 from the SC-ECM functionalised HP hydrogel when compared to HP alone. In the presented thoracic vertebrae 9-10 injury model, motor function and nerve fibre regeneration were significantly improved in the SC-ECM-HP containing FGF-2 with a synergistic effect observed between FGF-2 and SC-ECM.

Of the studies presented in Table 1.3, two used dECM hydrogels as carriers for cell delivery. Tukmachev et al. (2016) employed a SC-ECM populated with mesenchymal stem cells (MSC) in the repair of a rat model for spinal cord injury (SCI). MSC incorporated into SC-ECM increased neurofilament positive areas and significantly increased expression of GAP43 and VEGF-A compared to acellular SC-ECM. However, rather than site-appropriate tissue formation and regeneration, formation of a disorganised heterogeneous tissue of blood vessels and axons was observed. Wang et al. (2013) implanted neural stem cells (NSC) incorporated into urinary bladder matrix derived ECM (UB-ECM) into a traumatic

brain injury (TBI) rat model. UBM-ECM increased NSC survival when compared to implanted cells alone, whilst recovery of motor and cognitive function was further improved as well as a mitigation of white matter loss.

1.6.2.2   *Potential for dECM hydrogel incorporation into EngNT*

From Table 1.3 it can be seen that dECM-h have been predominantly used for the repair and regeneration of the CNS. Whilst 3 papers present data for use in PNI, none used dECM-h for cell delivery into nerve lesion sites and the research area in general remains relatively untouched. Current research into overcoming PNI revolves around the utilisation of tissue engineering for the design and development of NGCs; constructs that aim to bridge nerve injury sites to provide trophic and structural support to the regenerating axons (Kehoe et al., 2012, Carvalho et al., 2019, Sarker et al., 2018a). EngNT derived from a range of cell types and sources has been shown to introduce significant improvement in the promotion of *in vivo* axonal regeneration across nerve gaps (Georgiou et al., 2013, Georgiou et al., 2015, Sanen et al., 2017), however the material component has largely remained unchanged. dECM materials are distinct from purified collagen in their biological complexity; possessing ECM structural and soluble components that can modulate cell behaviour (Parmaksiz et al., 2020, Mazza et al., 2015a, Su et al., 2018, Smith et al., 2017, Shin et al., 2019) whilst they further have an increased affinity for binding of growth factors for presentation and/ or controlled release (Sonnenberg et al., 2015, Nakamura and Ijima, 2013). On the other hand, structural stability is often compromised in comparison to purified collagen, and so this must be taken into account when considering applications of dECM hydrogels. The incorporation of dECM hydrogels into EngNT may therefore prove to be beneficial; cell-ECM interactions will likely differ in the

process of EngNT production whilst improvements may be made in the modulation of the surrounding milieu when transplanted *in vivo*.

1.7 Thesis aims

The principal objective of this project was to identify suitable candidates from a range of decellularised extracellular matrix (dECM) derived hydrogels as alternatives to the current purified type I collagen used to produce engineered neural tissue (EngNT).

The projects main objectives may be summarised as:

- Using a range of tissues, that have been decellularised previously in the laboratory and in the literature, to create a portfolio of biochemically and mechanically characterised dECM hydrogels.

- To use established *in vitro* models to assess each materials' ability to undergo cellular contraction and alignment. Furthermore, to investigate the potential of each material for their suitability for use in EngNT through neurite extension studies.

- To assess the efficacy of a chosen dECM EngNT in a 10 mm sciatic nerve repair model, comparing to EngNT derived from purified collagen I.

Chapter 2 Materials and methods

This chapter describes the materials used throughout this thesis and the methods employed. Work relating to the decellularisation of tissue and its subsequent characterisation in Chapter 3 was performed at the Centre for Biomolecular Sciences (CBS), University of Nottingham, UK. The remainder of the work, outlined in Chapter's 4 and 5, was undertaken at the School of Pharmacy, UCL, UK.

Table 2.1 Table of materials and equipment.

Materials and equipment	Supplier
1,9-dimethylmethylene blue	Sigma Aldrich, 341088, UK
CellTiter-Glo	Promega, G9681, UK
Chloroform	Fisher Scientific, 67-66-3, UK
Chondroitin – 1,6 – sulphate	Sigma Aldrich, C4384, UK
Coffee grinder	Krups, F203, UK
Collagen I	FirstLink, 60-30-810, UK
Collagen I	Collagen solutions, 16CSA05, UK
Collagenase	Sigma Aldrich, C9407, UK
Coverslip	VWR, 631-0156, UK
Cytosine arabinoside	Sigma Aldrich, C176, UK
Dimethyl sulfoxide	Sigma Aldrich, D5879-1L, UK
Dulbecco's modified Eagles' media	Sigma Aldrich, D6429, UK
Ethylenediaminetetraacetic acid	Fisher Scientific, D/0700/53, UK
Foetal bovine serum	Sigma Aldrich, F74524, UK
Gentamicin	Sigma Aldrich, G1397, UK

Hibernate A	Gibco, A12475-01, UK
Hoechst	Invitrogen, 33342, UK
Hydrochloric acid	Sigma Aldrich, 435570, UK
Isoflurane	Zoetis, Vm42058/4195 UK
L-cysteine	Sigma Aldrich, C1276-50G, UK
Methanol	Fisher Scientific, 67-56-1, UK
Optimal cutting temperature solution	Fisher Scientific, KMA-0100-00A, UK
Orbital shaker	OHAUS, SHHD1619DG, USA
Papain	Sigma Aldrich, P3375-25MG, UK
Paraformaldehyde	Fischer Scientific, P/0840/53, UK
Pepsin	Sigma Aldrich, P7012-250MG, UK
Penicillin and Streptomycin	Sigma Aldrich, P0781-100ML, UK
Pentoject, pentobarbitone sodium solution	Animalcare, XVD132, UK
Peroxyacetic acid	Fischer Scientific, 257755000, UK
Phenol/Chloroform/Isoamyl	Sigma Aldrich, 77617, UK
Phosphate buffered saline	Sigma Aldrich, P4417-100TAB, UK
Pico green assay	Life technologies, P11496, UK
Plate reader	BioTek, Synergy HTX, UK
Poly-d-lysine	Sigma Aldrich, A-003-E, UK
Polypropylene mesh	McMaster-Carr, 9275T21, USA
Proteinase K	Invitrogen, 25530-049, UK
Rheometer	Anton Paar, Physica MCR 301, UK
RNeasy Plus Mini Kit	Qiagen, UK
RT kit	Promega, GoScript™ Reverse Transcription System, UK

Sodium Deoxycholate	Sigma Aldrich, D2510-100G, UK
Sodium dodecyl sulphate	Sigma Aldrich, L3771-500G, UK
Sodium hydroxide	Fisher Scientific, S/4930/17, UK
Sucrose	Fisher Scientific, S/8600/60, UK
SYBR Green mix	Fisher Scientific, UK
TE buffer	PanReac AppliChem, 7l012281, UK
Tecan plate reader	Tecan, Tecan Infinite 200, UK
Tris-HCL	Fisher Scientific, 77-86-1, USA
Triton-X-100	Sigma Aldrich, T-8787, UK
Trypan Blue	Sigma Aldrich, 72-57-1, UK
Trypsin	Thermo Fisher Scientific, 15090-046, UK
Trypsin/ EDTA	Sigma Aldrich, T3924, UK
VECTASHIELD	Vector Laboratories, H-1400, UK

2.1 Cell culture

2.1.1 F7 Schwann cell culture

A cell line SCL4.1/F7, derived from rat schwannoma, were maintained in Dulbecco's modified eagle's medium (DMEM) supplemented with penicillin (100 U/ml)/ streptomycin (100 mg/ml) and 10% v/v foetal bovine serum (DMEM-complete) in standard cell culture flasks and used from passage 7 to 20. Media was replaced every 2 to 3 days and kept in a humidified incubator maintained at 5 % CO_2 / 95 % air.

2.1.2 Dorsal root ganglion preparation and culture

All experimental procedures involving animals were conducted in accordance with the UK animals (Scientific Procedures) Act (1986) and approved by the UCL animal ethics advisory group. Dissected dorsal root ganglia (DRGs) were harvested from adult rats (200-300g) culled using rising levels of CO_2. The spinal column was removed, cut longitudinally and spinal cord removed to access the DRGs (Figure 2.1 A). Dorsal and ventral roots were removed with their spinal nerve, to isolate the DRG (outlined in red in Figure 2.1 B) and placed in serum free DMEM. DRGs were dissociated in 0.125% collagenase for 1.5 hours in a cell culture incubator at 37 °C and 5 % CO_2 / 95 % air. Dissociation was aided by trituration followed by two washes in DMEM-complete. The suspension was plated onto cell culture flasks coated with poly-d-lysine (PDL) and incubated for 24 hours with cytosine arabinoside (0.01 mM) to deplete glial cells.
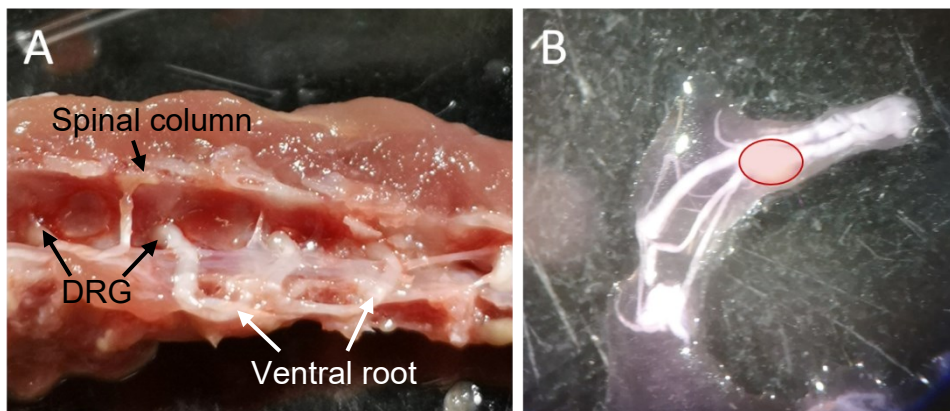
Figure 2.1 Rat spinal column dissection and dorsal root ganglion extraction. Spinal coluumn from adult Sprague Dawley rats with the spinal cord removed [A]. Rat DRG (shown in red) with ventral roots and spinal nerves attached [B].

2.2   dECM generation

Table 2.2. Decellularisation protocol selection for each tissue.

Tissue	Protocol
Cancellous bone	Existing in lab from previous work by Dr Lisa White.
Liver	Provided by Badylak laboratory.
Small intestine	Provided by Badylak laboratory.
Urinary bladder	dECM material provided by Dr Tim Keane.
Spinal cord	Provided by Dr Anne des Rieux

2.2.1   Bone preparation

Bovine tibias were sourced from an EU certified butcher (J. Broomhall Ltd., Dursely, UK), slaughtered at 12-24 months and the bones were sliced into 5 mm segments to be shipped on the same day (Figure 2.2 A). The segments were stored at -20 °C for later process. The bone was then processed to separate the bone marrow and cortical tissue from the cancellous bone (Figure 2.2 B). The cancellous material was then washed in phosphate-buffered saline (PBS) containing 0.1% w/v gentamicin. These segments were then snap frozen in liquid nitrogen and ground into pieces no larger than 4mm X 4mm X 4mm (Figure 2.2 C). The pieces were then further submerged in liquid nitrogen and ground into a powder in a commercial coffee grinder (Figure 2.2 D).
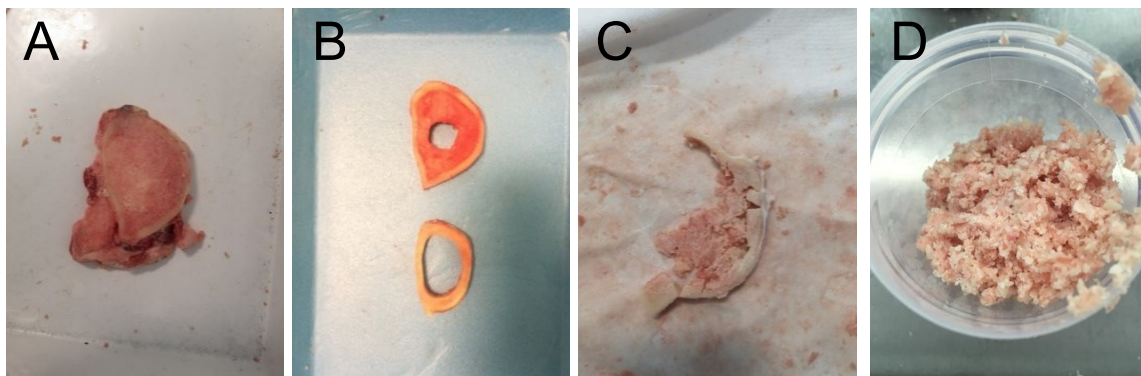
Figure 2.2 Cancellous bone powder generation. Cancellous bone as received [A], with connective and bone marrow removed [B]. Bone following crush [C], and milling in grinder [D].

2.2.2 Bone decellularisation

An adapted version of previous methods (Pietrzak et al., 2011) was utilised to remove the mineral content of the cancellous bone granules. The material was suspended in 0.5 N HCl (20 ml/ g bone) by agitating using a magnetic stirrer at 300 rpm for 24 hours at room temperature and then rinsed several times in distilled water. The demineralised bone matrix (DBM) had its lipid content extracted via a one-hour exposure to a mixture of 1:1 chloroform: methanol followed by rinsing in methanol and then PBS. The material was then snap frozen in liquid nitrogen, lyophilised for 48 hours and then stored at -20 °C.

The lyophilised DBM was then subjected to an adapted enzymatic decellularization treatment (Schenke-Layland et al., 2003). A solution of 0.05% trypsin and 0.02% ethylenediamine tetraacetic acid (EDTA) was used to decellularise the DBM under constant agitation at 300 rpm at room temperature for 24 hours. This material, now known as bovine decellularised matrix (B-ECM) was agitated in PBS for 24 hours at room temperature to remove any remaining cellular material. The B-ECM was then lyophilised into a powder for 48 hours and then stored at 4°C for later use.

2.2.3 Liver preparation

Porcine liver was harvested from animals 3-6 months old and shipped on the day of slaughter. Upon arrival, the liver was segmented, connective tissue removed and stored at -20°C for later use. Prior to decellularization, the liver segments were further processed into 10 cm x 2 cm x 5 mm slices using a mandoline slicer (Amazing Kitchenware, London, UK).
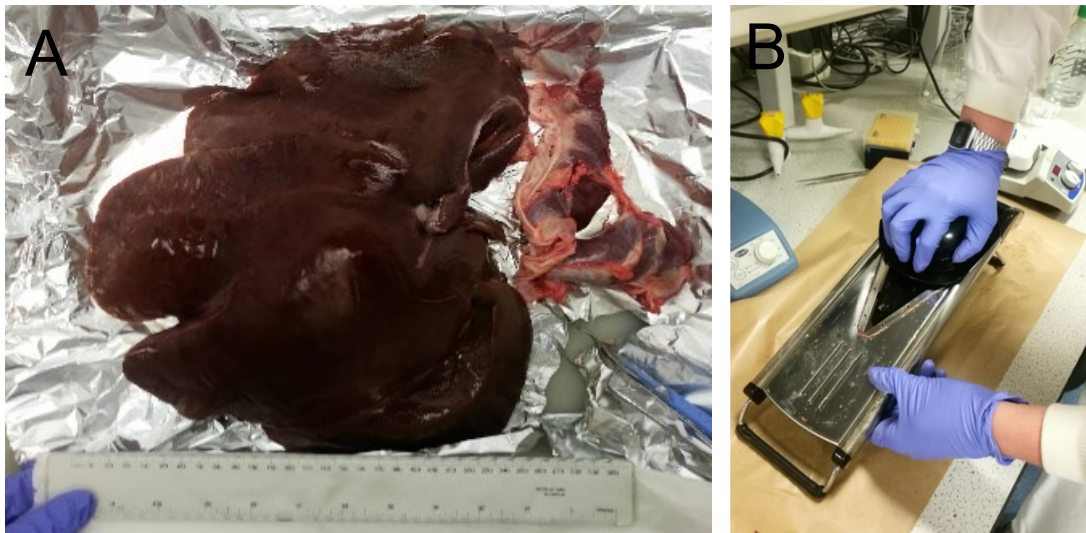
Figure 2.3 Liver preparation. Whole porcine livers as received [A]. Slicing liver with mandoline slicer [B].

2.2.4 Liver decellularisation

2.2.4.1 Liver decellularisation treatment optimisation

Two existing methods for liver decellularisation were explored. They are referred to in text as either method 1 (Loneker et al., 2016) or method 2; adapted from (Mazza et al., 2015a). With the application of implantation of encapsulated cells within these matrices in mind, the use of the cytotoxic (Friedrich et al., 2018) and potentially destructive SDS in method 2 prompted an investigation into the decellularisation potential of lower concentrations. This further led to the optimisation of the protocol through the alteration of each decellularisation agent, summarised in Table 2.3.

Table 2.3 Variations in decellularisation agent concentration for the production of LIV-ECM.

	1	2	2B	2C	2D	2E
TRYPSIN/ EDTA	0.02%/ 0.05%	0.02%/ 0.05%	0.02% / 0.05%	0.02% / 0.05%	0.02% / 0.05%	0.02% / 0.05%
TRITON X-100	3%	3%	5%	3%	3%	3%
SDS	NA	1%	0.5%	3%	0.5%	0.25%
SDC	4%	NA	NA	NA	NA	NA

EDTA: ethylenediaminetetraacetic acid, SDS: sodium dodecyl sulphate, SDC: sodium deoxycholate

A previously described method was adapted (Coronado et al., 2017). Liver slices were placed in conical flasks and first washed in dH2O for 15 minutes 3 times on a magnetic stirrer at 300 rpm at room temperature. The water was drained, and the slices placed back into the flasks. Three consecutive treatments were then applied; 0.02% trypsin 0.05% EDTA at 37°C, 3% Triton X-100 at room temperature and 4% sodium deoxycholate at room temperature. All treatments were performed at 300 rpm on a magnetic stirrer and between treatments the slices were gently massaged over a sieve before being washed 3 times at room temperature in dH2O at 300 rpm. The resultant LIV-ECM was stored at 4 °C in dH2O for 16 hours, dried and weighed. Depyrogenation was performed using a 1:20 w/v ratio of 0.1% peracetic acid for 2 hours at room temperature and at 300 rpm on a magnetic stirrer. After washing in PBS and dH2O the ECM was snap frozen, lyophilized into a powder and stored at 4°C for later use.

2.2.5 Small intestinal submucosa preparation and decellularisation

Porcine small intestine was harvested from animals 3-6 months old and shipped on day of slaughter. A previously described method was adapted (Badylak et al.,

1998). Upon arrival, the jejunum was separated from the large intestine (Figure 2.4 A), its connective tissue removed and was cut into lengths of approximately 1 m (Figure 2.4 B). The tissue was washed extensively by running H_2O through the lumen until the runoff became clear, before being sliced longitudinally.

The tissue was then turned over with the luminal side facing up and a portion of the tunica serosa removed through gentle abrasion (Figure 2.4 D). The tissue segment was then inverted to be abluminal side facing up and the muscular externis removed via mechanical delamination; a motion that further removes the tunica serosa underneath. The resultant submucosa (Figure 2.4 E) was washed in PBS on a mechanical shaker at 300 rpm at room temperature. Subsequently, the SIS was treated in a 1:20 w/v ratio of 0.1% peracetic acid for 2 hours followed by two sequential washes in PBS and deionised water; all treatments performed on a mechanical shaker at 300 rpm at room temperature. The resultant SIS-ECM sheets (Figure 2.4 E) were then frozen at -80° C for 24 hours, lyophilised and stored at 4° C. Sheets were then milled into a powder form and stored at -20° C.
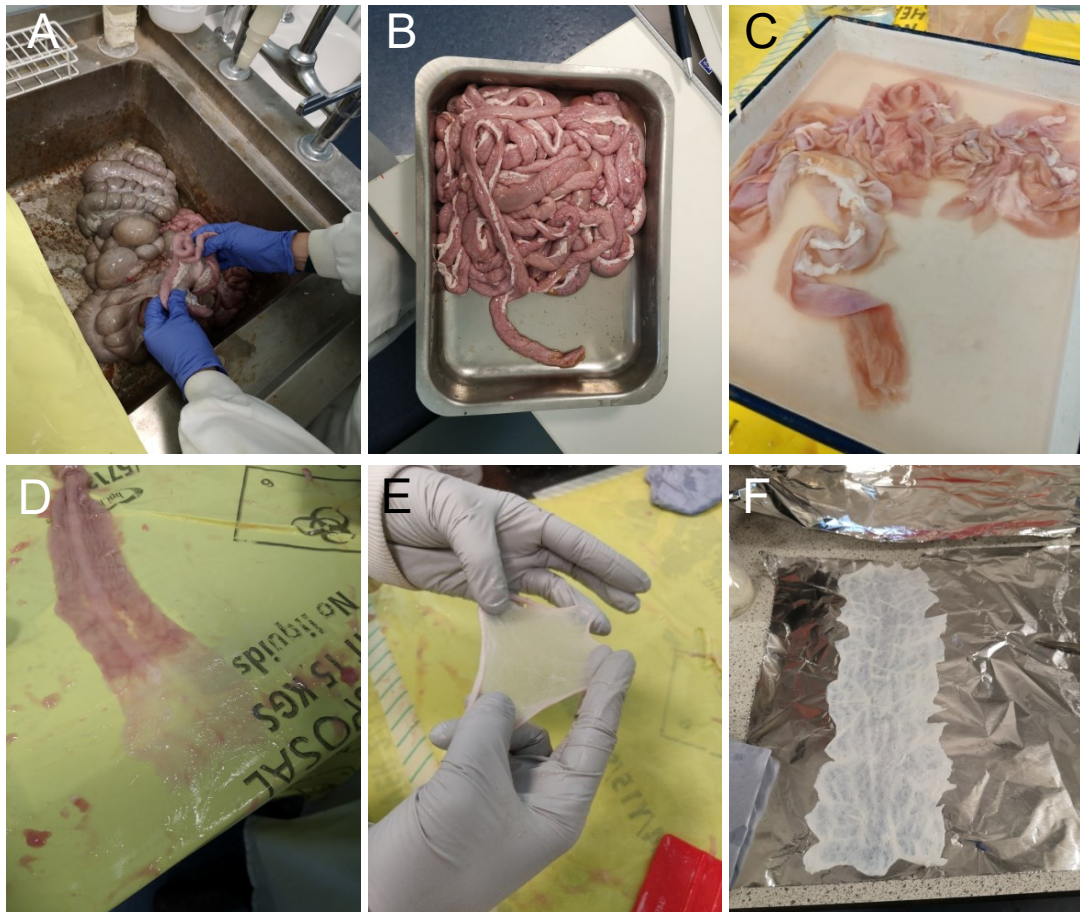
Figure 2.4 Preparation and decellularisation of small intestinal submucosa.
Separation of porcine large [A] and small [B] intestine. Longitudinal slicing of tissue to
produce sheets of small intestine [C]. Mechanical abrasion of the abluminal side of small
intestine [D] and resultant SIS sheet [E]. Sheets of SIS following PAA decellularisation
ready to be frozen and lyophilised [F].

2.2.6 Spinal cord preparation and decellularisation

Fresh porcine spinal cord was obtained from market weight animals. A previously

described procedure was followed (Crapo et al., 2013). Connective tissue, dura

mater and residual blood clots were removed from the tissue prior to being

segmented latitudinally at ≈ 4cm intervals. These segments were then sliced

longitudinally and rolled out to form sheets of spinal cord.

The sheets were washed for 12 hours in PBS at 4°C and then placed in 0.05%

trypsin 0.02% EDTA and agitated at 300 rpm at 37°C for 1 hour. The tissue was

then treated with 3% Triton X-100 followed by a 4% sodium deoxycholate treatment both at 300 rpm for 1 hour at room temperature. To ensure residual decellularization agents were removed, the tissue was agitated at 300 rpm for 1 hour at room temperature in PBS and then PBS. In between each stage the treatments were washed off in dH2O over a 300μm sieve whilst gently massaging the tissue between the thumb and index finger to aid in the decellularization process. The resultant SC-ECM was snap frozen in liquid nitrogen, lyophilized for 48 hours and stored at -20°C for later use.

2.3   dECM hydrogel formation

2.3.1   Digestion and solubilisation

A previously described method was employed to achieve ECM solubilisation (Freytes et al., 2008). Lyophilised ECM powders were added to 1 mg/ ml pepsin in 0.01 N HCl solution to make up a final ECM concentration of 10 mg/ml. In other words, 1 g dry ECM mixed with 100 mg pepsin in 100 ml 0.01 N HCl. The suspension was mixed on a magnetic stirrer at room temperature for 48 hours (LIV-ECM, SIS-ECM) or 96 hours (B-ECM) until no visible particulate was observed. Now known as an "ECM digest" these were subsequently centrifuged at 2000 rpm, aliquoted and stored at - 20°C or used immediately.

2.3.2   Neutralisation and gel formation

Gelation was achieved via basic neutralisation as previously described (Freytes et al., 2008). All solutions were kept at 4° C. Briefly, ECM digests were mixed with 0.1 N NaOH (1/10 volume of pre-gel solution) and 10X PBS (1/9 volume of pre-gel solution). 1X PBS was further used to adjust the solution to the desired concentration and volume before raising the temperature to 37°C to promote gelation.

2.4 Biochemical ECM characterisation

2.4.1 Histology

Histology was performed to enable microscopic visualisation of both cellular and extracellular structures.

Tissue was fixed in 3.7% (w/v) paraformaldehyde (PFA), using a 20:1 ratio (PFA:Tissue), straight after each experiment. The tissue was incubated in PFA for 48 hours before rinsing with the same volume PBS. An automated tissue processor (Leica TP1020) was used to penetrate the tissue with melted paraffin wax. Briefly,the tissue was dehydrated using increasing concentrations of ethanol (25%; 50%;75%; 95%; 100%) to fully remove water content from the tissue. Once the tissue was fully penetrated by ethanol, the ethanol was replaced by Histoclear, a clearing agent that is miscible in ethanol and paraffin wax. In the final step, Histoclear was replaced with melted paraffin wax (~60°C). The whole process took 16 hours. Following this process, the tissue was wax embedded using a wax embedder (Leica EG1160). Briefly, the tissue was placed in a stainless steel base mould, orientated as required and then covered with melted wax before left to set on a cooled plate (-20°C) until fully hardened. The histopathology unit at Queens Medical Centre (QMC) Nottingham (UK) conducted sectioning, staining and imaging. Tissue sections were cut into 5 mm sections. Three sections were taken per sample. A Hamamatsu Nanozoomer NDP slide scanner was used to scan all slides.

The following stains were chosen for histological analysis:

- Haematoxylin; (H) (basic dye) binds to the acidic components/structures (negatively charged) of the cell such as the nucleic acids. Stains purple/ blue.

- Eosin; (E) (acidic dye) will bind to the cationic (positively charged) or basic components/structures of the cell such as the amino groups in proteins in the cytoplasm. Stains pink.

- Alcian Blue; (AB) (basic dye) that binds to acidic polysaccharides (negatively charged) such as sulphated and non-sulphated glycosaminoglycans. Stains blue.

- Picro Sirius Red; (PSR) is a combination of Yellow Picric (acid dye), Sirius Red (acid dye) and a metal complex (basic dye). The Yellow Picric and Sirius dye stain the positively charged cell components such collagen fibres and connective tissue red as well as protein-enriched areas such as the cytoplasm various shades of yellow. The metal complex stains the anionic structures (negatively charged) of the cells, such as the nucleic acids in grey/brown.

2.4.2 dsDNA quantification

An adaption of a previously reported method was used to quantitatively measure double stranded DNA (dsDNA) content (Gilbert, Freund & Badylak 2009). ECM powders of known weight were digested in a Proteinase K solution containing 0.5 M EDTA, 10 % SDS, 5 M NaCl for 24 hours at 60 °C. DNA was extracted from the Proteinase K digests by addition of 25:24:1 (v/v/v) phenol/ chloroform/ isoamyl alcohol. A DNA pellet was formed through precipitation at -80°C from the aqueous phase via addition of 0.1 ml of volume of 3 M sodium acetate (pH 5.2) and 100 % ethanol followed by centrifugation at 10,000 g for 10 minutes. Pellets were washed in ethanol, dried and then resuspended in 1 X TE buffer. Total dsDNA

concentration was calculated using a Quant-iT™ PicoGreen dsDNA assay kit. Standard curves of 0 to 1000 ng/ ml were produced and the DNA extracts were diluted and absorbances read using a plate reader.

2.4.3 Glycosaminoglycan quantification

DMMB reagent, a light-sensitive cationic dye that specifically binds to sGAG, was produced via dissolving 16 mg/L of 1,9-dimethylmethylene blue in 5 mL of 100% ethanol and addition of 40 mM glycine 40 mM NaCl. The pH of the DMMB solution was adjusted to 1.5 pH using hydrochloric acid.

ECM powders of known weight were digested in 0.125 mg/ml papain in phosphate buffer supplemented with 0.01 M cysteine and 0.01 M EDTA at 60 °C for 24 hours. The digests were then diluted and placed in a 96 well-plate before adding DMMB solution. A standard curve was produced of 0-75 µg/ml chondroitin sulphate from shark cartilage and absorbance was measured at 540 nm with a reference of 620 nm using a Tecan 200 plate reader.

2.5 Rheological characterisation of dECM hydrogels

Rheological measurements were carried out using a Physica MCR 301 rheometer. 200 µl gels were placed at 4 °C in a 0.2 mm gap between two 25 mm parallel plates. The apparatus was cooled in a humidified chamber to 4 °C prior to gel insertion and then warmed to 37 °C to induce gelation. A time sweep of 20 minutes at constant angular frequency (1 rad/s) and amplitude (1% oscillatory strain) with readings every 30 s was first performed to view gelation kinetics. The gel was then subject to an amplitude sweep from 0.1% to 200% oscillatory strain with a constant angular frequency of 1 rad/s to view strain stiffening behaviour and maximum moduli.

Whilst possible to produce dECM hydrogels from certain tissues at higher concentrations (> 20 mg/ml) (Ijima et al., 2018), the requirement for the final material to support cellular self-alignment through contraction within tethered gels, and the relationship between cellular gel-contraction and gel concentration (O'Rourke et al., 2015), resulted in the formation of gels of a lower concentration. Our preliminary work had shown that dECM hydrogels of a concentration of 2 mg/ml lacked the structural integrity for easy gel manoeuvrability, and so 4 mg/ml was chosen as the lowest concentration. Consequently, rheological measurements were carried out on 3 hydrogel concentrations: 4, 6, and 8 mg/ml. These were chosen to make linear rheological profiles that could then be referred to in future experiments.

Rheological parameters are outlined in Table 2.3 and were chosen following a review of the literature on dECM hydrogel characterisation and preliminary experimental optimisation (Massensini et al., 2015, Tatic et al., 2019).

Table 2.4 Parameters for rheological characterisation of dECM hydrogels

	T (°C)	Angular frequency (ω)	Strain
Pre	4-37	0.01	0.01
Time sweep	37	0.01	0.01
Frequency	37	0.01-100	0.01
Strain sweep	37	0.01	1-200

2.6 3D cellular gel production

2.6.1 Collagen and dECM gel production

dECM digests were neutralised and made up to desired concentrations and volumes. ECM digests were mixed with 0.1 N NaOH (1/10 volume of pre-gel solution) and 10X MEM (1/9 volume of pre-gel solution). 1X PBS was further used

to adjust the solution to the desired concentration and volume before raising the temperature to 37°C to promote gelation. Following neutralisation, gels were prepared by using 90 % v/v ECM hydrogel with 10% v/v F7 Schwann cell suspensions with the correct cell number to achieve the desired cell seeding concentration.

Collagen gels were produced by mixing 80 % type I rat tail collagen 2 mg/ml in 0.6% acetic acid; FirstLink) with 10 % 10X MEM and around 50 µl sodium hydroxide (1:10 dilution in PBS). Adjustments were made to the pH by adding sodium hydroxide dropwise until a neutral pH was reached based on the colour change of phenol red indicator (1:20 dilution in phosphate buffered saline). 10 % F7 Schwann cell suspensions with the correct cell number (described in each experimental section) to achieve the desired final concentrations were then added.

75 µl gels were prepared for the 96-well plate contraction assay, whereas 400 µl gels were prepared and placed in tethered moulds in 6-well plates to create aligned anisotropic tissue. Gelation was induced by incubation at 37 °C for 30 minutes. For the contraction assay the gels were mechanically removed from the edge of the well plate and 200 µl of DMEM-complete added to each well to form "free-floating" cellular gels. For alignment, gelation was induced for 30 minutes, following which enough DMEM-complete was added to each 6-well plate (Figure 2.5 A) to cover the entire mould. All gels were further incubated at 37 °C in a humidified incubator with 5% CO_2/ 95% air for 24 hours.
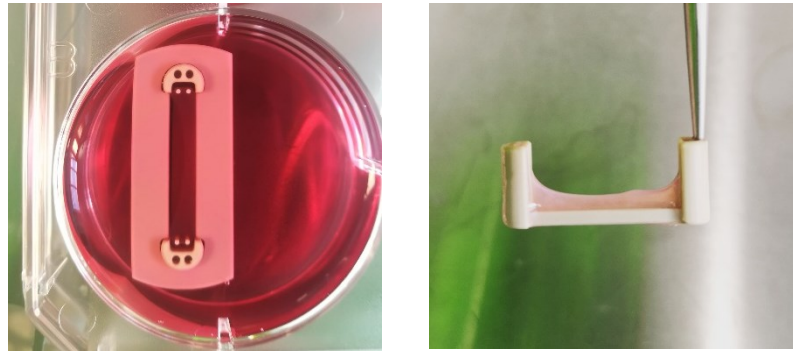
Figure 2.5 Tethered moulds to facilitate cellular self-alignment.

2.6.2 EngNT sheet production

Plastic compression was performed by removing the hydrated cellular gels from their 400 µl moulds and placing them underneath RAFT™ absorbers, separated by a fabric mesh (Figure 2.6) for 15 seconds (SIS-ECM), 25 seconds (B-ECM) and 45 seconds (LIV-ECM).
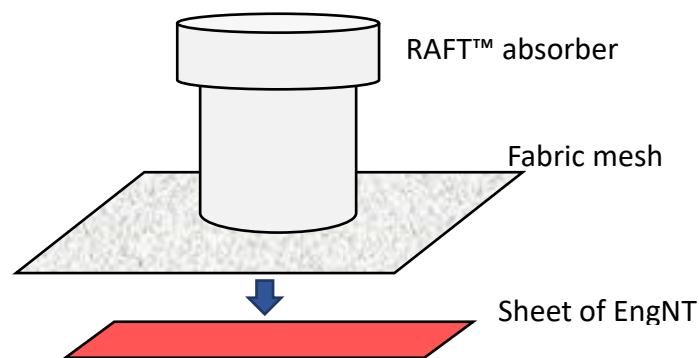
Figure 2.6 Schematic of plastic compression method to produce dECM EngNT.
Fabric mesh separating the RAFT™ absorber and the tissue to prevent disruption of the tissue.

2.7 Cell assays

2.7.1 3D CellTiter-Glo®

dECM and collagen I hydrogels of 6 mg/ ml were formed, seeded with F7 Schwann cells at a concentration of 0.5 x 10^6 cells/ ml, and placed in a cell culture incubator at 37°C and 5 % CO_2/ 95 % air for 1 hour. DMEM was aspirated and the gels placed in a black 96-well plate. 1:1 DMEM: CellTiter-Glo® reagent was added and the plate placed on a shaker at 120 rpm for 20 min. Luminescence was measured using a microplate reader.

2.7.2 DRG outgrowth assay

Neurons obtained from DRG cultures were seeded on top of 19 mm cover slips coated with 50 µg/ml PDL, followed by either 50 µg/ml collagen I or 50 µg/ml dECM. Cultures were covered in DMEM-complete and maintained at 37 °C in a humidified incubator with 5% CO_2/ 95% air for 72 hours, following which they were washed in PBS and fixed in 4% paraformaldehyde overnight at 4 °C for immunostaining.

2.7.3 DRG co-culture with EngNT

Neurons were seeded on top of EngNT sheets in 6-well plates, allowed to settle for 30 minutes before addition of enough DMEM-complete to completely cover the constructs and incubated at 37 °C in a humidified incubator with 5% CO_2/ 95% air for 72 hours. Following incubation, the constructs were washed with PBS and fixed in 4% paraformaldehyde overnight at 4 °C for immunostaining.

2.7.4 Gene expression of Schwann cells in dECM hydrogels

Total RNA from F7 Schwann cells was extracted using the RNeasy Plus Mini Kit according to the manufacturer's instructions. gDNA was removed using gDNA

Eliminator columns. cDNA was synthesized with a RT kit using oligo dT primers from 0.4µg of total RNA. PCR reactions were run using a SYBR Green mix. We measured each sample in duplicate during the same run. The following conditions were used for amplification: an initial holding stage of 10 min at 95 °C, then 45 cycles consisting of denaturation at 95 °C for 3 s and annealing/extension at 60 °C for 60 s. Products were analysed by performing a melting curve at the end of each PCR run. Data are normalized to 3-reference genes expression: beta-2 microglobulin (B2m), hypoxanthine phosphoribosyltransferase 1 (Hprt1), and ribosomal protein S18 (Rps18). The expression of these 3-reference genes was not affected by the different experimental conditions. The primers used were checked against sus scrofa (pig) and bos Taurus (cow) in order to strictly amplify amplicons from Rattus Norvegicus. The sequences of the primers used are listed in the following table.

2.8   Rat sciatic nerve repair

2.8.1 Animals

All experimental procedures involving animals were conducted in accordance with the UK animals (Scientific Procedures) Act (1986) and approved by the UCL animal ethics advisory group. Male Wistar rats (200-225 g) were used for the following experiments.

2.8.2 Surgical procedure
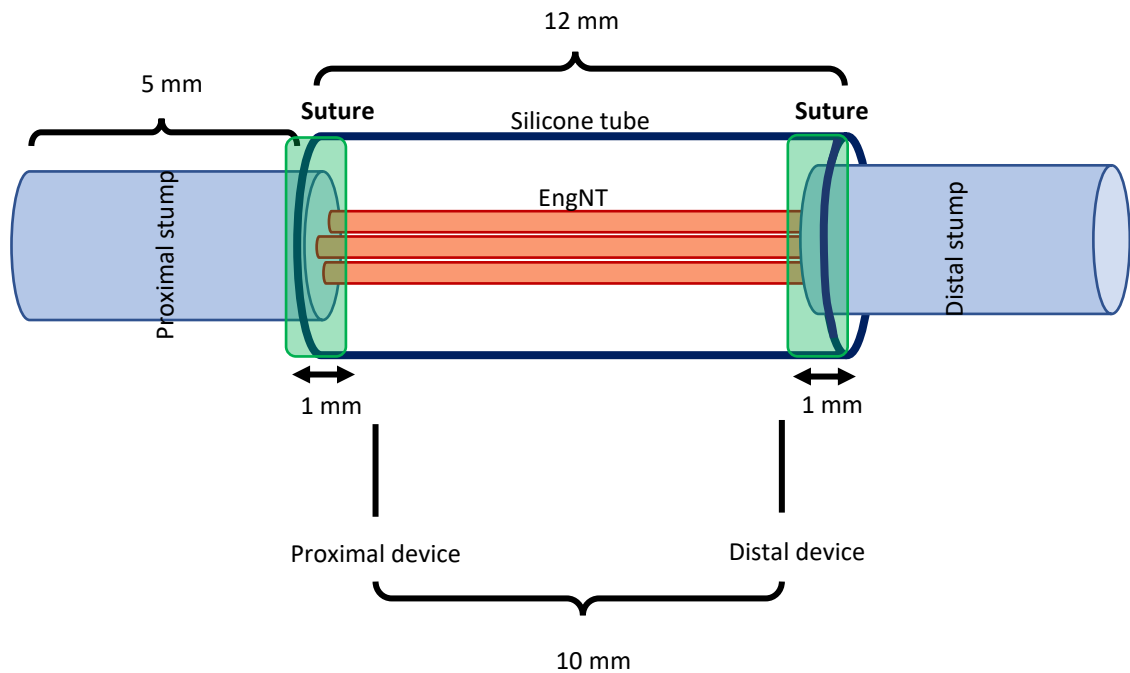
Figure 2.7 Schematic of surgical procedures for 10 mm sciatic nerve transection model.

The surgery was performed by Dr Victoria Roberton, whilst the author was responsible for conduit preparation and all tissue preparation and analysis post-surgery. Isoflurane inhalation was used to anaesthetise rats. The left sciatic nerves of each rat were transected at mid-thigh level to form a 10 mm gap. 12 mm tubes were introduced into the injury site either as empty tubes or filled with 400 µl EngNT derived from purified rat tail collagen I or B-ECM hydrogels. 1 mm of the distal and proximal nerve stumps were inserted into corresponding ends of the devices and sutured in place with epineural sutures (Ethilon 10/0: Ethilon-Johnson & Johnson, Brussels, Belgium). The muscular layer was closed with sutures (Ethilon 4/0) and the wounds closed with wound clips. Animals were monitored for 28 days post-surgery.
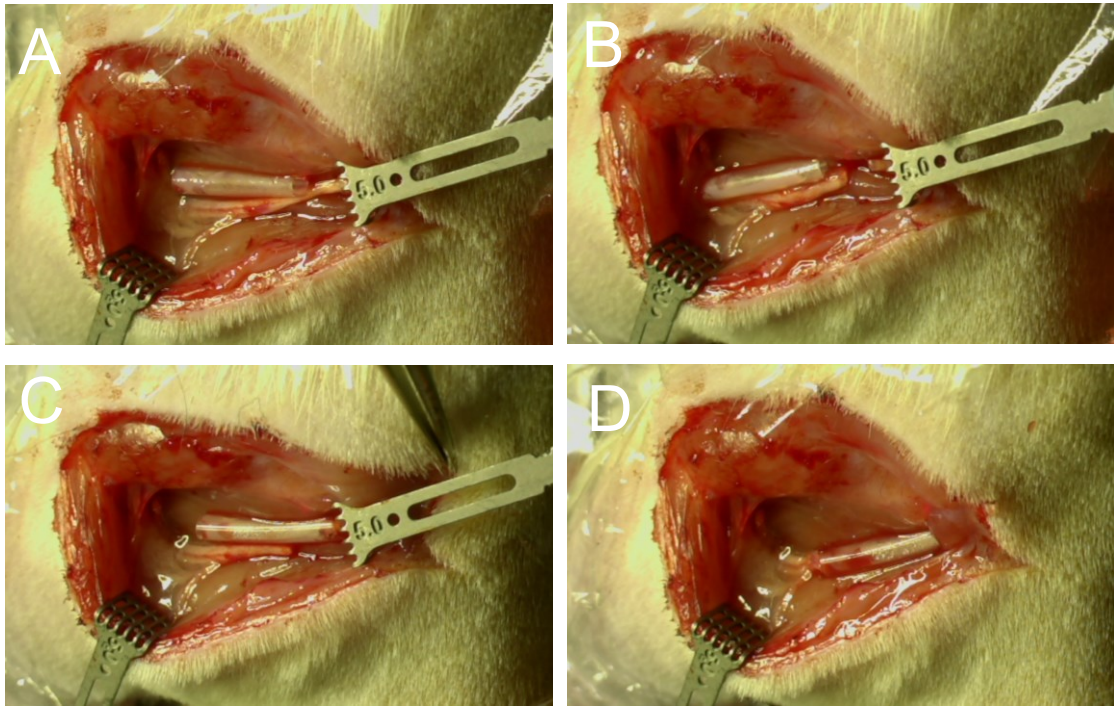
Figure 2.8 *In vivo* nerve injury model. Conduit and nerve side by side [A]. Transection [B] and suture of the proximal stump to the proximal device [C]. Suture of the distal nerve stump to the distal device [D].

2.8.3 Preparation of nerve tissue for histological analysis

Following the 28-day experimental period, animals were culled via overdose of anaesthesia. Sciatic nerves were harvested under a dissecting microscope: connective tissue around the conduits was separated from the muscle and the nerves cut approximately 6 mm from the distal and proximal sutures. Nerves were immediately placed in 4 % paraformaldehyde on ice and fixed overnight at 4 °C. The silicone tubes were then removed, and the nerves were then placed in 15 % sucrose in PBS overnight, or until sunk, before being placed in 30 % sucrose overnight. The nerves were then dissected as depicted in Figure 2.9 and embedded in 1:1 v/v sucrose in PBS: optimal cutting temperature (OCT; Leica) solution within a cryosection mould (TAAB). Moulds were placed in liquid nitrogen to snap-freeze the samples that were then stored at -20° C for sectioning.
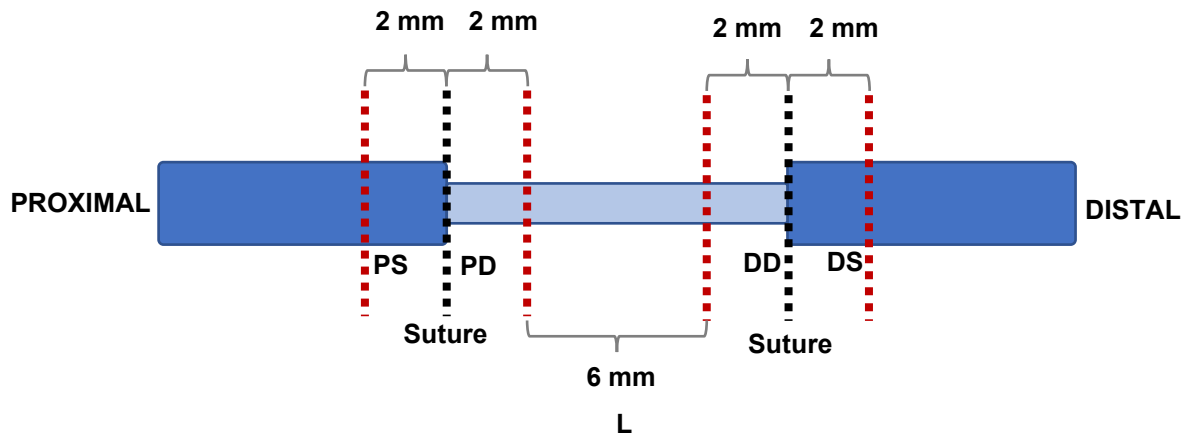
Figure 2.9 Nerve tissue preparation for sectioning. PS = proximal stump, PD = proximal device, DD = distal device, DS = distal stump, and L = longitudinal. Red dotted lines indicate dissection (3 samples per nerve).

16 μm cross sections were produced from the proximal and distal devices at predetermined distances (1 mm) from the suture site using a cryostat (Leica CM1860). 16 μm sections were also prepared from the longitudinal part of the device. Sections were then placed on glass slides (Superfrost TM Plus, Thermo Fisher Scientific) for staining and analysis.

2.9 Immunofluorescence staining

2.9.1 3D cellular gels

Cellular gels were fixed in 4 % paraformaldehyde overnight at 4° C. Two PBS washes for 5 min each followed, before permeabilisation in 0.5 % Triton X-100 for 15 minutes. Next, the gels were washed three times in PBS for 10 min, followed by a 30 min blocking incubation in 5 % goat serum (GS) at room temperature. GS was removed and primary antibodies added in the appropriate dilutions (Table 2.4) to be incubated overnight at 4° C. Constructs were then washed six times for 5 min in PBS followed by a 90 min incubation in the dark with secondary antibodies, appropriately diluted in PBS (Table 2.4). Gels were then washed in PBS for 5 min and then incubated in Hoechst 33342 diluted in

PBS (1:1000). A final wash in PBS for 5 min was performed before placing in fresh PBS for immediate imaging or stored at 4° C.

2.9.2 Tissue sections

Glass slides with adhered tissue sections were washed for 5 min immunostaining buffer (0.2 % Triton X-100, 0.02 % sodium aziide in PBS) to remove OCT. A blocking solution of 5 % GS and 5 % horse serum (HS) in immunostaining buffer was used for 20 min before incubation with primary antibodies, diluted to the appropriate concentration (Table 6) in immunostaining buffer, overnight at 4 °C in a humidified chamber. Slides were washed twice with immunostaining buffer, dried, and the secondary antibodies diluted in immunostaining buffer were applied for 45 min in a dark, humidified chamber at room temperature. Next, slides were washed in immunostaining buffer three times for 5 min, followed by incubation in Hoechst at 1:1000 dilution in immunostaining buffer. A final wash in immunostaining buffer was performed followed by removal of liquid and mounting with VECTASHIELD hard-set mounting medium.

Table 2.5 Primary and secondary antibodies used

Primary Antibodies			
Target antigen	**Host species**	**Brand**	**Dilution**
S-100	Rabbit	Dako	1:200
BIII-Tubulin	Mouse	Sigma-Aldrich	1:500
BIII-Tubulin	Rabbit	Sigma-Aldrich	1:500
Neurofilament	Mouse	Eurogentec	1:1000
Secondary Antibodies			
Anti-mouse Dylight 549 IgG	Goat	Sigma-Aldrich	1:200
Anti-mouse Dylight 488 IgG	Goat	Sigma-Aldrich	1:200
Anti-rabbit Dylight 549 IgG	Horse	Sigma-Aldrich	1:200
Anti-rabbit Dylight 488 IgG	Horse	Sigma-Aldrich	1:200

2.10 Microscopy

2.10.1 Confocal microscope

Images of fluorescently labelled cells were obtained using 10X and 20X objectives on a Zeiss LSM 710 confocal microscope. Parameters of wavelength intensity, laser power, and z-stack height were maintained across all of the images for each experiment. For EngNT constructs, 4 z-stacks were taken per construct and images were taken at 10 μm intervals. Alexa Fluor-488, -549, and DAPI were assigned to the green, red, and blue channels respectively.

2.10.2 Fluorescence microscope

A Zeiss AxioLab.A1 upright microscope (10x and 20x objectives) was used to image fluorescently labelled cells in 3D gels to observe and qualitatively assess alignment, as well as immunostained tissue sections for blood vessel quantification. ZEN lite Software was used to process images before analysis.

2.11 Image analysis

2.11.1 Measurement of contraction

Following their 24-hour incubation time, images were captured of each gel following removal of culture media. Percentage contraction was calculated in ImageJ by measuring the area of each gel as a percentage of the total area of the well.
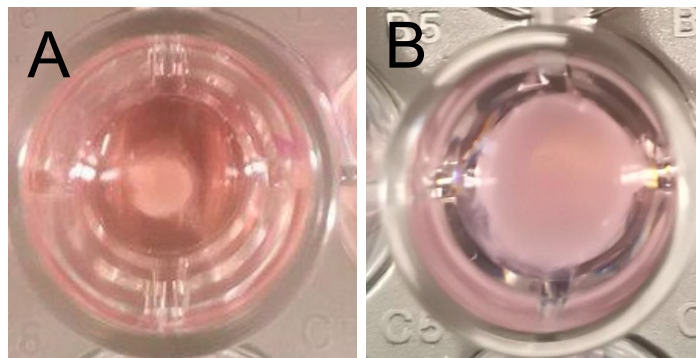
Figure 2.10 Cell mediated contraction in 96-well plates. B-ECM hydrogels seeded with 4 x 10^6 [A] and 0.5 x 10^6 [B] F7 Schwann cells.

2.11.2 Angle of cell deviation

Z-stacks of cellular constructs were imaged from specified regions of the gel (Figure 2.10 A) and imported into Volocity™ for 3D image analysis. The software was used to assign each cell as an "object" with parameters applied to separate touching objects and to exclude objects outside a designated size range. Each object was then assigned a length corresponding to their longest axis (Figure

2.10 B), and the software was then used to calculate their angle of deviation from the longitudinal axis of the construct. Each value was then assigned to bins of 0-10°. Objects of value close to 0° represent cells that are aligned in parallel to the longitudinal axis of the gel, whereas those closer to 90° represent those that are perpendicular.
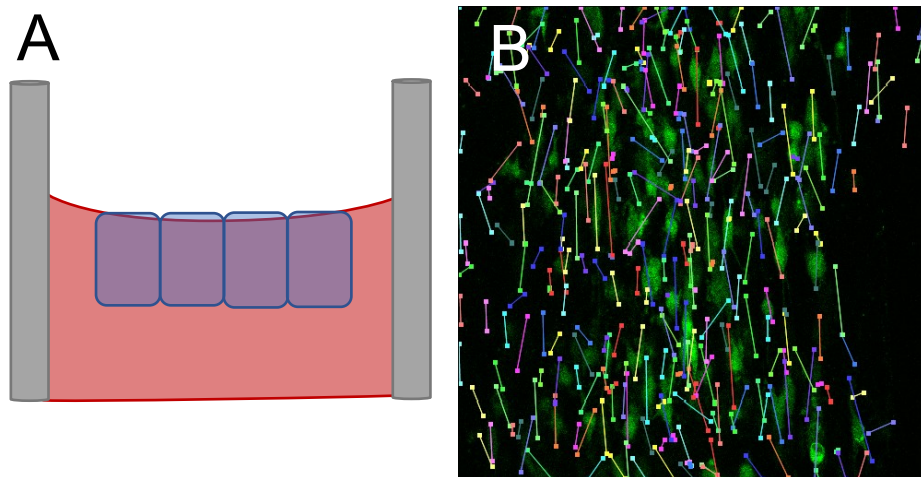
Figure 2.11 Alignment quantification. Schematic of Z-stack location during confocal microscopy [A]. Volocity assignment of cellular objects within dECM EngNT for quantification of angle of deviation from long axis of the construct [B].

2.11.3 Measurement of neurite length

Neurite length was automatically calculated using the "Simple Neurite Tracer" plugin in ImageJ. 3 whole gels per condition were used for data collection. Mean neurite length was calculated as the mean length of neurites attached to a single DRG neuron, whilst longest neurite was calculated as the longest neurite extending from each DRG neuron.
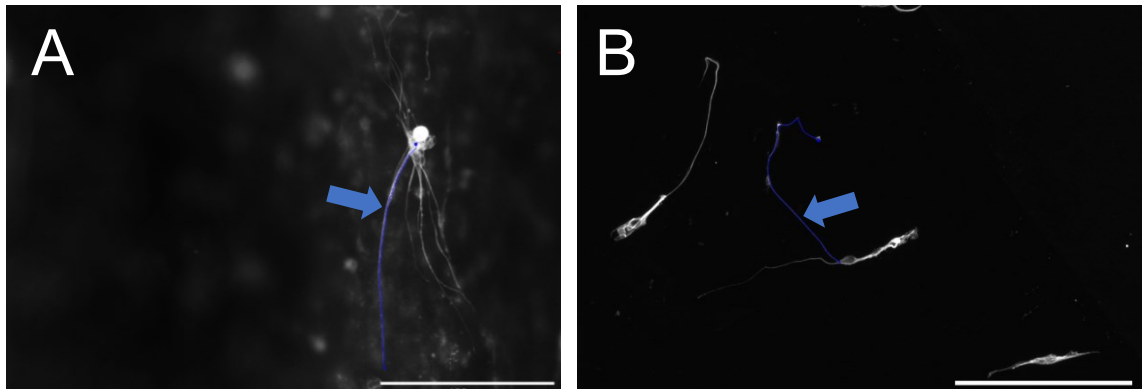
Figure 2.12 Neurite length quantification. DRG neurons seeded on EngNT construct. Images taken after 72 hours [A]. DRGs seeded on glass coverslips coated with dECM. Images taken after 48 hours [B]. Scale bars = 200 µm. Arrows indicate tracked neurite to be measured.

2.11.4 Automated quantification of axons in nerve tissue sections

Tile scan confocal images were obtained from a Zeiss LSM710 confocal microscope. These were used to quantify the number of neurofilament positive axons present in each region of the device. Volocity™ was used to automate this process. Briefly, the endoneurium was selected as the region of interest and the image cropped. This was followed by the assignment of objects of a minimum threshold of intensity, corresponding to axons, as well as size exclusion of objects and separation of touching objects (Figure 2.12 A). Three areas on each section were randomly selected for manual counting (Figure 2.12 B) to compare with the automated protocol to ensure accuracy. The protocol was accepted if the two separate counts fell within 10 % range, if not the parameters were adjusted until correct.
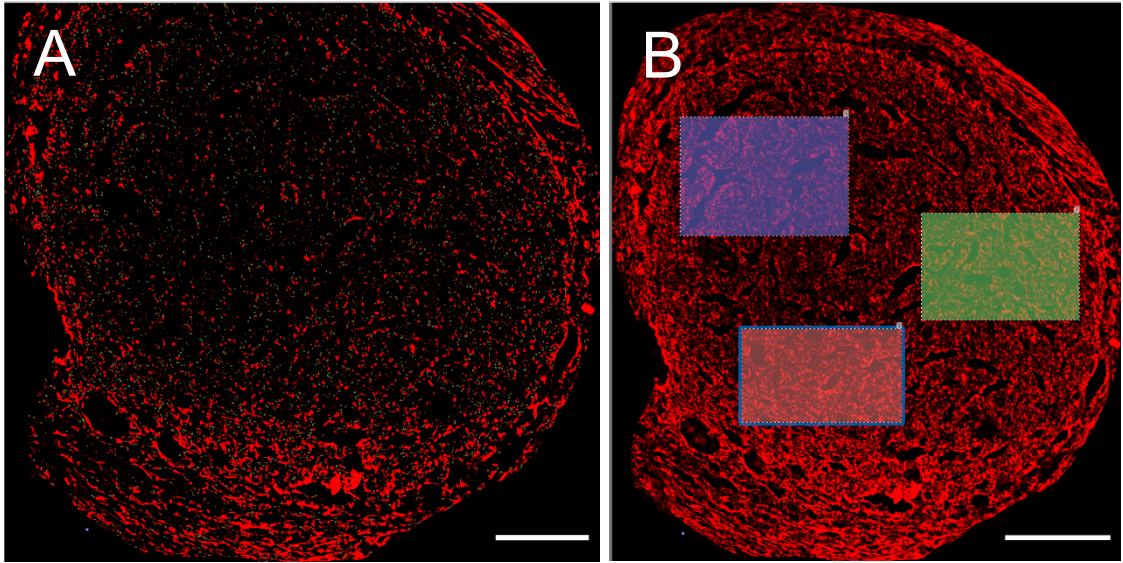
Figure 2.13 Automated quantification of neurofilament positive axons in cross sectional images of sciatic nerves analysed in Volocity using ultra-high contrast images to identify objects via threshold intensity. Object identification [A], random selection of areas for validation of the automated protocols [B]. Scale bar = 200 μm.

Chapter 3 Decellularised material generation and characterisation

3.1 Introduction

Decellularisation can be defined as the removal of cellular and antigenic material from tissue with the aim of preserving the ECM structure and its biologically active soluble factors. The resultant acellular scaffold is considered to be non-immunogenic and contains ECM components such as structural proteins, proteoglycans, glycosaminoglycans (GAGs) and growth factors (Voytik-Harbin et al., 1997, Hudson et al., 2004, Mendoza-Novelo et al., 2011, Walles et al., 2003). The past few decades have seen advances in whole organ and tissue decellularisation with a common aim to overcome graft/ transplant rejection and shortages of donor tissue (Crapo et al., 2011). The potential use of ECM materials derived from decellularised tissues has been diversified through solubilisation and reconstitution into hydrogels, soft materials that retain the dECM innate ability to modulate cell behaviour such as differentiation, migration and survival, with the proteolytic cleavage further releasing bioactive cryptic peptides (Brás and Frangogiannis, 2020).

3.1.1 Decellularisation techniques

There are a number of factors that need to be considered when decellularising a tissue, such as its cell density, thickness and constituent ECM components. Different chemical, biological or physical methods may be preferentially employed to optimally remove cellular material without compromising the resultant properties of the dECM (Crapo et al., 2011). Chemical agents include acids, bases, and non-ionic or ionic detergents, each with their merits and pitfalls regarding the practical use of the final product. Ionic detergents such as sodium

dodecyl sulphate (SDS) and sodium deoxycholate (SDC), whilst potent agents of decellularisation, can significantly affect material mechanical properties, most likely due to the disruption of collagen fibrils (Kasimir et al., 2003, Liu et al., 2018, White et al., 2017, Xu et al., 2014). It has been further shown that, even after thorough washing treatments, residual molecules of SDS remain in the scaffold later causing reduced metabolic activity of seeded cells and, in some cases, cytotoxicity (Fernández-Pérez and Ahearne, 2019, Friedrich et al., 2018, Syed et al., 2014, White et al., 2017). Triton X-100, a frequently used non-ionic detergent, may result in a dECM material with a higher retention of GAGs, collagen architecture, and a higher elastic modulus (Liu et al., 2018, Xu et al., 2014), although often at the expense of dsDNA removal (Fernández-Pérez and Ahearne, 2019, Liu et al., 2018, Xu et al., 2014). Enzymatic agents such as trypsin are commonly used to detach cells from their ECM. Although collagen is resistant to proteolytic cleavage by trypsin (Keech, 1954a), some studies have shown that the utilisation of trypsin as a decellularisation agent can cause detrimental effects to the fibrillar architecture (Kasimir et al., 2003, Keech, 1954b) and some report, although using a higher concentration of 0.5%, a reduction in GAG content (Xu et al., 2014).

3.1.2 Decellularised ECM characterisation

When considering a decellularised material, naturally of interest is what has been removed and what is retained in the scaffold. Removal of antigenic material is necessary to avoid immunogenic responses (Keane et al., 2012, Londono et al., 2017), yet conservation of ECM components is often desired. It is widely accepted to be impractical to remove 100% of cellular material as a point of diminishing returns arises in the damage the decellularisation agents impart,

resulting in loss of functionality in the decellularised tissue (Fernández-Pérez and Ahearne, 2019, White et al., 2017).

3.1.2.1   Cellular removal

Due to correlations between nuclear material and adverse host and cellular responses (Keane et al., 2012, Londono et al., 2017, Nagata et al., 2010a, Zheng et al., 2005) one of the metrics of decellularisation is assessing the removal of nuclei using histological staining and often quantifying residual double stranded DNA (dsDNA). Crapo et al. (2011) stated that a dsDNA content of less than 50 ng/ mg dry tissue weight with no visible nuclei are required parameters for a tissue to be accepted as decellularised and these values are often cited in the literature (Liu et al., 2018, Sawkins et al., 2013, Alshaikh et al., 2019). Whilst the literature is unclear on the precise quantities of dsDNA acceptable, 95% removal compared to the native tissue is often considered decellularised and this is supported by both *in vitro* and *in vivo* data whereby clean collagen scaffolds were supplemented with various concentrations of DNA; higher DNA concentrations resulted in increases in macrophage proinflammatory cytokine production *in vitro* which was further associated with an increase in M1 macrophage populations *in vivo* (Londono et al., 2017). Londono et al. (2017) stress that other cell debris such as lipids and mitochondrial remnants also result in adverse reactions however these parameters are less frequently assessed.

3.1.2.2   ECM components

Collagen is the most abundant protein of the ECM and is largely responsible for the mechanical properties, such as tensile strength, of living tissue (Balasubramanian et al., 2012, Kadler et al., 2007). Additionally, collagens are potent modulators of cell migration (Schor, 1980), adhesion (Somaiah et al.,

2015), proliferation (Najafi et al., 2008), and are involved in tissue repair (Krafts, 2010). Dependent on the tissue in question, different types of collagen will exist in the extracellular milieu; articular cartilage ECM is predominantly collagen II (Yin et al., 2012), liver contains equal amounts of collagen I, II and III as well as basement membrane collagens (Rojkind et al., 1979), dermis contains collagen I and III (Meigel et al., 1977), whereas the brain contains almost no collagen I in its extracellular matrix (Kucharz, 1992). The collagen content of decellularised matrices is therefore often quantified with techniques such as western blot (Pan et al., 2014), immunohistochemistry (Grauss et al., 2005) and mass spectrometry (Lee et al., 2014). The most common method used, however, is via the estimation of total collagen content through the colorimetric quantification of hydroxyproline (Neuman and Logan, 1950). Whilst able to estimate total collagen content of tissues (hydroxyproline being 12-14 % mass of collagen), the hydroxyproline assay does not reveal the different types of collagen within a tissue.

Glycosaminoglycans (GAGs) are chains of repeating disaccharide units, often highly sulphated and containing an amino sugar (Yamada et al., 2011). Six types of GAG exist: heparin (Hep), heparin sulphate (HS), chondroitin-6-sulphate (CS), dermatin sulphate (DS), keratan sulphate (KS) and hyaluronic acid (HA) (Köwitsch et al., 2018). GAG function is dependent on structure and biochemical composition; Aggrecan, a proteoglycan containing CS and HA, absorbs and retains water, acting as a shock absorber to enable cartilage to endure compressive forces (Roughley and Mort, 2014). HA is also the main component of the brain ECM and has been shown to regulate neural stem cell differentiation (Su et al., 2017). Different GAGs further bind to specific growth factors; HS may bind fibroblast growth factor (FGF) (Pellegrini, 2001) or tumour necrosis factor

alpha (TNFα) (Menart et al., 2002), whereas fibromodulin (a KS rich proteoglycan) has been shown to bind bone morphogenic protein-2 (BMP-2) (Bi et al., 2007). GAG functions are therefore varied, with the potential to affect both the mechanical and biochemical properties of tissues, and thus are commonly analysed following decellularisation (Fernández-Pérez and Ahearne, 2019, Grauss et al., 2005, Kočí et al., 2017, Liu et al., 2018). Alcian blue staining (Lev and Spicer, 1964) may be employed during histological analysis to qualitatively highlight sulphated glycans, whilst the dimethyl methylene blue (DMMB) assay is often used to quantify sulphated GAGs (Zheng and Levenston, 2015, Templeton, 1988).

3.1.3 ECM hydrogel characterisation

ECM hydrogels have been studied extensively. Applications vary from 3D tissue-specific cell culture *in vitro* (Alom et al., 2017, Loneker et al., 2016, Shin et al., 2019, Skardal et al., 2012), to injectable soft materials for tissue remodelling and wound healing (Cornelison et al., 2018, Ghuman et al., 2016). The mechanical properties of a material have a direct impact on cell behaviour (Discher et al., 2005) with material stiffness being a potent effector of cell migration, proliferation, adhesion and differentiation (Hadden et al., 2017, Sun et al., 2018, Vedadghavami et al., 2017). Characterisation of the material physical properties is therefore desired.

3.1.3.1 Viscoelastic behaviour

Hydrogels are viscoelastic, that is, they may present both viscous and elastic behaviours (Cacopardo et al., 2019). In elastic materials, energy is stored through the stretching of chemical bonds and the energy exerted is stored, whilst in viscous materials energy is dissipated through the material.

Viscoelastic behaviour, however, is observed when materials display characteristics of both a viscous and elastic material (Gargallo and Radic, 2009). Viscoelasticity is further dependent on time, temperature, polymer chemical composition, shear rate and strain (Zuidema et al., 2014).

3.1.3.2 Strain stiffening behaviour

Nonlinear viscoelasticity is observed in biological filamentous networks such as collagen, fibrin, cellulose, actin and neurofilaments and these materials are thus considered "semi-flexible" (Shao et al., 2019, Storm et al., 2005). These materials maintain viscoelasticity over a certain degree of shear extension, until they reach a point in which they begin to stiffen, finally reaching a critical strain, and peak elastic modulus, before softening. The proposed mechanism for this behaviour is that the filament network exists in a relaxed state (Figure 3.1 A). Once a strain is applied, this allows for network deformation and material extension (Figure 3.1 B) up to a critical point in which the interfilamentous chemical bonds break and the network ruptures (Figure 3.1 C). This process is reliant on individual filament elasticity/ rigidity as well as the number, strength and distance between the chemical crosslinks (Storm et al., 2005).
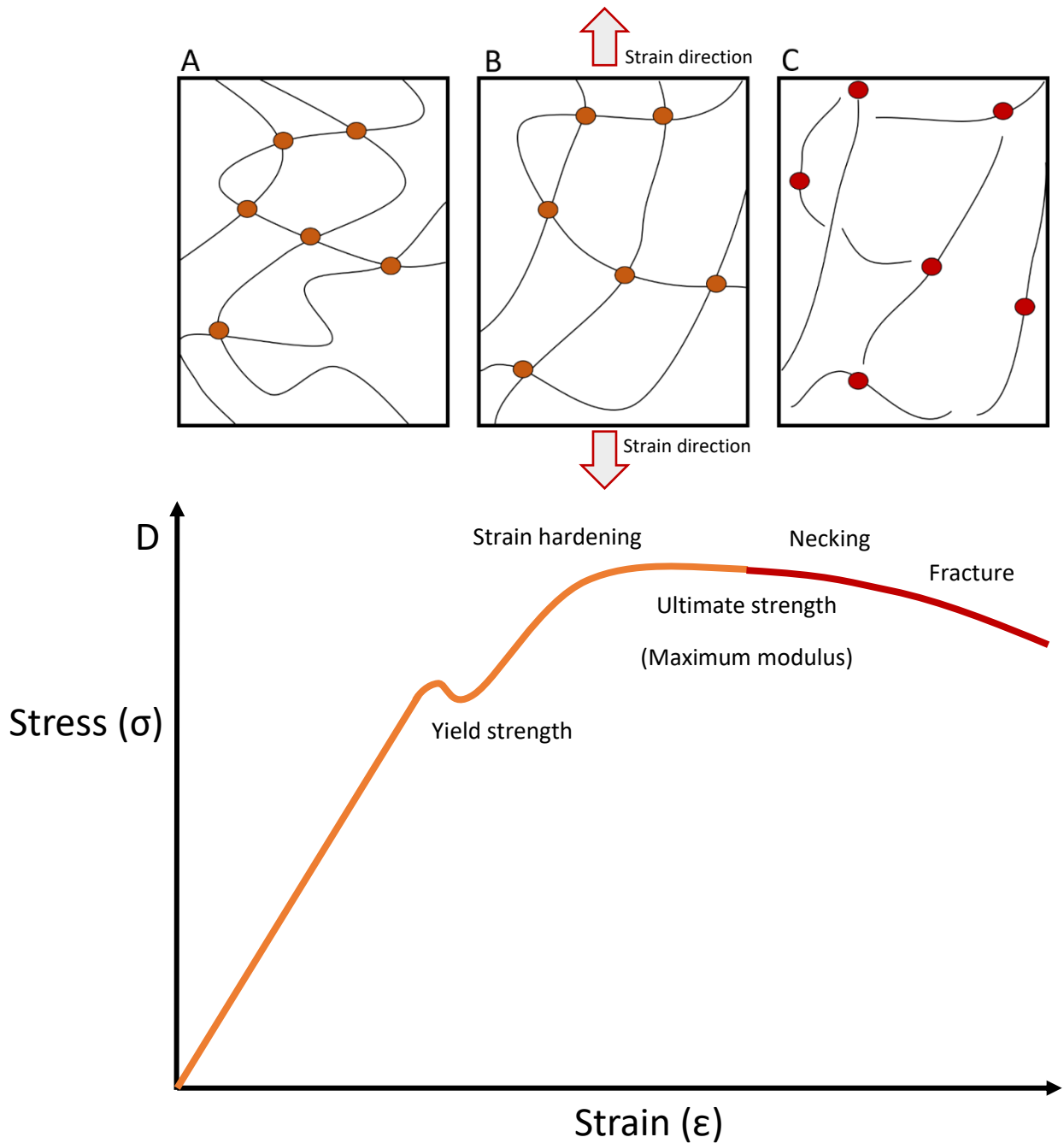
Figure 3.1 Strain stiffening of biological fibres. Relaxed filamentous network in which applying low levels of strain will not alter material stiffness [A], applying further strain causes extension and deformation of network causing an increase in elastic modulus [B]. Following critical strain, the chemical crosslinks break and network ruptures [C].

Strain stiffening is essential in biological tissues to protect from rupture, in such cases as the arterial wall, allowing the tissue to withstand extreme shear strains

without permanent deformation (Holzapfel et al., 2005). Furthermore, strain stiffening behaviour allows biological materials, such as collagen, to act as conduits for mechanotransduction of external forces directly to the cells residing in the tissue. In the context of biological tissues, as the network stiffens, cell-ECM interactions are altered and cellular cytoskeletal morphologies are changed, resulting in downstream processes of matrix deposition, matrix remodelling as well as cell-cell signalling over long distances (Cacopardo et al., 2019, Rudnicki et al., 2013, Storm et al., 2005).

3.1.3.3   *Rheology*

Rheology has been widely used to study the deformation and flow of structured fluids. More specifically, it can be utilised to identify the relationship different viscoelastic polymers possess with temperature, time, strain and shear rate (Vallée et al., 2009). By measuring storage and loss moduli as a function of oscillation frequency and angular displacement, rheological measurements may further elucidate the materials' relationship with shear rate and strain respectively (De Kee, 2016, Zuidema et al., 2014, Yan and Pochan, 2010). These experiments may be carried out on relatively small sample sizes and so rheology is an attractive option for mechanical characterisation of ECM hydrogels.
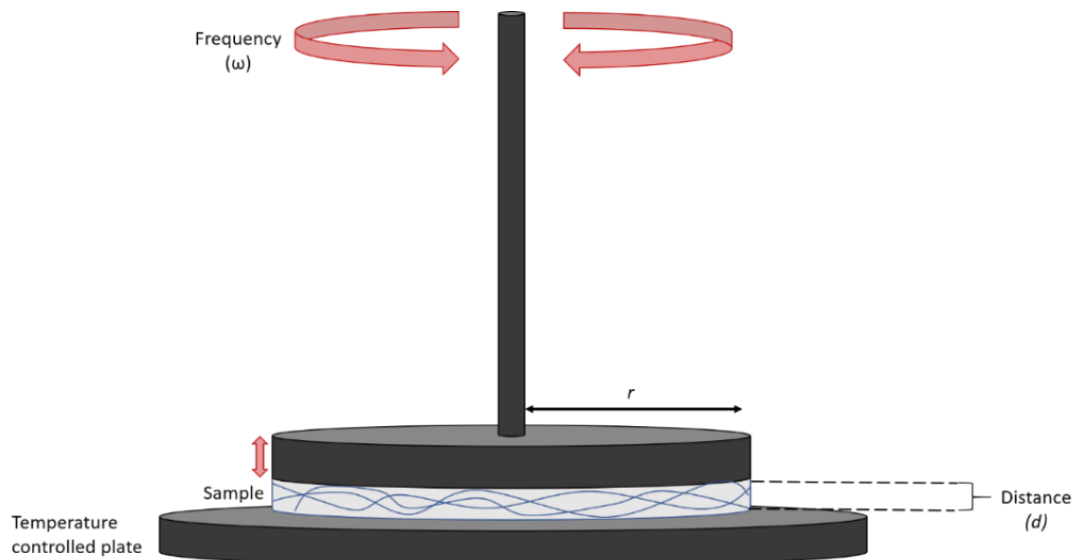
Figure 3.2 Hydrogel sample in a parallel plate rheometer. A hydrogel is formed on a temperature controlled plate of a specific volume and size (determined by the radius of the plate (r) and the height between the plates (h). To induce network formation, the plates are raised to physiological temperature. Rotational strain is applied at specific frequencies (ω) by the top plate and changes in storage and loss moduli calculated over time.

3.1.4 Remarks on ECM characterisation

In summation, and outlined in Section 1.6.2, dECM materials require extensive biochemical and mechanical characterisation due to their novelty and natural heterogeneity; biochemical and mechanical properties differ between tissues and between animal sources. Furthermore, different biochemical and mechanical properties may be of interest when considering the material application. Key metrics to consider are residual antigenic material in the scaffolds, such as dsDNA, biologically active soluble factors, such as sGAGs, and hydrogel stiffness.

3.2 Chapter aims

Due to the diversity in tissue sources available, the creation of a diverse portfolio of materials, that are likely to in turn produce a variety of different cellular

responses, was predicted. In this chapter we optimised established decellularisation processes on a range of different tissues and applied common biochemical and mechanical characterisation protocols to generate a portfolio of decellularised materials to be screened for their potential use in engineered neural tissue (EngNT). Selected materials from the portfolio were then taken forward in the next experimental chapter.

The aims of this chapter may be summarised:

• Elimination of cellular material. Quantification of dsDNA content has been shown to be a useful indicator of antigenicity with the aim of removing a minimum of 95% of dsDNA with residual nuclear material in the ng/ mg dry weight range.

• To reduce the elimination of biologically active factors within the dECM. This will be performed by quantifying the sulphated GAGs (sGAGs) content using the simple dimethylmethylene blue assay.

• Qualitative biochemical characterisation will be carried out through histological analysis of nuclei (DAPI), collagen (picosirius red), and sGAG (Alcian blue) staining.

• To use rheological measurements to characterise their mechanical behaviour. Rheology will be used in this study to reveal properties such as gelation kinetics, shear thinning and strain stiffening behaviours.

3.3 Experimental design

Tissue was taken from either bovine or porcine sources and existing protocols were employed and optimised to decellularise them and create a portfolio of dECM to be biochemically and mechanically characterised (Badylak et al., 1998,

Crapo et al., 2013, Loneker et al., 2016, Sawkins et al., 2013). A range of tissues were chosen to be investigated: bone, liver, spinal cord, small intestinal submucosa and urinary bladder. Liver and bone are known to be biochemically distinct with similar mechanical properties (Coronado et al., 2017, Sawkins et al., 2013), and so may provide useful comparative data when exploring cell behaviour. Small intestinal submucosa and urinary bladder were chosen due to their approved clinical use (Lanteri Parcells et al., 2014, Mosala Nezhad et al., 2016b) whilst both have additionally been successfully applied in nerve engineering (Arda et al., 2017, Nguyen et al., 2017b, Yi et al., 2013). Similarly, spinal cord ECM can modulate Schwann cell behaviour (Wrobel and Sundararaghavan, 2018) and therefore was also considered for this study. The characterisation for each of the materials is shown in Table 3.1.

Table 3.1 Characterisation for each of the native and decellularised tissues in the portfolio

Green boxes indicate characterisation methods that were carried out for each material

	Bone		Liver		Small intestine		Urinary bladder		Spinal cord	
	Native	dECM	Native	dECM	Native	dECM	Native	dECM	Native	dECM
dsDNA	🟩	🟩	🟩	🟩		🟩	*	🟩	**	🟩
sGAG		🟩		🟩		🟩		🟩		**
Nuclei (qualitative)		🟩	🟩	🟩	🟩	🟩		🟩		
sGAG (qualitative)		🟩	🟩	🟩	🟩	🟩		🟩		
Collagen (qualitative)		🟩	🟩	🟩	🟩	🟩		🟩		
G'		🟩		🟩		🟩		🟩		
G''		🟩		🟩		🟩		🟩		
Gelation		🟩		🟩		🟩		🟩		

Abbreviations: dECM – ECM derived from decellularised tissue, dsDNA – double stranded deoxyribonucleic acid content, G' – storage modulus, G'' – loss modulus, sGAG – sulphated glycosaminoglycan content,

*= Material kindly supplied in dECM powder form by Dr Tim Keane (Imperial College London)

**= Material initially produced for another student, Dr Natalija Tatic (University of Nottingham). No supply of native spinal cord prevented further batches from being made and characterised during this project.

3.4 Results

3.4.1 B-ECM generation and biochemical characterisation

A detailed account of the decellularisation process may be found in the Materials and Methods section (2.1.). Briefly, bovine tibias arrived laterally cut to 5 mm (Figure 3.3 A). Cancellous bone was separated from cortical bone (Figure 3.3 B) and ground into a fine powder initially using a mortar and pestle in liquid nitrogen (LN2) (Figure 3.3 C). Following demineralisation and delipidation (2.1.1), demineralised bone matrix (DBM) was produced, whilst a further enzymatic decellularisation treatment (2.1.2) produced decellularised bone ECM (B-ECM). Batch 1 of DBM and B-ECM were assessed for their dsDNA content (Figure 3.3 E) and were found to have 377.7 ± 12.3 and 250.9 ± 27.6 ng/mg dry tissue weight respectively.
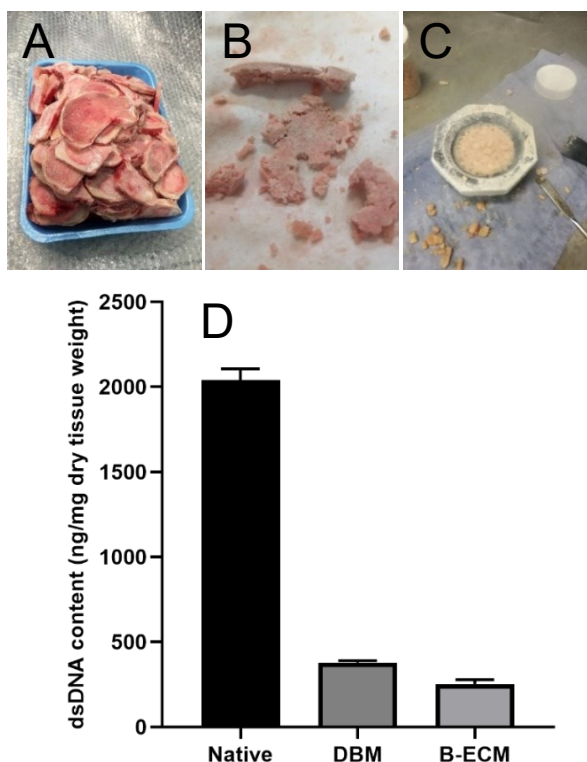
Figure 3.3 Bone preparation and decellularisation – Batch 1. Bovine bone (as received) [A]. Bone following mechanical separation of cancellous and cortical regions [B]. Pestle and mortar containing cancellous bone fragments and LN$_2$ [C]. Grinding of fragments in pestle and mortar to create uniform size particles of cancellous bone [D]. dsDNA content of native, DBM and B-ECM material. Data are presented as mean ± SD, N = 3 individual experiments, run in triplicate.
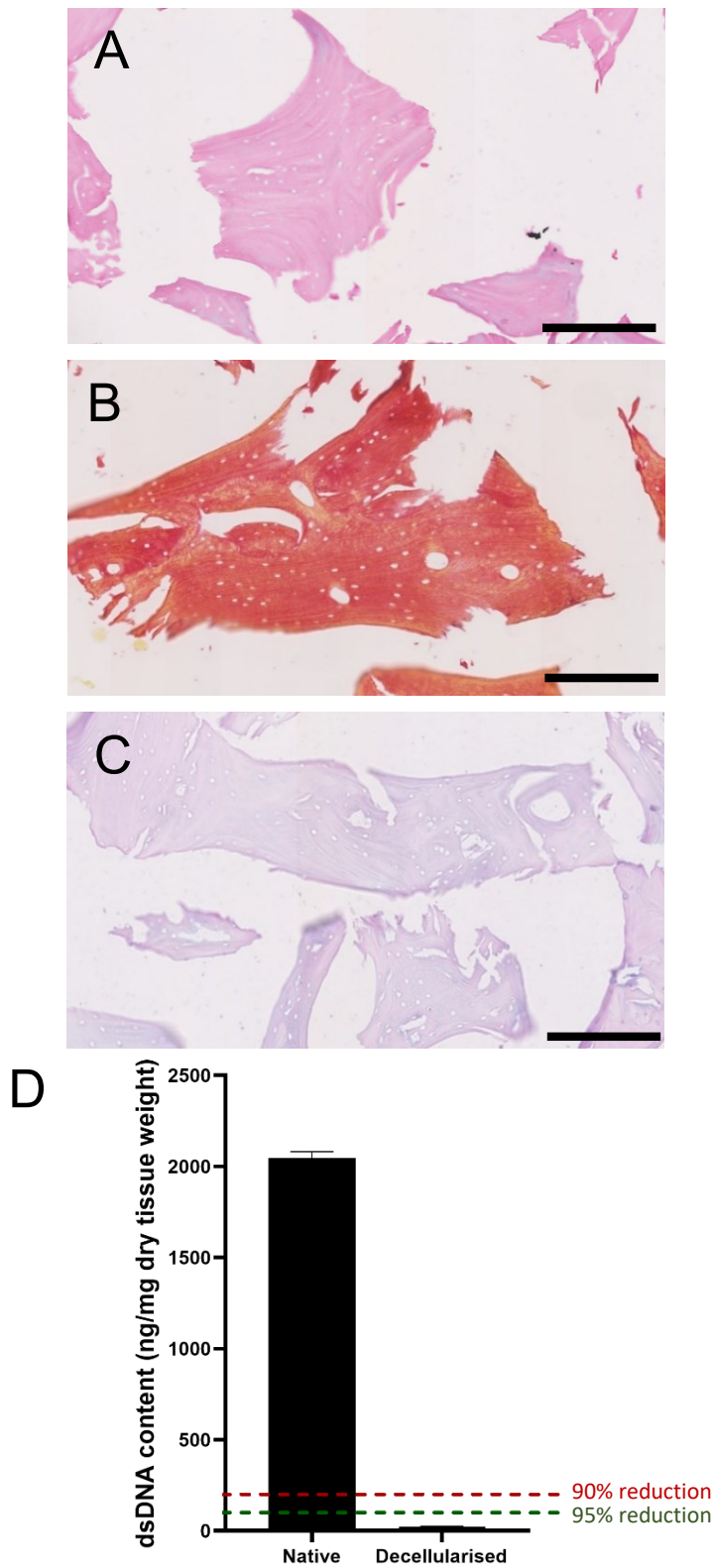
Figure 3.4 Biochemical profile for B-ECM – Batch 2. H & E [A], picosirius red [B} and alcian blue [C] staining. dsDNA content for native and decellularised tissue[D]. Data are presented as mean ± SD, N = 3 individual experiments, run in triplicate. Scale bars = 200 μm.

Figure 3.4 displays the entire biochemical characterisation of the final B-ECM material (batch 2). H&E staining (Figure 3.4 A) showed no visible nuclei and this is corroborated with the dsDNA content of 24.2 ± 4.3 ng /mg; a removal of ~99% of the nuclear material from the native tissue which contained 2044.7 ± 63.5 ng/mg (Figure 3.4 D). The picosirius red staining showed an abundance of fibrillar collagen (red) and the lack of yellow staining indicated a lack of cytoplasm (Figure 3.4 B). The alcian blue staining (Figure 3.4 C) revealed a distinct absence of sGAG within the B-ECM material and this was further seen in the quantification of 0.38 ± 0.1 μg/mg (Figure 3.12 B).

3.4.2 LIV-ECM generation and biochemical characterisation

The complete protocol may be found in the Materials and Methods section 2.1.3. Briefly, whole porcine livers (Figure 3.5 A) were roughly sliced into segments of 10 cm x 2 cm x 5 mm and stored at -20° C until the day of decellularisation. A mandolin slicer (Figure 3.5 B) was used to cut segments of frozen liver into 3 mm slices (Figure 3.5 C), ready for decellularisation. The process described in section 2.1.4 employed stages of one enzymatic and two detergent decellularisation agents separated by washes in PBS all performed on a mechanical shaker at 300 rpm. Following a 4 % peracetic acid treatment, colourless decellularised liver derived ECM (LIV-ECM) was produced (Figure 3.5 D).
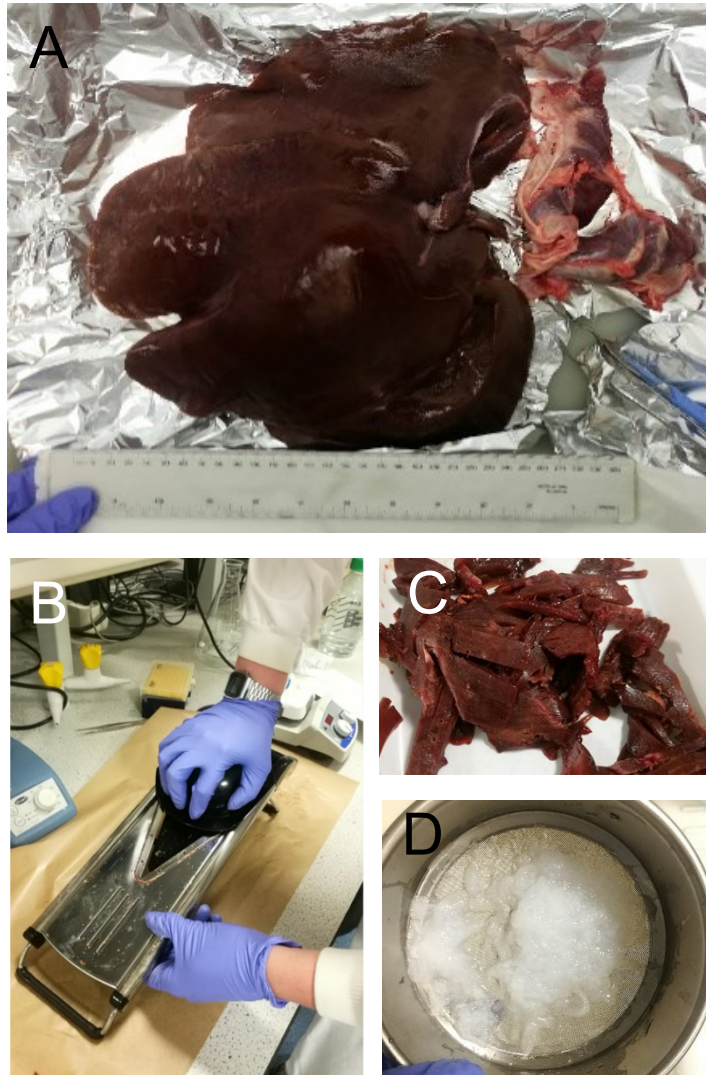
Figure 3.5 Liver preparation and decellularisation. Liver as received from abattoir [A]. Mandoline slicer [B]. Slices of native liver [C]. Resultant decellularised LIV-ECM [D].
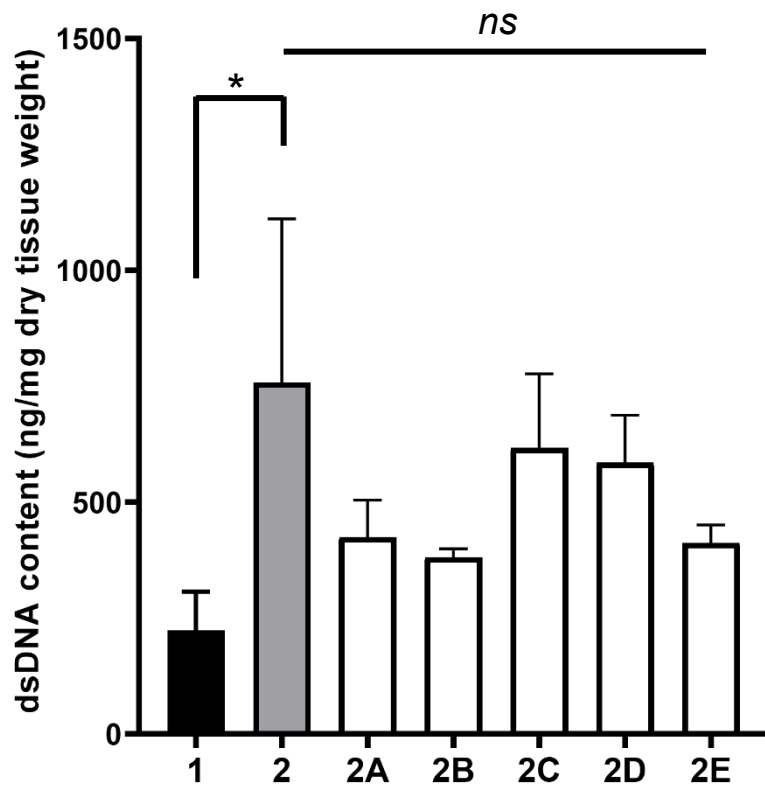
Figure 3.6 dsDNA content analysis of variations in liver decellularisation agent concentrations. Data are presented as mean ± SD, N = 3 individual experiments, run in triplicate. N = 3. One-way ANOVA with Tukey's multiple comparisons test showed a significant difference between method 1 and method 2 (*$p < 0.05$). ns = no significant difference observed.

Figure 3.6 shows the dsDNA content observed in LIV-ECM scaffolds when the tissue was taken through different decellularisation protocols (outlined in 3.2). Method 1 had the lowest dsDNA content at 223.4 ± 83.6 ng/mg whereas method 2 was significantly higher at 758.5 ± 352.8 ng/mg. No significant difference was found between method 2 and any of its variations.
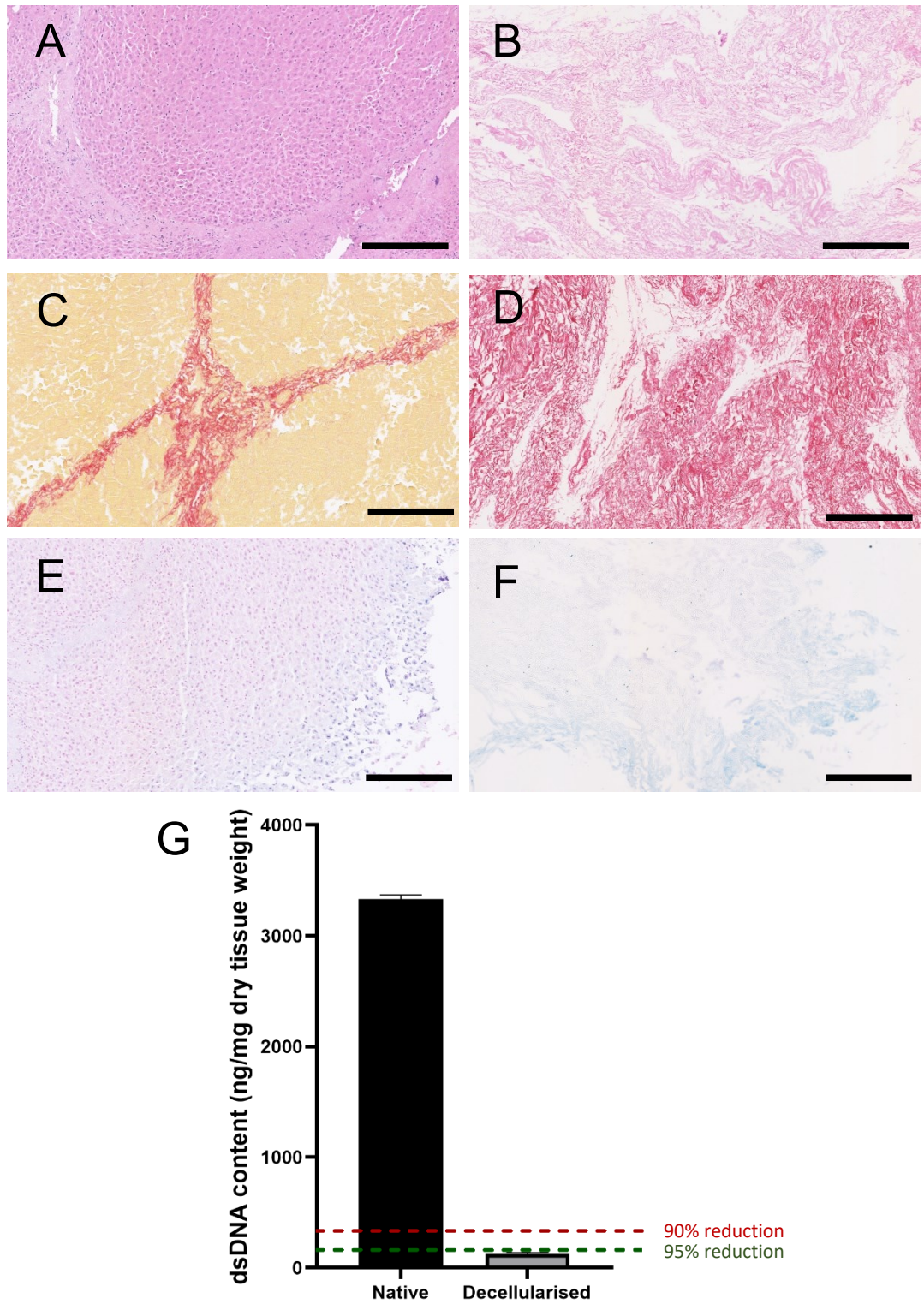
Figure 3.7 Biochemical profile for LIV-ECM. H & E staining for native [A] and decellularised [B] liver. Picosirius red staining for native [C] and decellularised [D] liver. Alcian blue staining for native [E] and decellularised [F] liver. staining. dsDNA content for native and decellularised tissues [G]. Data are presented as mean ± SD, N = 3 individual experiments, run in triplicate. Scale bars = 200 µm.

The biochemical characterisation for the LIV-ECM is shown in Figure 3.7. H&E staining of the native tissue (Figure 3.7 A) showed a partial hepatic lobule with its surrounding connective tissue, both containing many nuclei. Following decellularisation (Figure 3.7 B), no visible nuclei were remaining whilst the native structure of the liver was also absent. Picosirius red staining of the native liver (Figure 3.7 C) highlights the connective tissue abundant with fibrillar collagen (red) whereas the inside of the nodules appeared to be predominantly cytoplasm (yellow). The picosirius red staining for the decellularised material (Figure 3.7 D) further showed the collapsing of the native tissue structure and only fibrillar collagen (red) remained in the resultant LIV-ECM scaffold. Limited sGAG were observed in the native tissue (Figure 3.7 E) however this appeared to be maintained in the decellularised material (Figure 3.7 F). Quantitative analysis was further performed; dsDNA quantification showed that native liver contained 3331 ± 62.7 ng/mg dsDNA and subsequently 125.1 ± 20.0 ng/mg was found in the decellularised LIV-ECM. sGAG content in the decellularised LIV-ECM was found to be 2.0 ± 0.3 µg/mg (Figure (3.11).

3.4.3 SIS-ECM generation and biochemical characterisation

A detailed description of the process may be found in Material and Methods section 2.1.5. The large and small intestines (Figure 3.8 A) were separated to isolate the small intestine and the jejunum removed (Figure 3.8 B). The tubular small intestine was sliced longitudinally to form sheets (Figure 3.8 C). Delamination (Figure 3.8 D) of the mucosal, serosal, and muscular layers revealed the medial submucosal layer (Figure 3.8 E). This material was then washed in PBS before treatment with 4 % peracetic acid to create sheets of SIS (Figure 3.8 F).
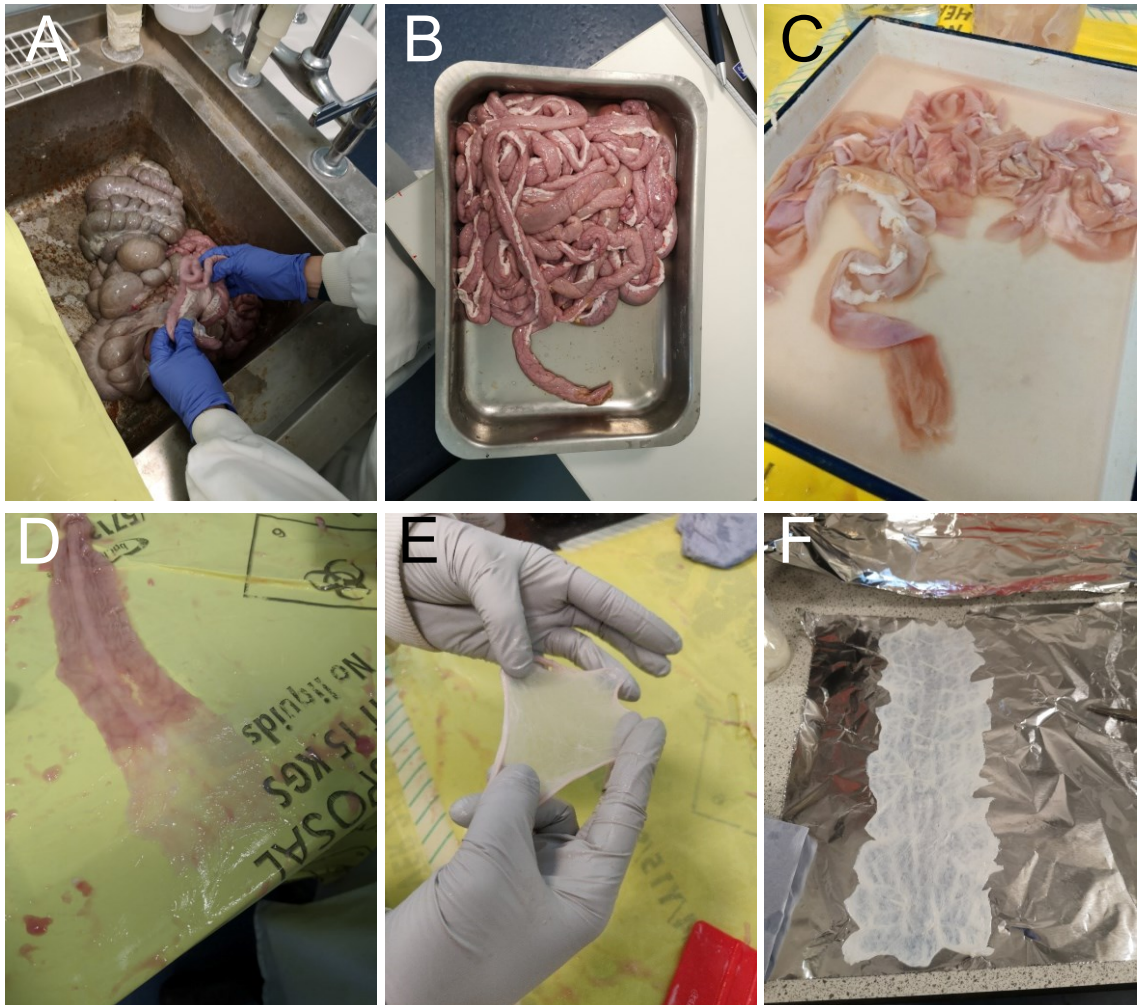
Figure 3.8 Preparation and decellularisation of small intestinal submucosa. Separation of porcine large [A] and small [B] intestine. Longitudinal slicing of tissue to produce sheets of small intestine [C]. Mechanical abrasion of the abluminal side of small intestine [D] and resultant SIS sheet [E]. Sheets of SIS following PAA decellularisation ready to be frozen and lyophilised [F].
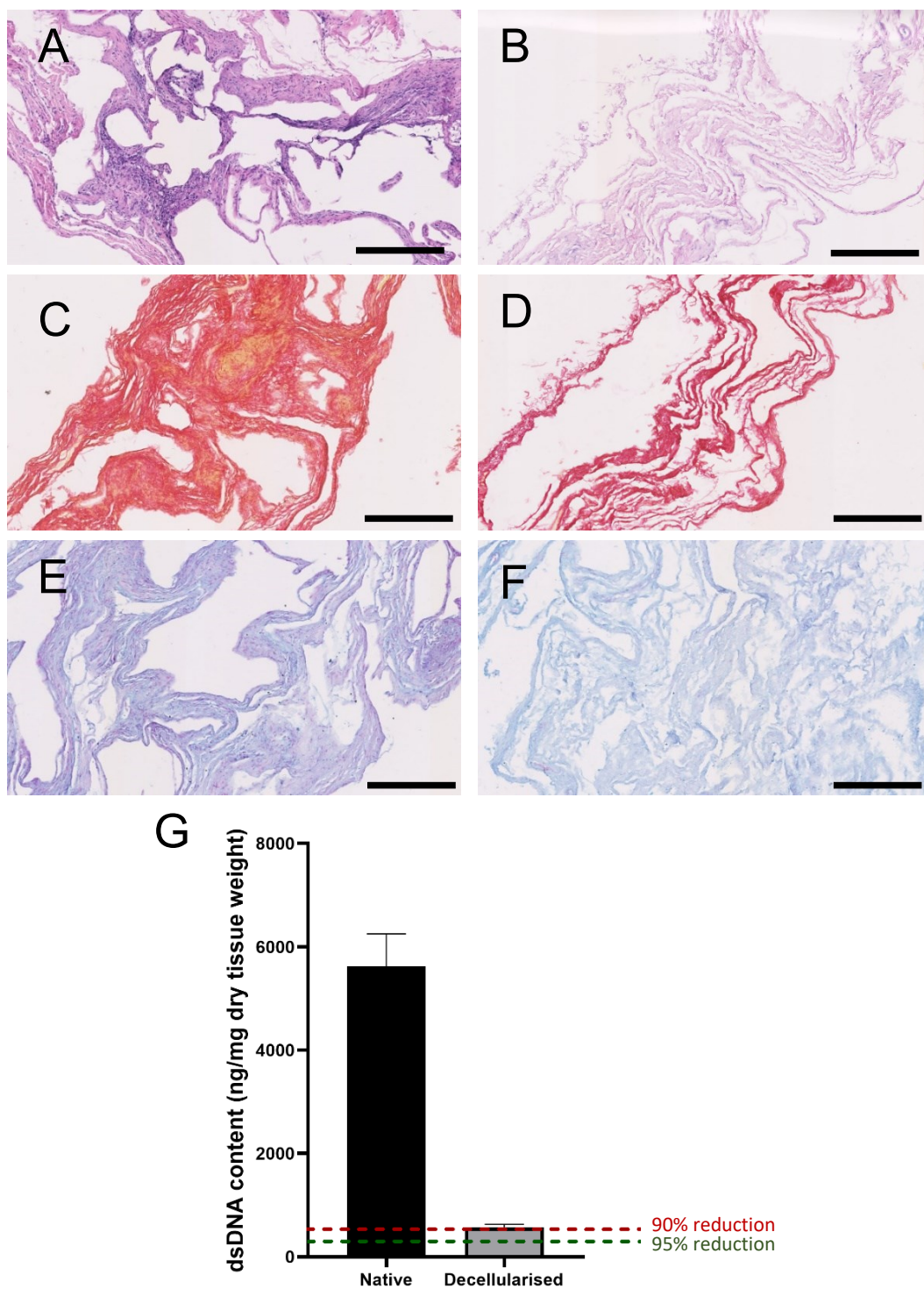
Figure 3.9 Biochemical profile for SIS-ECM. H & E staining for native [A] and decellularised [B] SIS. Picosirius red staining for native [C] and decellularised [D] SIS. Alcian blue staining for native [E] and decellularised [F] SIS. staining. dsDNA content for native and decellularised tissues [G]. Data are presented as mean ± SD, N = 3 individual experiments, run in triplicate. Scale bars = 200 μm.

The biochemical characterisation for the SIS-ECM is shown in Figure 3.9. Densely populated nuclei were observed within the native tissue in the H&E staining (Figure 3.9 A, the vast majority of which were removed following the decellularisation (Figure 3.9 B). Although some nuclei remained, the dsDNA quantification (Figure 3.9 G) showed that the process eradicated around 90 % of nuclear material from 5626.8 ± 1082.7 ng/mg to 572.0 ± 95.6 ng/mg. Collagen (red) dominates the picosirius red staining with a nominal cytoplasmic (yellow) presence that was not present in the decellularised SIS-ECM (Figure 3.9 D). The presence of sGAG was seen in the alcian blue staining for the native tissue (Figure 3.9 E) and was highly retained in the decellularised tissue (Figure 3.9 F). This was further reflected in the DMMB assay with an sGAG quantification of 3.9 ± 0.3 µg/mg for the decellularised SIS-ECM (3.11 B).

3.4.4 SC-ECM generation and biochemical characterisation

A full account of the process is outlined in the Materials and Methods section 2.1.6. Porcine spinal cords (Figure 3.10 A) had their dura and blood vessels trimmed (Figure 3.10 B) and were sliced longitudinally to open them into a sheet (Figure 3.10 C). After an overnight wash in dH_2O (Figure 3.10 D) the tissue was put through an intensive process using enzymatic, and detergent methods to produce the SC-ECM (Figure 3.11 F). The dsDNA content for SC-ECM was 31.8 ± 11.3 ng/mg (Figure 3.11).
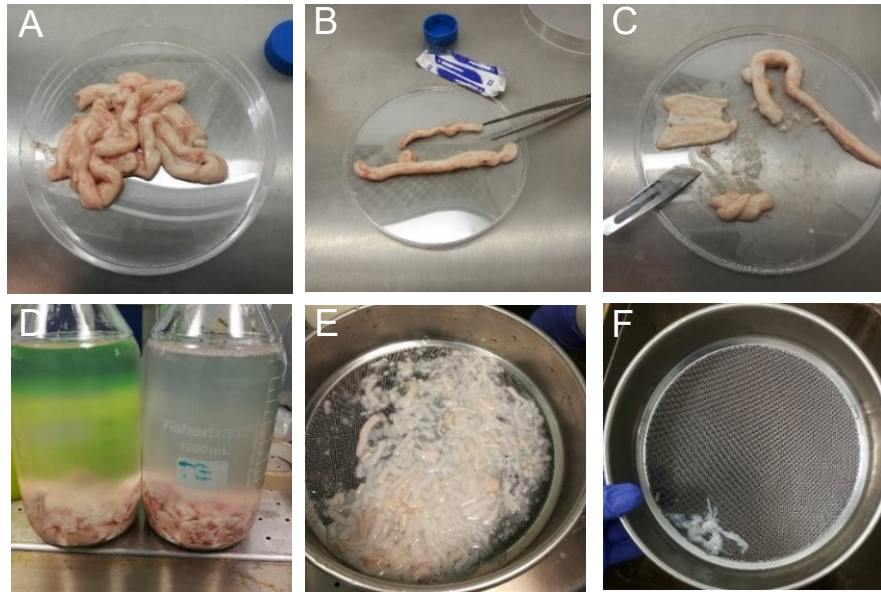
Figure 3.10 Preparation and decellularisation of spinal cord. Spinal cord as received [A]. Removal of dura [B] and longitudinal transection [C]. PBS wash [D] and decellularisation [E], and resultant SC-ECM [F].

3.4.5 Comparative dsDNA and sGAG quantitative analysis of dECM portfolio
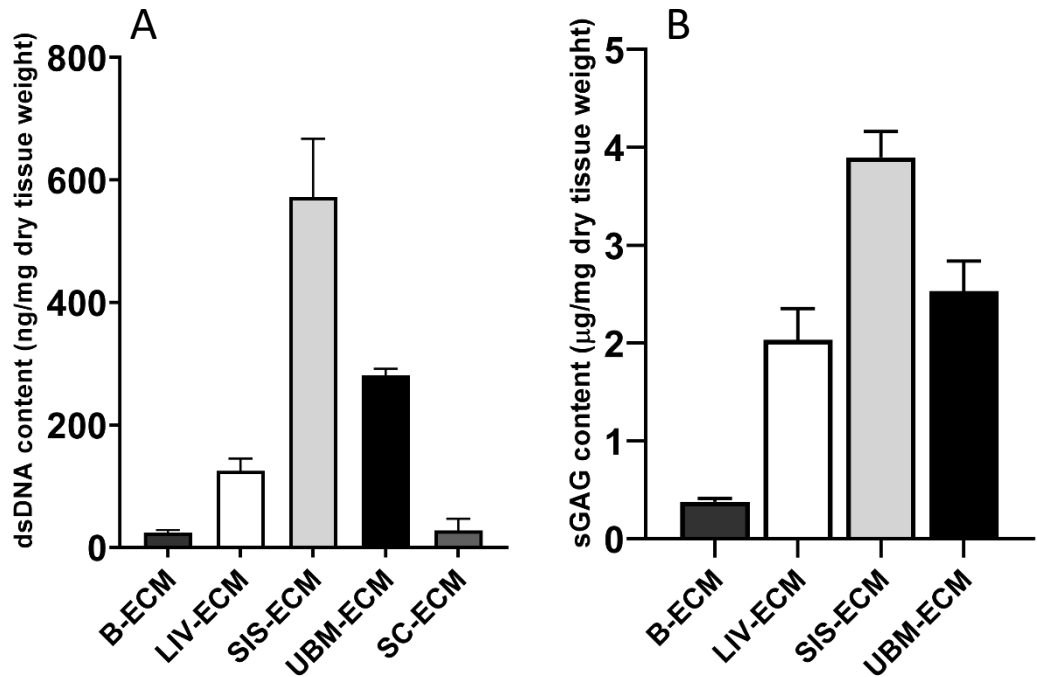
Figure 3.11 Trends in biochemical properties of dECM materials. dsDNA content for each of the materials decellularised [A]. sGAG content for each of the dECM produced [B].

Figure 3.11 shows the dsDNA and sGAG contents for each of the dECM materials. B-ECM had the lowest dsDNA content at 24.2 ± 4.3 ng/ mg dry tissue weight, however also had the lowest sGAG content at 0.38 ± 0.1 μg/mg. Similarly, dsDNA content was highest for SIS-ECM at 572.0 ± 95.6 ng/ mg, whilst its sGAG content was of 3.9 ± 0.3 μg/ mg.

3.4.6 dECM hydrogel formation
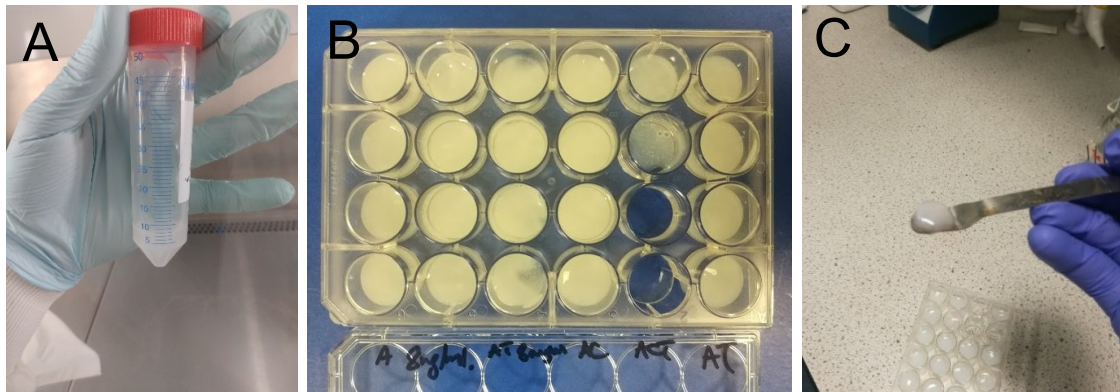
Figure 3.12 dECM hydrogel formation. 10 mg/ ml dECM digest [A]. 8 mg/ ml dECM hydrogels in 24-well plate [B] that were robust and easily handled [C].

dECM powder was solubilised in HCl into dECM "digests" (Figure 3.11 A). These were then neutralised to physiological pH to form opaque dECM hydrogels (Figure 3.11 B) that could be easily handled and manipulated (Figure 3.11 C).

3.4.7 Rheological characterisation of dECM hydrogels

Rheological characterisation of the ECM hydrogels was carried out on a parallel plate rheometer and was performed on 3 chosen concentrations to create rheological profiles: 4, 6 and 8 mg/ ml. The time sweeps (Figures 3.12, 3.13, 3.14 & 3.15 A) show that after neutralisation, all three concentrations in every material displayed solid-like behaviour as their storage modulus (G') becomes higher than their loss modulus (G'') by at least a factor of 10. Each material showed concentration dependent gelation kinetics with the 8 mg/ml concentrations displaying solid-like behaviour in the shortest time. The B-ECM hydrogels displayed a sigmoidal gelation profile (Figure 3.12 A) whereas the other materials exhibited more complex gelation; their storage moduli do not plateau, instead remaining on a steady incline throughout the measurement period. Furthermore,

the B-ECM exhibited solid-like properties in the fastest time followed by LIV-ECM and SIS-ECM (Figure 3.16).

A frequency sweep (Figures 3.13, 3.14, 3.15 C, D & E) was carried out immediately following the time sweep at a constant amplitude. Angular frequency was increased from 0.01 to 100 rad/s with viscosity and storage modulus observed. Viscosity of each material was seen to decrease due to increases in angular frequency, whilst storage moduli largely remained linear across all materials, with the exception of 4 and 6 mg/ml B-ECM and 4 mg/ml LIV-ECM hydrogels that began to stiffen at 54, 12 and 25 rad/s, respectively.

Following the frequency sweep, an amplitude sweep was carried out at a constant frequency of 0.01 Hz. Viscoelastic behaviour was observed up until critical strain values whereby non-linear regions were observed as G' values were raised, exhibiting a strain stiffening effect (Figures 3.13, 3.14, 3.15 B). The 6 mg/ml B-ECM gel had the highest maximum modulus at 1476.7 ± 104.4 Pa; the largest strain stiffening response from a storage modulus of 160.7 ± 8.3 Pa. Gels then weakened as their critical strains were reached, once again dependent on concentration, and by 166 % strain G' values fell to lower than their linear viscoelastic values.
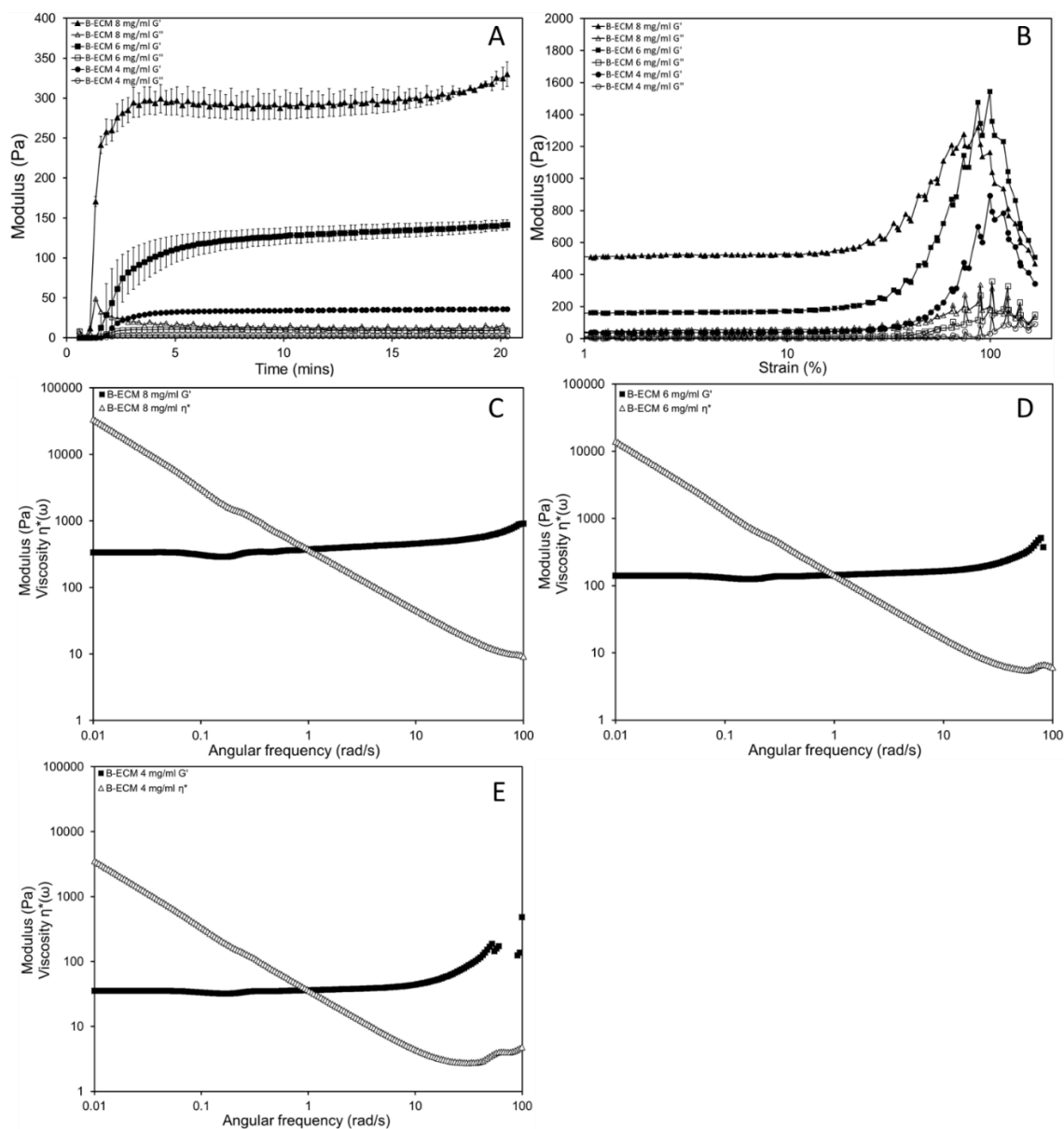
Figure 3.13 Rheological characterisation of B-ECM hydrogels. Time sweep showing storage (G') and loss modulus (G'') for 8, 6 and 4 mg/ml B-ECM hydrogels [A]. Strain sweep showing G' and G'' for 8, 6 and 4 mg/ml B-ECM hydrogels [B]. Frequency sweeps displaying G' and viscous modulus for 8 [C], 6 [D] and 4 [E] mg/ml B-ECM hydrogels. Data are presented as means ± SD, N = 3 independent gels.
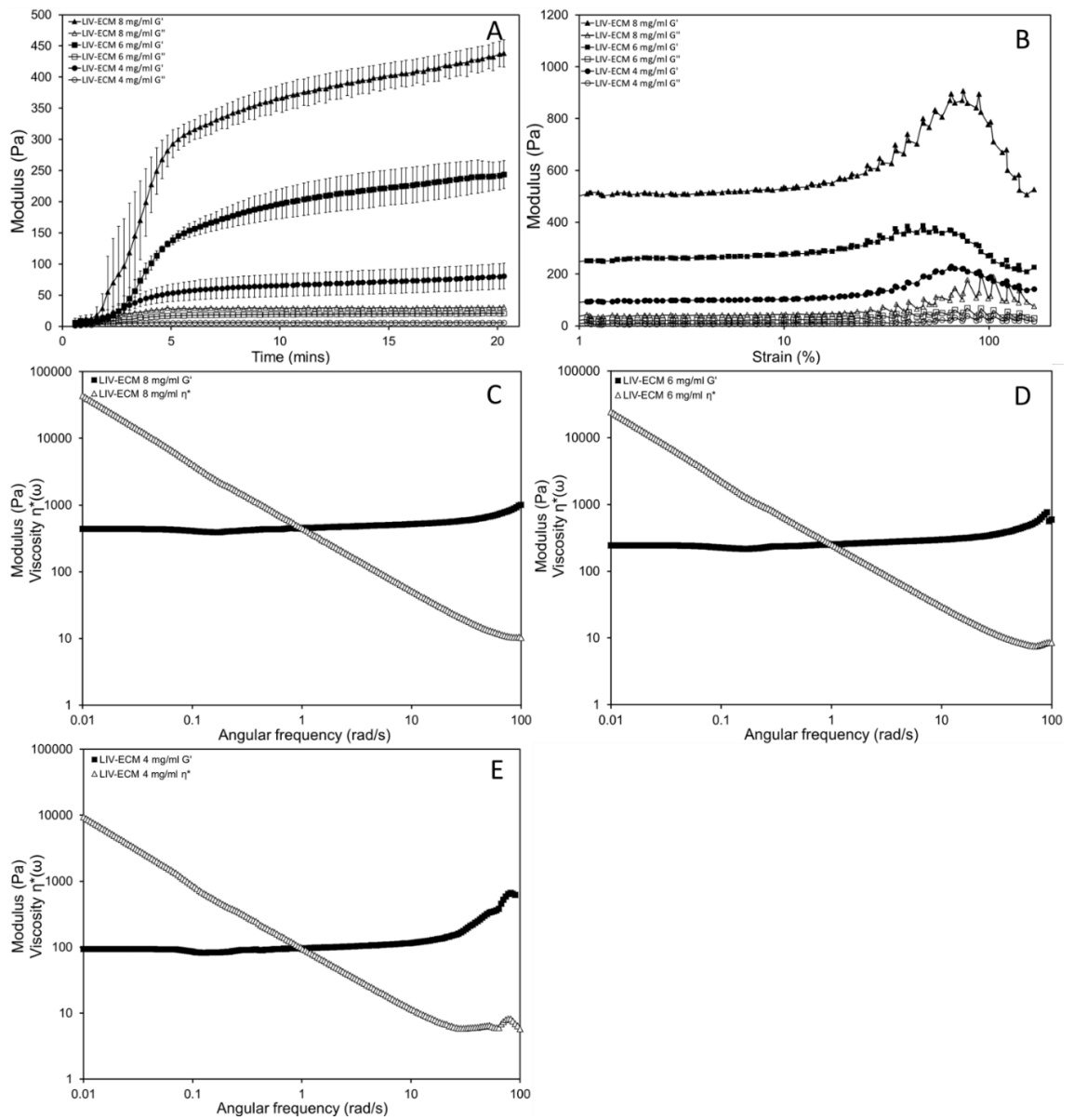
Figure 3.14 Rheological characterisation of LIV-ECM hydrogels. Time sweep showing storage (G') and loss modulus (G'') for 8, 6 and 4 mg/ml LIV-ECM hydrogels [A]. Strain sweep showing G' and G'' for 8, 6 and 4 mg/ml LIV-ECM hydrogels [B]. Frequency sweeps displaying G' and viscous modulus for 8 [C], 6 [D] and 4 [E] mg/ml LIV-ECM hydrogels. Data are presented as means ± SD, N = 3 independent gels.
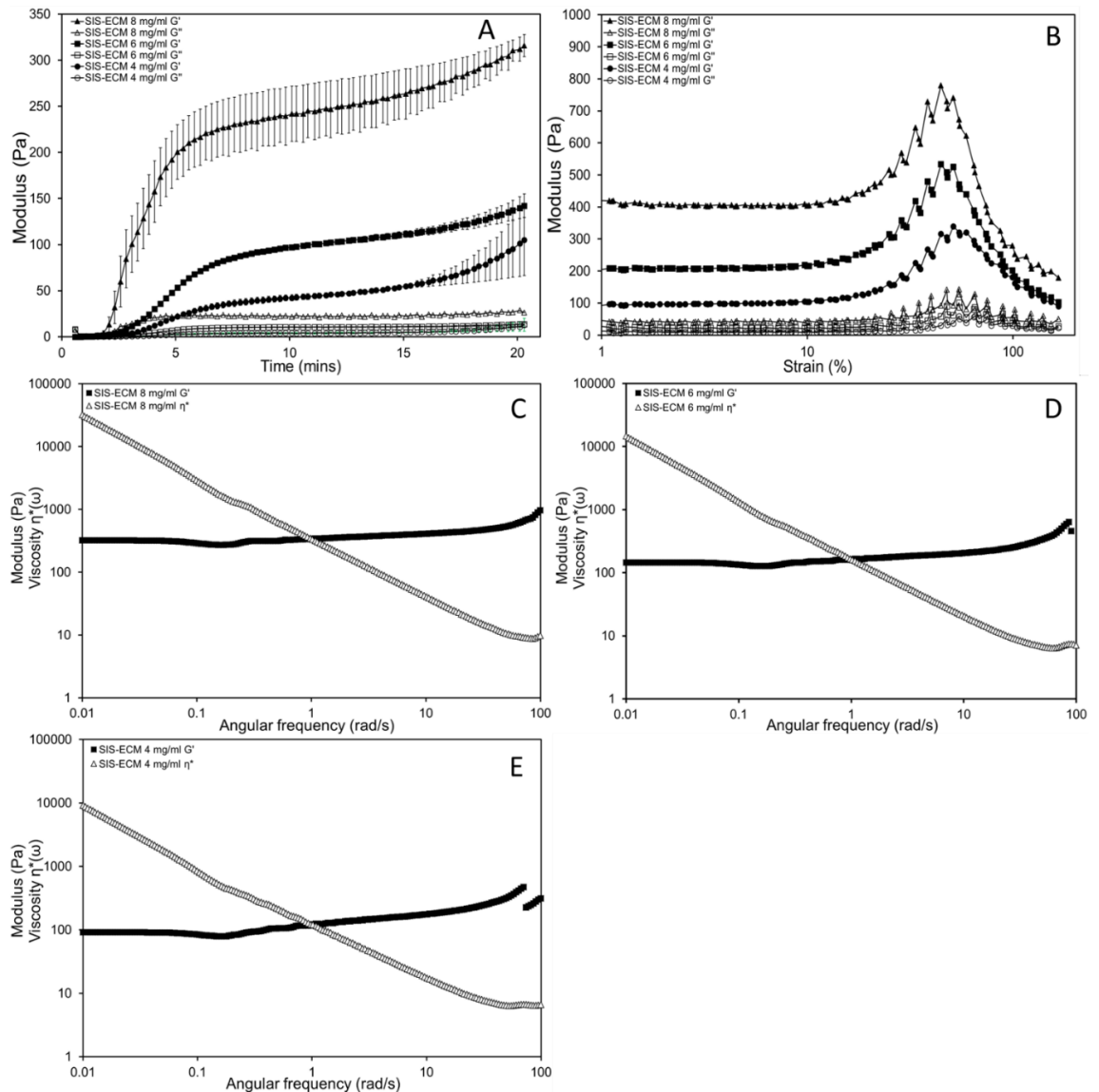
Figure 3.15 Rheological characterisation of SIS-ECM hydrogels. Time sweep showing storage (G') and loss modulus (G'') for 8, 6 and 4 mg/ml SIS-ECM hydrogels [A]. Strain sweep showing G' and G'' for 8, 6 and 4 mg/ml SIS-ECM hydrogels [B]. Frequency sweeps displaying G' and viscous modulus for 8 [C], 6 [D] and 4 [E] mg/ml SIS-ECM hydrogels. Data are presented as means ± SD, N = 3 independent gels.
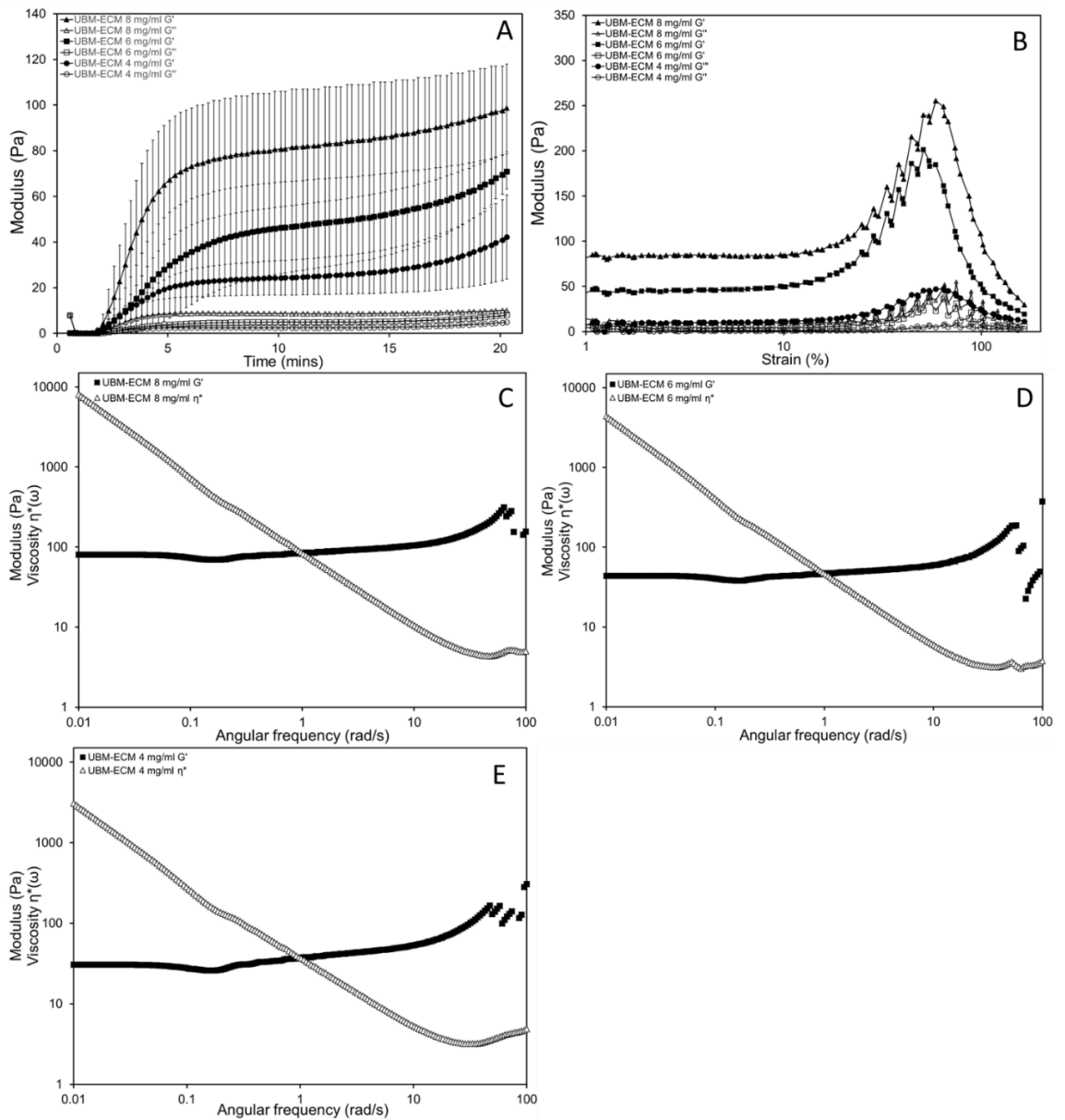
Figure 3.16 Rheological characterisation of UBM-ECM hydrogels. Time sweep showing storage (G') and loss modulus (G'') for 8, 6 and 4 mg/ml UBM-ECM hydrogels [A]. Strain sweep showing G' and G'' for 8, 6 and 4 mg/ml UBM-ECM hydrogels [B]. Frequency sweeps displaying G' and viscous modulus for 8 [C], 6 [D] and 4 [E] mg/ml UBM-ECM hydrogels. Data are presented as means ± SD, N = 3 independent gels.

3.4.7.1   Time to half gelation
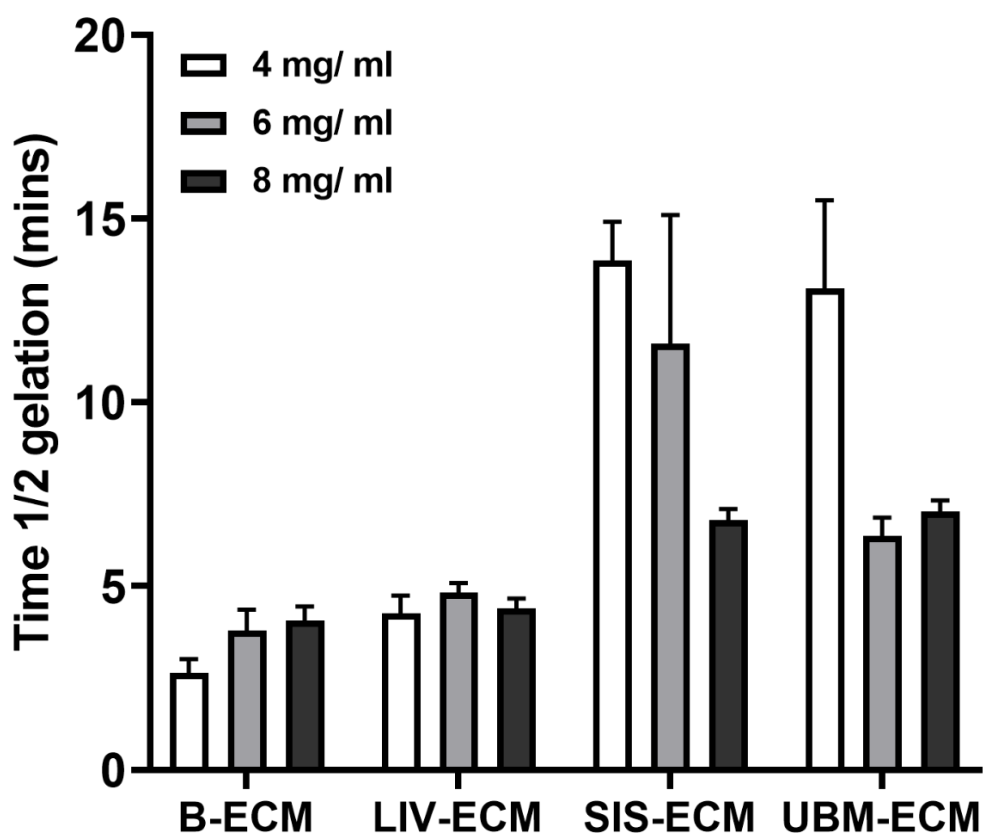
Figure 3.17 Time to half gelation for each dECM hydrogel at 4, 6 and 8 mg/ml gel concentrations. Data are shown as mean ± SD. N = 3 independent gels.

Time to half gelation was calculated as the time to reach half of the maximum modulus. SIS-ECM and UBM-ECM hydrogels exhibited concentration dependent gelation time. As was evident from the time sweep data, the B-ECM hydrogels exhibited the fastest gelation, followed by the LIV-ECM gels. Whilst the UBM-ECM and SIS-ECM displayed similar gelation kinetics for their 4 mg/ ml and 8 mg/ml hydrogels, the SIS-ECM 6 mg/ml gel reached gelation significantly slower than the UBM-ECM hydrogel. Moreover, the LIV-ECM and UBM-ECM 6 mg/ ml displayed similar gelation times.

3.5 Discussion

Decellularisation of tissues to produce biologic scaffolds is an effective method to generate biomaterials that are biocompatible and promote positive tissue remodelling responses *in vivo* (Crapo et al., 2011). These materials are rich in the biochemical constituents of ECM that affect cell behaviour such as structural proteins, proteoglycans, GAGs, growth factors, cryptic peptides and matrix bound vesicles, as well as presenting native ECM ultrastructure and macroscopic architecture (Crapo et al., 2011, Hussey et al., 2018). High degrees of evolutionary conservation across components of the ECM allow for effective xenogeneic applications and, furthermore, non-tissue specific ECM is often employed with comparable outcomes to tissue-specific ECM (Mosala Nezhad et al., 2016b, Nguyen et al., 2017b, Smith et al., 2004, Syed et al., 2014). Moreover, partial acidic digestion of dECM and solubilisation into thermo and pH-sensitive robust hydrogels has been extensively reported with applications ranging from injectable materials for wound healing (Farnebo et al., 2014, Engel et al., 2015) to the creation of 3D tissue-appropriate *in vitro* disease models (Tapias et al., 2015, Rijal and Li, 2017) or cell culture and differentiation (Alom et al., 2017, Loneker et al., 2016, Shin et al., 2019, Skardal et al., 2012, DeQuach et al., 2012).

When decellularising a tissue, considerations must be made for its cellular density, ECM components and its thickness (Crapo et al., 2011). Additionally, following decellularisation, of concern is the amount of cellular debris retained in the scaffold and the residual constituent ECM components remaining. These properties affect the biomaterials' immunogenicity and regenerative capacity, and so achieving a balance between cellular removal and ECM damage reduction may be seen as a core tenet of decellularisation. As such, thorough

characterisation of dECM biochemical properties is desired. Likewise, mechanical properties such as stiffness alter cellular responses (Janmey et al., 2020, Wells, 2008).

B-ECM underwent the most complete decellularisation process with >98 % of dsDNA removed from the tissue. The harsher acidic, solvent and enzymatic treatments the material was exposed to are likely responsible for this substantial removal of cellular material in the resultant scaffold, however this may also contribute to the lack of sGAGs observed. In comparison, the less severe decellularisation process of mechanical abrasion and dilute peracetic acid treatments undertaken with SIS resulted in a retention of 10 % of native dsDNA content with the potential advantage of a higher sGAG content. Decellularisation of liver resulted in approximately 98% reduction of dsDNA compared to the native liver control, likely due to the comparatively harsh treatment involving multiple detergents and trypsin. However, histological analysis of LIV-ECM indicated preservation of the low levels of sGAG seen in the native tissue in addition to the collagen architecture remaining intact. dsDNA quantification was performed on both SC-ECM and UBM-ECM however, their native tissues were omitted from the analysis due to a low yield (SC-ECM) and the lack of access to the native tissue (UBM-ECM). The low yield and a lack of availability of the SC-ECM resulted in its omission from further investigation.

dECM powders were successfully solubilised and formed into stable hydrogels of varying concentrations. Time sweeps were carried out on these hydrogels to produce gelation profiles for each material. Gelation was observed and occurred in all materials at each of the three chosen gel concentrations as their storage moduli increased to values higher than their loss moduli indicating solid-like

behaviour. Gelation kinetics were similar across each material; however, a sigmoidal profile was only seen in the B-ECM hydrogels whilst the others displayed a more complex mechanism whereby the storage modulus remains on a steady incline throughout the experiment. In the context of ECM hydrogels, gelation occurs through the cross-linking of collagen fibrils and so, the complex gelation observed may be attributed to the diversity of ECM components of LIV-, SIS- and UBM-ECM as the presence of network forming collagens, laminin, fibronectin and sGAGs can modulate gelation, possibly interfering with the fibrillogenesis (Filla et al., 2017, Milan et al., 2005, Vogel et al., 1984, Munakata et al., 1999). Additionally, the correlation observed between sGAG content and gelation kinetics appears to be concurrent with the findings of previous studies on umbilical cord and brain derived ECM (Kočí et al., 2017).

All materials displayed shear thinning behaviour as their viscous modulus decreased as a function of frequency. B-ECM, LIV-ECM and SIS-ECM hydrogels at concentrations of 8 and 6 mg/ml exhibited storage moduli independent of frequency up to 100 rad/s, indicating a stable, robust, and well-structured gel system containing strongly associated polymers; in this instance inter-collagen crosslinking. Conversely at 4 mg/ml, these materials began to destabilise at around 50% rad/s as G' increased as a function of frequency. Viscous modulus ceased to decrease implying non-linear viscoelastic behaviour and slight destabilisation of the gel system. In contrast, the UBM-ECM 8 and 6 mg/ml gels were less stable at frequencies above 50 rad/s whilst the 4 mg/ml appears to exit its linear viscoelastic region around 10 rad/s.

To assess their stress response to shear strain, materials were subjected to a strain sweep immediately following the frequency sweeps. This nonlinear

elasticity in response to shear strain is observed in biological polymers due to polymer "semi-flexibility" (Licup et al., 2015, Storm et al., 2005, Van Oosten et al., 2016) and this strain-induced nonlinear viscoelasticity can vary, dependent on elasticity and stiffness of the individual filaments and the strength of the interfilamentous network (Storm et al., 2005). All materials at each concentration exhibited strain stiffening behaviour, although this occurred at different strains and in a variety of amplitudes. For example, the 4 mg/ml B-ECM gel retained its linear viscoelasticity up to 15 % strain followed by a stiffening of the polymer network up to 90 % strain reaching an elastic modulus 3.5 times its original value. In contrast, G' for the 8 mg/ml SIS-ECM gel increased at 12 % strain and reached its peak elastic modulus at 50 % strain with a value 2.1 times its original value. The 8 mg/ml B-ECM gel withstood strains of over 100 % before beginning to rupture whereas the 8 mg/ml SIS-ECM withstood the lowest, reaching a critical strain of 50 % strain. It can therefore be assumed that the B-ECM gel contained a filamentous network held together with strong chemical bonds that was flexible to extension, whereas the SIS-ECM gel was more compliant and contained weaker crosslinks (Motte and Kaufman, 2013). LIV-ECM gels showed the smallest increase in G', however upon reaching their maximum shear modulus they displayed wider peaks than any of the other materials and required more extension past their critical strain to induce network collapse. To summarise, these materials differ in their sensitivity to shear mechanical loads, likely as a result of biochemical compositional variability, in which subtle differences of collagen isoforms or the presence of sGAG and other ECM components such as laminin or fibronectin may be affecting the elasticity of the filamentous network. Moreover, Motte & Kauffman (2013) found that strain stiffening in collagen I

hydrogels is dependent on solubilisation technique and the fact that B-ECM underwent a 96 hour pepsin solubilisation in comparison to 48 hours for the LIV-, SIS- and UBM-ECM should not be ignored when considering these differences in mechanical behaviour. Similarly, differences in tissue processing are likely to impact hydrogel mechanical properties with harsher decellularisation agents such as the TX-100/ SDS in the liver protocol or the HCl used for the bone may disrupt the collagen architecture resulting in a sub optimal stiffness (Fernández-Pérez and Ahearne, 2019, Lumpkins et al., 2008, White et al., 2017). The lack of structural integrity of the UBM-ECM resulted in its omission from further investigation in this study.

3.6 Conclusion

Materials derived from different tissues and with different processing conditions differed in biochemical profiles and physical properties. Decellularisation was achieved with the removal of over 90% of the native dsDNA in every material, whilst sGAG were further present. Thorough rheological analysis showed that material physical behaviour is diverse; gelation time, stiffness, and strain stiffening responses were different in every dECM-h. These differences in biochemical and physical properties will likely affect cell responses. Irreversible damage to the structural proteins of the ECM can be a consequence of the use of harsh decellularisation agents to achieve low dsDNA, resulting in damage to the binding motifs and native architecture that regulate cell adhesion and behaviour. Therefore, the capabilities for these materials to maintain and support cellular function must be addressed. Three dECM materials were chosen to be taken forward: B-ECM, LIV-ECM, and SIS-ECM.

Chapter 4 Assessment of material suitability for use in EngNT

4.1 Introduction

Possibly one of the most remarkable phenomena in biology is the ability of certain tissues to spontaneously regenerate following injury. Unlike the central nervous system (CNS), tissue in the injured peripheral nerve will undergo reorganisation on a macroscopic and molecular level in order to create an environment that is biochemically, mechanically and topographically supportive of axonal regrowth to aid regeneration of nerves toward their target organs (Deumens et al., 2010, Fu and Gordon, 1997). A challenge of nerve engineering is to effectually recreate, utilising biomaterials, therapeutic cells, and neurotrophic factors, this environment and to introduce it into the injury site.

4.1.1 Improving nerve regeneration

Central to the process of nerve regeneration is the reprogramming of SC from their myelin or Remak phenotypes into a repair phenotype; characteristically bipolar and elongated in morphology, aligning within their basal lamina in columnar structures known as the Bands of Büngner (Deumens et al., 2010, Jessen and Mirsky, 2016, Jessen and Mirsky, 2019). These Schwann cells upregulate the production and secretion of neurotrophic factors such as nerve growth factor (NGF), glial cell line derived neurotrophic factor (GDNF), and brain derived neurotrophic factor (BDNF) that may aid regeneration (Biernaskie et al., 2007, Jessen and Mirsky, 2019). Understanding these changes in morphology, biochemistry, and macroscopic organisation is critical when considering the incorporation of support cells into the design and fabrication of regenerative substrates/ tissues for nerve repair.

Hydrogels are attractive biomaterials for use in nerve repair due to their biomimicry of soft tissue mechanical properties (Chaudhuri, 2017). Moreover they may further provide implanted cells with a matrix and interstitial space within which to reside, subsequently resulting in increased cell survival compared with cell injection alone (Burdick et al., 2016, Marquardt and Heilshorn, 2016). In the application of peripheral nerve tissue engineering the implantation of aligned cells is often desired (Sarker et al., 2018b). Simple biomechanics of cell-hydrogel interactions may be exploited to provide an elegant solution to achieving alignment; utilising cell mediated contraction and planes of principal strain it is possible to simultaneously evenly populate a hydrogel with cells that self-align to form aligned strings of cells along a singular axis of the gel (Eastwood et al., 1998, Mudera et al., 2000).

4.1.2 Cell mediated contraction in hydrogels
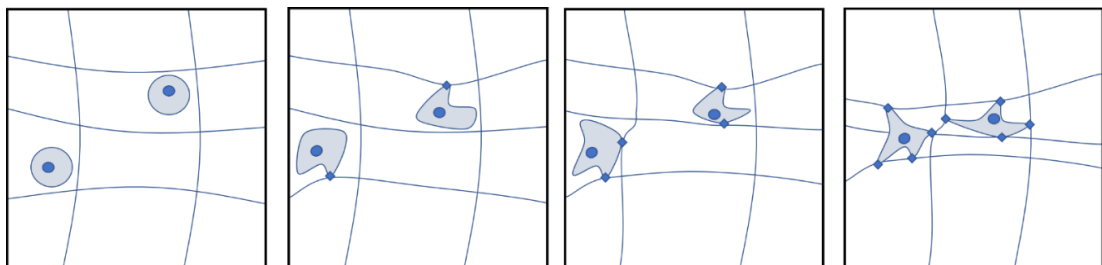
Figure 4.1. Schematic for cell-mediated contraction. Cells seeded into acellular hydrogel [A]. Initial cell-fibre interactions create tension throughout the network leading to an in increase in cell-fibre contact points [C]. Multiple cell-fibre contacts then cause the hydrogel to contract, resulting in a reduction in size [D].

Cellular attachment to its surrounding 3D environment instigates cellular morphology changes, resulting in elongation of the cell body and upregulation of expression in actin stress fibres as can be seen when comparing cell shape in collagen gels with gels made from agarose; a polymer with no cell adhesion sites (Ahearne, 2014). Fibres that are unable to endure the tension become warped at

the point of contact (Figure 4.1 B), often focal adhesion complexes, and as this action "pulls" the polymer network closer together (Figure 4.1 C), the hydrogel shrinks in size (Figure 4.1 D). In collagen I hydrogels these focal adhesions are formed primarily through integrin $\alpha 1\beta 1$ ligand binding and cell-mediated gel contraction as a function of this interaction can be up to an 80% reduction from its original size (Ahearne et al., 2010, O'Rourke et al., 2015). The level of contraction is dependent on the number of cell-ECM contacts, a variable that can be affected by increasing hydrogel concentration and modulating the number of available ligand binding sites (often changed via cell seeding density). Contraction is further dependent on the number of cross-links between the polymer fibres (Ahearne, 2014, Ahearne et al., 2010, O'Rourke et al., 2015). Through the tethering of the hydrogel at opposing ends, tension is created. Cells then align to this tension due to the prevention of contraction in the longitudinal axis as a result of the tethering (Eastwood et al., 1998, Mudera et al., 2000, Phillips et al., 2005).

4.1.3 Engineered neural tissue

Engineered neural tissue (EngNT) refers to a living artificial tissue comprised of a highly aligned purified collagen I hydrogel seeded with aligned therapeutic cells. (Georgiou et al., 2013). Cells are seeded into the hydrogel in a tethered mould (Figure 4.2) to promote longitudinal self-alignment of the cells and collagen fibres (Phillips et al., 2005). Following alignment, the construct is partially dehydrated via plastic compression using a RAFT™ absorber to produce a stabilised, robust sheet of aligned cells that can further be rolled into a conduit (Figure 4.2). To date, several types of cells have proven to be successful in producing EngNT, such as rat Schwann cells (Georgiou et al., 2013), adipose derived stem cells

(Georgiou et al., 2015) and clinically relevant human neural stem cells (O'Rourke et al., 2018). These have been tested in preclinical *in vivo* rat models of critical length (15 mm) gaps with comparable results to autograft groups.
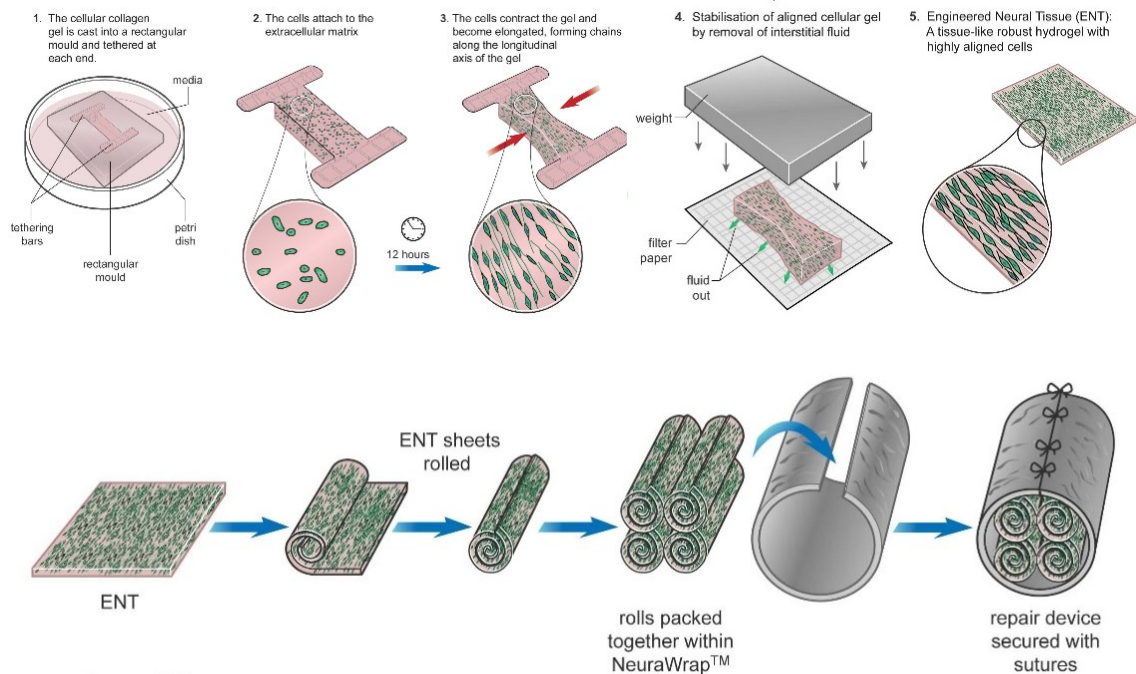
Figure 4.2 Production of EngNT sheets and rolling into conduits. Adapted from Georgiou et al., 2013 and jamesphillips.org

4.2   Chapter aims

In the previous chapter three hydrogels were produced via the decellularisation of mammalian tissues and characterised and these may provide an alternative to the currently used purified collagen I in EngNT. We hypothesise that diversity in the biochemical and mechanical properties of these dECM hydrogels is likely to affect cellular behaviour. The aim of this chapter was to implement the dECM materials into established *in vitro* assays and models to assess their suitability for use in EngNT.

4.3 Experimental design

In depth experimental procedures may be found in Chapter 2. A rat cell line, SCL4.1/F7 (cell culture procedures fully outlined in Materials and Methods section 2.1.1) was used for the *in vitro* assays in this chapter due to their previous utilisation in *in vivo* EngNT rat injury models (Georgiou et al., 2013). Adult rat DRGs were chosen for *in vitro* neurite extension assays for their accuracy in modelling neurite regeneration following injury (Kim et al., 2015, Kim et al., 2012, Lindsay, 1988, Menezes et al., 2019, Plantman et al., 2008). Established assays were employed to investigate the potential use of three dECM in EngNT: B-ECM, SIS-ECM and LIV-ECM. Firstly, we deemed it important to investigate material effect on Schwann cell metabolic activity, using collagen I as a comparator, to assess if any dECM caused a reduction in cell viability. Secondly, contraction profiles were of interest due to their previously proven ability to predict appropriate cell seeding densities and gel concentrations to achieve alignment. Two separate *in vitro* neurite extension assays were finally employed in the final screening process to identify the ideal candidate to be taken forward into possible *in vivo* nerve injury models.

Plastic compression to remove the interstitial fluid from cell laden collagen hydrogels has been reported (Georgiou et al., 2013, Georgiou et al., 2015, Sanen et al., 2017). Hydrogels derived from decellularised ECM differ from purified collagen hydrogels in their mechanical properties, dependent on tissue of origin and processing methods (Fernández-Pérez and Ahearne, 2019, Saldin et al., 2017, Sawkins et al., 2013). As such, the plastic compression process of the dECM based EngNT required optimisation due to issues with the structural integrity of the hydrogel constructs. Following compression, mechanical

detachment of the EngNT from the polypropylene mesh was performed via submersion in culture media and gentle agitation. The media was then removed from the well to leave sheets of dECM EngNT. The complete process is outlined in Figure 4.3.
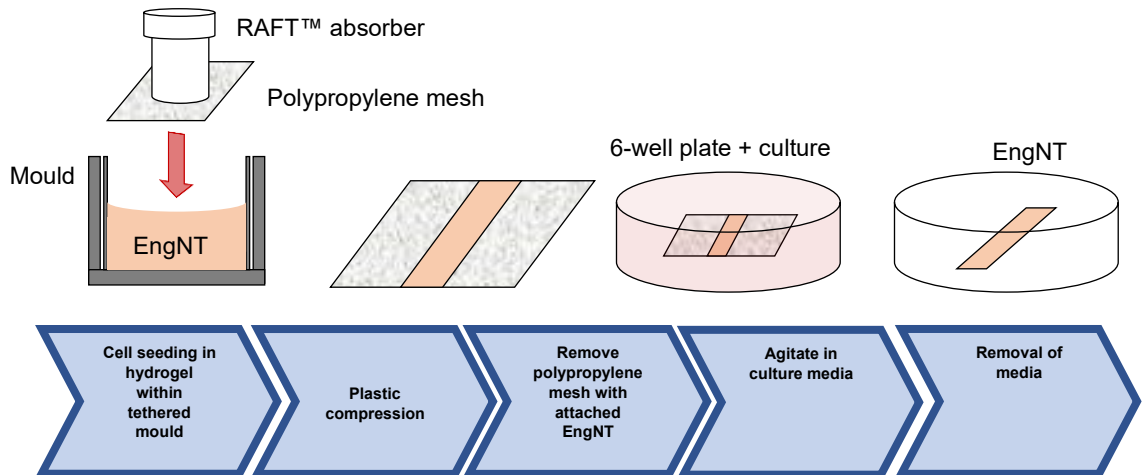
Figure 4.3 Schematic of EngNT sheet production process.

4.4 Results

4.4.1 dECM hydrogels differentially support F7 Schwann cell metabolic activity
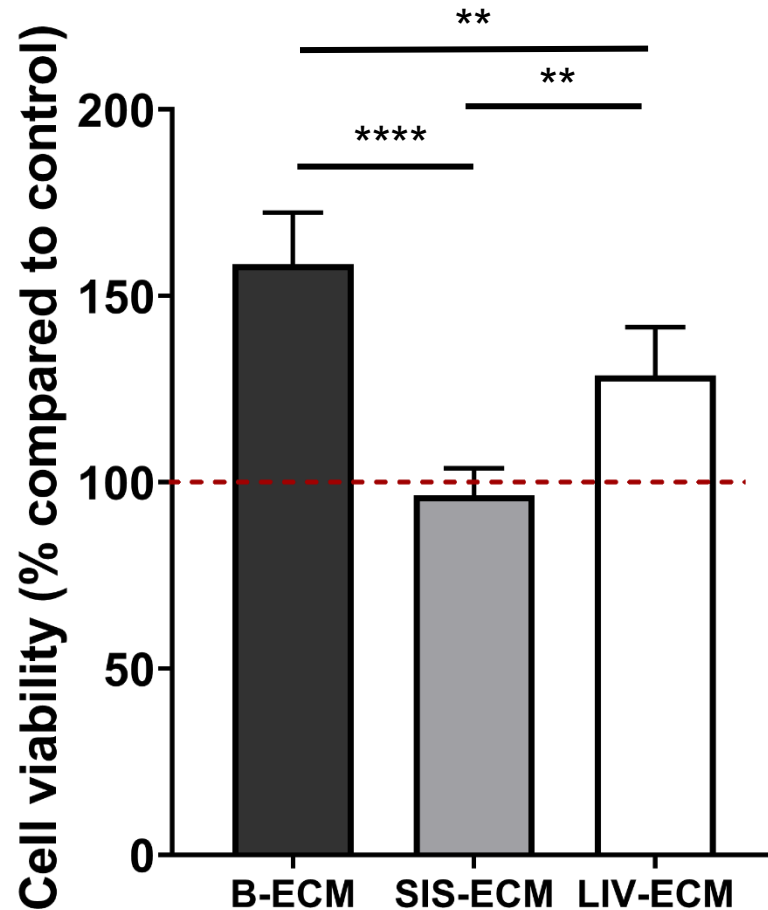
Figure 4.4 Effect of dECM on cell metabolic activity. Metaboic activity of F7 Schwann cells seeded at 0.5 x 10^6 cells/ ml in 6 mg/ml B-ECM, SIS-ECM and LIV-ECM hydrogels using the 3D cell-titer glo assay normalised to collagen I control (dotted line). Data are presented as means ± SD, N = 5 independent gels in quintuplicate. One-way ANOVA with Tukey's multiple comparisons test. **$p < 0.005$, ****$p < 0.0001$.

Figure 4.4 shows results from the 3D Cell-Titer Glo assay, employed to measure cell viability. F7 Schwann cell were seeded at 0.5 x 10^6 cells/ml in 6 mg/ml hydrogels. F7 Schwann cells in B-ECM gels possessed the highest metabolic activity at 158.4 ± 13.9 % of the collagen I control whereas F7 Schwann cells in the SIS-ECM had the lowest at 96.5 ± 7.3 %. F7 Schwann cells in the LIV-ECM on the other hand had 128.7 ± 13.0 % cell viability.

4.4.2 dECM hydrogel contraction is dependent on cell density and hydrogel composition and concentration
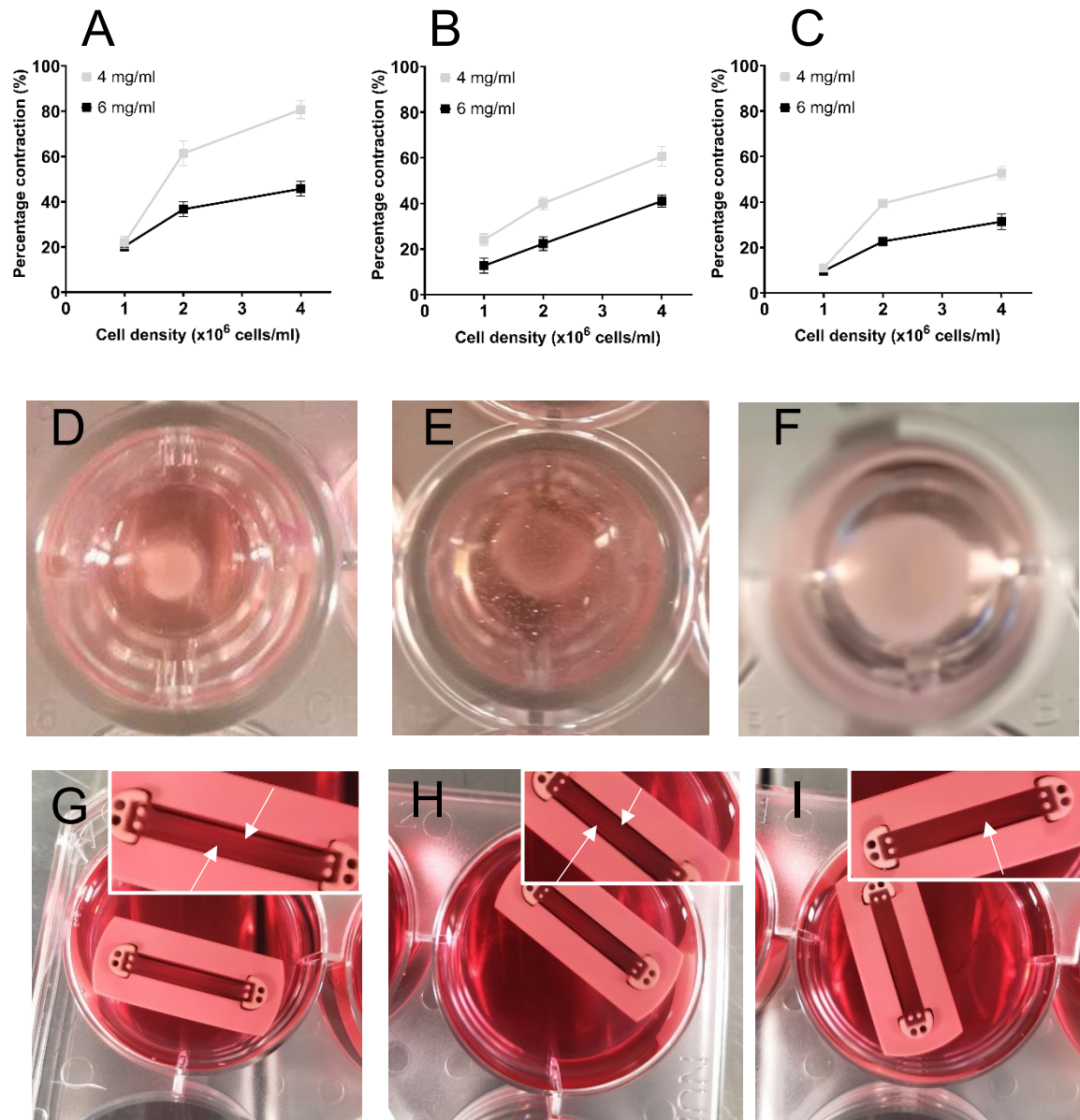
Figure 4.5 Effect of cell seeding density and hydrogel concentration on cell mediated contraction in the three dECM materials. Contraction profiles for 4 and 6 mg/ml hydrogels at different F7 Schwann cell densities for B-ECM [A], SIS-ECM [B] and LIV-ECM [C]. Contraction in 4 mg /ml hydrogels seeded with F7 Schwann cells at 4 x 10^6 cells/ml for B-ECM [D], SIS-ECM [E] and LIV-ECM [F]. Contraction in 4 mg/ml hydrogels in tethered moulds seeded with F7 Schwann cells at 4 x 10^6 cells/ml for B-ECM [G], SIS-ECM [H] and LIV-ECM [I]. White arrows denote the edges of the tethered hydrogels. N = 3 independent experiments run in quintuplicate. Data are presented as mean ± SEM.

Figure 4.5 shows results from the 96-well plate contraction assay (adapted from O'Rourke et al., 2015). Contraction was observed in all materials at both 4 and 6 mg/ ml and was dependent on gel concentration and cell seeding density (Fig 4.5 A, B & C); lower gel concentrations and higher cell densities resulted in higher contraction. Representative images of contraction in the 96-well plate assay may be seen in Figure 4.5 C-E. The B-ECM can be seen to be more responsive and showed the highest levels of contraction at 4 mg/ ml gel concentration and 4 x 10^6 cells/ ml cell seeding density at 80.7 ± 6.8 percentage contraction (Figure 4.5 A). The lowest level of contraction was observed in the LIV-ECM gels at 11.0 ± 2.2 percentage contraction (Figure 4.5 C). SIS-ECM gels were not as contractile as B-ECM, however still exhibited a relatively high percentage contraction of 60.7 ± 7.5 at 4 mg/ ml gel concentration and 4 x 10^6 cells/ ml cell seeding density (Figure 4.5 B). Following cell seeding in 400 µl of 4 mg/ ml gel concentration in tethered moulds (Figure 4.5 G, H & I) contraction was observed in all materials at 4 x 10^6 cells/ ml. In contrast to the 96-well plate assay, the magnitude of contraction appears to be similar in B-ECM and SIS-ECM gels (Figure 4.5 G & I). Tethered LIV-ECM gels were not as contractile (Figure 4.5 H).
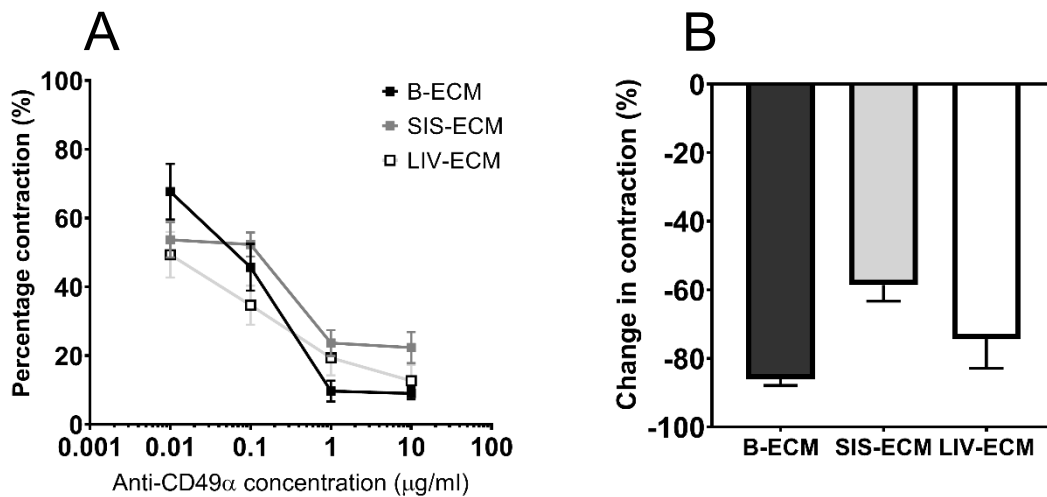
Figure 4.6 Effect of the incremental inactivation of integrin α1 in dECM. Dose response of anti-CD49α on B-ECM, SIS-ECM and LIV-ECM F7 Schwann cell containing hydrogels [A]. Percentage reduction in contraction from 0.01 µg/ ml to 10 µg/ml anti-CD49α in B-ECM, SIS-ECM and LIV-ECM F7 Schwann cell containing hydrogels [B]. N = 3 independent experiments run in quintuplicate. Data are presented as mean ± SD

To elucidate the mechanisms of cell-ECM interactions driving the contractile forces within the materials an anti-CD49α antibody was incubated at varying concentrations with hydrogels of 4 mg/ml and a cell density of 4 x 10^6 cells/ ml in the same 96-well plate model used previously (Figure 4.6 A). A dose response was observed as increasing anti-CD49α reduced contraction in all three materials. Contraction was reduced most in the B-ECM hydrogel, from 67.7 ± 8.1 % to 9.0 ± 1.7 %. Contraction was reduced from 49.3 ± 6.7 % to 12.7 ± 4.7 % and 53.7 ± 5.1 % to 22.3 ± 4.5 % in LIV-ECM and SIS-ECM hydrogels respectively. The effect of blocking CD49α as a function of percentage change in contraction is shown in Figure 4.6 B. The B-ECM hydrogel was most responsive with an 86.1 ± 1.8 % change in contraction reduction whereas the SIS-ECM hydrogel showed the least reduction in contraction (58.6 ± 4.7%).

144

4.4.3 dECM hydrogels modulate F7 Schwann cell phenotype

F7 Schwann cell gene expression shown in Figure 4.7 suggests that SIS-ECM hydrogels may be more active in the modulation of cell phenotype than the other dECM-h. An in-depth account of the protocol may be found in Materials and Methods Section 2.7.4. Briefly, 4 mg/ ml dECM-h and 2 mg/ ml collagen I hydrogels were seeded with F7 Schwann cells at 4×10^6 cells/ ml. Following a 24-hour incubation period, gels had contracted and were removed from culture media and immediately placed in buffer solution at -80 °C. RNA was extracted, and genes of interest amplified via PCR. Neurotrophic factors were investigated, including ciliary neurotrophic factor (CNTF) and GDNF. Inflammatory markers included interleukin 6 (IL-6) and leukaemia inhibitory factor (LIF), whereas Schwann cell markers investigated were roundabout homolog 1 (ROBO1) and transcription factor SOX-10 (SOX10). Expression was normalised to collagen controls.

No significant changes were observed in CNTF (Figure 4.7 A) and GDNF (Figure 4.7 B) when compared to the collagen control. All dECM significantly reduced the expression of IL-6 and increased expression of LIF (Figure 4.7 C and D, respectively). B-ECM and LIV-ECM hydrogels decreased ROBO1 expression (Figure 4.7 E) whilst no change was observed in SIS-ECM. SOX10 expression was elevated in SIS-ECM when compared to the collagen I control, however this was not statistically significant (n >0.05) (Figure 4.7 F).
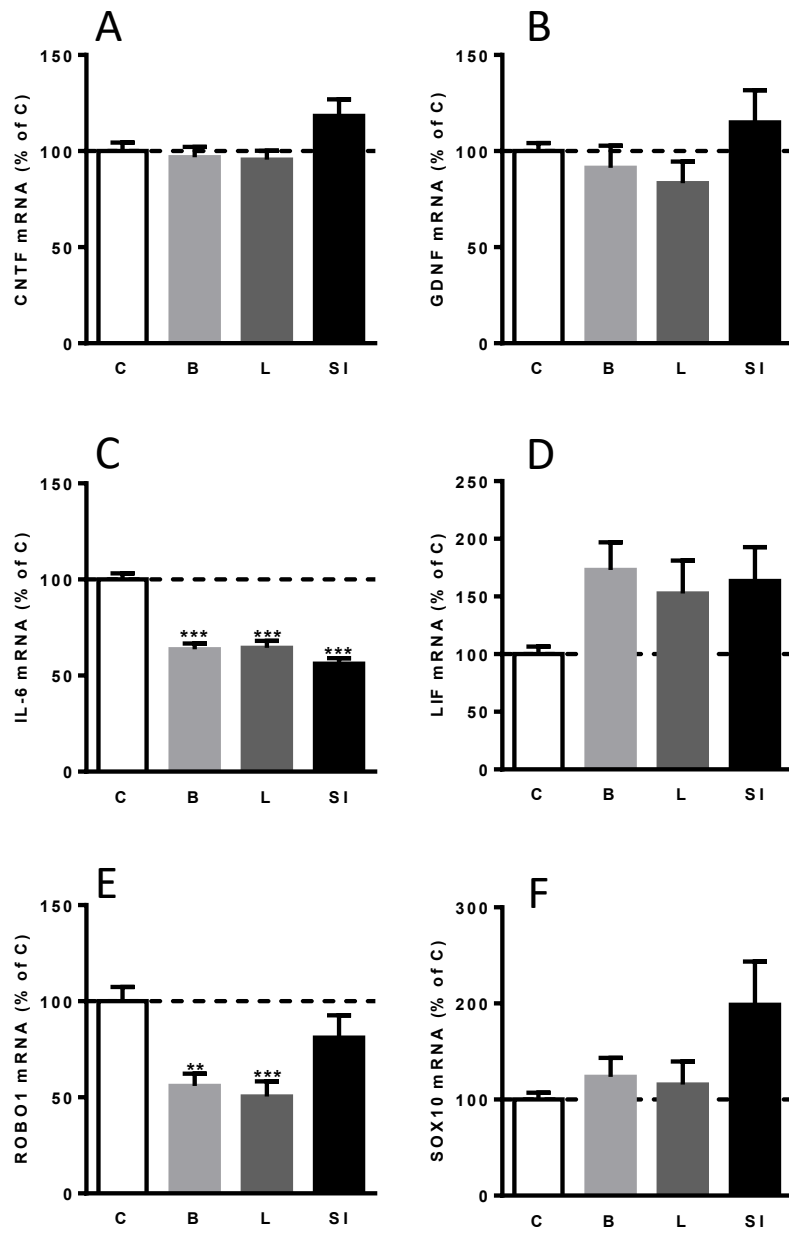
Figure 4.7 Schwann cell gene expression when incorporated into dECM hydrogels. Expression of CNTF [A], GDNF [B], IL-6 [C], LI [D], ROBO1 [E], and SOX10 [F] in F7 Schwann cells seeded in dECM hydrogels relative to collagen I controls. One-way ANOVA with Sidak's multiple comparisons with single pooled variance. **$p < 0.005$, ***$p < 0.001$, ****$p < 0.0001$. N = 4 independent experiments run in quadruplicate.

4.4.4 Cellular dECM hydrogels support F7 Schwann cell alignment
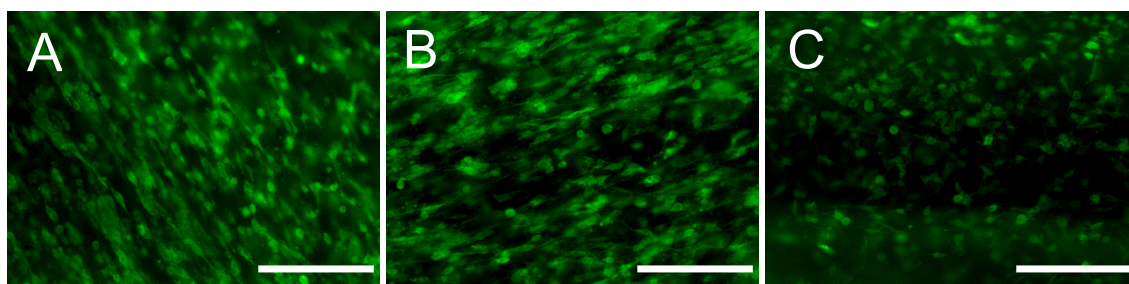
Figure 4.8 Qualitative assessment of F7 Schwann cell alignment in tethered dECM hydrogels. Fluorescence micrographs of F7 Schwann cells embedded in 4 mg/ ml B-ECM [A], SIS-ECM [B] and LIV-ECM [C] fully hydrated hydrogels. Scale bars = 200 µm.

Following the contraction assays, 4 mg/ml hydrogels were seeded with 4 x 10^6 rat F7 Schwann cells. F7 Schwann cell alignment was initially observed via immunostaining with anti-S100 and Hoechst (full procedures available in section 2.9.1) followed by fluorescence microscopy (Figure 4.7 A-C). F7 Schwann cells seeded in B-ECM and SIS-ECM hydrogels displayed cell elongation and a bipolar morphology as they aligned along the longitudinal axis of the material (Figure 4.7 A & B). Conversely, the F7 Schwann cells seeded in the LIV-ECM hydrogel presented a more spherical morphology with multi-directional protrusions of their cellular bodies, and whilst some were bipolar, these cells were not aligned along the longitudinal axis (Figure 4.8 C). To quantify the level of alignment, multiple images were taken via confocal microscopy (Figure 4.8 A-C), and the angle of F7 Schwann cell deviation from the longitudinal axis calculated in Volocity with each value placed into 10° bins from 0 to 90° (Figure 4.8 D). As in the fluorescence images, F7 Schwann cells were seen to be bipolar and elongated in B-ECM and SIS-ECM hydrogels (Figure 4.9 A and B respectively) and presented a spherical morphology in the LIV-ECM EngNT (Figure 4.9 C).
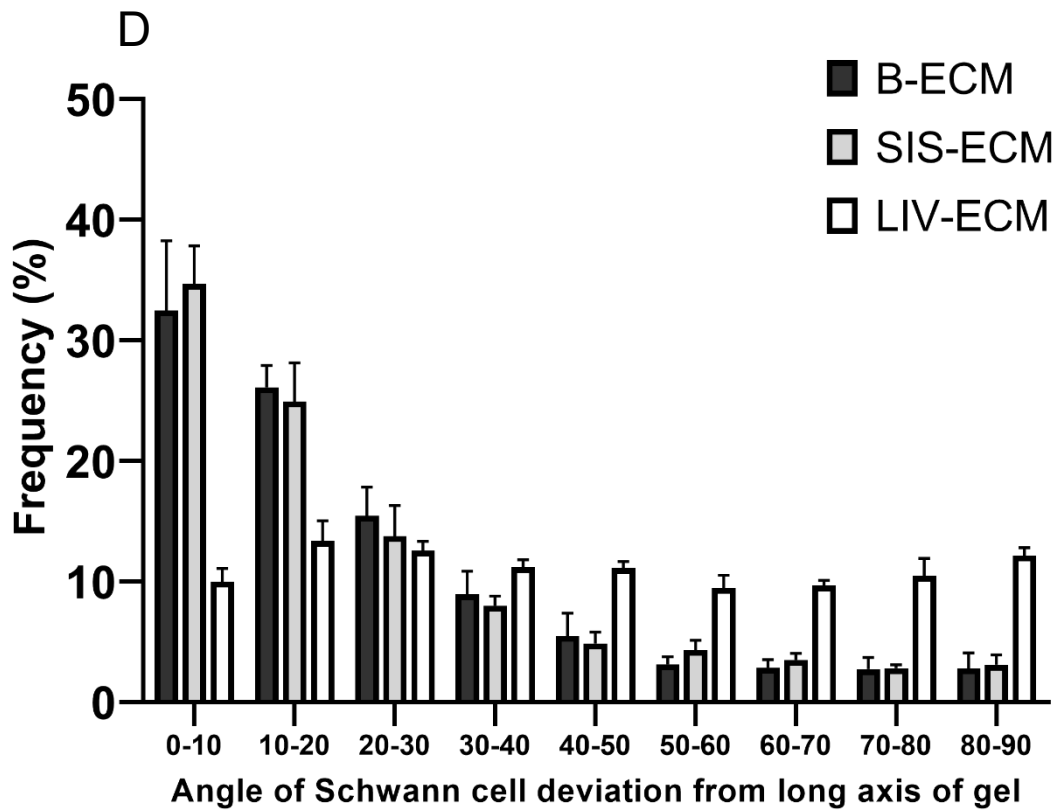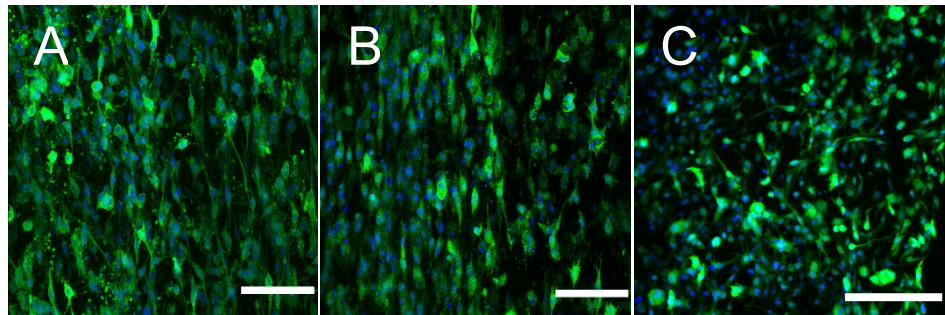
Figure 4.9 F7 SC alignment in dECM tethered hydrogels. Confocal micrographs of F7 SC embedded in 4 mg/ml B-ECM [A], SIS-ECM [B] and LIV-ECM [C] hydrogels. Angle of deviation of F7 Schwann cells in in 4 mg/ml B-ECM [A], SIS-ECM [B] and LIV-ECM [C] tethered hydrogels. Data are presented as mean ± SD, N = 4 independent constructs with 4 images from each construct. Scale bars = 100 μm

4.4.6 dECM coated coverslips can support DRG neurite extension
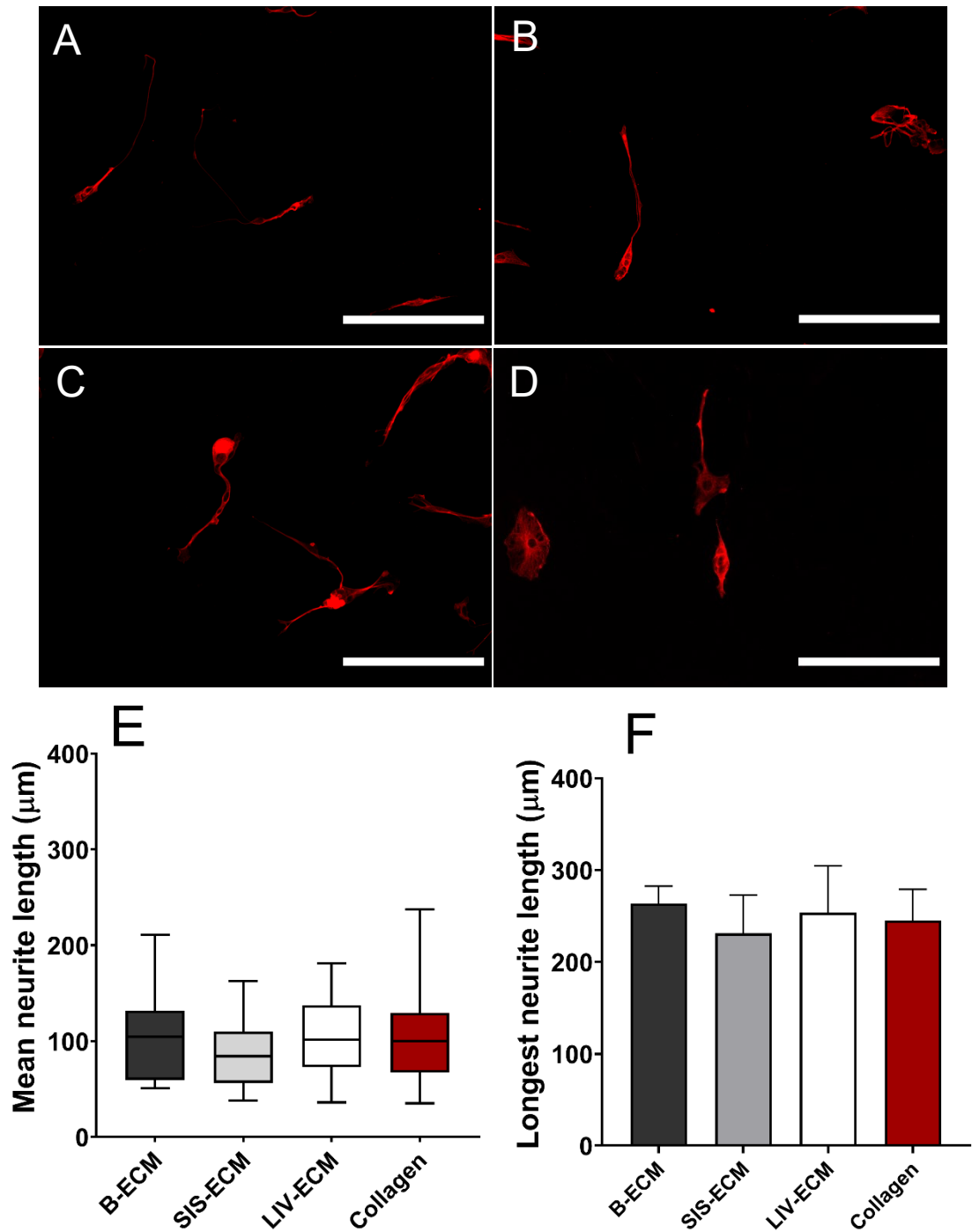
Figure 4.10 Effect of dECM and collagen coating on DRG neurite extension. Fluorescence images of isolated adult rat DRG neurons seeded on coverslips coated with 50 µg/ml B-ECM [A], SIS-ECM [B], LIV-ECM [C] and collagen I [D]. Scale bars = 200 µm. Quantification of neurite extension on dECM coated coverslips. Mean neurite length [A]. Boxes indicate upper and lower quartiles and whiskers indicate the maximum and minimum values of the data. Longest neurite [B]. Data are presented as mean ±SD. N = 8 coverslips with 4 images per coverslip.

PDL coated coverslips were coated with either 50 µg/ ml of B-ECM, SIS-ECM, LIV-ECM or collagen I and seeded with neurons isolated from rat DRG (cells from approx. 1 DRG per coverslip). After 72 hours extending neurites were observed on every material and extension from the cell body (full procedures and methods in section 2.7.2) was subsequently measured using ImageJ. Mean neurite length was around 100 µm for each material (Figure 4.9 E), whilst longest neurite length was further found to be comparable between materials at around 250 µm (Figure 4.9 F).

4.4.7 EngNT derived from dECM can support DRG neurite extension in vitro
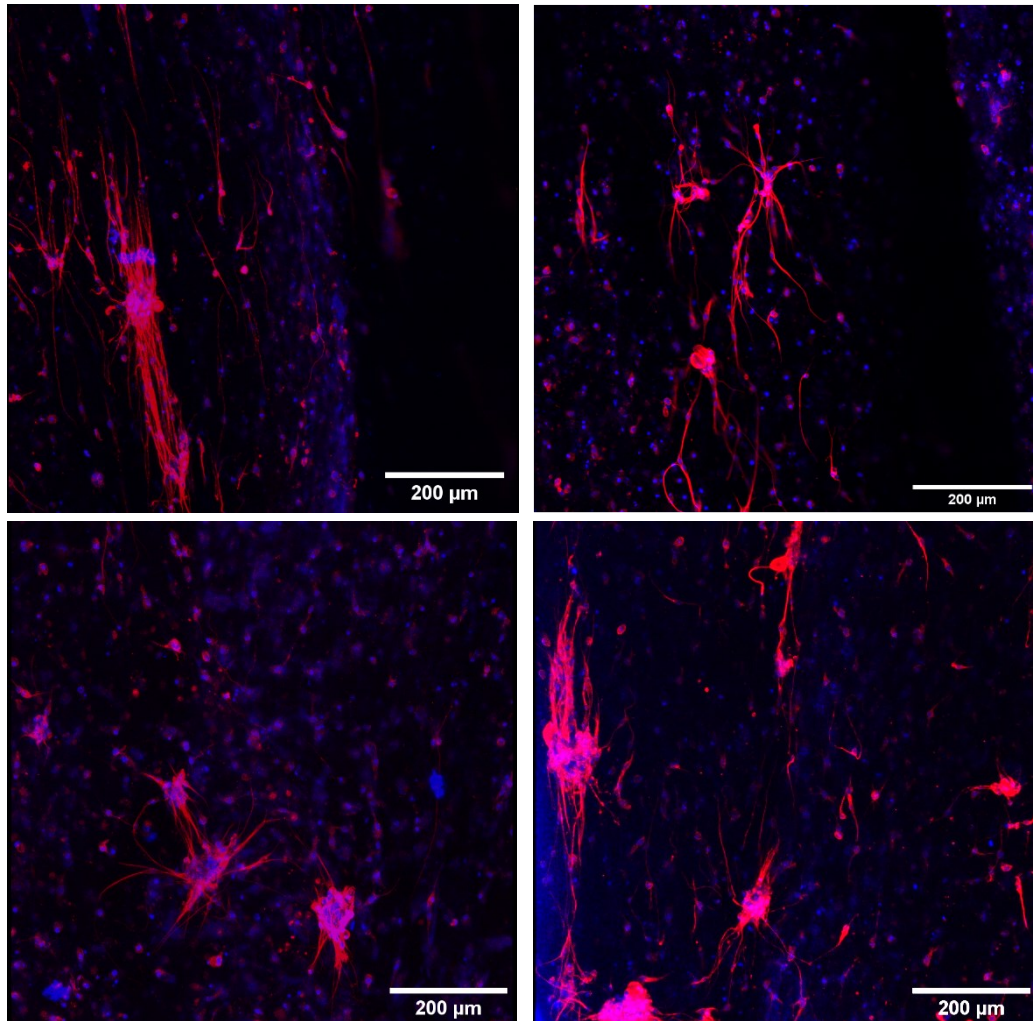
Figure 4.11 Effect of EngNT derived from different ECM materials on DRG neurite extension. Confocal micrographs of isolated rat DRG neurons seeded on 4 mg/ml B-ECM [A], SIS-ECM [B], LIV-ECM [C], and collagen I based EngNT with 4 x10^6/ml F7 Schwann cells. N = 3 independent constructs, with 3 DRGs seeded per construct, and imaged after 72 hours.

dECM EngNT and collagen based EngNT were seeded with DRG neurons. After 72 hours neurites were observed on every type of EngNT, visualised in the confocal micrographs (Figure 4.10 A-D) and the fluorescence images (Figure 4.11 A-D). However highly aligned neurites were only observed on B-ECM EngNT and collagen I EngNT (Figure 4.10 A & D and 4.12 A & D). Fluorescence images (Figure 4.11 A-D) were taken of every DRG and neurites were measured

in ImageJ (full protocol in section 2.11.2). B-ECM EngNT and collagen I EngNT were, on average, comparable for mean neurite length and for longest neurite. Likewise, SIS-ECM EngNT and LIV-ECM EngNT were comparable for mean neurite length (Figure 4.11 E) and longest neurite (Figure 4.11 F).
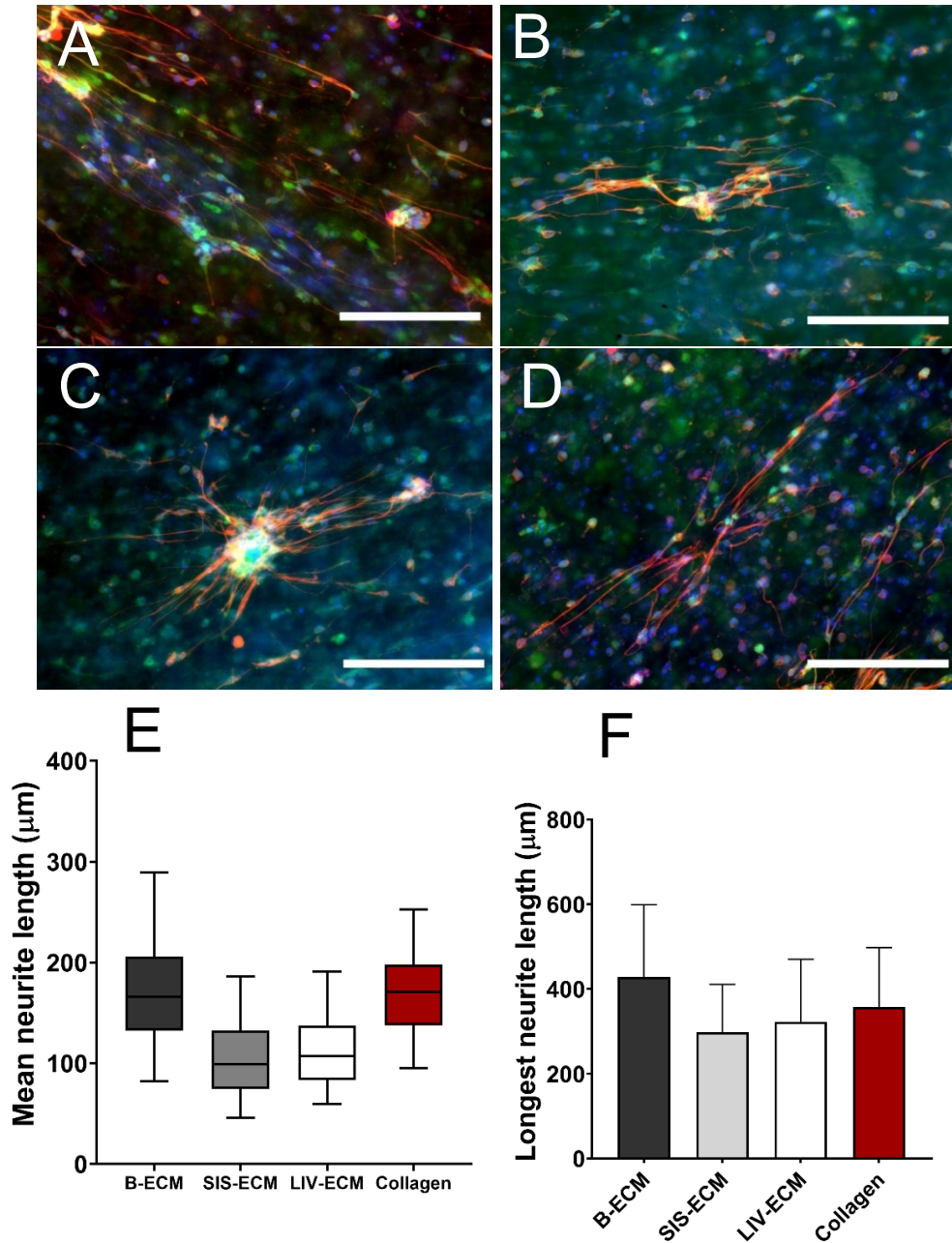
Figure 4.12 dECM derived EngNT constructs as substrates for neurite extension. Fluorescence images of rat DRGs seeded on EngNT derived from B-ECM [A], SIS-ECM [B], LIV-ECM [C], and collagen I [D]. Mean neurite extension [E]. Box plot boxes indicate upper and lower quartiles and whiskers indicate the maximum and minimum values of the data. Longest neurite [F]. Data are presented as mean ± SD. N = 4 constructs (approximately 15 – 25 DRGs measured per construct). Scale bars = 200 μm.

4.5   Discussion

Key components proven to improve the growth of axons include topographical cues, such as grooves or aligned fibres, or support cells that secrete ECM and neurotrophic factors (Muheremu and Ao, 2015, Tajdaran et al., 2019, Yi et al., 2019, Boni et al., 2018). When evaluating the application of Schwann cells, it is of importance to consider the biochemical and physical differences between their native and repair states; repair Schwann cell in the bands of Büngner are bipolar, elongated and possess a distinct biochemical profile secreting growth factors to promote neurite extension (Jessen and Mirsky, 2016, Jessen and Mirsky, 2019). We therefore established our fundamental criteria for producing successful EngNT for nerve repair as cellular alignment and neurotropism. The primary objective of this chapter was therefore to assess each of the dECM materials produced in Chapter 3 for their potential to produce aligned tissue engineered constructs that could further support neurite extension *in vitro*.

Studies on neurite behaviour have been numerous and *in vitro* work has illuminated complex multifactorial mechanisms affecting neurite extension. Neurites elongate further and faster on softer substrates (Balgude et al., 2001, Man et al., 2011, Yao et al., 2016). ECM components may further modulate neurite behaviour; laminin consistently improves neurite growth (Bailey et al., 1993, Deister et al., 2007, Fusaoka-Nishioka et al., 2011, Gonzalez-Perez et al., 2018), whilst certain sGAG such as chondroitin sulphate (CS) have proven to be inhibitory (Hynds and Snow, 1999, Yu and Bellamkonda, 2001). Additionally, culture media supplemented with matrix bound vesicles (mBVs) isolated from UBM resulted in increased neurite extension when compared to media alone (Faust et al., 2017). Anisotropy in the form of aligned fibres (Dodla and

Bellamkonda, 2006), microchannels (Shahriari et al., 2017) or cells (Georgiou et al., 2013, Georgiou et al., 2015) has further been shown to provide guidance cues to neurites resulting in superior regeneration. The introduction of neurotrophic factors further aids outgrowth and may be achieved through temporal release via incorporation into a biomaterial (Kim et al., 2007, Yang et al., 2005b) or by means of secretion from support cells (Woodhall et al., 2001, Zhang et al., 2020b, Carvalho et al., 2019). Support cells additionally provide axonal guidance through direct support and extracellular matrix remodelling and secretion (de Ruiter et al., 2009).

EngNT is a type of living artificial tissue containing highly aligned cells originally embedded in a purified collagen I hydrogel (Georgiou et al., 2013, Georgiou et al., 2015, Sanen et al., 2017). Previous work has investigated mechanisms of cellular contraction on collagen I hydrogels and the corresponding level of alignment in the resultant EngNT, with assays established to optimise cell seeding densities and gel concentrations to achieve this alignment (O'Rourke et al., 2015). In this study, this experimental design was adopted and applied to the dECM hydrogels seeded with F7 Schwann cells following an initial assessment of material influence on metabolic activity. We hypothesised that cell behaviour would likely differ between materials as a function of their variations in composition and physical characteristics.

Firstly, metabolic activity was measured using the 3D Cell Titer-Glo assay. B-ECM had the highest metabolic activity whereas SIS-ECM had the lowest of the dECM groups. Characterised differences in ECM composition or stiffness (Chapter 3) may account for this, as elevated dsDNA content has previously shown to negatively impact cell viability (Keane et al., 2012), whilst its lower

stiffness may further explicate the reduced metabolic activity (Gu et al., 2012). Conversely, the possibility of factors not quantified should not be dismissed, for instance, growth factor content; decellularised bone ECM is known to contain an array of BMPs that have been proven to modulate Schwann cell behaviour and therefore may possibly impact their metabolic activity (Kinameri and Matsuoka, 2003, Kokubu et al., 2018, Pietrzak et al., 2011, Thang et al., 2000). Moreover, differences in processing have further been proven to affect *in vitro* cell viability (Ren et al., 2013); residual detergent in the LIV-ECM from extensive processing may account for its lower cell viability when compared to the B-ECM of similar stiffness. Additionally, whether these differences in metabolic activity are a function of greater sustained cell survival or overall increases in F7 Schwann cell metabolic activity is unclear and this may require further investigation. The primary aim of this experiment was to identify any materials that had a clear detrimental impact on cell viability.

Contraction profiles based on those established in O'Rourke et al. (2015) were produced by seeding F7 Schwann cells at 1, 2 and 4 x 10^6 cells/ml in 4 and 6 mg/ml dECM hydrogels. Increasing the number of cells distributed within the hydrogel whilst reducing polymer concentration results in increased contraction, likely due to increases in the ratio of cell-fibril contact points (Ahearne, 2014). Consequently, as described for collagen by O'Rourke et al. (2015), the contraction of each material was dependent on both gel concentration and cell density. However, marked differences may be seen between the materials in their magnitude of contraction with the 4 mg/ml B-ECM cellular hydrogels being the most contractile. O'Rourke et al. (2015) present a threshold of around 60-80 % contraction in free-floating gels to be sufficient to predict acceptable alignment in

tethered gels made using the same material and cell parameters, and so, as this was approximately met by all three materials at 4 mg/ ml dECM hydrogels at 4 x 10^6 cells/ ml, they were taken forward to assess alignment. Following the identification of a cell seeding and hydrogel concentration to achieve appropriate levels of alignment, F7 Schwann cells were seeded into hydrogels in the tethered moulds used to produce EngNT. Lateral contraction was observed in all materials, although was most prominent in B-ECM and SIS-ECM, whilst it was lower in LIV-ECM. The dependency of contraction on cell-ECM interactions, specifically collagen I, was further investigated via blocking of integrin subunit α1 with anti-CD49α and, by observing the reduction in contraction, it can be determined the level of importance that collagen I interactions impose on the eventual formation of anisotropic tissue in each material (O'Rourke et al., 2015). Contraction is evidently dominated through cell-collagen I interactions in all three materials, however B-ECM hydrogels were most affected by the introduction of the anti-CD49α antibody. Although more contraction was observed in SIS-ECM compared to LIV-ECM hydrogels, the SIS-ECM was least affected by integrin α1 blocking. Drawing from data in the previous chapter and the literature, each ECM composition is known to be different (Coronado et al., 2017, Ji et al., 2019, Sierpowska et al., 2007). The presence of sGAGs, laminin, fibronectin and non-fibrillar collagens are likely to affect how cells interact with their ECM and the subsequent contractile forces imposed. Therefore, the differences in contraction observed may be attributed to the variation in ECM composition within the materials. Compositionally, bone matrix is estimated to be 90% collagen I (Sierpowska et al., 2007), likely influencing its similarity to collagen I hydrogels in contractile capabilities and further expounding the effect of α1 integrin blocking.

Conversely, LIV-ECM can contain up to 20% elastin (Coronado et al., 2017), a structural protein with limited integrin binding motifs, preferentially binding to elastin binding protein (EBP) instead. Proteomic analysis of porcine SIS (Ji et al., 2019) reveals an array of collagens present, the most abundant being collagen I, however, collagen V and VI (fibril/ beaded filament forming collagens respectively) were also present. The presence of additional fibril forming collagens in the SIS-ECM may uncover the mechanisms behind the materials' slighter response to α1 integrin blocking on the contractile forces; fibrillar collagens, along with other ECM components, may bind to other integrins and cell surface receptors to facilitate contraction.

PCR analysis of gene expression showed that, despite low protein concentrations of 4 mg/ ml, materials had differential effects on the expression of inflammatory, and Schwann cell phenotypic markers, whilst no difference was observed in the neurotrophic factors. IL-6 and LIF expression in Schwann cells show multiplicity in function; both recruiting macrophages (Tofaris et al., 2002) and promotion of axonal regeneration (REF). In fact, LIF has been shown to be a more potent promoter of neurite extension than brain derived neurotrophic factor (BDNF) (Gillespie et al., 2001). The downregulation of IL-6 and upregulation of LIF across all dECM-h therefore has interesting implications for the *in vivo* application of these materials. Both B-ECM and LIV-ECM hydrogels reduced expression of ROBO1 significantly. ROBO1 is upregulated in Schwann cells at the distal stump following injury (Chen et al., 2020) and coordinates macrophages and migratory Schwann cells in the nerve bridge following injury (Dun and Parkinson, 2020). SIS-ECM appeared to have the largest effect of the dECM-h, upregulating both GDNF and SOX10 (although not significantly). Yang et al. (2014) show that SIS-

ECM contains an array of neurotrophic factors such as BDNF, GDNF, and NGF. This may account for the slight differences observed in F7 Schwann cell gene expression between SIS-ECM and the other dECM materials.

Cellular self-alignment inside collagen hydrogels is known to be dependent on the level of cell-mediated contraction (O'Rourke et al., 2015). Following the formation of fully hydrated dECM-EngNT, constructs were assessed for alignment. Cellular alignment was comparable in B-ECM and SIS-ECM EngNT with cells presenting a more bipolarised, elongated morphology, that is more representative of a repair Schwann cell (Jessen and Mirsky, 2016, Jessen et al., 2015). These findings are further analogous to previous observations of cell morphology and alignment in collagen I based EngNT (Georgiou et al., 2013). In contrast F7 Schwann cells within the LIV-ECM EngNT were more spherical, non-polaraised and not aligned. As LIV-ECM exhibited around 50% contraction under these conditions, robust alignment was not expected. Elongation of cells and their nuclei are not only characteristic of a repair Schwann cell (Jessen and Mirsky, 2016, Wrobel and Sundararaghavan, 2018), but further upregulate c-Jun expression (Xu et al., 2020), a transcription factor that promotes downstream proregenerative neurotrophic signalling. Differences in material effect on Schwann cell behaviour is fundamental to this work when considering applications in nerve repair. The recreation of the conditions following nerve injury, wherein Schwann cells reprogramme into Büngner repair cells, is desirable for regeneration and so it may be reasoned that both B-ECM and SIS-ECM are suited to the production of EngNT.

DRG outgrowth on coated coverslips with dECM and collagen I was performed to observe material effect on the seeded neural cells. The resultant effects on

neurite extension would therefore be a function of the biochemical profiles of the materials on the DRG neurons or glial cells in the culture, as the stiffness of the glass coverslips dictate the mechanical properties exerted on the cells. In other words, the variation in stiffness between the dECM materials is removed. No discernible differences in average neurite length were observed, implying the differences in biochemical composition are insignificant and the molecular interactions between ECM and neurite are less impactful than their mechanical properties. A concentration of 50 µg/ml was chosen as it is within the standard range for coating with PDL and collagen (Cooke et al., 2008, Armstrong et al., 2007), however dECM hydrogels have been coated at higher concentrations with some studies using as high as 1 mg/ ml (Zou et al., 2018). A considerable increase in the quantity of biological factors, such as GAGs and cytokines, could make the differences in their effect on neurite behaviour more pronounced. Coating coverslips at varying protein concentrations may therefore be of interest in the future. Zou et al. (2018), for example, report DRG neurite length at 48 hours of over 1 mm with significant differences observed between dECM coatings, Matrigel, and collagen I coatings of 1 mg/ml. However, DRGs were harvested from neonatal rats (day 1), compared to the adult rats used in this chapter, possibly further accounting for the increases in neurite length (Argiro and Johnson, 1982, Ng and Lozano, 1999, Tsai et al., 1998).

Following optimisation for achievable plastic compression (as described in section 4.3), stabilised sheets of dECM EngNT were used as substrates for a further DRG outgrowth assay, using collagen I based EngNT as a comparator, to evaluate the potential of each dECM EngNT to support and guide axonal regrowth. It was chosen as the last experiment before material selection for *in*

vivo models as the outcome is dependent on multiple variables that have been investigated in this chapter: SC viability, behaviour and alignment, material stiffness, as well as soluble factors present within the dECM.

DRGs seeded on B-ECM EngNT had longer neurites than those of SIS-ECM and LIV-ECM and were comparable to those seeded on collagen I based EngNT. Moreover, neurites were directional on B-ECM EngNT extending outwardly from their cell bodies along the axis of F7 Schwann cell alignment. B-ECM EngNT showed high levels of alignment, whilst a higher F7 Schwann cell metabolic activity was observed in B-ECM hydrogels. These may contribute to promote elongated, unidirectional neurites. DRGs seeded on SIS-ECM EngNT were somewhat aligned along the axis of F7 Schwann cell alignment, they occasionally diverged and were shorter than those on B-ECM EngNT and collagen I EngNT. Despite the highly aligned SC observed, the lower stiffness and subsequent structural integrity of SIS-ECM EngNT may influence the nondirectional outgrowth of neurites, whilst further rationalisation may be attained from its lower F7 Schwann cell viability/ metabolic activity. Certain sGAGs are inhibitory to neurite growth (Yu and Bellamkonda, 2001), and this could have been a further explanation for the lower neurite extension observed in SIS-ECM and LIV-ECM EngNT, however, this was not reflected in the coverslip assay. Non-directional neurite elongation was observed on LIV-ECM, most likely due to lack of Schwann cell alignment. This was likely further cause for its comparatively shorter neurite lengths. Moreover, the low neurite extension in the SIS-ECM may be attributed to a lower F7 Schwann cell viability, or its lower structural integrity as a result of its stiffness (Chapter 3). Xu et al. (2020) show that encouraging morphological changes in Schwann cells, such as elongation, has an impact on protein

expression of c-Jun; a well-known "pro-regenerative" Schwann cell marker (Jessen and Mirsky, 2016, Jessen et al., 2015). Caution must therefore be applied when relating the phenotypic changes observed in the PCR data to differences in neurite extension. Expression of the immunomodulatory and neurotrophic factors in aligned EngNT constructs may therefore be of interest in further studies.

Taking into account both neurite extension studies, it may be asserted that differences in dECM composition have little direct impact on neurite extension. Whereas, the multifaceted influences from the dECM upon the cultured F7 Schwann cells, and the characteristics of the resultant EngNT, drive the differences observed in DRG neurite extension

4.6 Conclusions

Significant differences were observed in cell viability between every material with F7 Schwann cells seeded in B-ECM exhibiting higher metabolic activity than F7 Schwann cells seeded in every other material. Contraction and integrin blocking experiments indicated that cell-ECM interactions are driven via collagen I interactions. Highly aligned F7 Schwann cells were observed in B-ECM and SIS-ECM EngNT and alignment was similar to that observed previously in collagen I EngNT. No differences were observed in neurite extension on coated coverslips, implying differences in ECM composition have little direct impact on neurite outgrowth over a 48 hour period. Conversely, neurite extension varied on EngNT constructs, most likely as a function of ECM influence on Schwann cell behaviour as well as differences in EngNT structural integrity. This study, whilst not exhaustive, was an investigation into the effects different dECM impart on neural cells *in vitro*. As expected from their mechanical and biochemical differences

characterised previously, both Schwann cell and neuronal behaviour differed. From these assays a singular candidate material (B-ECM) was identified, to be taken forward into an *in vivo* rat nerve injury model.

Chapter 5 Comparative *in vivo* performance of B-ECM EngNT and collagen I EngNT

5.1 Introduction

Following the *in vitro* testing of the dECM-h in Chapter 3, one candidate (B-ECM) was deemed appropriate for further investigations in an *in vivo* model. B-ECM hydrogels seeded with F7 Schwann cells formed anisotropic tissue and promoted directional neurite extension similar to collagen I EngNT. It was therefore hypothesised that EngNT derived from B-ECM hydrogels would be able to promote axonal regeneration *in vivo.*

5.1.1 *Review of 10 mm sciatic nerve transection models*

At a gap length of 10 mm distance, nerve regeneration is eventually observed in empty tubes (Lundborg et al., 1982), and so, this length was chosen for the model to assess EngNT performance against spontaneous regeneration. Moreover, a time length of 4 weeks was chosen for this model to provide a rapid preliminary understanding of the material effect on axonal regeneration. Prior to the development of a device capable of being implanted *in vivo*, a literature search was performed to assess current trends in 10 mm sciatic nerve gap repair models' design. Table 5.1 outlines different NGC implanted into 10 mm sciatic nerve injury models from the past 5 years along with their positive and negative controls, measurement of histological and functional outcomes, and their key findings. Parameters to measure regeneration, as well as the use of positive and negative controls were evaluated to validate this model.

44 out of the 46 studies used a rat model whilst 1 opted for rabbit and another mouse. Possibly due to the relatively short gap length of 10 mm, only 15 studies incorporated support cells within the lumen. Over half of the studies chose to

evaluate NGC performance alongside an autograft, whilst 10 chose to compare with normal nerve, and 6 had no positive control whatsoever. Moreover, 7 out of 46 decided to not introduce a negative control. For the other 39 studies, the most common negative control was an empty tube, either an empty or unmodified conduit material, or a silicone tube. All studies that used an empty conduit as a negative control reported positive outcomes from tissue engineered/ modified experimental groups at earlier time periods that become more pronounced as the studies progressed. However, two studies that measured for longer time periods noticed that differences in functional measurements such as sciatic functional index (SFI) and nerve conductance velocity (NCV) were reduced as regeneration was observed within empty tubes (Hsieh et al., 2016, Hu et al., 2016).

5.1.1.1   *Outcome measure of regeneration*

One technique to evaluate regeneration is to assess the number of axons present at defined regions within the grafts and nerve tissue. The majority of the studies presented in Table 5.1 give axon counts at the midpoint of implantation (Roche et al., 2017, Hsieh et al., 2017, Pan et al., 2017, Chang et al., 2018, Gontika et al., 2018, Yen et al., 2019, Sayanagi et al., 2020). Others prefer to present the data as axon number at the midpoint of implantation per mm^2 of the cross sectional area (Mokarizadeh et al., 2016, Iman et al., 2017, Zhao et al., 2017b, Golzadeh and Mohammadi, 2016, Ilkhanizadeh et al., 2017, Mehrshad et al., 2017). Alternatively, some studies opt to count at the distal region of the device (Kim et al., 2018b, Liu et al., 2019b, Labroo et al., 2019, Gu et al., 2017). However, a more detailed account of the regeneration process may be gained through investigating axon counts at different parts of the device; Di Summa et al. (2018) show distinct differences in axon area between the midpoint and distal

devices. Muangsanit et al. (2020) develop this further by counting axons in the nerve tissues of the proximal and distal stumps, as well as the proximal and distal regions of the device. The counting of axons at the proximal end of the device, as a percentage of the proximal stump of the nerve, can indicate how accommodating the construct is to infiltration of axons from the proximal stump. Similarly, counting axons at the distal device, as a percentage of the proximal device, can indicate how supportive the inside of the NGC is to neurite outgrowth.

Blood vessel formation in nerve repair is also of interest, providing the regenerating tissue with essential nutrients as well as structural guidance for the infiltration of Schwann cells (Garcia-Diaz et al., 2019, Cattin et al., 2015) and axons (Grasman and Kaplan, 2017). Three studies chose to qualitatively assess blood vessel formation, whilst Wang et al. (2018) quantified blood vessels as a percentage of the area of the regenerated nerve, Yen et al. (2019) counted blood vessel number in representative images. Muangsanit et al. (2020), in contrast, counted total blood vessels in cross-sections at distinct regions of the device, as well as measuring lumen diameter.

Assessments such as SFI, sciatic static index (SSI), and electrophysiology may be employed when questions regarding functional recovery are raised. 10 of the studies did not include functional outcome assessments, likely as a result of relatively short experimental periods.

5.1.1.2   Tube material

Natural based conduit materials account for 44% of the studies presented, whereas 21% were formed from synthetic materials. The other 35 % were made using combinations of natural and synthetic polymers such as the polycaprolactone-collagen blend used in (Labroo et al., 2019) to deliver

tacrolimus. The most common natural material for conduits was chitosan (used in 10 studies) followed by type I collagen (8 studies).

Spontaneous nerve regeneration is facilitated within silicone chambers at gap lengths of 10 mm and under (Lundborg et al., 1982). Silicone was further shown to be relatively inert (Dahlin et al., 2001) and as such, was approved for clinical use. Ultimately, however, inflammatory reactions are observed over time periods of months to years, leading to the removal of the tubes (Merle et al., 1989). Three of the studies presented in Table 5.1 use silicone as the outer material for the NGC, whilst a further 3 employed an empty silicone tube as the negative control.

5.1.1.3   *Luminal fillers*

Possibly due to the short gap length, only 15 of the 46 studies opted for the inclusion of a cellular component within the lumen. Five studies transplanted Schwann cells or Schwann cell lines, whilst Di Summa et al. (2018) employed allogeneic adipose derived stem cells (ASC) differentiated into Schwann like cells. On the other hand, Klein et al. (2016b) and Hu et al. (2016) utilised undifferentiated autologous ASCs. The most common ECM component used as a luminal filler was collagen I (Farzamfar et al., 2017, Fukuda et al., 2018, Jeon et al., 2018a, Muangsanit et al., 2020). Gu et al. (2017), on the other hand employed a luminal filler of acellular matrix derived from bone marrow stem cells (BMSC), whereas Roche et al. (2017) used HA and laminin to deliver olfactory derived stem cells (OSC). Three of the 6 studies that incorporated growth factors opted for NGF whilst others used GDNF (Labroo et al., 2019), bFGF (Fukuda et al., 2018), or platelet-derived growth factor (PDGF) (Golzadeh and Mohammadi, 2016).

Table 5.1 Differences in conduit material, filler, support cell, and assessment of outcome measures for 10-mm sciatic nerve repair models over the past 5 years.
Search criteria: "nere repair" AND "sciatic" AND "conduit" AND "10-mm".
Exclusion criteria: no in vivo, repair of gaps under or over 10-mm, not sciatic

Conduit	Filler	Animal	Positive control	Negative control	Histology	Functional	Key findings / outcome	References
Chitin	CM chitosan	Rat	Autograft	Empty chitin tube	4, 12, 20 weeks	12, 20 weeks	Diameter and density of myelinated nerve fibres as well as NCV recover comparable to autograft after 20 weeks and superior to empty tube.	(Jiang et al., 2019)
Chitosan		Rat	Autograft	None	12 weeks	None	Proximal sections thicker suggesting ongoing regeneration at 12 weeks	(Yin et al., 2018)
Chitosan	Methylprednisolone hydrogel	Rat	Autograft	No treatment	16 weeks	4, 8, 12, 16 weeks	Axon counts for MP hydrogel comparabe to autograft, axon diameter higher than hdyrogel alone, myelin sheath not as thick as autograft.	(Mehrshad et al., 2017)
Chitosan	BMMC	Rat	Sham	Empty chitosan tube	12 weeks	12 weeks	BMMC filled conduit higher axon counts and better SFI compared to empty conduit.	(Ilkhanizadeh et al., 2017)
Chitosan	NGF-mPEG-PELG	Rat	Autograft	Empty chitosan tube	2, 12 weeks	12 weeks	NGF/mPEG-PELG group had similar axon count and myelin diameter to autograft as well as CMAP and MNCV. Hydrogel bound NGF far superior to IM NGF.	(Liu et al., 2019b)
Chitosan	Fibrin nanofibers	Rat	Autograft	Empty chitosan tube	12 weeks	12 weeks	Aligned fibrin nanofibers showed significantly improved CMAP, myelination, and Schwann cell infiltration to random fibrin fibres.	(Du et al., 2017)
Chitosan	P F-127/ P F-127 + simvastatin	Rat	Normal nerve	Empty chitosan tube	10 weeks	4, 6, 8, 10 weeks	Dose dependent response observed. SFI difference seen at all time points. Almost comparable to autograft.	(Guo et al., 2018)
Chitosan	PEG	Rat	Sham/ autograft	Empty chitosan tube	6 weeks	2, 4, 5, 6 weeks	Chitosan PEG lower SFI, higher muscle weight, and more axons/ mm2 than empty chitosan. Autograft remains superior.	(Mokarizadeh et al., 2016)
Chitosan	BMSC-ECM – silk fibroin	Rat	Normal nerve	Empty chitosan tube	1, 2, 12 weeks	12 weeks	Differences seen at 1 and 2 weeks between ECM group and empty conduit in regenerating axons. At 12 weeks CMAP similar to normal nerve in ECM group.	(Gu et al., 2017)
Chitosan/ ZnO		Rat	Sham	No treatment	12 weeks	4, 8, 12 weeks	Chitosan with ZnO better than empty tube in SFI and myelin at 4 weeks (faster recovery).	(Iman et al., 2017)
Collagen I	Collagen	Rabbit	Autograft	Silicone tube	13 weeks	13 weeks	Autograft far superior to collagen filled conduit, collagen conduit only significantly higher in axon diameter to empty tube	Jeon et al., (2018)
Collagen I	CSF	Rat	Autograft	Empty collagen tube	4, 12 weeks	1, 3, 6, 8, 16 weeks	Improved SFI. More blood vessels and myelinated fibres to empty collagen tube.	(Farjah et al., 2017)

Collagen I	ASC	Rat	None	Empty collagen tube	24 weeks	24 weeks	ASC improved conduction velocity vs empty conduit with thicker, more aligned cells within the conduit.	(Klein et al., 2016b)
Collagen I	microRNA-338 and microRNA-21	Rat	Normal nerve	Empty collagen tube	8 weeks	8 weeks	microRNA group showed imprved SFI, higher axon counts, and myelin thickness than empty conduit.	(Wang et al., 2016)
Collagen I	HA, laminin, OSCs/ OSCs + NGF	Rat	None	Empty tube	8 weeks	8 weeks	ONS + NGF>ONS>Empty tube. Improved SFI and higher axon counts.	(Roche et al., 2017)
CryoGelMA	ASC	Rat	Autograft	Empty CryoGelMA tube	16 weeks	4, 8, 16 weeks	ASCs improve conduit slightly compared to empty tube. Improvements in CMAP and NCV compared to empty tube seen at 4 weeks, not as apparent after 16 weeks.	(Hu et al., 2016)
Fibrin	dASC	Rat	Autograft	Empty fibrin tube	12 weeks	None	dASC filled conduit more axon coverage lower collagen coverage than empty conduit. Comparable myelin coverage to autograft.	(Di Summa et al., 2018)
Fibrin		Rat	Sham and autograft	None	12 weeks	4, 8, 12 weeks	Fibrin reached around 60 % axon density to autograft. SFI significantly poorer compared to autograft.	(Longo et al., 2016)
Gelatin/ PU	SC/ melatonin/ platelet rich plasma	Rat	Autograft	None	12 weeks	4, 8, 12 weeks	Conduits containing SCs, melatonin and platelet rich plasma outperformed all others aside from autograft.	(Salehi et al., 2018a)
HEC/ soy protein sponge		Rat	Autograft	None	12 weeks	None	Conduits with more pores showed higher axon counts and larger axon diameter as well as better CMAP recovery. Not comparable to autograft.	(Zhao et al., 2017b)
NHDF bioconduit		Rat	Autograft	Empty silicone tube	8 weeks	8 weeks	Comparable myelin thickness and axon diameter but poorer CMAP recovery to autograft.	(Takeuchi et al., 2019)
PCL	PCL nanofibres	Rat	Autograft	PCL tube	6 weeks	0, 2, 4, 6 weeks	Aligned fibres showed similar CMAP to autograf but lower axon counts and myelinated area.	Chang et al., (2018)
PCL	Agarose microchannels	Rat	None	Empty PCL tube	8 weeks	None	Conduits containing agarose channels showed directional axon growth and SC infiltration compared to disorientated axons and SCs in hollow tube.	(Shahriari et al., 2017)
PCL-collagen		Mouse	Normal nerve	Silicone tube	8 weeks	8 weeks	Experimental group higher nerve fibre, blood vessel number and nerve area than silicone tube. Not comparable to normal nerve.	(Yen et al., 2019)
PCL-collagen-nanobioglass	NGF	Rat	Autograft	No treatment	12 weeks	4, 8, 12 weeks	NGF supplemented conduits comparable to autograft at 12 weeks for CMAP and hot plate latency. Significantly outperformed empty conduit.	(Mohamadi et al., 2018)

Material	Cells/Factors	Model	Control	Conduit	Functional endpoint	Histological endpoint	Outcome	Reference
PCL/ Gelatin	USSC		Normal nerve	Empty PCL/ gelatin tube	14 weeks	14 weeks	USSC improved outcomes of hot plate latency, SFI, and CMAP recovery. Comparable muscle fibre are to autograft.	(Farzamfar et al., 2019)
PCL/ Gelatin	Collagen I and MenSCs	Rat	Autograft	PCL/ gelatin/ collagen conduit	None	4, 8 weeks	MenSCs in conduit performed better than conduit alone; less wet weight loss and better SFI.	(Farzamfar et al., 2017)
PDLLA/ RGD/ β-TCP		Rat	Normal nerve	PDLLA conduit	5 weeks	None	At 5 weeks clear increases in muscle and nerve fibre diameter and blood vessel formation in bioactive (RGD) PDLLA compared to unmodified PDLLA conduit.	(Li et al., 2016a)
PHBV	dASC	Rat	None	Empty PHBV tube	10 weeks	10 weeks	Aligned nanofibre + dASCs> ANF ASCs> Empty tube in walking track analysis, SFI, and percentage axon coverage.	(Hu et al., 2017)
PLA-ASC		Rat	Autograft	None	6 weeks	2, 4, 5, 6 weeks	Seeding cells on the outside of the conduit improved functional and histological outcomes, not comparable to autograft.	(Hsieh et al., 2016)
PLA/ MWCNTs/ Gelatin/ Chitosan	SC	Rat	Autograft	No treatment	14 weeks	4, 8, 14 weeks	Combination of cells, drug loaded nanoparticles, and MWCNTs, improved conduit outcomes in weight loss, muscle fibre mass, electrophysiology, and hot plate latency.	(Salehi et al., 2018b)
PLCL	MVSC	Rat		Empty PLCL conduit	8 weeks	4, 8 weeks	MVSC resulted in faster CMAP recovery than autograft. Qualitative analysis shows MVSCs differentiated into perivascular cells and formed blood vessels.	(Huang et al., 2019)
PLCL-MCL		Rat		Empty PLCL conduit	8 weeks	4, 8 weeks	Optimal MCL concentration of 15% observed for myelin fibre diameter and thickness. 25% improves NCV. All concentrations superior to unmodified PLCL films.	(Zhang et al., 2020a)
PLGA	PBMSCs and peptide gel	Rat	Normal nerve	Empty PLGA conduit	16 weeks	15 weeks	Axon count, myelination higher than empty, lower than autograft. Functional recovery better than empty conduit, poorer than autograft	(Pan et al., 2017)
PLGA	OBC-COL sponge	Rat	Autograft	Empty PLGA conduit	8 weeks	2, 4, 8 weeks	NGC with luminal filler was comparable to autograft after 8 weeks, some differences in function at 2 and 4 weeks.	(Hou et al., 2019)
PLGA-collagen	Collagen-bFGF	Rat	Normal nerve	Empty conduit	2, 4, 8, 20 weeks	None	bFGF improved SC migration into conduits and was associated with improved myelination	(Fukuda et al., 2018)
PTFE	FK506 – GDNF	Rat	None	Empty tube	10, 18 weeks	10, 18 weeks	FK506 and GDNF comparable after 10 weeks for muscle atrophy. More axons in GDNF group at 10 weeks, FK506 comparable to GDNF after 18 weeks.	(Labroo et al., 2019)
PU		Rat	Normal nerve	Neurotube	6 weeks	6 weeks	Regenerated axon area higher for PU than PLA. Improved SFI and CMAP to Neurotube.	(Hsu et al., 2017)

Material	Additive/Cells	Animal	Control	Comparison	Endpoint	Analysis time	Outcome	Reference
Silicone	PDGF	Rat	Normal nerve	Empty silicone tube	12 weeks	Weekly up to 12 weeks	Higher axon counts and myelin thickness, muslce weight similar to normal nerve in PDGF group	(Golzadeh and Mohammadi, 2016)
Silicone	Collagen I-SC	Rat	Autograft	Empty silicone tube	4 weeks	None	Axon counts in distal device lower than autograft but with similar blood vessel counts	(Muangsanit et al., 2020)
Silicone	COS - SC	Rat	NGF filled tube	Empty silicone tube	2 weeks	None	Inflammatory markers significantly reduced by COS after 7 days *in vivo* associated with faster regeneration than an NGF filled silicone tube.	(Zhao et al., 2017a)
Silk	SC	Rat	Autograft	Empty silk tube	16 weeks	None	Aligned tube with cells almost comparable to autograft in myelin, axon and muscle fibres	(Ebrahimi et al., 2018)
Silk fibroin-P(LLA-CL)		Rat	None	Pure P(LLA-CL)	3 weeks	None	SF/ P(LLA-CL) superior in regenerated axons, SC counts and blood vessels to unmodified P(LLA-CLL).	(Wang et al., 2018)
Silk fibroin-PLA	Microchannels	Rat	Autograft	None	20 weeks	Weekly up to 20 weeks	Microchannels improved regeneration, however micropores on conduit wall may cause infiltration of fibroblasts and impair regeneration.	(Zhou et al., 2017)
UBM		Rat	Autograft	None	6 weeks	3, 6 weeks	UBM conduit had more sensory neurons than autograft and similar motor. Foot fault and weight loss similar at 6 weeks between groups	(Nguyen et al., 2017a)
Zein	Microchannels	Rat	Autograft	Non-porous zein conduit	8 weeks, 16 weeks	2, 4, 8, 12, 16 weeks	Microchannels little effect on conduit in functional tests and myelinated axons. Both porous and porous microchannels better than non-porous conduit but not as good as autograft	(Wang et al., 2017a)

Abbreviations: ASC – adipose derived stem cells, bFGF – basic fibroblast growth factor, BMMC – bone marrow, BMSC-ECM – bone marrow mesenchymal stem cell derived ECM, CMAP – compound muscle action potential, COS – chitooligosaccharides, CryoGelMA - cryopolymerised gelatin methacryloyl, CSF – cerebrospinal fluid, dASC – differentiated adipose derived stem cells, HEC - hydroxyethyl cellulose, MVSC - multipotent vascular stem cells, MWCNT – multi-walled carbon nanotubes, NSC – neural stem cell, NGF – nerve growth factor, OSC – olfactory derived stem cells, PBMSC - peripheral blood-derived mesenchymal stem cells, PEG – polyethylene glycol, P F-127 – Pluronic F-127, PHGV - Poly (3-hydroxybutyrate-co-3-hydroxyvalerate), PLCL – poly(l-lactide-co-ε-caprolactone), PLGA - poly(lactic-co-glycolic acid), P(LLA-CL) - poly (l-lactide-co-E-caprolactone), SC – Schwann cells, UBM – urinary bladder matrix, USSC - Unrestricted Somatic Stem Cells

5.2   Chapter aims

Chapter 4 identified a singular candidate from our portfolio of decellularised ECM hydrogels (dECM-h) that could promote directional *in vitro* DRG neurite extension when incorporated into EngNT with F7 Schwann cells. B-ECM hydrogels of 4 mg/ml and a cell seeding density of 4×10^6 F7 Schwann cells was found to promote comparable neurite extension to EngNT derived from purified rat tail type I collagen of a concentration of 2 mg ml. dECM are complex materials that can induce unique cellular responses *in vitro* and *in vivo*, promoting positive tissue remodelling in injury sites (Crapo et al., 2011). It was therefore hypothesised that B-ECM EngNT would be able to promote neurite extension *in vivo*.

The primary objective of this chapter was to explore B-ECM derived EngNT as a possible alternative to the currently used purified rat tail type I collagen derived EngNT. Direct comparison of the B-ECM and collagen EngNT within silicone conduits using an *in vivo* nerve transection model was carried out to assess axonal regeneration and vascularisation, specifically quantifying number of axons and blood vessels in different regions of the devices, and qualitatively assessing Schwann cell infiltration.

5.3   Experimental design

As Angius et al. (2012) state, the specific research question is critical to *in vivo* study design. This study aimed to compare two materials that perform similarly *in vitro* for their *in vivo* capabilities of promoting axonal regeneration. As such, a short gap repair with a relatively short time period (4 weeks) was chosen alongside a negative control of an empty tube with an autograft as a positive control. From reviewing the literature (Table 5.1), a recovery time of 4-weeks in a gap length of 10 mm, empty tubes will not effectively support robust

regeneration, whilst regenerating axons are likely to be seen at the distal end of an autograft. This model was therefore chosen as it will provide a scale of regeneration, ranging from negligible (empty tube) to robust (autograft), within which the two EngNT groups may be compared. Additionally, due to the short time period it was deemed appropriate to employ a silicone tube as the outer sheath material; adverse inflammatory reactions and fibrosis were expected to be insignificant.

A detailed account of the graft preparation and surgical procedures may be found in Section 2.8.2. EngNT was produced as described (Chapter 4.3) and cut to a length of 10 mm before insertion into a 12 mm long silicone tube. 1 mm of the proximal and distal stumps were placed into the proximal and distal ends of the tube respectively and sutured in place.

Nerves were prepared for histological analysis as shown in Figure 5.1. Nerves were dissected 2 mm either side of the suture sites to provide 4 mm long regions of interest. For this study, proximal and distal devices were sectioned and imaged as described in Section 2.8.3.
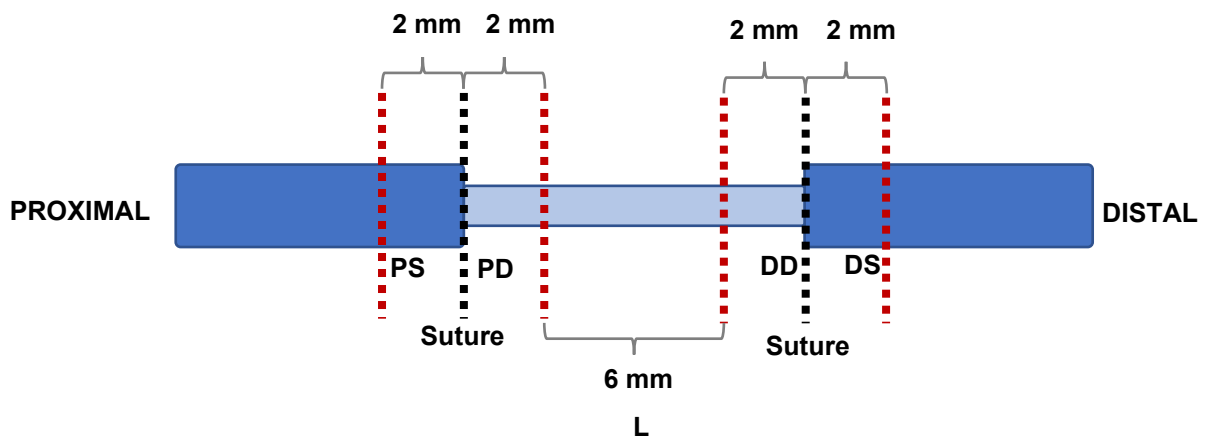
Figure 5.1 Nerve tissue preparation for sectioning. PS = proximal stump, PD = proximal device, DD = distal device, DS = distal stump, and L = longitudinal. Red dotted lines indicate dissection (3 samples per nerve).

5.4 Results

5.4.1 Robust tissue-bridge observed in B-ECM EngNT and collagen EngNT 28 days after implantation

Following a one-day incubation period with 4 x 10^6 F7 Schwann cells to achieve contraction and subsequent alignment, EngNT constructs derived from either B-ECM hydrogels or rat tail type I collagen were placed in a silicone tube that was longitudinally cut open prior to EngNT insertion, and sealed using superglue. Conduits were then sutured into a 10 mm sciatic nerve transection model and the animals left for 4 weeks (Surgery performed by Dr. Roberton). Due to autotomy of the hind paw, one animal from the autograft group was terminated before the designated study end point.

Following the 4-week study period rats underwent termination via an overdose of anaesthesia and the ipsilateral and contralateral nerves were removed for analysis.
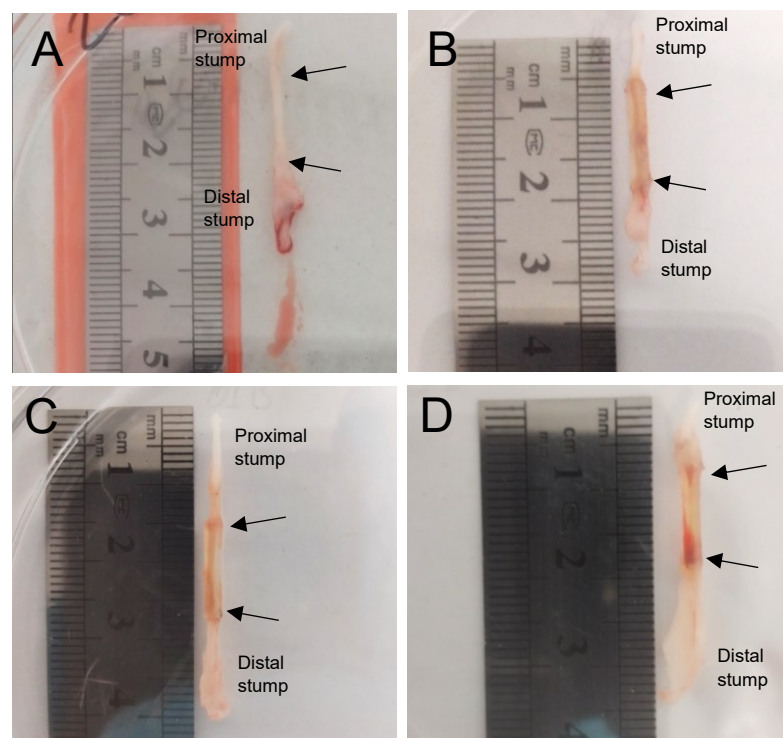
Figure 5.2 Harvested constructs 28-day post implantation. Autograft [A]. EngNT from collagen [B] and B-ECM [C] derived hydrogels, and empty silicone tube [D]. Arrows indicate suture sites.

At the endpoint a thin tissue bridge may be seen traversing the 10 mm between the proximal and distal stumps of the empty conduit (Figure 5.2 D). Both EngNT groups possess a more robust tissue bridge (Figure 5.2 B & C) whilst the autograft showed no signs of aberrant growth with continuity of the epineurium at both suture points (Figure 5.2 A).

5.4.2 Quantitative analysis of neurofilament positive axons at the proximal and distal devices after 28 days

The magnitude of axonal regeneration was assessed via counting of axons in the proximal and distal devices of empty tubes, B-ECM and collagen derived EngNT, and autografts. Densely populated axons were observed in the proximal device locations in all groups (Figure 5.4 A). Quantification of axons at the proximal device showed the highest number for the autograft with 8144 ± 929, whilst the empty tube axon count was the lowest with 6323 ± 531 (Figure 5.4 B). In comparison B-ECM and collagen I EngNT had 7583 ± 1139 and 7030 ± 396, respectively. Axons were also observed in the distal device of B-ECM EngNT, collagen EngNT, and autograft groups (Figure 5.4 A). Axonal counts at the distal device were highest in the autograft group with 6098 ± 660 axons present (Figure 5.4 B). Axons in the distal devices of B-ECM and collagen derived EngNT were 2461 ± 1083 and 1967 ± 403 respectively (Figure 5.4 B). Very few axons were observed in the distal device of empty tubes (Figure 5.4 A) and this can further be seen in the quantitative data (Figure 5.5 B). Percentage regeneration from the proximal to distal devices was highest in the autograft at 75.2 ± 6.4 %, compared to collagen and B-ECM EngNT; 28.1 ± 6.5 and 32.4 ± 12.8 %, respectively (Figure 5.4 C).
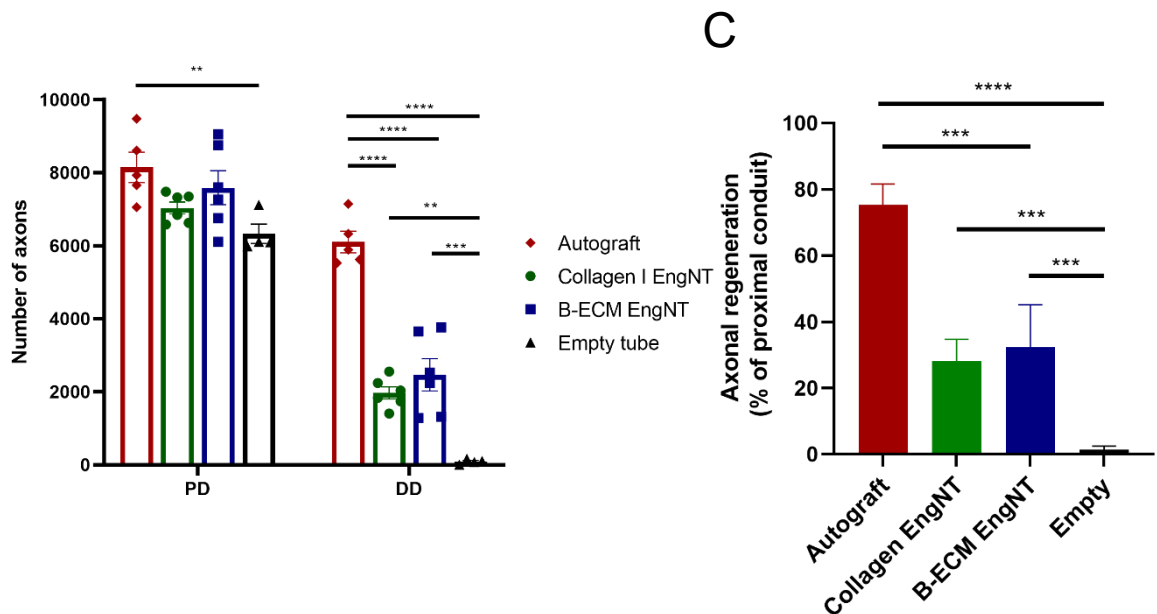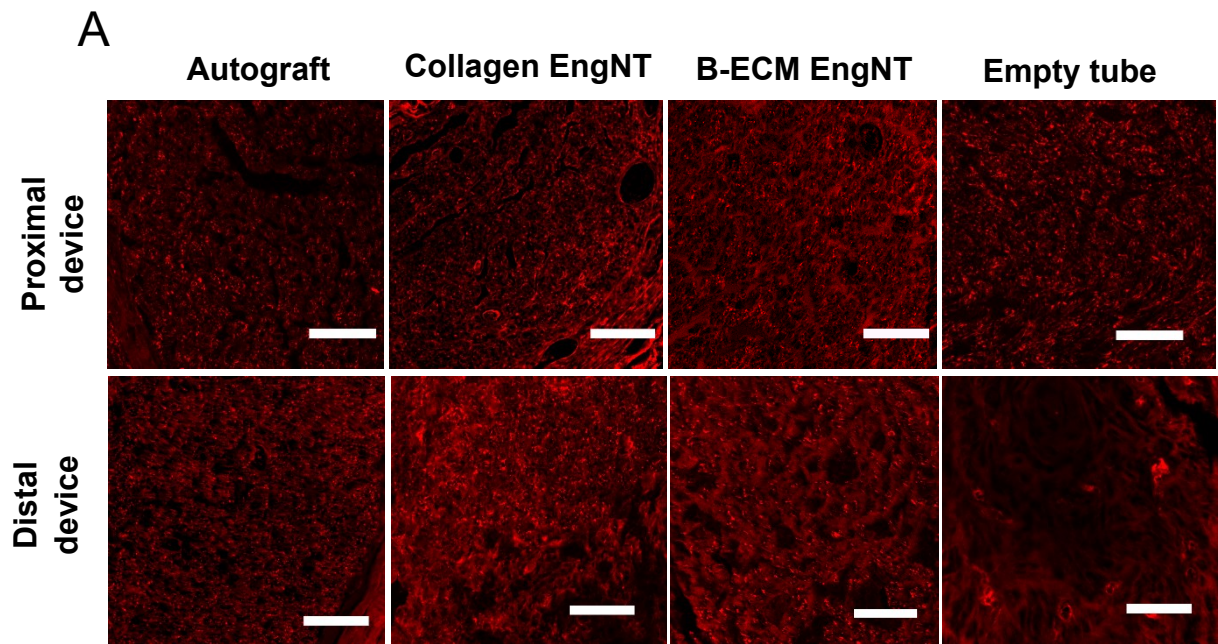
Figure 5.3 Engineered neural tissue (EngNT) derived from collagen and B-ECM hydrogels promote axonal regeneration. Representative confocal micrographs of neurofilament positive axons in the proximal and distal devices of empty tubes, collagen EngNT, B-ECM EngNT, and autografts 28 days post-surgery. Scale bar = 100 μm [A]. Axon counts for the proximal and distal devices of each group via the quantification of neurofilament positive axons in each region [B]. Percentage of axons in distal device compared to proximal device [C]. Data are mean ± SD n = 6 animals for B-ECM and collagen EngNT, n=5 animals for autograft, and n = 4 animals for empty tube with 3 images analysed per region. Two-way ANOVA with Tukey's multiple comparisons test (with Kramer correction for unequal sample sizes) [A]. One-way ANOVA with Tukey's multiple comparisons test (with Kramer correction for unequal sample sizes) [B]. Statistical significance is designated as **$p < 0.01$, ***$p < 0.001$, ****$p < 0.0001$.

5.4.3   Qualitative analysis of S100 positive cells and neurofilament positive axons within devices
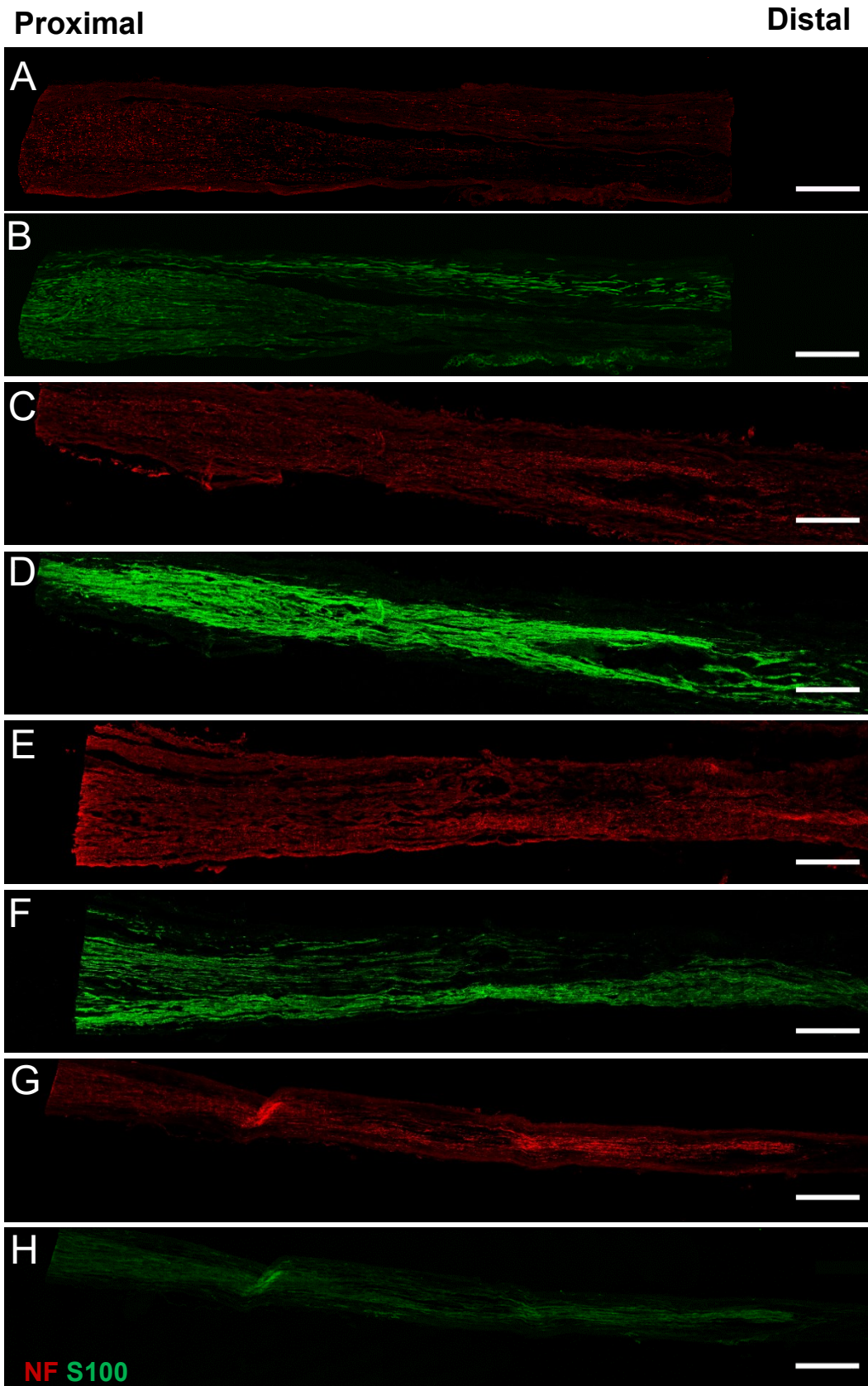
Figure 5.4 Neurofilament positive axons and S100 positive cells within the implanted devices. Representative confocal micrographs of NF and S100 staining of 6 mm long 15 μm longitudinal sections of Autograft [A, B], collagen I EngNT [C, D], B-ECM EngNT [E, F], and empty tubes [G, H- 28 days post-surgery. Scale bar = 500 μm.

Figure 5.4 shows representative longitudinal sections of neurofilament and S100 staining within an autograft (A, B), collagen EngNT (C, D), B-ECM EngNT (E, F), and an empty tube (G, H). Densely populated S100 positive cells may be seen in the collagen EngNT and B-ECM EngNT groups (Figure 5.4 D and E, respectively). S100 staining in the autograft group shows a sparser organisation of Schwann cells (Figure 5.4 B), and this structure is largely maintained toward the distal device. S100 staining within the empty tube revealed small, yet organised tissue. Neurofilament positive axons may be seen in all of the devices, however, in both EngNT groups the area occupied by axons becomes smaller towards the distal device and in the empty tube it almost disappears entirely (Figure 5.4 G).

Closely associated Schwann cell-axon groupings were observed at the proximal devices of all of the devices (Figure 5.5 A – D). In both of the EngNT groups this organised structure was seen to become slightly disrupted towards the distal device (Figure 5.5 B & C), whilst in the autograft group it was maintained (Figure 5.5 D). Less intense staining for S100 was observed within the autograft group compared to the relatively bright EngNT groups, and very few S100 positive cells were observed at the distal end of the empty silicone conduit (Figure 5.5 A).

Proximal　　　　　　　　　　　　　　　　　　**Distal**
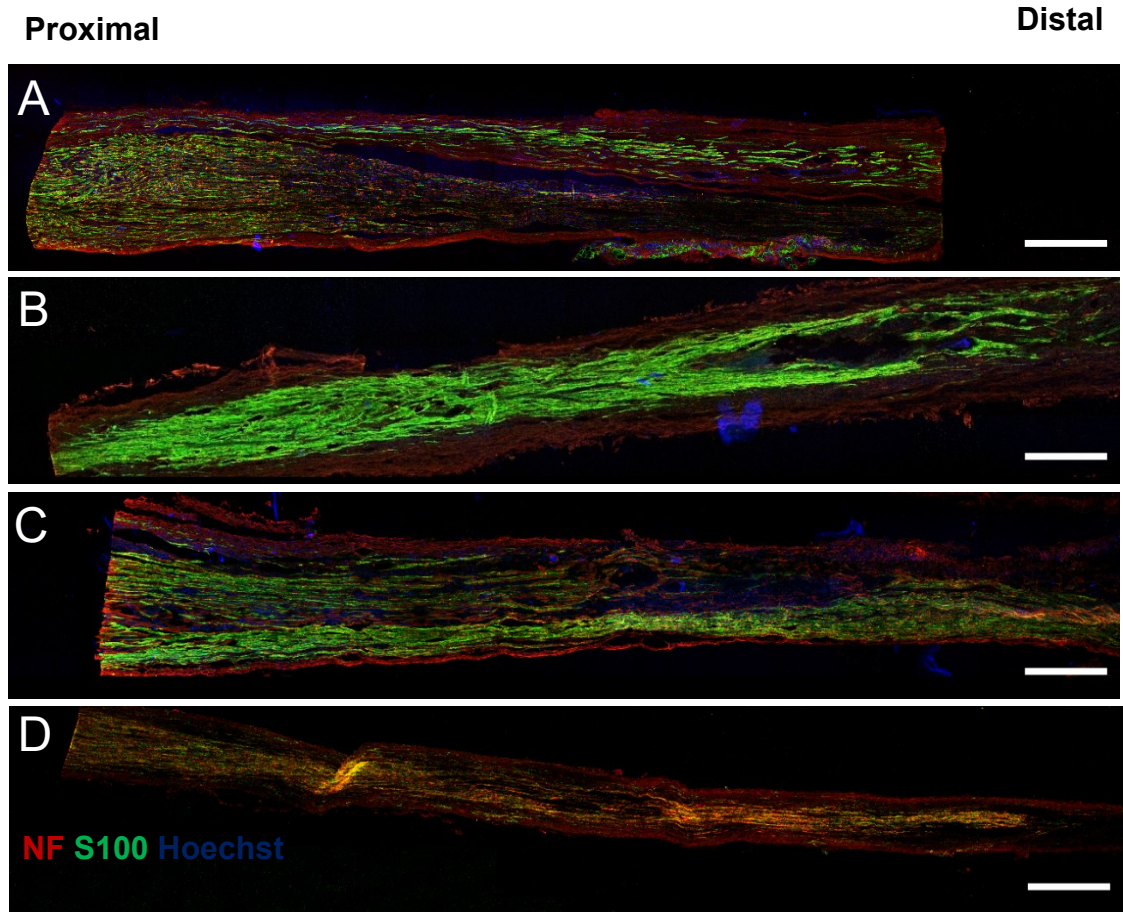
Figure 5.5 Neurofilament positive axons and S100 positive cells within the implanted devices (merged). Representative confocal micrographs of NF and S100 staining of 6 mm long 15 longitudinal sections of autograft [A], collagen I EngNT [B], B-ECM EngNT [C], and empty tube [D] 28 days post-surgery. Sections. Scale bar = 500 µm.

5.4.4 Analysis of blood vessel formation after 28 days

Blood vessels at the proximal and distal devices were assessed via immunofluorescence staining with an anti-endothelial cell antibody (RECA-1). Representative images at 20X magnification may be seen in Figure 5.6 A for autografts, collagen EngNT, B-ECM EngNT and empty tubes. Vessels were counted under a fluorescence microscope at 40X magnification (Figure 5.6 B). Similar numbers of blood vessels were observed for all groups at either end of the devices.
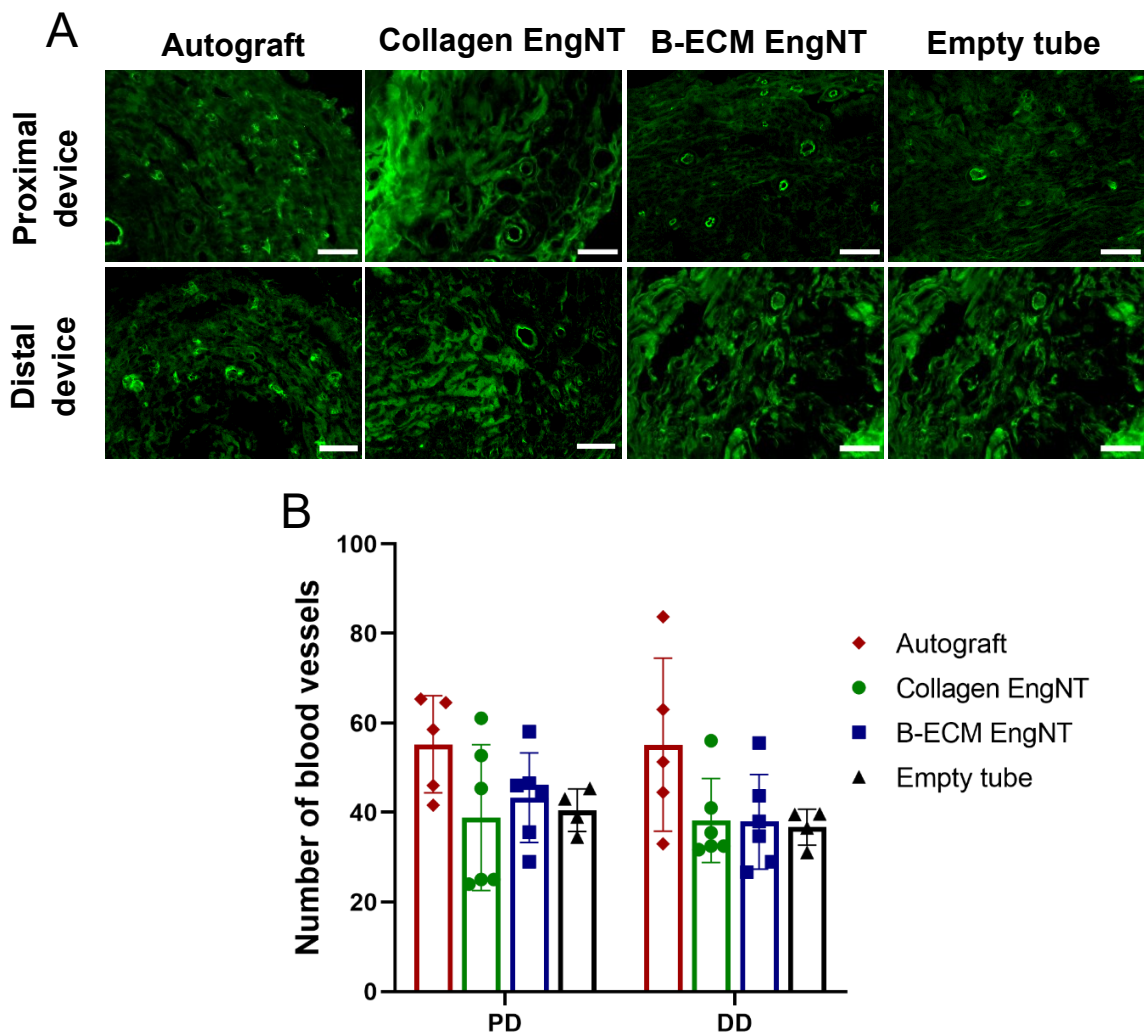
Figure 5.6 Assessment of vascularisation at the proximal and distal devices of empty tubes, autografts, and engineered neural tissue derived from either B-ECM or collagen I hydrogels. Representative fluorescence images of cross sections from the proximal and distal devices of each group [A]. Blood vessel counts for the proximal (PD) and distal devices (DD) [B]. Data are presented as mean ± SD. Scale bar = 100 μm.

5.5 Discussion

In the previous Chapter B-ECM was identified as a possible candidate for use in the repair of peripheral nerve injury (PNI). Neurite extension *in vivo* is reliant on multiple factors. Axons require a mechanically supportive environment that provides structural cues for directional axonal regeneration (Nachemson et al., 1988). Furthermore, neurotropism is desired to accelerate the outgrowth of axons across the defect (Gordon, 2009). In Chapter 4, 4 mg/ml B-ECM hydrogels were seeded with F7 Schwann cells to produce highly aligned EngNT that could promote directional neurite outgrowth *in vitro*. This suggested that hydrogels derived from decellularised bone ECM could have the potential to promote neurite extension *in vivo*.

In this chapter, EngNT derived from 4 mg/ ml B-ECM hydrogels was taken forward into an *in vivo* sciatic nerve 10 mm transection model in rats. The material was compared alongside three other experimental groups: autograft, empty tube, and EngNT derived from a purified rat tail type I collagen hydrogel. This model was chosen following review of the literature (Section 5.1.1) and from previous work in our lab by Muangsanit et al. (2020) that showed, at the designated gap length and experiment duration, empty tubes support minimal axonal regeneration, whilst axons will be regenerated through autografts; therefore allowing comparison between EngNT constructs derived from B-ECM or collagen I hydrogels and either control group. To reduce variability, collagen EngNT was plastically compressed in the same method used for dECM-h derived EngNT (Section 4.3); sheets of EngNT were separated from the RAFT™ absorber by surgical mesh, as opposed to in direct contact. B-ECM EngNT and collagen

EngNT were formed and placed within 12 mm silicone tubes that were longitudinally opened prior to EngNT insertion to be later sealed with super glue.

Both EngNT groups significantly improved axonal regeneration when compared to the empty tube, however, were not comparable to the autograft. This is concurrent with previous work on EngNT tested using the rat sciatic nerve model (Muangsanit et al., 2020, Georgiou et al., 2013). Other previous work has shown that EngNT seeded with neural stem cells had similar axonal counts to the autograft at the distal device in a 12 mm gap, however this was following a regeneration period of 8 weeks (O'Rourke et al., 2018). Axonal counts at the proximal and distal devices were slightly higher for the B-ECM EngNT group in comparison to the collagen I EngNT, although this was not found to be significant. Percentage of proximal axons reaching the distal device was further found to be slightly higher for B-ECM EngNT when compared to collagen I EngNT, although this was also not significant. F7 Schwann cells in the B-ECM and collagen I EngNT groups appeared to aid in the infiltration of axons at the proximal end of longitudinal sections however, the more narrow and less organised distal regions may account for the lower axonal counts observed at the distal devices. Nevertheless, percentages of proximal axons reaching the distal device are consistent with a number of studies of same gap length and similar time points (Farjah et al., 2017, Nguyen et al., 2017a, Muangsanit et al., 2020, Farahpour and Ghayour, 2014, Mottaghitalab et al., 2013, Wang et al., 2011).

On the other hand, B-ECM EngNT did show more variability in axonal regeneration; two of the animals presenting a relatively high axon count at the distal device whilst two others were relatively low. These may be due to variations in axon number observed at the proximal device; one of the two animals in the B-

ECM EngNT group with lower counts at the distal device had correspondingly lower counts at the proximal device. Moreover, the notion that B-ECM EngNT is mechanically distinct from collagen I EngNT should not be dismissed when considering the variation observed. EngNT derived from B-ECM hydrogels has a reduced structural integrity when compared to collagen I EngNT, and so, processes such as rolling, manoeuvring, and transit may have impacted the material, resulting in the variation within the B-ECM EngNT group.

Central to the process of nerve regeneration is the repair Schwann cell and its presence within the injury site (Ide et al., 1983, Jessen and Mirsky, 2016, Gulati et al., 1995, Gao et al., 2014b). Differences in S100 staining of longitudinal sections between the two control groups and the two EngNT groups suggests evidence of implanted F7 Schwann cell persistence within both EngNT groups, as well as possible migratory Schwann cells around the implanted cells at the proximal device. Without quantification, however, it is unclear the extent of this effect and this is a focus of ongoing research for this study.

Due to the angiogenic potential of dECM-h (Ungerleider et al., 2016, Qiu et al., 2020a, Fercana et al., 2017), and the implications of increased vascularisation improving nerve repair outcomes (Hobson et al., 2000, Podhajsky and Myers, 1995, Hobson, 2002), blood vessel formation was further assessed. However, no observable difference was found between any of the groups at either of the regions assessed. This is similar to previous research that found no differences in number of blood vessels observed in the proximal and distal devices of autografts, empty tubes, and EngNT seeded with CTX cells (O'Rourke et al., 2018). On the other hand, Yen et al. (2019) report distinct differences in blood vessel numbers between four groups of native nerve, PCL and collagen I

conduits, silicone, and PCL conduits (in descending order of blood vessel number), although this may be due to the longer experimental time period of 8 weeks. In a 3 week study differences were observed in blood vessel area between an empty tube and a silk fibroin filled tube, however as blood vessels were not counted this could be due to larger vessels in the experimental group (Wang et al., 2018). Conversely, significant differences have been observed in the vascularisation of devices comparing F7 Schwann cell EngNT with EngNT co-cultured with endothelial cells (Muangsanit, 2020). Regardless, both EngNT constructs were vascularised to the same extent as the controls.

5.6   Conclusions and future work

This chapter reported preliminary data from an *in vivo* rat sciatic nerve transection model, comparing EngNT derived from B-ECM or collagen I hydrogels. For 10 mm nerve gaps, empty tubes are sufficient to promote axonal regeneration and functional recovery. This study has shown that both EngNT groups showed significant improvements in axonal regeneration in comparison to the empty tube control. Although slightly higher axon counts were observed in B-ECM EngNT compared to collagen I EngNT, the findings were not significant. Regardless, this is the first time a material other than collagen I has promoted axonal regeneration *in vivo* when incorporated into EngNT. Similar performances of *in vivo* axonal regeneration further support the validity in the *in vitro* findings in the DRG models outlined in Chapter 4. Improved neovascularisation was not present in B-ECM EngNT, however, it may be of interest to investigate how dECM-h can influence endothelial cell behaviour in co-cultures with F7 Schwann cells. Moreover, future work is focussed around completing the analysis of proximal and distal stumps as well as quantitative assessment of S100 positive cells and macrophage

populations in each of the groups. Studies involving EngNT for a longer recovery time period have shown to promote comparable regeneration to autografts (O'Rourke et al., 2018) and so it may be of interest to see if this is observed in B-ECM EngNT conduits, whilst further assessing functional outcomes in addition to axonal regeneration. Additionally, this study could be used as a framework to develop other alternatives derived from dECM materials.

Chapter 6 Discussion, conclusions, and future work

The primary aim of this work was to explore the ability of different hydrogel materials derived from ECM from decellularised tissues to produce EngNT seeded with F7 Schwann cells. The hypothesis was that the innate ability of dECM hydrogels to modulate cell behaviour would make them suitable for use as a carrier for therapeutic cells within EngNT. Each material was taken from production, through thorough characterisation and *in vitro* screening, with a final material chosen for use in a preclinical *in vivo* model for peripheral nerve regeneration.

The application of dECM-h for peripheral nerve repair is relatively incipient; to date, six studies have employed dECM-h for use in the repair and regeneration of peripheral nerve defects (outlined in Section 1.6.2.1), of which four were published since the beginning of 2020. dECM-h in these studies were administered either as acellular gels (Lin et al., 2018, Prest et al., 2017) or incorporated with growth factors (Li et al., 2020, Rao et al., 2021). dECM-h functioning as cell delivery systems for a number of regenerative applications have been reported (Jang et al., 2017, Sun et al., 2020, Yuan et al., 2017). When considering the benefits of cellular support in NGC for robust repair of peripheral nerve defects (Gao et al., 2014a, Gulati, 1988, Hoben et al., 2015), it is surprising that studies have yet to use dECM-h as cell carriers for peripheral nerve repair. This thesis has made efforts to introduce an approach in the utilisation of dECM-h for peripheral nerve repair, via utilising the interactions between cell and matrix to improve therapeutic cell implantation within EngNT.

6.1 Discussion of key findings

6.1.1 dECM materials are biochemically and mechanically diverse

In Chapter 3, a portfolio of starting tissues that were decellularised and biochemically characterised was presented. Subsequently the different dECM were quantitatively assessed for dsDNA content and sGAG content and qualitatively assessed via histology for the presence of nuclei, sGAG, and collagen. Materials were biochemically distinct and were therefore expected to differentially affect cellular behaviour. The presence of residual cellular material within decellularised ECM, such as nucleic content, can result in unfavourable responses *in vitro*, for example the upregulation of inflammatory markers in macrophages (Londono et al., 2017), as well as aberrant inflammatory reactions *in vivo* (Zheng *et* al., 2005). B-ECM had the lowest dsDNA content with over 98 % cellular removal compared to the native control. SIS-ECM in contrast had more residual nucleic content with 10 % of the native dsDNA remaining within the scaffold. On the other hand, whilst B-ECM was the most completely decellularised, it also had the lowest sGAG content, whilst SIS-ECM had the highest, likely due to the differences decellularisation agents used during the treatment processes.

dECM powder was solubilised into pH and temperature sensitive digests that were neutralised to form pre-gel solutions; hydrogel formation and mechanical properties were characterised using a rheometer. Gelation time and kinetics, as well as storage and loss moduli, were found to be different for each material; further predicted to affect cell behaviour. Material stiffness can affect cell viability (Shi et al., 2017), migration (Perea-Gil et al., 2015), mitogenesis (Shi et al., 2017), and differentiation (Wells, 2008, Sun et al., 2018, Mao et al., 2016). More

specifically, material stiffness regulates *in vitro* Schwann cell morphology and phenotype (Xu et al., 2020), as well as *in vitro* neurite extension (Willits and Skornia, 2004, Balgude et al., 2001). LIV-ECM and B-ECM were similar in stiffness, whilst SIS-ECM was relatively softer in comparison, and UBM-ECM was far softer. UBM-ECM was not selected to be taken forward due to its lack of structural integrity causing problems in hydrogel manipulation and manoeuvrability. B-ECM, LIV-ECM, and SIS-ECM were subsequently deemed suitable for further use based on tissue availability, dECM yield and hydrogel structural integrity.

6.1.2 Neural cell response to dECM hydrogels

In Chapter 4 dECM hydrogels were assessed for their effect on F7 Schwann cell viability and their ability to undergo cell mediated contraction. F7 Schwann cells seeded in B-ECM hydrogels were found to have the highest metabolic activity. B-ECM and SIS-ECM hydrogels were shown to be most contractile and in-turn resulted in the highest levels of F7 Schwann cell alignment. The correlation of cell and gel concentrations on contraction is largely in agreement with previous studies on collagen I hydrogels and C6 glioma cells (O'Rourke et al., 2015), as well as mesenchymal stem cells in collagen I (Klumpers et al., 2013). Similarly, thresholds of contraction are required to achieve cellular alignment in tethered moulds, although these thresholds appeared to differ from those described in O'Rourke et al. (2015). SIS-ECM was able to produce highly aligned tissue at 4 x 10^6 cells/ ml with approximately 60 % contraction, whereas LIV-ECM at the same seeding density and slightly lower levels of contraction did not align.

Every dECM-h was found to be able to support neurite growth when coated on coverslips with similar neurite lengths observed in each material and collagen I

controls. It could therefore be assumed that neurite extension is largely independent of the biochemical composition of the dECM. However, higher protein concentrations have shown distinct differences in *in vitro* neurite extension between different dECM (Zou et al., 2018), and so this could be a focus of further research. In contrast, neurons seeded onto sheets of dECM EngNT differed; neurites on B-ECM EngNT were found to grow longer and orientated, whereas this was found to be less prominent in SIS-ECM EngNT. Neurites seeded on LIV-ECM EngNT were not found to be aligned. Differences in neurite extension may be attributed to differences in material stiffness (Xu et al., 2020), or higher concentrations of biochemical factors that may affect cellular behaviour; for example SIS-ECM had a higher dsDNA content as well as a higher sGAG content that could include neurite inhibitory chondroitin sulphate (Zuo et al., 2002, Yu and Bellamkonda, 2001). Regardless, the results of the *in vitro* models were clear, and out of the three materials, B-ECM hydrogels were taken forward in this study.

6.1.3 *In vivo* performance of EngNT derived from a dECM hydrogel

Finally, Chapter 5 saw the resolution of the project with the incorporation of B-ECM EngNT into an *in vivo* nerve injury model. Results showed that axonal regeneration through B-ECM EngNT was comparable to EngNT derived from purified collagen I. Both groups showed significantly more robust regeneration to empty tubes at 10 mm whilst neither were comparable to the autograft group. Levels of regeneration, moreover, were comparable to previous work on EngNT and other studies of similar length and time points (Farjah et al., 2017, Nguyen et al., 2017a, Muangsanit et al., 2020, Farahpour and Ghayour, 2014, Mottaghitalab et al., 2013, Wang et al., 2011). On the other hand, previous work using EngNT

comprising neural stem cells and collagen I exhibited more robust regeneration, over a 12 mm gap at 8 weeks, with comparable axon counts to the autograft (O'Rourke et al., 2018). It is possible that this effect may be observed with further experimentation on longer gap lengths and time periods with dECM EngNT. Moreover, differences between dECM EngNT and collagen I EngNT may be more pronounced at longer time periods. No difference was found in number of blood vessels between autografts, B-ECM EngNT, collagen I EngNT, and empty silicone tubes. This is consistent with previous work on collagen I EngNT seeded with neural stem cells (O'Rourke et al., 2018).

6.2   Limitations

Whilst the work in this thesis presents promising start in the investigations of the use of dECM hydrogels for use in EngNT for peripheral nerve repair, multiple limitations exist within the work presented, and the field as a whole. This section addresses these limitations as well as general limitations of dECM-h and the problems they must overcome for practical clinical translation.

6.2.1 Clinical translation

6.2.1.1   Cellular component

The principal aim of this work was to investigate the material component of EngNT, and so the SCL4.1/F7 Schwann cell line that had previously been applied in *in vitro* and *in vivo* models for neurite extension was chosen (Georgiou et al., 2013, Muangsanit et al., 2020). However, it is derived from a rat schwannoma. High proliferative rates result in ease of expansion and seeding of scaffolds, making immortalised cell lines like the F7 Schwann cell an appropriate choice for *in vitro* testing biomaterial effect on cell behaviour, as outlined in Chapter 4. On the other hand, this creates complications when considering effective clinical

translation. Cell passaging can cause genetic drift, over time affecting changes in cell genotype and phenotype, resulting in cells that are distinct from other passages and are atypical in protein and gene expression (Kaur and Dufour, 2012). This therefore must be taken into account when considering the cellular assays presented in this study and future research should investigate more therapeutically relevant cells, as well as the possibility of primary Schwann cell cultures, to better understand cell-matrix interactions with dECM.

6.2.1.2   Material component

The ECM is heterogeneous. Variations are observed in biochemical composition and mechanical properties as a result of tissue source (Xu et al., 2021), animal species (Loneker et al., 2016, Kočí et al., 2017), processing methods (Lu et al., 2012, Kočí et al., 2017, Kajbafzadeh et al., 2013), as well as the age of the tissue (Willits and Skornia, 2004, Tottey et al., 2011). As a result, batch-to-batch variation can be observed when generating dECM, even following extensive optimisation and standardisation of decellularisation protocols. Ideally, extensive biochemical and mechanical characterisation is required on each dECM batch produced, however, as shown in Table 1.3 (Section 1.6.2.1) this is not always the case. Research groups appear to characterise initial batches and use this characterisation as validation for the use of subsequent dECM batches in later publications. This may be explained by the amount of dECM required to fully biochemically and mechanically characterise these materials coupled with relatively low yields. Using material derived from animal tissue partially characterised can have severe implications for practicality in clinical use. For example, the implantation of Restore™, an approved "acellular" graft derived from porcine SIS caused adverse inflammatory responses when introduced into

a mouse rotator cuff repair model as a result of incomplete decellularisation (Zheng et al., 2005). Solutions for scaling up the process are essential before these materials could be considered for translation to the clinic. Moreover, standardisation of variables such as animal species and ages, and maintaining strict regulation of protocols in the decellularisation and characterisation processes is essential to maintain quality control between batches. This should then be followed with extensive *in vitro* and pre-clinical *in vivo* testing. An example of the complete process is presented in the development of a cardiac dECM-h for the repair and regeneration of heart tissue following myocardial infarction. Since its initial development and characterisation in 2009 (Singelyn et al., 2009), the material has gone through *in vitro* testing (Gaetani et al., 2016, French et al., 2012), implementation into *in vivo* models (Seif-Naraghi et al., 2013), and been applied clinically in a first-in-human trial (Traverse et al., 2019), a 10 year process.

Synthetic materials pose an alternative solution to natural polymers. Synthetic polymers can be made to precision in larger quantities and have well described properties with little batch-to-batch variation (Gunatillake et al., 2006). Research into improving cell-matrix interactions and performance of synthetic polymers has revolved around introducing binding motifs for cell adhesion (Yang et al., 2005a, Li et al., 2015) and making biohybrid formulations to create mechanically responsive materials that mimic the strain stiffening behaviour observed in natural polymers (Jaspers et al., 2014, de Almeida et al., 2019). Whilst these materials no doubt constitute a large proportion of the future research within tissue engineering, materials such as dECM are more representative of the native tissue milieu and their bioactive degradation products promote positive tissue remodelling (Banerjee et al., 2015, Agrawal et al., 2011a). The future of

biomaterials in nerve tissue engineering therefore likely involves combinations of synthetic and natural polymers to overcome the limitations associated with each.

6.3   Future work

This section outlines possible future work that can address the limitations presented previously to explore the future of dECM and its potential for further use in peripheral nerve repair.

Chapter 4 showed how the contractile properties of the dECM hydrogels differed. Whilst investigations into the blocking of integrin α1 indicate this is a collagen I dependent process, this could be clarified by investigating the collagen I content. Chapter 4 also established B-ECM as the most appropriate dECM material for neurite outgrowth based on *in vitro* neurite extension models. However, F7 Schwann cell gene expression profiles indicate SIS-ECM could be superior in the influence of certain pro-regenerative Schwann cell markers. It is possible that the lower structural integrity of the SIS-ECM hydrogels results in the decreased *in vitro* neurite outgrowth observed in Chapter 4. By improving the mechanical strength, SIS-ECM may prove superior to the B-ECM in its *in vitro* and *in vivo* potential for peripheral nerve repair. This could be achieved through composing blends of SIS-ECM and collagen I hydrogels at different concentrations and screening these in the *in vitro* neurite extension assays established in this project. Similarly, some studies have reported the effects of dECM-h in combination with more robust synthetic (Zheng et al., 2021) and natural (Xu et al., 2018) polymers to improve the mechanical properties. Alternatively, due to the presence of matrix-bound vesicles (MBV) in SIS-ECM (Huleihel et al., 2016), and their apparent ability to improve *in vitro* neurite extension (Faust et al., 2017) as well as modulate macrophage phenotype (Huleihel et al., 2017), isolation of SIS-ECM

derived MBV and their subsequent supplementation into either collagen I or B-ECM derived EngNT may further prove beneficial.

The use of stem cells for neural tissue engineering has been developing over the past 20 years (Bhangra et al., 2016). Adipose stem cells, neural stem cells, and dental pulp stem cells have been used to create EngNT (Georgiou et al., 2015, O'Rourke et al., 2018, Sanen et al., 2017), whilst clinical application potential may further be improved via the use of induced pluripotent stem cells. It is therefore of interest to assess dECM effect on maintaining stem cell cultures *in vitro* and the effect they may have on the expression of the Schwann cell and inflammatory markers, as well as the neurotrophic factors presented in Chapter 4. Moreover, the maintenance of differentiated stem cell phenotype *in vivo* should be explored. *In vitro* data has shown that Schwann cell-like differentiated adipose derived stem cells reverted back to a stem cell phenotype in the absence of stimulating differentiation media (Faroni et al., 2016); a process that may be mitigated by the introduction of a bioactive material that have the ability to modulate cell phenotype. As shown in Chapter 4, dECM-h have the potential to modulate F7 Schwann cell phenotype and behaviour, and so it may be of interest to explore dECM-h effect on the maintenance of therapeutic cells.

6.3.1 Tissue-specific dECM generation

The source tissues used in this study were nonspecific to the site of injury. Providing injury sites with site-appropriate tissue is a common theme when reviewing literature on *in vivo* applications of decellularised materials (Section 1.6.2.1). As such, groundwork in the dissection and decellularisation of porcine sciatic nerves has been established. Pig leg dissections have been carried out to extract sciatic nerves (Appendix A, Figure A1). Nerves were laterally sliced into

pieces of approximately 1 cm in length to be later subjected to the same decellularisation protocol for the production of spinal cord ECM (SC-ECM), outlined in Section 2.2.6 and used for peripheral nerve decellularisation in Prest et al. (2017). This is may be of interest to investigate further, however, was not able to be performed in the present study due to the limited amount of tissue extracted per leg and lack of tissue availability.

6.3.2 A nerve sheath derived from dECM

dECM application may not be exclusive to incorporation into EngNT. The silicone conduits used in this study do not degrade, and as such, would eventually need a second surgery to be removed, whilst adverse reactions have further been reported clinically (Merle et al., 1989). Resorbable conduits that do not cause nerve compression have been developed (Gaudin et al., 2016, Dienstknecht et al., 2013, Di Summa et al., 2014), including a nerve wrap made from porcine SIS-ECM (Smith et al., 2004, Arda et al., 2017). As such preliminary work on the design of a multilamellar conduit comprised of SIS-ECM sheets has been performed. Up to four SIS-ECM sheets underwent plastic compression and were formed into stable multilamellar sheets (Appendix B, Figure B1). Future work could be carried out into possibilities of cross-linking SIS-ECM sheets with agents such as genipin (Výborný et al., 2019) and degradation studies carried out using collagenase to assess degradation rates that could be tuned for *in vivo* experiments.

6.4   Conclusions

The primary objective of this work was to investigate avenues for the possible improvement of the material component of EngNT through the incorporation of dECM-h. This thesis showed, for the first time, that alternatives to the current rat

tail purified collagen I hydrogel may be explored in the production of EngNT. Various dECM hydrogels were able to be integrated into *in vitro* models using different neuronal cell types and showed diversity in cell responses. Drawing from the data of these *in vitro* models, EngNT derived from B-ECM was selected to be investigated in an *in vivo* rat model and was shown to promote comparable axonal regeneration to EngNT derived from collagen I.

Ultimately, this thesis has paved a path for future research into the possibilities of the utilisation of dECM-h for incorporation into EngNT; the prospects of site appropriate, tissue-specific ECM could be studied, as well as investigations into altering the mechanical properties of dECM hydrogels to improve their clinical application potential.

Bibliography

ABIDIAN, M. R., DANESHVAR, E. D., EGELAND, B. M., KIPKE, D. R., CEDERNA, P. S. & URBANCHEK, M. G. 2012. Hybrid conducting polymer-hydrogel conduits for axonal growth and neural tissue engineering. *Adv Healthc Mater,* 1**,** 762-7.

AGRAWAL, V., KELLY, J., TOTTEY, S., DALY, K. A., JOHNSON, S. A., SIU, B. F., REING, J. & BADYLAK, S. F. 2011a. An Isolated Cryptic Peptide Influences Osteogenesis and Bone Remodeling in an Adult Mammalian Model of Digit Amputation. *Tissue Engineering Part A,* 17**,** 3033-3044.

AGRAWAL, V., TOTTEY, S., JOHNSON, S. A., FREUND, J. M., SIU, B. F. & BADYLAK, S. F. 2011b. Recruitment of progenitor cells by an extracellular matrix cryptic peptide in a mouse model of digit amputation. *Tissue Eng Part A,* 17**,** 2435-43.

AGRAWAL, V., TOTTEY, S., JOHNSON, S. A., FREUND, J. M., SIU, B. F. & BADYLAK, S. F. 2011c. Recruitment of Progenitor Cells by an Extracellular Matrix Cryptic Peptide in a Mouse Model of Digit Amputation. *Tissue Engineering Part A,* 17**,** 2435-2443.

AHEARNE, M. 2014. Introduction to cell–hydrogel mechanosensing. *Interface Focus,* 4**,** 20130038-20130038.

AHEARNE, M., LIU, K. K., EL HAJ, A. J., THEN, K. Y., RAUZ, S. & YANG, Y. 2010. Online monitoring of the mechanical behavior of collagen hydrogels: Influence of corneal fibroblasts on elastic modulus. *Tissue Engineering - Part C: Methods*.

ALESSANDRINO, A., FREGNAN, F., BIAGIOTTI, M., MURATORI, L., BASSANI, G. A., RONCHI, G., VINCOLI, V., PIERIMARCHI, P., GEUNA, S. & FREDDI, G. 2019. SilkBridge™: A novel biomimetic and biocompatible silk-based nerve conduit. *Biomaterials Science,* 7**,** 4112-4130.

ALOM, N., PETO, H., KIRKHAM, G. R., SHAKESHEFF, K. M. & WHITE, L. J. 2017. Bone extracellular matrix hydrogel enhances osteogenic differentiation of C2C12 myoblasts and mouse primary calvarial cells. *Journal of Biomedical Materials Research - Part B Applied Biomaterials***,** 1-9.

ALSHAIKH, A. B., PADMA, A. M., DEHLIN, M., AKOURI, R., SONG, M. J., BRANNSTROM, M. & HELLSTROM, M. 2019. Decellularization of the mouse ovary: comparison of different scaffold generation protocols for future ovarian bioengineering. *J Ovarian Res,* 12**,** 58.

ANGIUS, D., WANG, H., SPINNER, R. J., GUTIERREZ-COTTO, Y., YASZEMSKI, M. J. & WINDEBANK, A. J. 2012. A systematic review of animal models used to study nerve regeneration in tissue-engineered scaffolds. *Biomaterials,* 33**,** 8034-9.

ARCHIBALD, S. J., KRARUP, C., SHEFNER, J., LI, S. T. & MADISON, R. D. 1991. A collagen-based nerve guide conduit for peripheral nerve repair: an electrophysiological study of nerve regeneration in rodents and nonhuman primates. *J Comp Neurol,* 306**,** 685-96.

ARDA, M. S., KOÇMAN, E. A., ÖZKARA, E., SÖZTUTAR, E., ÖZATIK, O., KÖSE, A. & ÇETIN, C. 2017. Can a small intestine segment be an

alternative biological conduit for peripheral nerve regeneration? *Balkan Medical Journal,* 34**,** 246-254.

ARGIRO, V. & JOHNSON, M. I. 1982. Patterns and kinetics of neurite extension from sympathetic neurons in culture are age dependent. *J Neurosci,* 2**,** 503-12.

ARMSTRONG, S. J., WIBERG, M., TERENGHI, G. & KINGHAM, P. J. 2007. ECM Molecules Mediate Both Schwann Cell Proliferation and Activation to Enhance Neurite Outgrowth. *Tissue Engineering,* 13**,** 2863-2870.

ASK, P., LEVITAN, H., ROBINSON, P. J. & RAPOPORT, S. I. 1983. Peripheral nerve as an osmometer: role of the perineurium in frog sciatic nerve. *Am J Physiol,* 244**,** C75-81.

AUMAILLEY, M., BRUCKNER-TUDERMAN, L., CARTER, W. G., DEUTZMANN, R., EDGAR, D., EKBLOM, P., ENGVALL, E., HOHENESTER, E., JONES, J. C. R., KLEINMAN, H. K., MARINKOVICH, M. P., MARTIN, G. R., MAYER, U., MENEGUZZI, G., MINER, J. H., MIYAZAKI, K., PATARROYO, M., PAULSSON, M., QUARANTA, V., SANES, J. R., SASAKI, T., SEKIGUCHI, K., SOROKIN, L. M., TALTS, J. F., TRYGGVASON, K., UITTO, J., VIRTANEN, I., MARK, K. V. D., WEWER, U. M., YAMADA, Y. & YURCHENCO, P. D. 2005. Mini review A simplified laminin nomenclature. *Matrix Biology,* 24**,** 326-332.

BADYLAK, S. F., KROPP, B., MCPHERSON, T., LIANG, H. & SNYDER, P. W. 1998. Small intestinal submucosa: a rapidly resorbed bioscaffold for augmentation cystoplasty in a dog model. *Tissue engineering,* 4**,** 379-387.

BAILEY, S. B., EICHLER, M. E., VILLADIEGO, A. & RICH, K. M. 1993. The influence of fibronectin and laminin during Schwann cell migration and peripheral nerve regeneration through silicon chambers. *Journal of Neurocytology,* 184**,** 176-184.

BALASUBRAMANIAN, P., PRABHAKARAN, M. P., SIREESHA, M. & RAMAKRISHNA, S. 2012. Collagen in Human Tissues: Structure, Function, and Biomedical Implications from a Tissue Engineering Perspective.

BALGUDE, A. P., YU, X., SZYMANSKI, A. & BELLAMKONDA, R. V. 2001. Agarose gel stiffness determines rate of DRG neurite extension in 3D cultures. *Biomaterials,* 22**,** 1077-1084.

BANERJEE, P., SUGUNA, L. & SHANTHI, C. 2015. Wound healing activity of a collagen-derived cryptic peptide. *Amino Acids,* 47**,** 317-328.

BARTLETT, R. D., ELEFTHERIADOU, D., EVANS, R., CHOI, D. & PHILLIPS, J. B. 2020. Mechanical properties of the spinal cord and brain: Comparison with clinical-grade biomaterials for tissue engineering and regenerative medicine. *Biomaterials,* 258**,** 120303.

BAYRAK, A., PRUGER, P., STOCK, U. A. & SEIFERT, M. 2013. Absence of immune responses with xenogeneic collagen and elastin. *Tissue Eng Part A,* 19**,** 1592-600.

BELIN, S., ZULOAGA, K. L. & POITELON, Y. 2017. Influence of Mechanical Stimuli on Schwann Cell Biology. *Front Cell Neurosci,* 11**,** 347.

BELLA, J. & HULMES, D. J. S. 2017. Fibrillar Collagens. *In:* PARRY, D. A. D. & SQUIRE, J. M. (eds.) *Fibrous Proteins: Structures and Mechanisms.* Cham: Springer International Publishing.

BELLAMKONDA, R. V. 2006. Peripheral nerve regeneration: an opinion on channels, scaffolds and anisotropy. *Biomaterials,* 27**,** 3515-8.

BHANGRA, K. S., BUSUTTIL, F., PHILLIPS, J. B. & RAHIM, A. A. 2016. Using Stem Cells to Grow Artificial Tissue for Peripheral Nerve Repair. *Stem Cells Int,* 2016**,** 7502178.

BI, H., YE, K. & JIN, S. 2020. Proteomic analysis of decellularized pancreatic matrix identifies collagen V as a critical regulator for islet organogenesis from human pluripotent stem cells. *Biomaterials,* 233**,** 119673.

BI, Y., EHIRCHIOU, D., KILTS, T. M., INKSON, C. A., EMBREE, M. C., SONOYAMA, W., LI, L., LEET, A. I., SEO, B. M., ZHANG, L., SHI, S. & YOUNG, M. F. 2007. Identification of tendon stem/progenitor cells and the role of the extracellular matrix in their niche. *Nat Med,* 13**,** 1219-27.

BIERNASKIE, J., SPARLING, J. S., LIU, J., SHANNON, C. P., PLEMEL, J. R., XIE, Y., MILLER, F. D. & TETZLAFF, W. 2007. Skin-derived precursors generate myelinating Schwann cells that promote remyelination and functional recovery after contusion spinal cord injury. *J Neurosci,* 27**,** 9545-59.

BIRK, D. E. & SILVER, F. H. 1984. Collagen fibrillogenesis in vitro: comparison of types I, II, and III. *Arch Biochem Biophys,* 235**,** 178-85.

BIXBY, J. L. & JHABVALA, P. 1990. Extracellular matrix molecules and cell adhesion molecules induce neurites through different mechanisms. *J Cell Biol,* 111**,** 2725-32.

BONI, R., ALI, A., SHAVANDI, A. & CLARKSON, A. N. 2018. Current and novel polymeric biomaterials for neural tissue engineering. *J Biomed Sci,* 25**,** 90.

BRÁS, L. E. D. C. & FRANGOGIANNIS, N. G. 2020. Extracellular matrix-derived peptides in tissue remodeling and fibrosis. *Matrix Biology,* 1-12.

BRIGHTMAN, A., RAJWA, B., STURGIS, J., MCCALLISTER, M., ROBINSON, J. & VOYTIK-HARBIN, S. 2000a. Time-Lapse Confocal Reflection Microcopy of Collagen Fibrillogenesis and Extracellular Matrix Assembly In Vitro. *Biopolymers,* 54**,** 222-234.

BRIGHTMAN, A. O., RAJWA, B. P., STURGIS, J. E., MCCALLISTER, M. E., ROBINSON, J. P. & VOYTIK-HARBIN, S. L. 2000b. Time-lapse confocal reflection microscopy of collagen fibrillogenesis and extracellular matrix assembly in vitro. *Biopolymers,* 54**,** 222-234.

BROWN, B. N., VALENTIN, J. E., STEWART-AKERS, A. M., MCCABE, G. P. & BADYLAK, S. F. 2009. Biomaterials Macrophage phenotype and remodeling outcomes in response to biologic scaffolds with and without a cellular component. *Biomaterials,* 30**,** 1482-1491.

BURDICK, J. A., MAUCK, R. L. & GERECHT, S. 2016. To Serve and Protect: Hydrogels to Improve Stem Cell-Based Therapies. *Cell Stem Cell,* 18**,** 13-15.

BURNETT, M. G. & ZAGER, E. L. 2004. Pathophysiology of peripheral nerve injury : a brief review. *Neurosurgical focus,* 16**,** 1-7.

BUTTNER, R., SCHULZ, A., REUTER, M., AKULA, A. K., MINDOS, T., CARLSTEDT, A., RIECKEN, L. B., BAADER, S. L., BAUER, R. & MORRISON, H. 2018. Inflammaging impairs peripheral nerve maintenance and regeneration. *Aging Cell,* 17**,** e12833.

CACOPARDO, L., GUAZZELLI, N., NOSSA, R., MATTEI, G. & AHLUWALIA, A. 2019. Engineering hydrogel viscoelasticity. *Journal of the Mechanical Behavior of Biomedical Materials,* 89**,** 162-167.

CANTY, E. G. & KADLER, K. E. 2005. Procollagen trafficking, processing and fibrillogenesis. *J Cell Sci,* 118**,** 1341-53.

CARRI, N. G., RUBIN, K., GULLBERG, D. & EBENDAL, T. 1992. Neuritogenesis on collagen substrates. Involvement of integrin-like matrix receptors in retinal fibre outgrowth on collagen. *Int J Dev Neurosci,* 10**,** 393-405.

CARVALHO, C. R., OLIVEIRA, J. M. & REIS, R. L. 2019. Modern Trends for Peripheral Nerve Repair and Regeneration: Beyond the Hollow Nerve Guidance Conduit. *Front Bioeng Biotechnol,* 7**,** 337.

CASALI, D. M., HANDLETON, R. M., SHAZLY, T. & MATTHEWS, M. A. 2018. A novel supercritical CO_2-based decellularization method for maintaining scaffold hydration and mechanical properties. *Journal of Supercritical Fluids,* 131**,** 72-81.

CATTIN, A. L., BURDEN, J. J., VAN EMMENIS, L., MACKENZIE, F. E., HOVING, J. J., GARCIA CALAVIA, N., GUO, Y., MCLAUGHLIN, M., ROSENBERG, L. H., QUEREDA, V., JAMECNA, D., NAPOLI, I., PARRINELLO, S., ENVER, T., RUHRBERG, C. & LLOYD, A. C. 2015. Macrophage-Induced Blood Vessels Guide Schwann Cell-Mediated Regeneration of Peripheral Nerves. *Cell,* 162**,** 1127-39.

CHAFIK, D., BEAR, D., BUI, P., PATEL, A., JONES, N. F., KIM, B. T., HUNG, C. T. & GUPTA, R. 2003. Optimization of Schwann cell adhesion in response to shear stress in an in vitro model for peripheral nerve tissue engineering. *Tissue Eng,* 9**,** 233-41.

CHANG, W., SHAH, M. B., LEE, P. & YU, X. 2018. Tissue-engineered spiral nerve guidance conduit for peripheral nerve regeneration. *Acta Biomaterialia,* 73**,** 302-311.

CHAUDHURI, O. 2017. Viscoelastic hydrogels for 3D cell culture. *Biomaterials Science,* 5**,** 1480-1490.

CHEN, B., CARR, L. & DUN, X. P. 2020. Dynamic expression of Slit1-3 and Robo1-2 in the mouse peripheral nervous system after injury. *Neural Regen Res,* 15**,** 948-958.

CHEN, P., CESCON, M., MEGIGHIAN, A. & BONALDO, P. 2013. Collagen VI regulates peripheral nerve myelination and function. *The FASEB Journal,* 28**,** 1145-1156.

CHEN, P., CESCON, M., ZUCCOLOTTO, G., NOBBIO, L., COLOMBELLI, C., FILAFERRO, M., VITALE, G., FELTRI, M. L. & BONALDO, P. 2015. Collagen VI regulates peripheral nerve regeneration by modulating macrophage recruitment and polarization. *Acta Neuropathol,* 129**,** 97-113.

CHEN, Z.-L., YU, W.-M. & STRICKLAND, S. 2007. Peripheral Regeneration. *Annual Review of Neuroscience,* 30**,** 209-233.

CHERNOUSOV, M. A., ROTHBLUM, K., STAHL, R. C., EVANS, A., PRENTISS, L. & CAREY, D. J. 2006. Glypican-1 and a4 (V) Collagen Are Required for Schwann Cell Myelination. *The Journal of neuroscience,* 26**,** 508-517.

CHERNOUSOV, M. A., YU, W.-M., CHEN, Z.-L., CAREY, D. J. & STRICKLAND, S. 2008. Regulation of Schwann cell function by the extracellular matrix. *Glia,* 56**,** 1498-1507.

COOKE, M. J., PHILLIPS, S. R., SHAH, D. S., ATHEY, D., LAKEY, J. H. & PRZYBORSKI, S. A. 2008. Enhanced cell attachment using a novel cell culture surface presenting functional domains from extracellular matrix proteins. *Cytotechnology,* 56**,** 71-9.

CORNBROOKS, C. J., CAREY, D. J., MCDONALD, J. A., TIMPLE, R. & BUNGE, R. P. 1983. In vivo and in vitro observations on laminin production by Schwann cells. *Proceedings of the National Academy of Sciences of the United States of America,* 80**,** 3850-3854.

CORNELISON, R. C., GONZALEZ-ROTHI, E., PORVASNIK, S. L., WELLMAN, S. M., PARK, J. H., FULLER, D. D. & SCHMIDT, C. E. 2018. Injectable hydrogels of optimized acellular nerve for injection in the injured spinal cord. *Biomedical Materials*.

CORONADO, R. E., SOMARAKI-CORMIER, M., NATESAN, S., CHRISTY, R. J., ONG, J. L. & HALFF, G. A. 2017. Decellularization and Solubilization of Porcine Liver for Use as a Substrate for Porcine Hepatocyte Culture. *Cell Transplantation,* 26**,** 1840-1854.

COURT, F. A., WRABETZ, L. & FELTRI, M. L. 2006. Basal lamina: Schwann cells wrap to the rhythm of space-time. *Current Opinion in Neurobiology,* 16**,** 501-507.

CRAIG, A. S., BIRTLES, M. J., CONWAY, J. F. & PARRY, D. A. 1989. An estimate of the mean length of collagen fibrils in rat tail-tendon as a function of age. *Connect Tissue Res,* 19**,** 51-62.

CRAPO, P. M., GILBERT, T. W. & BADYLAK, D. V. M. 2011. An overview of tissue and whole organ decellularization processes. *Biomaterials,* 32**,** 3233-3243.

CRAPO, P. M., MEDBERRY, C. J., REING, J. E., TOTTEY, S., VAN, Y., MERWE, D., JONES, K. E. & BADYLAK, S. F. 2013. Biologic scaffolds composed of central nervous system extracellular matrix. *Biomaterials,* 33**,** 3539-3547.

CUEVAS, J. 2007. The somatic nervous system. *xPharm: The Comprehensive Pharmacology Reference***,** 1-13.

DAAMEN, W. F., VAN MOERKERK, H. T., HAFMANS, T., BUTTAFOCO, L., POOT, A. A., VEERKAMP, J. H. & VAN KUPPEVELT, T. H. 2003. Preparation and evaluation of molecularly-defined collagen-elastin-glycosaminoglycan scaffolds for tissue engineering. *Biomaterials,* 24**,** 4001-9.

DAHLIN, L. B., ANAGNOSTAKI, L. & LUNDBORG, G. 2001. Tissue response to silicone tubes used to repair human median and ulnar nerves. *Scandinavian Journal of Plastic and Reconstructive Surgery and Hand Surgery,* 35**,** 29-34.

DAVIS, J. B. & STROOBANT, P. 1990. Platelet-derived Growth Factors and Fibroblast Growth Factors Are Mitogens for Rat Schwalm Cells. *The Journal of cell biology,* i**,** 1353-1360.

DE ALMEIDA, P., JASPERS, M., VAESSEN, S., TAGIT, O., PORTALE, G., ROWAN, A. E. & KOUWER, P. H. J. 2019. Cytoskeletal stiffening in synthetic hydrogels. *Nat Commun,* 10**,** 609.

DE KEE, D. 2016. Note: Rheological properties of structured fluids: Improvements on the slotted-plate apparatus. *Rev Sci Instrum,* 87**,** 066109.

DE QUEIROZ ANTONINO, R., LIA FOOK, B. R. P., DE OLIVEIRA LIMA, V. A., DE FARIAS RACHED, R. I., LIMA, E. P. N., DA SILVA LIMA, R. J., PENICHE COVAS, C. A. & LIA FOOK, M. V. 2017. Preparation and Characterization of Chitosan Obtained from Shells of Shrimp (Litopenaeus vannamei Boone). *Mar Drugs,* 15.

DE RUITER, G. C. W., MALESSY, M. J. A., YASZEMSKI, M. J., WINDEBANK, A. J. & SPINNER, R. J. 2009. Designing ideal conduits for peripheral nerve repair. *Neurosurgical Focus,* 26**,** 1-9.

DEISTER, C., ALJABARI, S. & SCHMIDT, C. E. 2007. Effects of collagen 1, fibronectin, laminin and hyaluronic acid concentration in multi-component gels on neurite extension. *Journal of Biomaterials Science, Polymer Edition,* 18**,** 983-997.

DEQUACH, J. A., LIN, J. E., CAM, C., HU, D., SALVATORE, M. A., SHEIKH, F. & CHRISTMAN, K. L. 2012. Injectable skeletal muscle matrix hydrogel promotes neovascularization and muscle cell infiltration in a hindlimb ischemia model. *Eur Cell Mater,* 23**,** 400-12; discussion 412.

DEUMENS, R., BOZKURT, A., MEEK, M. F., MARCUS, M. A. E., JOOSTEN, E. A. J., WEIS, J. & BROOK, G. A. 2010. Repairing injured peripheral nerves: Bridging the gap. *Progress in Neurobiology,* 92**,** 245-276.

DEW, L., ENGLISH, W. R., CHONG, C. K. & MACNEIL, S. 2016. Investigating Neovascularization in Rat Decellularized Intestine: An In Vitro Platform for Studying Angiogenesis. *Tissue Eng Part A,* 22**,** 1317-1326.

DI SUMMA, P. G., KINGHAM, P. J., CAMPISI, C. C., RAFFOUL, W. & KALBERMATTEN, D. F. 2014. Collagen (NeuraGen®) nerve conduits and stem cells for peripheral nerve gap repair. *Neuroscience Letters,* 572**,** 26-31.

DI SUMMA, P. G., SCHIRALDI, L., CHERUBINO, M., ORANGES, C. M., KALBERMATTEN, D. F., RAFFOUL, W. & MADDURI, S. 2018. Adipose Derived Stem Cells Reduce Fibrosis and Promote Nerve Regeneration in Rats. *Anatomical Record,* 301**,** 1714-1721.

DIENSTKNECHT, T., KLEIN, S., VYKOUKAL, J., GEHMERT, S., KOLLER, M., GOSAU, M. & PRANTL, L. 2013. Type i collagen nerve conduits for median nerve repairs in the forearm. *Journal of Hand Surgery,* 38**,** 1119-1124.

DILWALI, S., PATEL, P. B., ROBERTS, D. S., BASINSKY, G. M., HARRIS, G. J., EMERICK, K. S. & STANKOVIC, K. M. 2014. Primary culture of human Schwann and schwannoma cells: improved and simplified protocol. *Hear Res,* 315**,** 25-33.

DING, T., LUO, Z. J., ZHENG, Y., HU, X. Y. & YE, Z. X. 2010. Rapid repair and regeneration of damaged rabbit sciatic nerves by tissue-engineered scaffold made from nano-silver and collagen type I. *Injury,* 41**,** 522-527.

DISCHER, D. E., JANMEY, P. & WANG, Y. L. 2005. Tissue cells feel and respond to the stiffness of their substrate. *Science,* 310**,** 1139-43.

DODLA, M. C. & BELLAMKONDA, R. V. 2006. Anisotropic scaffolds facilitate enhanced neurite extensionin vitro. *Journal of Biomedical Materials Research Part A,* 78A**,** 213-221.

DOEGE, K. J. & FESSLER, J. H. 1986. Folding of carboxyl domain and assembly of procollagen I. *J Biol Chem,* 261**,** 8924-35.

DOYU, M., SOBUE, G., KEN, E., KIMATA, K., SHINOMURA, T., YAMADA, Y., MITSUMA, T. & TAKAHASHI, A. 1993. Laminin A, B1, and B2 chain gene expression in transected and regenerating nerves: regulation by axonal signals. *J Neurochem,* 60**,** 543-51.

DU, J., LIU, J., YAO, S., MAO, H., PENG, J., SUN, X., CAO, Z., YANG, Y., XIAO, B., WANG, Y., TANG, P. & WANG, X. 2017. Prompt peripheral nerve regeneration induced by a hierarchically aligned fibrin nanofiber hydrogel. *Acta Biomaterialia,* 55**,** 296-309.

DUBOVÝ, P., KLUSÁKOVÁ, I. & SVÍŽENSKÁ, I. 2002. A quantitative immunohistochemical study of the endoneurium in the rat dorsal and ventral spinal roots. *Histochemistry and Cell Biology,* 117**,** 473-480.

DUN, X. P. & PARKINSON, D. B. 2020. Classic axon guidance molecules control correct nerve bridge tissue formation and precise axon regeneration. *Neural Regen Res,* 15**,** 6-9.

EASTWOOD, M., MUDERA, V. C., MCGROUTHER, D. A. & BROWN, R. A. 1998. Effect of precise mechanical loading on fibroblast populated collagen lattices: Morphological changes. *Cell Motility and the Cytoskeleton,* 40**,** 13-21.

EBRAHIMI, M., AI, J., BIAZAR, E., EBRAHIMI-BAROUGH, S., KHOJASTEH, A., YAZDANKHAH, M., SHARIFI, S., AI, A. & HEIDARI-KESHEL, S. 2018. In vivo assessment of a nanofibrous silk tube as nerve guide for sciatic nerve regeneration. *Artificial Cells, Nanomedicine and Biotechnology,* 46**,** 394-401.

EGGERS, R., DE WINTER, F., TANNEMAAT, M. R., MALESSY, M. J. A. & VERHAAGEN, J. 2020. GDNF Gene Therapy to Repair the Injured Peripheral Nerve. *Front Bioeng Biotechnol,* 8**,** 583184.

ELDRIDGE, C. F., SANES, J. R., CHIU, A. Y., BUNGE, R. P. & CORNBROOKS, C. J. 1986. Basal lamina-associated heparan sulphate proteoglycan in the rat PNS: characterization and localization using monoclonal antibodies. *J Neurocytol,* 15**,** 37-51.

ENGEL, H., KAO, S. W., LARSON, J., URIEL, S., JIANG, B., BREY, E. M. & CHENG, M. H. 2015. Investigation of Dermis-derived hydrogels for wound healing applications. *Biomed J,* 38**,** 58-64.

ENGEL, J., ODERMATT, E., ENGEL, A., MADRI, J. A., FURTHMAYR, H., ROHDE, H. & TIMPL, R. 1981. Shapes, domain organizations and flexibility of laminin and fibronectin, two multifunctional proteins of the extracellular matrix. *J Mol Biol,* 150**,** 97-120.

ESCO, M. A., WANG, Z., MCDERMOTT, M. L. & KURPAKUS-WHEATER, M. 2001. Potential role for laminin 5 in hypoxia-mediated apoptosis of human corneal epithelial cells. *Journal of cell science,* 114**,** 4033-4040.

EVANKO, S. P., POTTER-PERIGO, S., BOLLYKY, P. L., NEPOM, G. T. & WIGHT, T. N. 2012. Hyaluronan and versican in the control of human T-lymphocyte adhesion and migration. *Matrix Biol,* 31**,** 90-100.

FADIA, N. B., BLILEY, J. M., DIBERNARDO, G. A., CRAMMOND, D. J., SCHILLING, B. K., SIVAK, W. N., SPIESS, A. M., WASHINGTON, K. M., WALDNER, M., LIAO, H. T., JAMES, I. B., MINTEER, D. M., TOMPKINS-RHOADES, C., COTTRILL, A. R., KIM, D. Y., SCHWEIZER, R., BOURNE, D. A., PANAGIS, G. E., ASHER SCHUSTERMAN, M.,

2ND, EGRO, F. M., CAMPWALA, I. K., SIMPSON, T., WEBER, D. J., GAUSE, T., 2ND, BROOKER, J. E., JOSYULA, T., GUEVARA, A. A., REPKO, A. J., MAHONEY, C. M. & MARRA, K. G. 2020. Long-gap peripheral nerve repair through sustained release of a neurotrophic factor in nonhuman primates. *Sci Transl Med,* 12.

FARAHPOUR, M. R. & GHAYOUR, S. J. 2014. Effect of in situ delivery of acetyl-L-carnitine on peripheral nerve regeneration and functional recovery in transected sciatic nerve in rat. *International Journal of Surgery,* 12**,** 1409-1415.

FARJAH, G. H., DOLATKHAH, M. A., POURHEIDAR, B. & HESHMATIAN, B. 2017. The effect of cerebrospinal fluid in collagen guide channel on sciatic nerve regeneration in rats. *Turkish Neurosurgery,* 27**,** 453-459.

FARNEBO, S., WOON, C. Y., SCHMITT, T., JOUBERT, L. M., KIM, M., PHAM, H. & CHANG, J. 2014. Design and characterization of an injectable tendon hydrogel: a novel scaffold for guided tissue regeneration in the musculoskeletal system. *Tissue Eng Part A,* 20**,** 1550-61.

FARONI, A., SMITH, R. J., LU, L. & REID, A. J. 2016. Human Schwann-like cells derived from adipose-derived mesenchymal stem cells rapidly de-differentiate in the absence of stimulating medium. *Eur J Neurosci,* 43**,** 417-30.

FARZAMFAR, S., EHTERAMI, A., SALEHI, M., VAEEZ, A., ATASHI, A. & SAHRAPEYMA, H. 2019. Unrestricted Somatic Stem Cells Loaded in Nanofibrous Conduit as Potential Candidate for Sciatic Nerve Regeneration. *Journal of Molecular Neuroscience,* 67**,** 48-61.

FARZAMFAR, S., NASERI-NOSAR, M., GHANAVATINEJAD, A., VAEZ, A., ZARNANI, A. H. & SALEHI, M. 2017. Sciatic nerve regeneration by transplantation of menstrual blood-derived stem cells. *Molecular Biology Reports,* 44**,** 407-412.

FAUST, A., KANDAKATLA, A., MERWE, Y. V. D., REN, T., HULEIHEL, L., HUSSEY, G., NARANJO, J. D., JOHNSON, S., BADYLAK, S. & STEKETEE, M. 2017. Urinary bladder extracellular matrix hydrogels and matrix-bound vesicles differentially regulate central nervous system neuron viability and axon growth and branching. *Biomaterials applications,* 31**,** 1277-1295.

FERCANA, G. R., YERNENI, S., BILLAUD, M., HILL, J. C., VANRYZIN, P., RICHARDS, T. D., SICARI, B. M., JOHNSON, S. A., BADYLAK, S. F., CAMPBELL, P. G., GLEASON, T. G. & PHILLIPPI, J. A. 2017. Perivascular extracellular matrix hydrogels mimic native matrix microarchitecture and promote angiogenesis via basic fibroblast growth factor. *Biomaterials,* 123**,** 142-154.

FERNÁNDEZ-PÉREZ, J. & AHEARNE, M. 2019. The impact of decellularization methods on extracellular matrix derived hydrogels. *Scientific Reports,* 9**,** 1-12.

FERNANDEZ-VALLE, C., GWYNN, L., WOOD, P. M., CARBONETTO, S. & BUNGE, M. B. 1994. Anti-beta 1 integrin antibody inhibits Schwann cell myelination. *J Neurobiol,* 25**,** 1207-26.

FERNG, A. S., CONNELL, A. M., MARSH, K. M., QU, N., MEDINA, A. O., BAJAJ, N., PALOMARES, D., IWANSKI, J., TRAN, P. L., LOTUN, K., JOHNSON, K. & KHALPEY, Z. 2017. Acellular porcine heart matrices:

whole organ decellularization with 3D-bioscaffold & vascular preservation. *J Clin Transl Res,* 3**,** 260-270.

FILLA, M. S., DIMEO, K. D., TONG, T. & PETERS, D. M. 2017. Disruption of fibronectin matrix affects type IV collagen, fibrillin and laminin deposition into extracellular matrix of human trabecular meshwork (HTM) cells. *Exp Eye Res,* 165**,** 7-19.

FLEISCHMAJER, R., PERLISH, J. S., MACDONALD, E. D., 2ND, SCHECHTER, A., MURDOCH, A. D., IOZZO, R. V. & YAMADA, Y. 1998. There is binding of collagen IV to beta 1 integrin during early skin basement membrane assembly. *Ann N Y Acad Sci,* 857**,** 212-27.

FONTANA, X., HRISTOVA, M., DA COSTA, C., PATODIA, S., THEI, L., MAKWANA, M., SPENCER-DENE, B., LATOUCHE, M., MIRSKY, R., JESSEN, K. R., KLEIN, R., RAIVICH, G. & BEHRENS, A. 2012. c-Jun in Schwann cells promotes axonal regeneration and motoneuron survival via paracrine signaling. *J Cell Biol,* 198**,** 127-41.

FRENCH, K. M., BOOPATHY, A. V., DEQUACH, J. A., CHINGOZHA, L., LU, H., CHRISTMAN, K. L. & DAVIS, M. E. 2012. A naturally derived cardiac extracellular matrix enhances cardiac progenitor cell behavior in vitro. *Acta Biomater,* 8**,** 4357-64.

FREYTES, D. O., MARTIN, J., VELANKAR, S. S., LEE, A. S. & BADYLAK, S. F. 2008. Preparation and rheological characterization of a gel form of the porcine urinary bladder matrix. *Biomaterials,* 29**,** 1630-1637.

FRIEDE, R. L. & BISCHHAUSEN, R. 1978. The organization of endoneural collagen in peripheral nerves as revealed with the scanning electron microscope. *Journal of the Neurological Sciences,* 38**,** 83-88.

FRIEDRICH, E. E., LANIER, S. T., NIKNAM-BIENIA, S., ARENAS, G. A., RAJENDRAN, D., WERTHEIM, J. A. & GALIANO, R. D. 2018. Residual sodium dodecyl sulfate in decellularized muscle matrices leads to fibroblast activation in vitro and foreign body response in vivo. *Journal of Tissue Engineering and Regenerative Medicine,* 12**,** e1704-e1715.

FU, S. Y. & GORDON, T. 1997. The cellular and molecular basis of peripheral nerve regeneration. *Molecular Neurobiology,* 14**,** 67-116.

FUJII, K., TSUJI, M. & MUROTA, K. 1986. Isolation of Peripheral Nerve Collagen. *Neurochemical Research,* 11**,** 1439-1446.

FUKUDA, T., KUSUHARA, H., NAKAGOSHI, T., ISOGAI, N. & SUEYOSHI, Y. 2018. A basic fibroblast growth factor slow-release system combined to a biodegradable nerve conduit improves endothelial cell and Schwann cell proliferation: A preliminary study in a rat model. *Microsurgery,* 38**,** 899-906.

FUSAOKA-NISHIOKA, E., SHIMONO, C., TANIGUCHI, Y., TOGAWA, A., YAMADA, A., INOUE, E., ONODERA, H., SEKIGUCHI, K. & IMAI, T. 2011. Differential effects of laminin isoforms on axon and dendrite development in hippocampal neurons. *Neuroscience Research,* 71**,** 421-426.

GAETANI, R., YIN, C., SRIKUMAR, N., BRADEN, R., DOEVENDANS, P. A., SLUIJTER, J. P. & CHRISTMAN, K. L. 2016. Cardiac-Derived Extracellular Matrix Enhances Cardiogenic Properties of Human Cardiac Progenitor Cells. *Cell Transplant,* 25**,** 1653-1663.

GAMBLE, H. J. & EAMES, R. A. 1964. An Electron Microscope Study of the Connective Tissues of Human Peripheral Nerve. *J Anat,* 98**,** 655-63.

GAO, S., ZHENG, Y., CAI, Q., DENG, Z., YAO, W., WANG, J., WANG, X. & ZHANG, P. 2014a. Combination of acellular nerve graft and schwann cells-like cells for rat sciatic nerve regeneration. *Neural Plast,* 2014**,** 139085.

GAO, S., ZHENG, Y., CAI, Q., DENG, Z., YAO, W., WANG, J., WANG, X. & ZHANG, P. 2014b. Combination of acellular nerve graft and Schwann cells-like cells for rat sciatic nerve regeneration. *Neural Plasticity,* 2014.

GARCIA-DIAZ, B., BACHELIN, C., COULPIER, F., GERSCHENFELD, G., DEBOUX, C., ZUJOVIC, V., CHARNAY, P., TOPILKO, P. & BARON-VAN EVERCOOREN, A. 2019. Blood vessels guide Schwann cell migration in the adult demyelinated CNS through Eph/ephrin signaling. *Acta Neuropathol,* 138**,** 457-476.

GARGALLO, L. & RADIC, D. 2009. Viscoelastic Behaviour of Polymers. Dordrecht: Springer Netherlands.

GATTAZZO, F., URCIUOLO, A. & BONALDO, P. 2014. Extracellular matrix: a dynamic microenvironment for stem cell niche. *Biochim Biophys Acta,* 1840**,** 2506-19.

GAUDIN, R., KNIPFER, C., HENNINGSEN, A., SMEETS, R., HEILAND, M. & HADLOCK, T. 2016. Approaches to peripheral nerve repair: Generations of biomaterial conduits yielding to replacing autologous nerve grafts in craniomaxillofacial surgery. *BioMed Research International,* 2016.

GEORGIOU, M., BUNTING, S. C. J., DAVIES, H. A., LOUGHLIN, A. J., GOLDING, J. P. & PHILLIPS, J. B. 2013. Engineered neural tissue for peripheral nerve repair. *Biomaterials,* 34**,** 7335-7343.

GEORGIOU, M., GOLDING, J. P., LOUGHLIN, A. J., KINGHAM, P. J. & PHILLIPS, J. B. 2015. Engineered neural tissue with aligned, differentiated adipose-derived stem cells promotes peripheral nerve regeneration across a critical sized defect in rat sciatic nerve. *Biomaterials,* 37**,** 242-251.

GHIDINELLI, M., POITELON, Y., SHIN, Y. K., AMEROSO, D., WILLIAMSON, C., FERRI, C., PELLEGATTA, M., ESPINO, K., MOGHA, A., MONK, K., PODINI, P., TAVEGGIA, C., NAVE, K. A., WRABETZ, L., PARK, H. T. & FELTRI, M. L. 2017. Laminin 211 inhibits protein kinase A in Schwann cells to modulate neuregulin 1 type III-driven myelination. *PLoS Biology,* 15.

GHUMAN, H., GERWIG, M., NICHOLLS, F. J., LIU, J. R., DONNELLY, J., BADYLAK, S. F. & MODO, M. 2017. Long-term retention of ECM hydrogel after implantation into a sub-acute stroke cavity reduces lesion volume. *Acta Biomaterialia,* 63**,** 50-63.

GHUMAN, H., MASSENSINI, A. R., DONNELLY, J., KIM, S. M., MEDBERRY, C. J., BADYLAK, S. F. & MODO, M. 2016. ECM hydrogel for the treatment of stroke: Characterization of the host cell infiltrate. *Biomaterials,* 91**,** 166-181.

GILBERT, T. W., FREUND, J. M. & BADYLAK, S. F. 2009. Quantification of DNA in Biologic Scaffold Materials. *Journal of Surgical Research,* 152**,** 135-139.

GILLESPIE, L. N., CLARK, G. M., BARTLETT, P. F. & MARZELLA, P. L. 2001. LIF is more potent than BDNF in promoting neurite outgrowth of mammalian auditory neurons in vitro. *Neuroreport,* 12**,** 275-9.

GILPIN, S. E., GUYETTE, J. P., GONZALEZ, G., REN, X., ASARA, J. M., MATHISEN, D. J., VACANTI, J. P. & OTT, H. C. 2014. Perfusion decellularization of human and porcine lungs: Bringing the matrix to clinical scale. *Journal of Heart and Lung Transplantation,* 33**,** 298-308.

GIRALDO-GOMEZ, D. M., LEON-MANCILLA, B., DEL PRADO-AUDELO, M. L., SOTRES-VEGA, A., VILLALBA-CALOCA, J., GARCIADIEGO-CAZARES, D. & PIÑA-BARBA, M. C. 2016. Trypsin as enhancement in cyclical tracheal decellularization: Morphological and biophysical characterization. *Materials Science and Engineering C,* 59**,** 930-937.

GOETHALS, S., YDENS, E., TIMMERMAN, V. & JANSSENS, S. 2010. Toll-like receptor expression in the peripheral nerve. *Glia,* 58**,** 1701-1709.

GOLZADEH, A. & MOHAMMADI, R. 2016. Effect of local administration of platelet-derived growth factor B on functional recovery of peripheral nerve regeneration: A sciatic nerve transection model. *Dental Research Journal,* 13**,** 225-232.

GONTIKA, I., KATSIMPOULAS, M., ANTONIOU, E., KOSTAKIS, A., STAVROPOULOS-GIOKAS, C. & MICHALOPOULOS, E. 2018. Decellularized Human Umbilical Artery Used as Nerve Conduit. *Bioengineering,* 5**,** 100-100.

GONZALEZ-PEREZ, F., COBIANCHI, S., HEIMANN, C., PHILLIPS, J. B., UDINA, E. & NAVARRO, X. 2017. Stabilization, Rolling, and Addition of Other Extracellular Matrix Proteins to Collagen Hydrogels Improve Regeneration in Chitosan Guides for Long Peripheral Nerve Gaps in Rats. *Neurosurgery,* 80**,** 465-474.

GONZALEZ-PEREZ, F., HERNÁNDEZ, J., HEIMANN, C., PHILLIPS, J. B., UDINA, E. & NAVARRO, X. 2018. Schwann cells and mesenchymal stem cells in laminin- or fibronectin-aligned matrices and regeneration across a critical size defect of 15 mm in the rat sciatic nerve. *Journal of Neurosurgery: Spine,* 28**,** 109-118.

GORDON, T. 2009. The role of neurotrophic factors in nerve regeneration. *Neurosurg Focus,* 26**,** E3.

GORIO, A., LESMA, E., VERGANI, L. & DI GIULIO, A. M. 1997. Glycosaminoglycan supplementation promotes nerve regeneration and muscle reinnervation. *European Journal of Neuroscience,* 9**,** 1748-1753.

GRASMAN, J. M. & KAPLAN, D. L. 2017. Human endothelial cells secrete neurotropic factors to direct axonal growth of peripheral nerves. *Sci Rep,* 7**,** 4092.

GRAUSS, R. W., HAZEKAMP, M. G., OPPENHUIZEN, F., VAN MUNSTEREN, C. J., GITTENBERGER-DE GROOT, A. C. & DERUITER, M. C. 2005. Histological evaluation of decellularised porcine aortic valves: Matrix changes due to different decellularisation methods. *European Journal of Cardio-thoracic Surgery,* 27**,** 566-571.

GROVE, M., LEE, H., ZHAO, H. & SON, Y. J. 2020. Axon-dependent expression of YAP/TAZ mediates Schwann cell remyelination but not proliferation after nerve injury. *Elife,* 9.

GU, J., FUJIBAYASHI, A., YAMADA, K. M. & SEKIGUCHI, K. 2002. Laminin-10/11 and fibronectin differentially prevent apoptosis induced by serum removal via phosphatidylinositol 3-kinase/Akt- and MEK1/ERK-dependent pathways. *Journal of Biological Chemistry,* 277**,** 19922-19928.

GU, Y., JI, Y., ZHAO, Y., LIU, Y., DING, F., GU, X. & YANG, Y. 2012. The influence of substrate stiffness on the behavior and functions of Schwann cells in culture. *Biomaterials,* 33**,** 6672-6681.

GU, Y., LI, Z., HUANG, J., WANG, H., GU, X. & GU, J. 2017. Application of marrow mesenchymal stem cell-derived extracellular matrix in peripheral nerve tissue engineering. *Journal of Tissue Engineering and Regenerative Medicine,* 11**,** 2250-2260.

GULATI, A. K. 1988. Evaluation of acellular and cellular nerve grafts in repair of rat peripheral nerve. *J Neurosurg,* 68**,** 117-23.

GULATI, A. K., RAI, D. R. & ALI, A. M. 1995. The influence of cultured Schwann cells on regeneration through acellular basal lamina grafts. *Brain Research,* 705**,** 118-124.

GUNATILLAKE, P., MAYADUNNE, R. & ADHIKARI, R. 2006. Recent developments in biodegradable synthetic polymers. *Biotechnol Annu Rev,* 12, 301-47.

GUO, Q., LIU, C., HAI, B., MA, T., ZHANG, W., TAN, J., FU, X., WANG, H., XU, Y. & SONG, C. 2018. Chitosan conduits filled with simvastatin/Pluronic F-127 hydrogel promote peripheral nerve regeneration in rats. *Journal of Biomedical Materials Research - Part B Applied Biomaterials,* 106**,** 787-799.

HADDEN, W. J., YOUNG, J. L., HOLLE, A. W., MCFETRIDGE, M. L., KIM, D. Y., WIJESINGHE, P., TAYLOR-WEINER, H., WEN, J. H., LEE, A. R., BIEBACK, K., VO, B. N., SAMPSON, D. D., KENNEDY, B. F., SPATZ, J. P., ENGLER, A. J. & CHO, Y. S. 2017. Stem cell migration and mechanotransduction on linear stiffness gradient hydrogels. *Proceedings of the National Academy of Sciences of the United States of America,* 114**,** 5647-5652.

HALFTER, W., DONG, S., YIP, Y. P., WILLEM, M. & MAYER, U. 2002. A critical function of the pial basement membrane in cortical histogenesis. *J Neurosci,* 22**,** 6029-40.

HAN, Z. & LU, Z. R. 2017. Targeting Fibronectin for Cancer Imaging and Therapy. *J Mater Chem B,* 5**,** 639-654.

HARTY, B. L. & MONK, K. R. 2017. Unwrapping the unappreciated: recent progress in Remak Schwann cell biology. *Curr Opin Neurobiol,* 47**,** 131-137.

HEIDEMANN, S. R., LAMOUREUX, P. & BUXBAUM, R. E. 1995. Cytomechanics of axonal development. *Cell Biochem Biophys,* 27**,** 135-55.

HENNING, N. F., LEDUC, R. D., EVEN, K. A. & LARONDA, M. M. 2019. Proteomic analyses of decellularized porcine ovaries identified new matrisome proteins and spatial differences across and within ovarian compartments. *Sci Rep,* 9**,** 20001.

HILL, R. E. & WILLIAMS, R. E. 2002. A quantitative analysis of perineurial cell basement membrane collagen IV, laminin and fibronectin in diabetic and non-diabetic human sural nerve. *J Anat,* 201**,** 185-92.

HO, P. R., COAN, G. M., CHENG, E. T., NIELL, C., TARN, D. M., ZHOU, H., SIERRA, D. & TERRIS, D. J. 1998. Repair with collagen tubules linked with brain-derived neurotrophic factor and ciliary neurotrophic factor in a rat sciatic nerve injury model. *Arch Otolaryngol Head Neck Surg,* 124**,** 761-6.

HOBEN, G., YAN, Y., IYER, N., NEWTON, P., HUNTER, D. A., MOORE, A. M., SAKIYAMA-ELBERT, S. E., WOOD, M. D. & MACKINNON, S. E. 2015. Comparison of acellular nerve allograft modification with Schwann cells or VEGF. *Hand (N Y),* 10**,** 396-402.

HOBSON, M. I. 2002. Increased vascularisation enhances axonal regeneration within an acellular nerve conduit. *Ann R Coll Surg Engl,* 84**,** 47-53.

HOBSON, M. I., GREEN, C. J. & TERENGHI, G. 2000. VEGF enhances intraneural angiogenesis and improves nerve regeneration after axotomy. *J Anat,* 197 Pt 4**,** 591-605.

HODDE, J. & HILES, M. 2002. Virus safety of a porcine-derived medical device: Evaluation of a viral inactivation method. *Biotechnology and Bioengineering,* 79**,** 211-216.

HODDE, J. P., BADYLAK, S. F., BRIGHTMAN, A. O. & VOYTIK-HARBIN, S. L. 1996. Glycosaminoglycan Content of Small Intestinal Submucosa: A Bioscaffold for Tissue Replacement. *Tissue Engineering,* 2**,** 209-217.

HOFFMAN, A. S. 2001. Hydrogels for biomedical applications. *Ann N Y Acad Sci,* 944**,** 62-73.

HOHENESTER, E. 2019. Structural biology of laminins. *Essays Biochem,* 63**,** 285-295.

HOLZAPFEL, G. A., STADLER, M. & GASSER, T. C. 2005. Changes in the mechanical environment of stenotic arteries during interaction with stents: computational assessment of parametric stent designs. *J Biomech Eng,* 127**,** 166-80.

HONG, J. Y., SEO, Y., DAVAA, G., KIM, H. W., KIM, S. H. & HYUN, J. K. 2020. Decellularized brain matrix enhances macrophage polarization and functional improvements in rat spinal cord injury. *Acta Biomaterialia,* 101**,** 357-371.

HOU, Y., WANG, X., ZHANG, Z., LUO, J., CAI, Z., WANG, Y. & LI, Y. 2019. Repairing Transected Peripheral Nerve Using a Biomimetic Nerve Guidance Conduit Containing Intraluminal Sponge Fillers. *Advanced Healthcare Materials,* 8**,** 1-13.

HOZUMI, K., SUZUKI, N., NIELSEN, P. K., NOMIZU, M. & YAMADA, Y. 2006. Laminin alpha1 chain LG4 module promotes cell attachment through syndecans and cell spreading through integrin alpha2beta1. *J Biol Chem,* 281**,** 32929-40.

HSIEH, J. Y., SMITH, T. D., MELI, V. S., TRAN, T. N., BOTVINICK, E. L. & LIU, W. F. 2017. Differential regulation of macrophage inflammatory activation by fibrin and fibrinogen. *Acta Biomaterialia,* 47**,** 14-24.

HSIEH, S. C., CHANG, C. J., CHENG, W. T., TSENG, T. C. & HSU, S. H. 2016. Effect of an epineurial-like biohybrid nerve conduit on nerve regeneration. *Cell Transplantation,* 25**,** 559-574.

HSU, S. H., CHANG, W. C. & YEN, C. T. 2017. Novel flexible nerve conduits made of water-based biodegradable polyurethane for peripheral nerve regeneration. *Journal of Biomedical Materials Research - Part A,* 105**,** 1383-1392.

HU, F., ZHANG, X., LIU, H., XU, P., DOULATHUNNISA, TENG, G. & XIAO, Z. 2017. Neuronally differentiated adipose-derived stem cells and aligned PHBV nanofiber nerve scaffolds promote sciatic nerve regeneration. *Biochemical and Biophysical Research Communications,* 489**,** 171-178.

HU, X., CAI, J., YANG, J. & SMITH, G. M. 2010. Sensory axon targeting is increased by NGF gene therapy within the lesioned adult femoral nerve. *Exp Neurol,* 223**,** 153-65.

HU, Y., WU, Y., GOU, Z., TAO, J., ZHANG, J., LIU, Q., KANG, T., JIANG, S., HUANG, S., HE, J., CHEN, S., DU, Y. & GOU, M. 2016. 3D-engineering of cellularized conduits for peripheral nerve regeneration. *Scientific Reports,* 6**,** 1-12.

HUANG, C. W., HSUEH, Y. Y., HUANG, W. C., PATEL, S. & LI, S. 2019. Multipotent vascular stem cells contribute to neurovascular regeneration of peripheral nerve. *Stem Cell Research and Therapy,* 10**,** 1-9.

HUDSON, T. W., ZAWKO, S., DEISTER, C., LUNDY, S., HU, C. Y., LEE, K. & SCHMIDT, C. E. 2004. Optimized Acellular Nerve Graft Is Immunologically Tolerated and Supports Regeneration. *Tissue Engineering,* 10**,** 1641-1651.

HULEIHEL, L., BARTOLACCI, J. G., DZIKI, J. L., VOROBYOV, T., ARNOLD, B., SCARRITT, M. E., MOLINA, C. P., LOPRESTI, S. T., BROWN, B. & BADYLAK, S. F. 2017. Matrix-bound nanovesicles recapitulate extracellular matrix effects on macrophage phenotype. *Tissue Engineering Part A,* 23**,** 1283-1294.

HULEIHEL, L., HUSSEY, G. S., NARANJO, J. D., ZHANG, L., DZIKI, J. L., TURNER, N. J., STOLZ, D. B. & BADYLAK, S. F. 2016. Matrix-bound nanovesicles within ECM bioscaffolds. *Sci Adv,* 2**,** e1600502.

HUNDEPOOL, C. A., NIJHUIS, T. H. J., KOTSOUGIANI, D., FRIEDRICH, P. F., BISHOP, A. T. & SHIN, A. Y. 2017. Optimizing decullularization techniques to create a new nerve allograft: an in vitro study using rodent nerve segments. *Neurosurgery Focus,* 42**,** 1-7.

HUSSEY, G. S., DZIKI, J. L. & BADYLAK, S. F. 2018. Extracellular matrix-based materials for regenerative medicine. *Nature Reviews Materials,* 3**,** 159-173.

HUSSEY, G. S., DZIKI, J. L., LEE, Y. C., BARTOLACCI, J. G., BEHUN, M., TURNQUIST, H. R. & BADYLAK, S. F. 2019. Matrix bound nanovesicle-associated IL-33 activates a pro-remodeling macrophage phenotype via a non-canonical, ST2-independent pathway. *Journal of Immunology and Regenerative Medicine,* 3**,** 26-35.

HYNDS, D. L. & SNOW, D. M. 1999. Neurite outgrowth inhibition by chondroitin sulfate proteoglycan: Stalling/stopping exceeds turning in human neuroblastoma growth cones. *Experimental Neurology,* 160**,** 244-255.

HYYSALO, A., RISTOLA, M., MÄKINEN, M. E., HÄYRYNEN, S., NYKTER, M. & NARKILAHTI, S. 2017. Laminin α 5 substrates promote survival , network formation and functional development of human pluripotent stem cell-derived neurons in vitro. *Stem Cell Research,* 24**,** 118-127.

IDE, C., TOHYAMA, K., YOKOTA, R., NITATORI, T. & ONODERA, S. 1983. Schwann cell basal lamina and nerve regeneration. *Brain Res,* 288**,** 61-75.

IJIMA, H., NAKAMURA, S., BUAL, R., SHIRAKIGAWA, N. & TANOUE, S. 2018. Physical Properties of the Extracellular Matrix of Decellularized Porcine Liver. *Gels,* 4.

IJIMA, H., NAKAMURA, S., BUAL, R. P. & YOSHIDA, K. 2019. Liver-specific extracellular matrix hydrogel promotes liver-specific functions of

hepatocytes in vitro and survival of transplanted hepatocytes in vivo. *Journal of Bioscience and Bioengineering,* 128**,** 365-372.

IJPMA, F., VAN DE GRAAF, R. C. & MEEK, M. F. 2008. The early history of tubulation in nerve repair. *J Hand Surg Eur Vol,* 33**,** 581-6.

ILKHANIZADEH, B., ZAREI, L., FARHAD, N., BAHRAMI-BUKANI, M. & MOHAMMADI, R. 2017. Mast cells improve functional recovery of transected peripheral nerve: A novel preliminary study. *Injury,* 48**,** 1480-1485.

IMAN, M., ARAGHI, M., PANAHI, Y. & MOHAMMADI, R. 2017. Effects of Chitosan-Zinc Oxide Nanocomposite Conduit on Transected Sciatic Nerve: An Animal Model Study. *Bulletin of Emergency and Trauma,* 5**,** 240-248.

JANG, J., PARK, H. J., KIM, S. W., KIM, H., PARK, J. Y., NA, S. J., KIM, H. J., PARK, M. N., CHOI, S. H., PARK, S. H., KIM, S. W., KWON, S. M., KIM, P. J. & CHO, D. W. 2017. 3D printed complex tissue construct using stem cell-laden decellularized extracellular matrix bioinks for cardiac repair. *Biomaterials,* 112**,** 264-274.

JÄNIG, W. 1989. Autonomic Nervous System. *In:* SCHMIDT, R. F. & THEWS, G. (eds.) *Human Physiology.* Berlin, Heidelberg: Springer Berlin Heidelberg.

JANMEY, P. A., FLETCHER, D. A. & REINHART-KING, C. A. 2020. Stiffness Sensing by Cells. *Physiological reviews,* 100**,** 695-724.

JASPERS, M., DENNISON, M., MABESOONE, M. F. J., MACKINTOSH, F. C., ROWAN, A. E. & KOUWER, P. H. J. 2014. Ultra-responsive soft matter from strain-stiffening hydrogels. *Nature Communications,* 5**,** 1-8.

JEON, T., VUTESCU, E. S., SALTZMAN, E. B., VILLA, J. C., WOLFE, S. W., LEE, S. K., FEINBERG, J. H., POWNDER, S. L., DYKE, J. P. & SNEAG, D. B. 2018a. Evaluation of two collagen conduits and autograft in rabbit sciatic nerve regeneration with quantitative magnetic resonance DTI, electrophysiology, and histology. *European Radiology Experimental,* 2**,** 1-10.

JEON, T., VUTESCU, E. S., SALTZMAN, E. B., VILLA, J. C., WOLFE, S. W., LEE, S. K., FEINBERG, J. H., POWNDER, S. L., DYKE, J. P. & SNEAG, D. B. 2018b. Evaluation of two collagen conduits and autograft in rabbit sciatic nerve regeneration with quantitative magnetic resonance DTI, electrophysiology, and histology. *Eur Radiol Exp,* 2**,** 19.

JESSEN, K. R. & MIRSKY, R. 2016. The repair Schwann cell and its function in regenerating nerves. *The Journal of Physiology,* 594**,** 3521-3531.

JESSEN, K. R. & MIRSKY, R. 2019. The success and failure of the schwann cell response to nerve injury. *Frontiers in Cellular Neuroscience,* 13**,** 1-14.

JESSEN, K. R., MIRSKY, R. & LLOYD, A. C. 2015. Schwann Cells : Development and Role in Nerve Repair. *Cold Spring Harb Perspect Biol,* 7**,** 1-15.

JESURAJ, N. J., SANTOSA, K. B., MACEWAN, M. R., MOORE, A. M., KASUKURTHI, R., RAY, W. Z., FLAGG, E. R., HUNTER, D. A., BORSCHEL, G. H., JOHNSON, P. J., MACKINNON, S. E. & SAKIYAMA-ELBERT, S. E. 2014. Schwann cells seeded in acellular nerve grafts improve functional recovery. *Muscle Nerve,* 49**,** 267-76.

JI, Y., ZHOU, J., SUN, T., TANG, K., XIONG, Z., REN, Z., YAO, S., CHEN, K., YANG, F., ZHU, F. & GUO, X. 2019. Diverse preparation methods for small intestinal submucosa (SIS): Decellularization, components, and structure. *Journal of Biomedical Materials Research - Part A,* 107**,** 689-697.

JIANG, Z., SONG, Y., QIAO, J., YANG, Y., ZHANG, W., LIU, W. & HAN, B. 2019. Rat sciatic nerve regeneration across a 10-mm defect bridged by a chitin/CM-chitosan artificial nerve graft. *International Journal of Biological Macromolecules,* 129**,** 997-1005.

JIN, R., YANG, G. & LI, G. 2010. Inflammatory mechanisms in ischemic stroke: role of inflammatory cells. *J Leukoc Biol,* 87**,** 779-89.

KADLER, K. E., BALDOCK, C., BELLA, J. & BOOT-HANDFORD, R. P. 2007. Collagens at a glance. *Journal of Cell Science,* 120**,** 1955-1958.

KAJBAFZADEH, A. M., JAVAN-FARAZMAND, N., MONAJEMZADEH, M. & BAGHAYEE, A. 2013. Determining the optimal decellularization and sterilization protocol for preparing a tissue scaffold of a human-sized liver tissue. *Tissue Eng Part C Methods,* 19**,** 642-51.

KARGAR-ABARGHOUEI, E., VOJDANI, Z., HASSANPOUR, A., ALAEE, S. & TALAEI-KHOZANI, T. 2018. Characterization, recellularization, and transplantation of rat decellularized testis scaffold with bone marrow-derived mesenchymal stem cells. *Stem Cell Res Ther,* 9**,** 324.

KASIMIR, M. T., RIEDER, E., SEEBACHER, G., SILBERHUMER, G., WOLNER, E., WEIGEL, G. & SIMON, P. 2003. Comparison of different decellularization procedures of porcine heart valves. *International Journal of Artificial Organs,* 26**,** 421-427.

KAUR, G. & DUFOUR, J. M. 2012. Cell lines: Valuable tools or useless artifacts. *Spermatogenesis,* 2**,** 1-5.

KAZUYA, M. M., KATSUNORI, O. M., TETSUYA, K. M., TAKASHI, S. M., UEDA, H., ENG, M., TATSUO, N. M., KATSUAKI, E. M. & YASUHIKO, S. M. 2000. Peripheral nerve regeneration across an 80-mm gap bridged by a polyglycolic acid (PGA)– collagen tube filled with laminin-coated collagen fibers : a histological and electrophysiological evaluation of regenerated nerves. *Brain Research,* 868**,** 315-328.

KEANE, T. J., LONDONO, R., TURNER, N. J. & BADYLAK, S. F. 2012. Consequences of ineffective decellularization of biologic scaffolds on the host response. *Biomaterials,* 33**,** 1771-1781.

KEECH, M. 1954a. The effect of collagenase and trypsin on collagen. *The Anatomical Record,* 119**,** 139-159.

KEECH, M. K. 1954b. The effect of collagenase and trypsin on collagen; an electron microscopic study. *Anat Rec,* 119**,** 139-59.

KEHOE, S., ZHANG, X. F. & BOYD, D. 2012. FDA approved guidance conduits and wraps for peripheral nerve injury: a review of materials and efficacy. *Injury,* 43**,** 553-72.

KIM, H., W. CASPAR, T., SHAH, S. B. & HSIEH, A. H. 2015. Effects of proinflammatory cytokines on axonal outgrowth from adult rat lumbar dorsal root ganglia using a novel three-dimensional culture system. *Spine Journal,* 15**,** 1823-1831.

KIM, K. & KIM, M. S. 2016. An injectable hydrogel derived from small intestine submucosa as a stem cell carrier. *Journal of Biomedical Materials Research - Part B Applied Biomaterials,* 104**,** 1544-1550.

KIM, S., MAYNARD, J. C., STRICKLAND, A., BURLINGAME, A. L. & MILBRANDT, J. 2018a. Schwann cell O-GlcNAcylation promotes peripheral nerve remyelination via attenuation of the AP-1 transcription factor JUN. *Proc Natl Acad Sci U S A,* 115**,** 8019-8024.

KIM, S. M., LEE, M. S., JEON, J., LEE, D. H., YANG, K., CHO, S. W., HAN, I. & YANG, H. S. 2018b. Biodegradable Nerve Guidance Conduit with Microporous and Micropatterned Poly(lactic-co-glycolic acid)-Accelerated Sciatic Nerve Regeneration. *Macromolecular Bioscience,* 18**,** 1-14.

KIM, S. M., LEE, S. K. & LEE, J. H. 2007. Peripheral nerve regeneration using a three dimensionally cultured Schwann cell conduit. *Journal of Craniofacial Surgery,* 18**,** 475-488.

KIM, Y.-P., LEE, G.-S., KIM, J.-W., KIM, M. S., AHN, H.-S., LIM, J.-Y., KIM, H.-W., SON, Y.-J., KNOWLES, J. C. & HYUN, J. K. 2012. Phosphate glassfibres promote neurite outgrowth and early regeneration in a peripheral nerve injury model. *Journal of tissue engineering and regenerative medicine,* 9**,** 236-246.

KIM, Y., KO, H., KWON, I. K. & SHIN, K. 2016. Extracellular Matrix Revisited: Roles in Tissue Engineering. *Int Neurourol J,* 20**,** S23-29.

KINAMERI, E. & MATSUOKA, I. 2003. Autocrine action of BMP2 regulates expression of GDNF-mRNA in sciatic Schwann cells. *Molecular Brain Research,* 117**,** 221-227.

KLEIN, S., PRANTL, L., VYKOUKAL, J., LOIBL, M. & FELTHAUS, O. 2016a. Differential Effects of Coating Materials on Viability and Migration of Schwann Cells. *Materials (Basel),* 9.

KLEIN, S. M., VYKOUKAL, J., LI, D. P., PAN, H. L., ZEITLER, K., ALT, E., GEIS, S., FELTHAUS, O. & PRANTL, L. 2016b. Peripheral motor and sensory nerve conduction following transplantation of undifferentiated autologous adipose tissue-derived stem cells in a biodegradable U.S. food and drug administration-approved nerve conduit. *Plastic and Reconstructive Surgery,* 138**,** 132-139.

KLEINMAN, H. K., LUCKENBILL-EDDS, L., CANNON, F. W. & SEPHEL, G. C. 1987. Use of extracellular matrix components for cell culture. *Anal Biochem,* 166**,** 1-13.

KLIEMT, S., LANGE, C., OTTO, W., HINTZE, V., MOLLER, S., VON BERGEN, M., HEMPEL, U. & KALKHOF, S. 2013. Sulfated hyaluronan containing collagen matrices enhance cell-matrix-interaction, endocytosis, and osteogenic differentiation of human mesenchymal stromal cells. *J Proteome Res,* 12**,** 378-89.

KLUMPERS, D. D., ZHAO, X., MOONEY, D. J. & SMIT, T. H. 2013. Cell mediated contraction in 3D cell-matrix constructs leads to spatially regulated osteogenic differentiation. *Integr Biol (Camb),* 5**,** 1174-83.

KOČÍ, Z., VÝBORNÝ, K., DUBIŠOVÁ, J., VACKOVÁ, I., JÄGER, A., LUNOV, O., JIRÁKOVÁ, K. & KUBINOVÁ, Š. 2017. Extracellular Matrix Hydrogel Derived from Human Umbilical Cord as a Scaffold for Neural Tissue Repair and Its Comparison with Extracellular Matrix from Porcine Tissues. *Tissue Engineering Part C: Methods,* 23**,** 333-345.

KOKUBU, N., TSUJII, M., AKEDA, K., IINO, T. & SUDO, A. 2018. BMP-7/Smad expression in dedifferentiated Schwann cells during axonal regeneration and upregulation of endogenous BMP-7 following administration of PTH

(1-34). *Journal of Orthopaedic Surgery,* 26**,** 230949901881295-230949901881295.

KOOPMANS, G., HASSE, B. & SINIS, N. 2009. *Chapter 19 The Role of Collagen in Peripheral Nerve Repair*, Elsevier Inc.

KÖWITSCH, A., ZHOU, G. & GROTH, T. 2018. Medical application of glycosaminoglycans: a review.

KRAFTS, K. P. 2010. Tissue repair: The hidden drama. *Organogenesis,* 6**,** 225-33.

KRASSIOUKOV, A. V. 2002. Peripheral Nervous System. *In:* RAMACHANDRAN, V. S. (ed.) *Encyclopedia of the Human Brain.* New York: Academic Press.

KUANG, D. M., WU, Y., CHEN, N., CHENG, J., ZHUANG, S. M. & ZHENG, L. 2007. Tumor-derived hyaluronan induces formation of immunosuppressive macrophages through transient early activation of monocytes. *Blood,* 110**,** 587-95.

KUCHARZ, E. J. 1992. Collagen in the Nervous System. Berlin, Heidelberg: Springer Berlin Heidelberg.

KUFFLER, D. P., SOSA, I. J. & REYES, O. 2009. Schwann cell chondroitin sulfate proteoglycan inhibits dorsal root ganglion neuron neurite outgrowth and substrate specificity via a soma and not a growth cone mechanism. *J Neurosci Res,* 87**,** 2863-71.

KURTZ, A. & OH, S. J. 2012. Age related changes of the extracellular matrix and stem cell maintenance. *Prev Med,* 54 Suppl**,** S50-6.

LA FLEUR, M., UNDERWOOD, J. L., RAPPOLEE, D. A. & WERB, Z. 1996. Basement membrane and repair of injury to peripheral nerve: defining a potential role for macrophages, matrix metalloproteinases, and tissue inhibitor of metalloproteinases-1. *J Exp Med,* 184**,** 2311-26.

LABRADOR, R. O., BUTÍ, M. & NAVARRO, X. 1998. Influence of collagen and laminin gels concentration on nerve regeneration after resection and tube repair. *Experimental Neurology,* 149**,** 243-252.

LABROO, P., HILGART, D., DAVIS, B., LAMBERT, C., SANT, H., GALE, B., SHEA, J. E. & AGARWAL, J. 2019. Drug-delivering nerve conduit improves regeneration in a critical-sized gap. *Biotechnology and Bioengineering,* 116**,** 143-154.

LANTERI PARCELLS, A., ABERNATHIE, B. & DATIASHVILI, R. 2014. The use of urinary bladder matrix in the treatment of complicated open wounds. *Wounds*.

LASSNER, F., BECKER, M. & BERGER, A. 1995. Degeneration and regeneration in nerve autografts and allografts. *Microsurgery,* 16**,** 4-8.

LATTOUF, R., YOUNES, R., LUTOMSKI, D., NAAMAN, N., GODEAU, G., SENNI, K. & CHANGOTADE, S. 2014. Picrosirius red staining: a useful tool to appraise collagen networks in normal and pathological tissues. *J Histochem Cytochem,* 62**,** 751-8.

LAURENT, G. J. 1987. Dynamic state of collagen: pathways of collagen degradation in vivo and their possible role in regulation of collagen mass. *Am J Physiol,* 252**,** C1-9.

LEE, H. K., SEO, I. A., PARK, H. K., PARK, Y. M., AHN, K. J., YOO, Y. H. & PARK, H. T. 2007. Nidogen is a prosurvival and promigratory factor for adult Schwann cells. *J Neurochem,* 102**,** 686-98.

LEE, H. K., SEO, I. A., SUH, D. J. & PARK, H. T. 2009. Nidogen plays a role in the regenerative axon growth of adult sensory neurons through Schwann cells. *J Korean Med Sci,* 24**,** 654-9.

LEE, J.-Y., GIUSTI, G., FRIEDRICH, P. F., ARCHIBALD, S. J., KEMNITZER, J. E., PATEL, J., DESAI, N., BISHOP, A. T. & SHIN, A. Y. 2012. The Effect of Collagen Nerve Conduits Filled with Collagen-Glycosaminoglycan Matrix on Peripheral Motor Nerve Regeneration in a Rat Model. *The Journal of Bone and Joint Surgery-American Volume,* 94**,** 2084-2091.

LEE, J. S., SHIN, J., PARK, H. M., KIM, Y. G., KIM, B. G., OH, J. W. & CHO, S. W. 2014. Liver extracellular matrix providing dual functions of two-dimensional substrate coating and three-dimensional injectable hydrogel platform for liver tissue engineering. *Biomacromolecules,* 15**,** 206-218.

LEE, S. J., ZHU, W., NOWICKI, M., LEE, G., HEO, D. N., KIM, J., ZUO, Y. Y. & ZHANG, L. G. 2018. 3D printing nano conductive multi-walled carbon nanotube scaffolds for nerve regeneration. *J Neural Eng,* 15**,** 016018.

LEE, S. K. & WOLFE, S. W. 2000. Peripheral nerve injury and repair. *The Journal of the American Academy of Orthopaedic Surgeons,* 8**,** 243-252.

LEFCORT, F., VENSTROM, K., MCDONALD, J. A. & REICHARDT, L. F. 1992. Regulation of expression of fibronectin and its receptor, alpha 5 beta 1, during development and regeneration of peripheral nerve. *Development,* 116**,** 767-82.

LEIVO, I. & ENGVALL, E. 1988. Merosin, a protein specific for basement membranes of Schwann cells, striated muscle, and trophoblast, is expressed late in nerve and muscle development. *Proceedings of the National Academy of Sciences of the United States of America,* 85**,** 1544-1548.

LEV, R. & SPICER, S. S. 1964. Specific Staining of Sulphate Groups with Alcian Blue at Low Ph. *J Histochem Cytochem,* 12**,** 309.

LI, B., QIU, T., IYER, K. S., YAN, Q., YIN, Y., XIE, L., WANG, X. & LI, S. 2015. PRGD/PDLLA conduit potentiates rat sciatic nerve regeneration and the underlying molecular mechanism. *Biomaterials,* 55**,** 44-53.

LI, B. B., YIN, Y. X., YAN, Q. J., WANG, X. Y. & LI, S. P. 2016a. A novel bioactive nerve conduit for the repair of peripheral nerve injury. *Neural Regeneration Research,* 11**,** 150-155.

LI, H., TERENGHI, G. & HALL, S. M. 1997. Effects of delayed re-innervation on the expression of c-erbB receptors by chronically denervated rat Schwann cells in vivo. *Glia,* 20**,** 333-47.

LI, Q., UYGUN, B. E., GEERTS, S., OZER, S., SCALF, M., GILPIN, S. E., OTT, H. C., YARMUSH, M. L., SMITH, L. M., WELHAM, N. V. & FREY, B. L. 2016b. Proteomic analysis of naturally-sourced biological scaffolds. *Biomaterials,* 75**,** 37-46.

LI, R., XU, J., RAO, Z., DENG, R., XU, Y., QIU, S., LONG, H., ZHU, Q., LIU, X., BAI, Y. & QUAN, D. 2020. Facilitate Angiogenesis and Neurogenesis by Growth Factors Integrated Decellularized Matrix Hydrogel. *Tissue Eng Part A.*

LI, S., LIQUARI, P., MCKEE, K. K., HARRISON, D., PATEL, R., LEE, S. & YURCHENCO, P. D. 2005. Laminin-sulfatide binding initiates basement membrane assembly and enables receptor signaling in Schwann cells and fibroblasts. *J Cell Biol,* 169**,** 179-89.

LI, S., VAN DEN DIEPSTRATEN, C., D'SOUZA, S. J., CHAN, B. M. & PICKERING, J. G. 2003. Vascular smooth muscle cells orchestrate the assembly of type I collagen via alpha2beta1 integrin, RhoA, and fibronectin polymerization. *Am J Pathol,* 163**,** 1045-56.

LIANG, R., YANG, G., KIM, K. E., D'AMORE, A., PICKERING, A. N., ZHANG, C. & WOO, S. L. 2015. Positive effects of an extracellular matrix hydrogel on rat anterior cruciate ligament fibroblast proliferation and collagen mRNA expression. *J Orthop Translat,* 3**,** 114-122.

LIAO, Y.-F., GOTWALS, P. J., KOTELIANSKY, V. E., SHEPPARD, D. & DE WATER, L. V. 2002. The EIIIA Segment of Fibronectin Is a Ligand for Integrins alpha 9beta 1 and alpha 4beta 1 Providing a Novel Mechanism for Regulating Cell Adhesion by Alternative Splicing. *Journal of Biological Chemistry,* 227**,** 14467-14474.

LIAW, C. Y., JI, S. & GUVENDIREN, M. 2018. Engineering 3D Hydrogels for Personalized In Vitro Human Tissue Models. *Adv Healthc Mater,* 7.

LICUP, A. J., MÜNSTER, S., SHARMA, A., SHEINMAN, M., JAWERTH, L. M., FABRY, B., WEITZ, D. A. & MACKINTOSH, F. C. 2015. Stress controls the mechanics of collagen networks. *PNAS,* 112.

LIN, C. Q. & BISSELL, M. J. 1993. Multi-faceted regulation of cell differentiation by extracellular matrix. *FASEB journal : official publication of the Federation of American Societies for Experimental Biology,* 7**,** 737-43.

LIN, T., LIU, S., CHEN, S., QIU, S., RAO, Z., LIU, J., ZHU, S., YAN, L., MAO, H., ZHU, Q., QUAN, D. & LIU, X. 2018. Hydrogel derived from porcine decellularized nerve tissue as a promising biomaterial for repairing peripheral nerve defects. *Acta Biomaterialia,* 73**,** 326-338.

LINDBERG, K. & BADYLAK, S. F. 2001. Porcine small intestinal submucosa (SIS): A bioscaffold supporting in vitro primary human epidermal cell differentiation and synthesis of basement membrane proteins. *Burns,* 27**,** 254-266.

LINDSAY, R. M. 1988. Nerve growth factors (NGF, BDNF) enhance axonal regeneration but are not required for survival of adult sensory neurons. *The Journal of neuroscience,* 8**,** 2394-2405.

LIU, C., LI, X., ZHAO, Q., XIE, Y., YAO, X., WANG, M. & CAO, F. 2021. Nanofibrous bicomponent scaffolds for the dual delivery of NGF and GDNF: controlled release of growth factors and their biological effects. *J Mater Sci Mater Med,* 32**,** 9.

LIU, M., ZENG, X., MA, C., YI, H., ALI, Z., MOU, X., LI, S., DENG, Y. & HE, N. 2017. Injectable hydrogels for cartilage and bone tissue engineering. *Bone Res,* 5**,** 17014.

LIU, P., PENG, J., HAN, G. H., DING, X., WEI, S., GAO, G., HUANG, K., CHANG, F. & WANG, Y. 2019a. Role of macrophages in peripheral nerve injury and repair. *Neural Regen Res,* 14**,** 1335-1342.

LIU, X., LI, N., GONG, D., XIA, C. & XU, Z. 2018. Comparison of detergent-based decellularization protocols for the removal of antigenic cellular components in porcine aortic valve. *Xenotransplantation,* 25**,** 1-13.

LIU, X., WU, H., BYRNE, M., KRANE, S. & AENISCH, R. U. J. 1997. Type III collagen is crucial for collagen I fibrillogenesis and for and for normal cardiovascular development. *Developmental Biology,* 94**,** 1852-1856.

LIU, Y., YU, S., GU, X., CAO, R. & CUI, S. 2019b. Tissue-engineered nerve grafts using a scaffold-independent and injectable drug delivery system:

A novel design with translational advantages. *Journal of Neural Engineering,* 16.

LONDONO, R., DZIKI, J. L., HALJASMAA, E., TURNER, N. J., LEIFER, C. A. & BADYLAK, S. F. 2017. The effect of cell debris within biologic scaffolds upon the macrophage response. *Journal of Biomedical Materials Research - Part A,* 105**,** 2109-2118.

LONEKER, A. E., FAULK, D. M., HUSSEY, G. S., D'AMORE, A. & BADYLAK, S. F. 2016. Solubilized liver extracellular matrix maintains primary rat hepatocyte phenotype in-vitro. *Journal of Biomedical Materials Research - Part A,* 104**,** 957-965.

LONGO, M. V. L., MARQUES DE FARIA, J. C., ISAAC, C., NEPOMUCENO, A. C., TEIXEIRA, N. H. & GEMPERLI, R. 2016. Comparisons of the results of peripheral nerve defect repair with fibrin conduit and autologous nerve graft: An experimental study in rats. *Microsurgery,* 36**,** 59-65.

LORIMIER, P., MEZIN, P., MOLEUR, F. L., PINEL, N., PEYROL, S. & STOEBNER, P. 1992. Ultrastructural localization of the major components of the extracellular matrix in normal rat nerve. *Journal of Histochemistry and Cytochemistry,* 40**,** 859-868.

LU, H., HOSHIBA, T., KAWAZOE, N. & CHEN, G. 2012. Comparison of decellularization techniques for preparation of extracellular matrix scaffolds derived from three-dimensional cell culture. *Journal of Biomedical Materials Research - Part A,* 100 A**,** 2507-2516.

LU, P., TAKAI, K., WEAVER, V. M. & WERB, Z. 2011. Extracellular matrix degradation and remodeling in development and disease. *Cold Spring Harb Perspect Biol,* 3.

LUMPKINS, S. B., PIERRE, N. & MCFETRIDGE, P. S. 2008. A mechanical evaluation of three decellularization methods in the design of a xenogeneic scaffold for tissue engineering the temporomandibular joint disc. *Acta Biomaterialia,* 4**,** 808-816.

LUNDBORG, G., DAHLIN, L. B., DANIELSEN, N., GELBERMAN, R. H., LONGO, F. M., POWELL, H. C. & VARON, S. 1982. Nerve regeneration in silicone chambers: Influence of gap length and of distal stump components. *Experimental Neurology,* 76**,** 361-375.

LUNDBORG, G. R., DAHLIN, L. B., DANIELSEN, N. P., HANSSON, H. A. & LARSSON, K. 1981. Reorganization and orientation of regenerating nerve fibres, perineurium, and epineurium in preformed mesothelial tubes - an experimental study on the sciatic nerve of rats. *Journal of Neuroscience Research,* 6**,** 265-281.

LUQUE, E. H., ANGULO, E. & MONTES, G. S. 1983. A histochemical and electron microscopic study on the collagen of nerves in the domestic fowl. *J Anat,* 137 (Pt 1)**,** 171-6.

MADHUSUDANAN, P., RAJU, G. & SHANKARAPPA, S. 2020. Hydrogel systems and their role in neural tissue engineering. *J R Soc Interface,* 17**,** 20190505.

MADRI, J. A. & BASSON, M. D. 1992. Extracellular matrix-cell interactions: dynamic modulators of cell, tissue and organism structure and function. *Lab Invest,* 66**,** 519-21.

MALAFAYA, P. B., SILVA, G. A. & REIS, R. L. 2007. Natural-origin polymers as carriers and scaffolds for biomolecules and cell delivery in tissue engineering applications. *Adv Drug Deliv Rev,* 59**,** 207-33.

MAN, A. J., DAVIS, H. E., ITOH, A., LEACH, J. K. & BANNERMAN, P. 2011. Neurite outgrowth in fibrin gels is regulated by substrate stiffness. *Tissue Engineering - Part A,* 17**,** 2931-2942.

MAO, A. S., SHIN, J. W. & MOONEY, D. J. 2016. Effects of substrate stiffness and cell-cell contact on mesenchymal stem cell differentiation. *Biomaterials,* 98**,** 184-191.

MARQUARDT, L. M. & HEILSHORN, S. C. 2016. Design of Injectable Materials to Improve Stem Cell Transplantation. *Current Stem Cell Reports,* 2**,** 207-220.

MARUSINA, A. I., MERLEEV, A. A., LUNA, J. I., OLNEY, L., HAIGH, N. E., YOON, D., GUO, C., OVADIA, E. M., SHIMODA, M., LUXARDI, G., BODDU, S., LAL, N. N., TAKADA, Y., LAM, K. S., LIU, R., ISSEROFF, R. R., LE, S., NOLTA, J. A., KLOXIN, A. M. & MAVERAKIS, E. 2020. Tunable hydrogels for mesenchymal stem cell delivery: Integrin-induced transcriptome alterations and hydrogel optimization for human wound healing. *Stem Cells,* 38**,** 231-245.

MASSENSINI, A. R., GHUMAN, H., SALDIN, L. T., MEDBERRY, C. J., KEANE, T. J., NICHOLLS, F. J., VELANKAR, S. S., BADYLAK, S. F. & MODO, M. 2015. Concentration-dependent rheological properties of ECM hydrogel for intracerebral delivery to a stroke cavity. *Acta Biomaterialia,* 27**,** 116-130.

MATUSKA, A. M. & MCFETRIDGE, P. S. 2015. The effect of terminal sterilization on structural and biophysical properties of a decellularized collagen-based scaffold; Implications for stem cell adhesion. *Journal of Biomedical Materials Research - Part B Applied Biomaterials,* 103**,** 397-406.

MAZZA, G., ROMBOUTS, K., RENNIE HALL, A., URBANI, L., VINH LUONG, T., AL-AKKAD, W., LONGATO, L., BROWN, D., MAGHSOUDLOU, P., DHILLON, A. P., FULLER, B., DAVIDSON, B., MOORE, K., DHAR, D., DE COPPI, P., MALAGO, M. & PINZANI, M. 2015a. Decellularized human liver as a natural 3D-scaffold for liver bioengineering and transplantation. *Sci Rep,* 5**,** 13079.

MAZZA, G., ROMBOUTS, K., RENNIE HALL, A., URBANI, L., VINH LUONG, T., AL-AKKAD, W., LONGATO, L., BROWN, D., MAGHSOUDLOU, P., DHILLON, A. P., FULLER, B., DAVIDSON, B., MOORE, K., DHAR, D., DE COPPI, P., MALAGO, M. & PINZANI, M. 2015b. Decellularized human liver as a natural 3D-scaffold for liver bioengineering and transplantation. *Scientific Reports,* 5**,** 1-15.

MCKAY HART, A., WIBERG, M. & TERENGHI, G. 2003. Exogenous leukaemia inhibitory factor enhances nerve regeneration after late secondary repair using a bioartificial nerve conduit. *Br J Plast Surg,* 56**,** 444-50.

MCKEE, A. C. & DANESHVAR, D. H. 2015. The neuropathology of traumatic brain injury. *Handb Clin Neurol,* 127**,** 45-66.

MCKEE, K. K., YANG, D. H., PATEL, R., CHEN, Z. L., STRICKLAND, S., TAKAGI, J., SEKIGUCHI, K. & YURCHENCO, P. D. 2012. Schwann cell myelination requires integration of laminin activities. *Journal of Cell Science,* 125**,** 4609-4619.

MCWHORTER, F. Y., DAVIS, C. T. & LIU, W. F. 2015. Physical and mechanical regulation of macrophage phenotype and function. *Cellular and Molecular Life Sciences,* 72**,** 1303-1316.

MEDBERRY, C. J., CRAPO, P. M., SIU, B. F., CARRUTHERS, C. A., WOLF, M. T., NAGARKAR, S. P., AGRAWAL, V., JONES, K. E., KELLY, J., JOHNSON, S. A., VELANKAR, S. S., WATKINS, S. C., MODO, M. & BADYLAK, S. F. 2013. Hydrogels derived from central nervous system extracellular matrix. *Biomaterials,* 34**,** 1033-1040.

MEHRSHAD, A., SHAHRAKI, M. & EHTESHAMFAR, S. 2017. Local Administration of Methylprednisolone Laden Hydrogel Enhances Functional Recovery of Transected Sciatic Nerve in Rat. *Bulletin of Emergency and Trauma,* 5**,** 231-239.

MEHTA, H. 1985. Synthesis by Schwann cells of basal lamina and membrane-associated heparan sulfate proteoglycans. *The Journal of Cell Biology,* 101**,** 660-666.

MEIGEL, W. N., GAY, S. & WEBER, L. 1977. Dermal architecture and collagen type distribution. *Archives for Dermatological Research,* 259**,** 1-10.

MENART, V., FONDA, I., KENIG, M. & POREKAR, V. G. 2002. Increased in vitro cytotoxicity of TNF-alpha analog LK-805 is based on the interaction with cell surface heparan sulfate proteoglycan. *Ann N Y Acad Sci,* 973**,** 194-206.

MENDOZA-NOVELO, B., AVILA, E. E., CAUICH-RODRÍGUEZ, J. V., JORGE-HERRERO, E., ROJO, F. J., GUINEA, G. V. & MATA-MATA, J. L. 2011. Decellularization of pericardial tissue and its impact on tensile viscoelasticity and glycosaminoglycan content. *Acta Biomaterialia,* 7**,** 1241-1248.

MENEZES, R., HASHEMI, S., VINCENT, R., COLLINS, G., MEYER, J., FOSTON, M. & ARINZEH, T. L. 2019. Investigation of glycosaminoglycan mimetic scaffolds for neurite growth. *Acta Biomaterialia,* 90**,** 169-178.

MENG, F. W., SLIVKA, P. F., DEARTH, C. L. & BADYLAK, S. F. 2015. Solubilized extracellular matrix from brain and urinary bladder elicits distinct functional and phenotypic responses in macrophages. *Biomaterials,* 46**,** 131-140.

MERLE, M., DELLON, A. L., CAMPBELL, J. N. & CHANG, P. S. 1989. Complications from silicon-polymer intubulation of nerves. *Microsurgery,* 10**,** 130-3.

MILAN, A. M., SUGARS, R. V., EMBERY, G. & WADDINGTON, R. J. 2005. Modulation of collagen fibrillogenesis by dentinal proteoglycans. *Calcif Tissue Int,* 76**,** 127-35.

MILNER, R., WILBY, M., NISHIMURA, S., BOYLEN, K., EDWARDS, G., FAWCETT, J., STREULI, C., PYTELA, R. & FFRENCH-CONSTANT, C. 1997. Division of labor of Schwann cell integrins during migration on peripheral nerve extracellular matrix ligands. *Dev Biol,* 185**,** 215-28.

MOHAMADI, F., EBRAHIMI-BAROUGH, S., NOURANI, M. R., AHMADI, A. & AI, J. 2018. Use new poly (ε-caprolactone/collagen/NBG) nerve conduits along with NGF for promoting peripheral (sciatic) nerve regeneration in a rat. *Artificial Cells, Nanomedicine and Biotechnology,* 46**,** 34-45.

MOKARIZADEH, A., MEHRSHAD, A. & MOHAMMADI, R. 2016. Local Polyethylene Glycol in Combination with Chitosan Based Hybrid Nanofiber Conduit Accelerates Transected Peripheral Nerve Regeneration. *Journal of Investigative Surgery,* 29**,** 167-174.

MONNIER, P. P., SIERRA, A., SCHWAB, J. M., HENKE-FAHLE, S. & MUELLER, B. K. 2003. The Rho/ROCK pathway mediates neurite growth-inhibitory activity associated with the chondroitin sulfate proteoglycans of the CNS glial scar. *Molecular and Cellular Neuroscience,* 22**,** 319-330.

MOSAHEBI, A., FULLER, P., WIBERG, M. & TERENGHI, G. 2002a. Effect of allogeneic Schwann cell transplantation on peripheral nerve regeneration. *Exp Neurol,* 173**,** 213-23.

MOSAHEBI, A., FULLER, P., WIBERG, M. & TERENGHI, G. 2002b. Effect of allogeneic schwann cell transplantation on peripheral nerve regeneration. *Experimental Neurology,* 173**,** 213-223.

MOSALA NEZHAD, Z., PONCELET, A., DE KERCHOVE, L., GIANELLO, P., FERVAILLE, C. & EL KHOURY, G. 2016a. Small intestinal submucosa extracellular matrix (CorMatrix(R)) in cardiovascular surgery: a systematic review. *Interact Cardiovasc Thorac Surg,* 22**,** 839-50.

MOSALA NEZHAD, Z., PONCELET, A., DE KERCHOVE, L., GIANELLO, P., FERVAILLE, C. & EL KHOURY, G. 2016b. Small intestinal submucosa extracellular matrix (CorMatrix®) in cardiovascular surgery: A systematic review. *Interactive Cardiovascular and Thoracic Surgery,* 22**,** 839-850.

MOSTAFAVI-POUR, Z., ASKARI, J. A., WHITTARD, J. D. & HUMPHRIES, M. J. 2001. Identification of a novel heparin-binding site in the alternatively spliced IIICS region of fibronectin: roles of integrins and proteoglycans in cell adhesion to fibronectin splice variants. *Matrix Biology,* 20**,** 63-73.

MOTTAGHITALAB, F., FAROKHI, M., ZAMINY, A., KOKABI, M., SOLEIMANI, M., MIRAHMADI, F., SHOKRGOZAR, M. A. & SADEGHIZADEH, M. 2013. A Biosynthetic Nerve Guide Conduit Based on Silk/SWNT/Fibronectin Nanocomposite for Peripheral Nerve Regeneration. *PLoS ONE,* 8**,** 6-17.

MOTTE, S. & KAUFMAN, L. J. 2013. Strain stiffening in collagen I networks. *Biopolymers,* 99**,** 35-46.

MOW, V. C., KUEI, S. C., LAI, W. M. & ARMSTRONG, C. G. 1980. Biphasic creep and stress relaxation of articular cartilage in compression? Theory and experiments. *J Biomech Eng,* 102**,** 73-84.

MUANGSANIT, P. 2020. *Aligned endothelial cell and Schwann cell structures in 3D hydrogels for peripheral nerve tissue engineering.* Ph.D, UCL (University College London).

MUANGSANIT, P., DAY, A., DIMIOU, S., ATAC, A. F., KAYAL, C., PARK, H., NAZHAT, S. N. & PHILLIPS, J. B. 2020. Rapidly formed stable and aligned dense collagen gels seeded with Schwann cells support peripheral nerve regeneration. *J Neural Eng,* 17**,** 046036.

MUDERA, V. C., PLEASS, R., EASTWOOD, M., TARNUZZER, R., SCHULTZ, G., KHAW, P., MCGROUTHER, D. A. & BROWN, R. A. 2000. Molecular responses of human dermal fibroblasts to dual cues: contact guidance and mechanical load. *Cell Motil Cytoskeleton,* 45**,** 1-9.

MUHEREMU, A. & AO, Q. 2015. Past, Present, and Future of Nerve Conduits in the Treatment of Peripheral Nerve Injury. *BioMed Research International,* 2015**,** 1-6.

MUNAKATA, H., TAKAGAKI, K., MAJIMA, M. & ENDO, M. 1999. Interaction between collagens and glycosaminoglycans investigated using a surface plasmon resonance biosensor. *Glycobiology,* 9**,** 1023-7.

MUNCIE, J. M. & WEAVER, V. M. 2018. *The Physical and Biochemical Properties of the Extracellular Matrix Regulate Cell Fate*, Elsevier Inc.

NACHEMSON, A. K., HANSSON, H. A. & LUNDBORG, G. 1988. Neurotropism in nerve regeneration: an immunohistochemical study. *Acta Physiol Scand,* 133**,** 139-48.

NAGAO, R. J., LUNDY, S., KHAING, Z. Z. & SCHMIDT, C. E. 2011. Functional characterization of optimized acellular peripheral nerve graft in a rat sciatic nerve injury model. *Neurological Research,* 33**,** 600-608.

NAGATA, S., HANAYAMA, R. & KAWANE, K. 2010a. Autoimmunity and the Clearance of Dead Cells. *Cell,* 140**,** 619-630.

NAGATA, S., HANAYAMA, R. & KAWANE, K. 2010b. Autoimmunity and the clearance of dead cells. *Cell,* 140**,** 619-30.

NAKAMURA, S. & IJIMA, H. 2013. Solubilized matrix derived from decellularized liver as a growth factor-immobilizable scaffold for hepatocyte culture. *Journal of Bioscience and Bioengineering,* 116**,** 746-753.

NATH, R. K., MACKINNON, S. E., JENSEN, J. N. & PARKS, W. C. 1997. Spatial pattern of type I collagen expression in injured peripheral nerve. *J Neurosurg,* 86**,** 866-70.

NEUMAN, R. E. & LOGAN, M. A. 1950. The determination of hydroxyproline. *The Journal of biological chemistry,* 184**,** 299-306.

NG, W. P. & LOZANO, A. M. 1999. Neuronal age influences the response to neurite outgrowth inhibitory activity in the central and peripheral nervous systems. *Brain Res,* 836**,** 49-61.

NGUYEN, L., AFSHARI, A., KELM, N. D., POLLINS, A. C., SHACK, R. B., DOES, M. D. & THAYER, W. P. 2017a. Bridging the gap: Engineered porcine-derived urinary bladder matrix conduits as a novel scaffold for peripheral nerve regeneration. *Annals of Plastic Surgery,* 78**,** S328-S334.

NGUYEN, L., AFSHARI, A., KELM, N. D., POLLINS, A. C., SHACK, R. B., DOES, M. D. & THAYER, W. P. 2017b. Engineered Porcine-derived Urinary Bladder Matrix Conduits as a Novel Scaffold for Peripheral Nerve Regeneration. *Annals of Plastic Surgery,* 78**,** S328-S334.

NISHIUCHI, R., TAKAGI, J., HAYASHI, M., IDO, H., YAGI, Y., SANZEN, N., TSUJI, T., YAMADA, M. & SEKIGUCHI, K. 2006. Ligand-binding specificities of laminin-binding integrins: a comprehensive survey of laminin-integrin interactions using recombinant alpha3beta1, alpha6beta1, alpha7beta1 and alpha6beta4 integrins. *Matrix Biol,* 25**,** 189-97.

NIU, Y., CHEN, K. C., HE, T., YU, W., HUANG, S. & XU, K. 2014. Scaffolds from block polyurethanes based on poly(ε-caprolactone) (PCL) and poly(ethylene glycol) (PEG) for peripheral nerve regeneration. *Biomaterials,* 35**,** 4266-4277.

O'ROURKE, C., DRAKE, R. A. L., CAMERON, G. W. W., LOUGHLIN, A. J. & PHILLIPS, J. B. 2015. Optimising contraction and alignment of cellular collagen hydrogels to achieve reliable and consistent engineered anisotropic tissue. *Journal of Biomaterials Applications,* 30**,** 599-607.

O'ROURKE, C., DAY, A. G. E., MURRAY-DUNNING, C., THANABALASUNDARAM, L., COWAN, J., STEVANATO, L., GRACE, N., CAMERON, G., DRAKE, R. A. L., SINDEN, J. & PHILLIPS, J. B. 2018. An allogeneic 'off the shelf' therapeutic strategy for peripheral

nerve tissue engineering using clinical grade human neural stem cells. *Scientific Reports,* 8, 2951-2951.

OPENSTAX 2016. *Anatomy & physiology*, OpenStax.

PADUANO, F., MARRELLI, M., ALOM, N., AMER, M., LISA, J., SHAKESHEFF, K. M., TATULLO, M., PADUANO, F., MARRELLI, M., ALOM, N. & AMER, M. 2017. Decellularized bone extracellular matrix and human dental pulp stem cells as a construct for bone regeneration. *Journal of Biomaterials Science, Polymer Edition,* 28, 730-748.

PAN, M., WANG, X., CHEN, Y., CAO, S., WEN, J., WU, G., LI, Y., LI, L., QIAN, C., QIN, Z., LI, Z., TAN, D., FAN, Z., WU, W. & GUO, J. 2017. Tissue engineering with peripheral blood-derived mesenchymal stem cells promotes the regeneration of injured peripheral nerves. *Experimental Neurology,* 292, 92-101.

PAN, M. X., HU, P. Y., CHENG, Y., CAI, L. Q., RAO, X. H., WANG, Y. & GAO, Y. 2014. An efficient method for decellularization of the rat liver. *Journal of the Formosan Medical Association,* 113, 680-687.

PANKOV, R. 2002. Fibronectin at a glance. *Journal of Cell Science,* 115, 3861-3863.

PARMAKSIZ, M., ELCIN, A. E. & ELCIN, Y. M. 2020. Decellularized Cell Culture ECMs Act as Cell Differentiation Inducers. *Stem Cell Rev Rep,* 16, 569-584.

PARRINELLO, S., NAPOLI, I., RIBEIRO, S., DIGBY, P. W., FEDOROVA, M., PARKINSON, D. B., DODDRELL, R. D. S., NAKAYAMA, M., ADAMS, R. H. & LLOYD, A. C. 2010. EphB signaling directs peripheral nerve regeneration through Sox2-dependent Schwann cell Sorting. *Cell,* 143, 145-155.

PATTON, B. L. 2000. Laminins of the neuromuscular system. *Microsc Res Tech,* 51, 247-61.

PATTON, B. L., MINER, J. H., CHIU, A. Y. & SANES, J. R. 1997. Distribution and Function of Laminins in the Neuromuscular System of Developing, Adult, and Mutant Mice. *Journal of Cell Biology,* 139, 1507-1521.

PAULSSON, M. 1992. The role of laminin in attachment, growth, and differentiation of cultured cells: a brief review. *Cytotechnology,* 9, 99-106.

PELLEGRINI, L. 2001. Role of heparan sulfate in fibroblast growth factor signalling: a structural view. *Curr Opin Struct Biol,* 11, 629-34.

PELTONEN, S., ALANNE, M. & PELTONEN, J. 2013. Barriers of the peripheral nerve. *Tissue Barriers,* 1, e24956-e24956.

PEREA-GIL, I., URIARTE, J. J., PRAT-VIDAL, C., GÁLVEZ-MONTÓN, C., ROURA, S., LLUCIÀ-VALLDEPERAS, A., SOLER-BOTIJA, C., FARRÉ, R., NAVAJAS, D. & BAYES-GENIS, A. 2015. In vitro comparative study of two decellularization protocols in search of an optimal myocardial scaffold for recellularization. *American Journal of Translational Research,* 7, 558-573.

PERRY, V. H. & BROWN, M. C. 1992. Macrophages and nerve regeneration. *Current Opinion in Neurobiology,* 2, 679-682.

PETERSEN, T. H., CALLE, E. A., ZHAO, L., LEE, E. J., GUI, L., RAREDON, M. S. B., GAVRILOV, K., YI, T., ZHUANG, Z. W., BREUER, C., HERZOG, E. & NIKLASON, L. E. 2010. Tissue-engineered lungs for in vivo implantation. *Science,* 329, 538-541.

PETREACA, M. & MARTINS-GREEN, M. 2020. Chapter 6 - The dynamics of cell–extracellular matrix interactions, with implications for tissue engineering. *In:* LANZA, R., LANGER, R., VACANTI, J. P. & ATALA, A. (eds.) *Principles of Tissue Engineering (Fifth Edition).* Academic Press.

PETROSYAN, A., DA SACCO, S., TRIPURANENI, N., KREUSER, U., LAVARREDA-PEARCE, M., TAMBURRINI, R., DE FILIPPO, R. E., ORLANDO, G., CRAVEDI, P. & PERIN, L. 2017. A step towards clinical application of acellular matrix: A clue from macrophage polarization. *Matrix Biology,* 57-58**,** 334-346.

PETTERSSON, J., KALBERMATTEN, D., MCGRATH, A. & NOVIKOVA, L. N. 2010. Biodegradable fibrin conduit promotes long-term regeneration after peripheral nerve injury in adult rats. *J Plast Reconstr Aesthet Surg,* 63**,** 1893-9.

PFEIFFER, E., VICKERS, S. M., FRANK, E., GRODZINSKY, A. J. & SPECTOR, M. 2008. The effects of glycosaminoglycan content on the compressive modulus of cartilage engineered in type II collagen scaffolds. *Osteoarthritis and Cartilage,* 16**,** 1237-1244.

PHILLIPS, J. B., BUNTING, S. C. J., HALL, S. M. & BROWN, R. A. 2005. Neural Tissue Engineering: A Self-Organizing Collagen Guidance Conduit. *Tissue Engineering,* 11**,** 1611-1617.

PICKERING, J. G. 2001. Regulation of vascular cell behavior by collagen : form is function. *Circ Res,* 88**,** 458-9.

PIETRZAK, W. S., ALI, S. N., CHITTURI, D., JACOB, M. & WOODELL-MAY, J. E. 2011. BMP depletion occurs during prolonged acid demineralization of bone: Characterization and implications for graft preparation. *Cell and Tissue Banking,* 12**,** 81-88.

PINA-OVIEDO, S. & ORTIZ-HIDALGO, C. 2008. The Normal and Neoplastic Perineurium. *Adv Anat Pathol,* 15**,** 147-164.

PLANTMAN, S., PATARROYO, M., FRIED, K., DOMOGATSKAYA, A., TRYGGVASON, K., HAMMARBERG, H. & CULLHEIM, S. 2008. Integrin-laminin interactions controlling neurite outgrowth from adult DRG neurons in vitro. *Molecular and Cellular Neuroscience,* 39**,** 50-62.

PODHAJSKY, R. J. & MYERS, R. R. 1995. A diffusion-reaction model of nerve regeneration. *J Neurosci Methods,* 60**,** 79-88.

PODRATZ, J. L., RODRIGUEZ, E. & WINDEBANK, A. J. 2001. Role of the extracellular matrix in myelination of peripheral nerve. *Glia,* 35**,** 35-40.

PODUSLO, J. F., LOW, P. A., NICKANDER, K. K. & DYCK, P. J. 1985. Mammalian endoneurial fluid: Collection and protein analysis from normal and crushed nerves. *Brain Research,* 332**,** 91-102.

POLLINS, A. C., BOYER, R. B., NUSSENBAUM, M. & THAYER, W. P. 2018. Comparing Processed Nerve Allografts and Assessing Their Capacity to Retain and Release Nerve Growth Factor. *Ann Plast Surg,* 81**,** 198-202.

POTAS, J. R., HAQUE, F., MACLEAN, F. L. & NISBET, D. R. 2015. Interleukin-10 conjugated electrospun polycaprolactone (PCL) nanofibre scaffolds for promoting alternatively activated (M2) macrophages around the peripheral nerve in vivo. *Journal of Immunological Methods,* 420**,** 38-49.

PREST, T. A., YEAGER, E., LOPRESTI, S. T., ZYGELYTE, E., MARTIN, M. J., DONG, L., GIBSON, A., OLUTOYE, O. O., BROWN, B. N. & CHEETHAM, J. 2017. Nerve-specific, xenogeneic extracellular matrix

hydrogel promotes recovery following peripheral nerve injury. *Journal of Biomedical Materials Research Part A,* 450-459.

QIU, P., LI, M., CHEN, K., FANG, B., CHEN, P., TANG, Z., LIN, X. & FAN, S. 2020a. Periosteal matrix-derived hydrogel promotes bone repair through an early immune regulation coupled with enhanced angio- and osteogenesis. *Biomaterials,* 227**,** 119552-119552.

QIU, S., RAO, Z., HE, F., WANG, T., XU, Y., DU, Z., YAO, Z., LIN, T., YAN, L., QUAN, D., ZHU, Q. & LIU, X. 2020b. Decellularized nerve matrix hydrogel and glial-derived neurotrophic factor modifications assisted nerve repair with decellularized nerve matrix scaffolds. *Journal of Tissue Engineering and Regenerative Medicine***,** 1-13.

RAHMAN, S., GRIFFIN, M., NAIK, A., SZARKO, M. & BUTLER, P. E. M. 2018. Optimising the decellularization of human elastic cartilage with trypsin for future use in ear reconstruction. *Scientific Reports,* 8**,** 3097-3097.

RAO, N., AGMON, G., TIERNEY, M. T., UNGERLEIDER, J. L., BRADEN, R. L., SACCO, A. & CHRISTMAN, K. L. 2017. Engineering an Injectable Muscle-Specific Microenvironment for Improved Cell Delivery Using a Nanofibrous Extracellular Matrix Hydrogel. *ACS Nano,* 11**,** 3851-3859.

RAO, Z., LIN, T., QIU, S., ZHOU, J., LIU, S., CHEN, S., WANG, T., LIU, X., ZHU, Q., BAI, Y. & QUAN, D. 2021. Decellularized nerve matrix hydrogel scaffolds with longitudinally oriented and size-tunable microchannels for peripheral nerve regeneration. *Mater Sci Eng C Mater Biol Appl,* 120**,** 111791.

RASULIC, L., SAVIC, A., ZIVKOVIC, B., VITOSEVIC, F., MICOVIC, M., BASCAREVIC, V., PUZOVIC, V., NOVAKOVIC, N., LEPIC, M., SAMARDZIC, M. & MANDIC-RAJCEVIC, S. 2017. Outcome after brachial plexus injury surgery and impact on quality of life. *Acta Neurochir (Wien),* 159**,** 1257-1264.

RAY, W. Z. & MACKINNON, S. E. 2010. Management of nerve gaps: Autografts, allografts, nerve transfers, and end-to-side neurorrhaphy. *Experimental Neurology,* 223**,** 77-85.

REDERSTORFF, E., WEISS, P., SOURICE, S., PILET, P., XIE, F., SINQUIN, C., COLLIEC-JOUAULT, S., GUICHEUX, J. & LAIB, S. 2011. An in vitro study of two GAG-like marine polysaccharides incorporated into injectable hydrogels for bone and cartilage tissue engineering. *Acta Biomater,* 7**,** 2119-30.

REID, A. J., SUN, M., WIBERG, M., DOWNES, S., TERENGHI, G. & KINGHAM, P. J. 2011. Nerve repair with adipose-derived stem cells protects dorsal root ganglia neurons from apoptosis. *Neuroscience,* 199**,** 515-22.

REN, H., SHI, X., TAO, L., XIAO, J., HAN, B., ZHANG, Y., YUAN, X. & DING, Y. 2013. Evaluation of two decellularization methods in the development of a whole-organ decellularized rat liver scaffold. *Liver International,* 33**,** 448-458.

RICARD-BLUM, S. 2011. The Collagen Family. *Cold Spring Harbor Perspectives in Biology,* 3**,** 1-19.

RIEDER, E., KASIMIR, M. T., SILBERHUMER, G., SEEBACHER, G., WOLNER, E., SIMON, P. & WEIGEL, G. 2004. Decellularization protocols of porcine heart valves differ importantly in efficiency of cell

removal and susceptibility of the matrix to recellularization with human vascular cells. *J Thorac Cardiovasc Surg,* 127**,** 399-405.

RIJAL, G. & LI, W. 2017. A versatile 3D tissue matrix scaffold system for tumor modeling and drug screening. *Sci Adv,* 3**,** e1700764.

ROCHE, P., ALEKSEEVA, T., WIDAA, A., RYAN, A., MATSIKO, A., WALSH, M., DUFFY, G. P. & O'BRIEN, F. J. 2017. Olfactory Derived Stem Cells Delivered in a Biphasic Conduit Promote Peripheral Nerve Repair In Vivo. *Stem Cells Translational Medicine,* 6**,** 1894-1904.

ROJKIND, M., GIAMBRONE, M. A. & BIEMPICA, L. 1979. Collagen Types in Normal and Cirrhotic Liver. *Gastroenterology,* 76**,** 710-719.

ROTHER, S., KRONERT, V., HAUCK, N., BERG, A., MOELLER, S., SCHNABELRAUCH, M., THIELE, J., SCHARNWEBER, D. & HINTZE, V. 2019. Hyaluronan/collagen hydrogel matrices containing high-sulfated hyaluronan microgels for regulating transforming growth factor-beta1. *J Mater Sci Mater Med,* 30**,** 65.

ROUGHLEY, P. J. & MORT, J. S. 2014. The role of aggrecan in normal and osteoarthritic cartilage. *J Exp Orthop,* 1**,** 8.

RUDNICKI, M. S., CIRKA, H. A., AGHVAMI, M., SANDER, E. A., WEN, Q. & BILLIAR, K. L. 2013. Nonlinear strain stiffening is not sufficient to explain how far cells can feel on fibrous protein gels. *Biophysical Journal,* 105**,** 11-20.

RYDEVIK, B. L., KWAN, M. K., MYERS, R. R., BROWN, R. A., TRIGGS, K. J., WOO, S. L. & GARFIN, S. R. 1990. An in vitro mechanical and histological study of acute stretching on rabbit tibial nerve. *J Orthop Res,* 8**,** 694-701.

SACKETT, S. D., TREMMEL, D. M., MA, F., FEENEY, A. K., MAGUIRE, R. M., BROWN, M. E., ZHOU, Y., LI, X., O'BRIEN, C., LI, L., BURLINGHAM, W. J. & ODORICO, J. S. 2018. Extracellular matrix scaffold and hydrogel derived from decellularized and delipidized human pancreas. *Scientific Reports,* 8**,** 10452-10452.

SAEKI, M., TANAKA, K., IMATANI, J., OKAMOTO, H., WATANABE, K., NAKAMURA, T., GOTANI, H., OHI, H., NAKAMURA, R. & HIRATA, H. 2018. Efficacy and safety of novel collagen conduits filled with collagen filaments to treat patients with peripheral nerve injury: A multicenter, controlled, open-label clinical trial. *Injury,* 49**,** 766-774.

SAHEB-AL-ZAMANI, M., YAN, Y., FARBER, S. J., HUNTER, D. A., NEWTON, P., WOOD, M. D., STEWART, S. A., JOHNSON, P. J. & MACKINNON, S. E. 2013. Limited regeneration in long acellular nerve allografts is associated with increased Schwann cell senescence. *Exp Neurol,* 247**,** 165-77.

SALDIN, L. T., CRAMER, M. C., VELANKAR, S. S., WHITE, L. J. & BADYLAK, S. F. 2017. Extracellular matrix hydrogels from decellularized tissues: Structure and function. *Acta Biomaterialia,* 49**,** 1-15.

SALEHI, M., NASERI-NOSAR, M., EBRAHIMI-BAROUGH, S., NOURANI, M., KHOJASTEH, A., FARZAMFAR, S., MANSOURI, K. & AI, J. 2018a. Polyurethane/Gelatin Nanofibrils Neural Guidance Conduit Containing Platelet-Rich Plasma and Melatonin for Transplantation of Schwann Cells. *Cellular and Molecular Neurobiology,* 38**,** 703-713.

SALEHI, M., NASERI-NOSAR, M., EBRAHIMI-BAROUGH, S., NOURANI, M., KHOJASTEH, A., HAMIDIEH, A. A., AMANI, A., FARZAMFAR, S. & AI,

J. 2018b. Sciatic nerve regeneration by transplantation of Schwann cells via erythropoietin controlled-releasing polylactic acid/multiwalled carbon nanotubes/gelatin nanofibrils neural guidance conduit. *Journal of Biomedical Materials Research - Part B Applied Biomaterials,* 106**,** 1463-1476.

SALTZMAN, E. B., VILLA, J. C., DOTY, S. B., FEINBERG, J. H., LEE, S. K. & WOLFE, S. W. 2019. A Comparison Between Two Collagen Nerve Conduits and Nerve Autograft: A Rat Model of Motor Nerve Regeneration. *J Hand Surg Am,* 44**,** 700 e1-700 e9.

SANEN, K., MARTENS, W., GEORGIOU, M., AMELOOT, M., LAMBRICHTS, I. & PHILLIPS, J. 2017. Engineered neural tissue with Schwann cell differentiated human dental pulp stem cells: potential for peripheral nerve repair? *Journal of Tissue Engineering and Regenerative Medicine,* 11**,** 3362-3372.

SAPUDOM, J., MOHAMED, W. K. E., GARCIA-SABATE, A., ALATOOM, A., KARAMAN, S., MAHTANI, N. & TEO, J. C. 2020. Collagen Fibril Density Modulates Macrophage Activation and Cellular Functions during Tissue Repair. *Bioengineering (Basel),* 7.

SARKER, M., NAGHIEH, S., MCINNES, A. D., SCHREYER, D. J. & CHEN, X. 2018a. Strategic Design and Fabrication of Nerve Guidance Conduits for Peripheral Nerve Regeneration. *Biotechnology Journal,* 13**,** 1-16.

SARKER, M. D., NAGHIEH, S., MCINNES, A. D., SCHREYER, D. J. & CHEN, X. 2018b. Regeneration of peripheral nerves by nerve guidance conduits: Influence of design, biopolymers, cells, growth factors, and physical stimuli. *Prog Neurobiol,* 171**,** 125-150.

SAWKINS, M. J., BOWEN, W., DHADDA, P., MARKIDES, H., SIDNEY, L. E., TAYLOR, A. J., ROSE, F. R. A. J., BADYLAK, S. F., SHAKESHEFF, K. M. & WHITE, L. J. 2013. Hydrogels derived from demineralized and decellularized bone extracellular matrix. *Acta Biomaterialia,* 9**,** 7865-7873.

SAYANAGI, J., TANAKA, H., EBARA, M., OKADA, K., OKA, K., MURASE, T. & YOSHIKAWA, H. 2020. Combination of Electrospun Nanofiber Sheet Incorporating Methylcobalamin and PGA-Collagen Tube for Treatment of a Sciatic Nerve Defect in a Rat Model. *The Journal of Bone and Joint Surgery,* 102**,** 245-253.

SCHENKE-LAYLAND, K., VASILEVSKI, O., OPITZ, F., KÖNIG, K., RIEMANN, I., HALBHUBER, K. J., WAHLERS, T. & STOCK, U. A. 2003. Impact of decellularization of xenogeneic tissue on extracellular matrix integrity for tissue engineering of heart valves. *Journal of Structural Biology,* 143**,** 201-208.

SCHENSE, J. C., BLOCH, J., AEBISCHER, P. & HUBBELL, J. A. 2000. Enzymatic incorporation of bioactive peptides into fibrin matrices enhances neurite extension. *Nat Biotechnol,* 18**,** 415-9.

SCHIFF, R. & ROSENBLUTH, J. 1986. Ultrastructural localization of laminin in rat sensory ganglia. *J Histochem Cytochem,* 34**,** 1691-9.

SCHIMMEL, S. J., ACOSTA, S. & LOZANO, D. 2017. Neuroinflammation in traumatic brain injury: A chronic response to an acute injury. *Brain Circ,* 3**,** 135-142.

SCHOLZ, T., SUMARTO, A., KRICHEVSKY, A. & EVANS, G. R. 2011. Neuronal differentiation of human adipose tissue-derived stem cells for peripheral nerve regeneration in vivo. *Arch Surg,* 146**,** 666-74.

SCHOR, S. L. 1980. Cell proliferation and migration on collagen substrata in vitro. *Journal of Cell Science,* Vol. 41**,** 159-175.

SEDDON, H. J., MEDAWAR, P. B. & SMITH, H. 1943. Rate of regeneration of peripheral nerves in man. *The Journal of Physiology,* 102**,** 191-215.

SEIF-NARAGHI, S. B., SINGELYN, J. M., SALVATORE, M. A., OSBORN, K. G., WANG, J. J., SAMPAT, U., KWAN, O. L., STRACHAN, G. M., WONG, J., SCHUP-MAGOFFIN, P. J., BRADEN, R. L., BARTELS, K., DEQUACH, J. A., PREUL, M., KINSEY, A. M., DEMARIA, A. N., DIB, N. & CHRISTMAN, K. L. 2013. Safety and efficacy of an injectable extracellular matrix hydrogel for treating myocardial infarction. *Sci Transl Med,* 5**,** 173ra25.

SEITZ, R. J., REINERS, K., HIMMELMANN, F., HEININGER, K., HARTUNG, H. P. P. & TOYKA, K. V. 1989. The blood–nerve barrier in Wallerian degeneration: A sequential long-term study. *Muscle & Nerve,* 12**,** 627-635.

SERGEYENKO, A. M., ROSENFELD, D. J. & TSOUKAS, M. M. 2018. Chronic immunosuppression in the mature patient. *Clin Dermatol,* 36**,** 255-263.

SHAHRIARI, D., SHIBAYAMA, M., LYNAM, D. A., WOLF, K. J., KUBOTA, G., KOFFLER, J. Y., TUSZYNSKI, M. H., CAMPANA, W. M. & SAKAMOTO, J. S. 2017. Peripheral nerve growth within a hydrogel microchannel scaffold supported by a kink-resistant conduit. *Journal of Biomedical Materials Research - Part A,* 105**,** 3392-3399.

SHAO, C., MENG, L., WANG, M., CUI, C., WANG, B., HAN, C. R., XU, F. & YANG, J. 2019. Mimicking Dynamic Adhesiveness and Strain-Stiffening Behavior of Biological Tissues in Tough and Self-Healable Cellulose Nanocomposite Hydrogels. *ACS Applied Materials and Interfaces*.

SHI, P., LAUDE, A. & YEONG, W. Y. 2017. Investigation of cell viability and morphology in 3D bio-printed alginate constructs with tunable stiffness. *J Biomed Mater Res A,* 105**,** 1009-1018.

SHIN, K., KOO, K. H., JEONG, J., PARK, S. J., CHOI, D. J., KO, Y.-G. & KWON, H. 2019. Three-Dimensional Culture of Salivary Gland Stem Cell in Orthotropic Decellularized Extracellular Matrix Hydrogels. *Tissue Engineering Part A*, 1-25.

SIERPOWSKA, J., LAMMI, M. J., HAKULINEN, M. A., JURVELIN, J. S., LAPPALAINEN, R. & TÖYRÄS, J. 2007. Effect of human trabecular bone composition on its electrical properties. *Medical Engineering and Physics,* 29**,** 845-852.

SIIRONEN, J., SANDBERG, M., VUORINEN, V. & ROYTTA, M. 1992a. Expression of type I and III collagens and fibronectin after transection of rat sciatic nerve. Reinnervation compared with denervation. *Lab Invest,* 67**,** 80-7.

SIIRONEN, J., SANDBERG, T. M., VUORINEN, V. & ROYTTA, M. 1992b. Laminin B1 and Collagen Type IV Gene Expression in Transected Peripheral Nerve : Reinnervation Compared to Denervation. *Journal of Neurobiology***,** 2184-2192.

SIIRONEN, J., VUORIO, E., SANDBERG, M. & ROYTTA, M. 1996. Expression of type I and III collagen and laminin beta1 after rat sciatic nerve crush injury. *J Peripher Nerv Syst,* 1**,** 209-21.

SIKKEMA, A. H., STOFFELS, J. M. J., WANG, P., BASEDOW, F. J., BULSINK, R., BAJRAMOVIC, J. J. & BARON, W. 2018. Fibronectin aggregates promote features of a classically and alternatively activated phenotype in macrophages. *J Neuroinflammation,* 15**,** 218.

SIMON, T. & BROMBERG, J. S. 2017. Regulation of the Immune System by Laminins. *Trends Immunol,* 38**,** 858-871.

SINGELYN, J. M., DEQUACH, J. A., SEIF-NARAGHI, S. B., LITTLEFIELD, R. B., SCHUP-MAGOFFIN, P. J. & CHRISTMAN, K. L. 2009. Naturally derived myocardial matrix as an injectable scaffold for cardiac tissue engineering. *Biomaterials,* 30**,** 5409-16.

SKARDAL, A., SMITH, L., BHARADWAJ, S., ATALA, A., SOKER, S. & ZHANG, Y. 2012. Tissue specific synthetic ECM hydrogels for 3-D in vitro maintenance of hepatocyte function. *Biomaterials,* 33**,** 4565-4575.

SLIVKA, P. F., DEARTH, C. L., KEANE, T. J., MENG, F. W., MEDBERRY, C. J., RIGGIO, R. T., REING, J. E. & BADYLAK, S. F. 2014. Fractionation of an ECM hydrogel into structural and soluble components reveals distinctive roles in regulating macrophage behavior. *Biomater. Sci.,* 2**,** 1521-1534.

SMITH, C. A., BOARD, T. N., ROONEY, P., EAGLE, M. J., RICHARDSON, M. & HOYLAND, J. A. 2017. Human decellularized bone scaffolds from aged donors show improved osteoinductive capacity compared to young donor bone. *PLoS ONE,* 1-15.

SMITH, G. V. & STEVENSON, J. A. 1988. Peripheral nerve grafts lacking viable Schwann cells fail to support central nervous system axonal regeneration. *Exp Brain Res,* 69**,** 299-306.

SMITH, R. M., WIEDL, C., CHUBB, P. & GREENE, C. H. 2004. Role of small intestine submucosa (SIS) as a nerve conduit: Preliminary report. *Journal of Investigative Surgery,* 17**,** 339-344.

SOMAIAH, C., KUMAR, A., MAWRIE, D., SHARMA, A., PATIL, S. D., BHATTACHARYYA, J., SWAMINATHAN, R. & JAGANATHAN, B. G. 2015. Collagen promotes higher adhesion, survival and proliferation of mesenchymal stem cells. *PLoS ONE,* 10**,** 1-15.

SONNENBERG, S. B., RANE, A. A., LIU, C. J., RAO, N., AGMON, G., SUAREZ, S., WANG, R., MUNOZ, A., BAJAJ, V., ZHANG, S., BRADEN, R., SCHUP-MAGOFFIN, P. J., KWAN, O. L., DEMARIA, A. N., COCHRAN, J. R. & CHRISTMAN, K. L. 2015. Delivery of an engineered HGF fragment in an extracellular matrix-derived hydrogel prevents negative LV remodeling post-myocardial infarction. *Biomaterials,* 45**,** 56-63.

SRIDHARAN, R., RYAN, E. J., KEARNEY, C. J., KELLY, D. J. & O'BRIEN, F. J. 2019. Macrophage Polarization in Response to Collagen Scaffold Stiffness Is Dependent on Cross-Linking Agent Used To Modulate the Stiffness. *ACS Biomater Sci Eng,* 5**,** 544-552.

STERN, R., KOGAN, G., JEDRZEJAS, M. J. & SOLTES, L. 2007. The many ways to cleave hyaluronan. *Biotechnol Adv,* 25**,** 537-57.

STOLINSKI, C. 1995. Structure and composition of the outer connective tissue sheaths of peripheral nerve. *J Anat,* 186 (Pt 1)**,** 123-30.

STORM, C., PASTORE, J. J., MACKINTOSH, F. C., LUBENSKY, T. C. & JANMEY, P. A. 2005. Nonlinear elasticity in biological gels. *Nature,* 435**,** 191-194.

STOVER, D. A. & VERRELLI, B. C. 2011. Comparative vertebrate evolutionary analyses of type I collagen: potential of COL1a1 gene structure and intron variation for common bone-related diseases. *Mol Biol Evol,* 28**,** 533-42.

STRATTON, J. A., HOLMES, A., ROSIN, N. L., SINHA, S., VOHRA, M., BURMA, N. E., TRANG, T., MIDHA, R. & BIERNASKIE, J. 2018. Macrophages Regulate Schwann Cell Maturation after Nerve Injury. *Cell Rep,* 24**,** 2561-2572 e6.

SU, J., SATCHELL, S. C., SHAH, R. N. & WERTHEIM, J. A. 2018. Kidney decellularized extracellular matrix hydrogels: Rheological characterization and human glomerular endothelial cell response to encapsulation. *Journal of Biomedical Materials Research - Part A,* 106**,** 2448-2462.

SU, W., FOSTER, S. C., XING, R., FEISTEL, K., OLSEN, R. H., ACEVEDO, S. F., RABER, J. & SHERMAN, L. S. 2017. CD44 Transmembrane Receptor and Hyaluronan Regulate Adult Hippocampal Neural Stem Cell Quiescence and Differentiation. *J Biol Chem,* 292**,** 4434-4445.

SUMNER, A. J. 1990. Aberrant reinnervation. *Muscle Nerve,* 13**,** 801-3.

SUN, J., LYU, J., XING, F., CHEN, R., DUAN, X. & XIANG, Z. 2020. A biphasic, demineralized, and Decellularized allograft bone-hydrogel scaffold with a cell-based BMP-7 delivery system for osteochondral defect regeneration. *J Biomed Mater Res A,* 108**,** 1909-1921.

SUN, M., CHEN, S., ADAMS, S. M., FLORER, J. B., LIU, H., KAO, W. W., WENSTRUP, R. J. & BIRK, D. E. 2011. Collagen V is a dominant regulator of collagen fibrillogenesis: dysfunctional regulation of structure and function in a corneal-stroma-specific Col5a1-null mouse model. *J Cell Sci,* 124**,** 4096-105.

SUN, M., CHI, G., LI, P., LV, S., XU, J., XU, Z., XIA, Y., TAN, Y., XU, J., LI, L. & LI, Y. 2018. Effects of Matrix Stiffness on the Morphology, Adhesion, Proliferation and Osteogenic Differentiation of Mesenchymal Stem Cells. *International Journal of Medical Sciences,* 15**,** 257-268.

SUNDERLAND, I. R. P., BRENNER, M. J., SINGHAM, J., RICKMAN, S. R., HUNTER, D. A. & MACKINNON, S. E. 2004. Effect of tension on nerve regeneration in rat sciatic nerve transection model. *Annals of Plastic Surgery,* 53**,** 382-387.

SUNDERLAND, S. 1951. A classification of peripheral nerve injuries producing loss of function. *Brain,* 74**,** 491-516.

SURI, S. & SCHMIDT, C. E. 2010. Cell-Laden Hydrogel Constructs of Hyaluronic Acid, Collagen, and Laminin for Neural Tissue Engineering. *Tissue Engineering Part A,* 16**,** 1703-1716.

SWINDLE-REILLY, K. E., PAPKE, J. B., KUTOSKY, H. P., THROM, A., HAMMER, J. A., HARKINS, A. B. & WILLITS, R. K. 2012. The impact of laminin on 3D neurite extension in collagen gels. *J Neural Eng,* 9**,** 046007.

SYED, O., WALTERS, N. J., DAY, R. M., KIM, H. W. & KNOWLES, J. C. 2014. Evaluation of decellularization protocols for production of tubular small

intestine submucosa scaffolds for use in oesophageal tissue engineering. *Acta Biomaterialia,* 10**,** 5043-5054.

TAJDARAN, K., CHAN, K., GORDON, T. & BORSCHEL, G. H. 2019. Matrices, scaffolds, and carriers for protein and molecule delivery in peripheral nerve regeneration. *Experimental Neurology,* 319**,** 112817-112817.

TAKEUCHI, H., IKEGUCHI, R., AOYAMA, T., ODA, H., YURIE, H., MITSUZAWA, S., TANAKA, M., OHTA, S., AKIEDA, S., MIYAZAKI, Y., NAKAYAMA, K. & MATSUDA, S. 2019. A scaffold-free Bio 3D nerve conduit for repair of a 10-mm peripheral nerve defect in the rats. *Microsurgery,* 207-216.

TAPIAS, L. F., GILPIN, S. E., REN, X., WEI, L., FUCHS, B. C., TANABE, K. K., LANUTI, M. & OTT, H. C. 2015. Assessment of Proliferation and Cytotoxicity in a Biomimetic Three-Dimensional Model of Lung Cancer. *Ann Thorac Surg,* 100**,** 414-21.

TATIC, N., ROSE, F., DES RIEUX, A. & WHITE, L. J. 2019. Stem cells from the dental apical papilla in extracellular matrix hydrogels mitigate inflammation of microglial cells. *Sci Rep,* 9**,** 14015.

TELEJKO, E., WROBEL, K., WISNIEWSKI, K. & BANKOWSKI, E. 1992. Pharmacological and physicochemical properties of collagen breakdown-products. *Acta Neurobiol Exp (Wars),* 52**,** 223-32.

TEMPLETON, D. M. 1988. The basis and applicability of the dimethylmethylene blue binding assay for sulfated glycosaminoglycans. *Connect Tissue Res,* 17**,** 23-32.

TERRIS, D. J., TOFT, K. M., MOIR, M., LUM, J. & WANG, M. 2001. Brain-derived neurotrophic factor-enriched collagen tubule as a substitute for autologous nerve grafts. *Arch Otolaryngol Head Neck Surg,* 127**,** 294-8.

THANG, S. H., KOBAYASHI, M. & MATSUOKA, I. 2000. Regulation of glial cell line-derived neurotrophic factor responsiveness in developing rat sympathetic neurons by retinoic acid and bone morphogenetic protein-2. *Journal of Neuroscience,* 20**,** 2917-2925.

THEOCHARIS, A. D., SKANDALIS, S. S., GIALELI, C. & KARAMANOS, N. K. 2016. Extracellular matrix structure. *Adv Drug Deliv Rev,* 97**,** 4-27.

THOMAS, P. K. 1963. The connective tissue of peripheral nerve: an electron microscope study. *J Anat,* 97**,** 35-44.

TIMPL, R., WIEDEMANN, H., DELDEN, V. V. A. N., FURTHMAYR, H., KLAUS, K. U. H. N. & IV, T. 2000. A Network Model for the Organization of Type IV Collagen Molecules in Basement Membranes. *Eur. J. Biochem,* 211**,** 203-211.

TOBA, T., NAKAMURA, T., LYNN, A. K., MATSUMOTO, K., FUKUDA, S., YOSHITANI, M., HORI, Y. & SHIMIZU, Y. 2002. Evaluation of peripheral nerve regeneration across an 80-mm gap using a polyglycolic acid (PGA)--collagen nerve conduit filled with laminin-soaked collagen sponge in dogs. *Int J Artif Organs,* 25**,** 230-7.

TOFARIS, G. K., PATTERSON, P. H., JESSEN, K. R. & MIRSKY, R. 2002. Denervated Schwann cells attract macrophages by secretion of leukemia inhibitory factor (LIF) and monocyte chemoattractant protein-1 in a process regulated by interleukin-6 and LIF. *J Neurosci,* 22**,** 6696-703.

TOS, P., CROSIO, A., PUGLIESE, P., ADANI, R., TOIA, F. & ARTIACO, S. 2015. Painful scar neuropathy: principles of diagnosis and treatment. *Plastic and Aesthetic Research,* 2**,** 156-156.

TOTTEY, S., JOHNSON, S. A., CRAPO, P. M., REING, J. E., ZHANG, L., JIANG, H., MEDBERRY, C. J., REINES, B. & BADYLAK, S. F. 2011. The effect of source animal age upon extracellular matrix scaffold properties. *Biomaterials,* 32**,** 128-36.

TRAVERSE, J. H., HENRY, T. D., DIB, N., PATEL, A. N., PEPINE, C., SCHAER, G. L., DEQUACH, J. A., KINSEY, A. M., CHAMBERLIN, P. & CHRISTMAN, K. L. 2019. First-in-Man Study of a Cardiac Extracellular Matrix Hydrogel in Early and Late Myocardial Infarction Patients. *JACC Basic Transl Sci,* 4**,** 659-669.

TSAI, R. K., SHEU, M. M. & WANG, H. Z. 1998. Capability of neurite regeneration of rat retinal explant at different ages. *Kaohsiung J Med Sci,* 14**,** 192-6.

TSILIBARY, E. C., KOLIAKOS, G. G., CHARONIS, A. S., VOGEL, A. M., REGER, L. A. & FURCHT, L. T. 1988. Heparin type IV collagen interactions: equilibrium binding and inhibition of type IV collagen self-assembly. *J Biol Chem,* 263**,** 19112-8.

TUKMACHEV, D., FOROSTYAK, S., KOCI, Z., ZAVISKOVA, K., VACKOVA, I., VYBORNY, K., SANDVIG, I., SANDVIG, A., MEDBERRY, C. J., BADYLAK, S. F., SYKOVA, E. & KUBINOVA, S. 2016. Injectable Extracellular Matrix Hydrogels as Scaffolds for Spinal Cord Injury Repair. *Tissue Engineering Part A,* 22**,** 306-317.

ULERY, B. D., NAIR, L. S. & LAURENCIN, C. T. 2011. Biomedical Applications of Biodegradable Polymers. *J Polym Sci B Polym Phys,* 49**,** 832-864.

UNGERLEIDER, J. L., JOHNSON, T. D., HERNANDEZ, M. J., ELHAG, D. I., BRADEN, R. L., DZIECIATKOWSKA, M., OSBORN, K. G., HANSEN, K. C., MAHMUD, E. & CHRISTMAN, K. L. 2016. Extracellular Matrix Hydrogel Promotes Tissue Remodeling, Arteriogenesis, and Perfusion in a Rat Hindlimb Ischemia Model. *JACC: Basic to Translational Science,* 1**,** 32-44.

VALLÉE, F., MÜLLER, C., DURAND, A., SCHIMCHOWITSCH, S., DELLACHERIE, E., KELCHE, C., CASSEL, J. C. & LEONARD, M. 2009. Synthesis and rheological properties of hydrogels based on amphiphilic alginate-amide derivatives. *Carbohydrate Research,* 344**,** 223-228.

VAN DER MERWE, Y., FAUST, A. & STEKETEE, M. 2017. Matrix bound vesicles and miRNA cargoes are bioactive factors within extracellular matrix bioscaffolds. *Neural Regeneration Research,* 12**,** 1597-1597.

VAN OOSTEN, A. S. G., VAHABI, M., LICUP, A. J., SHARMA, A., GALIE, P. A., MACKINTOSH, F. C. & JANMEY, P. A. 2016. Uncoupling shear and uniaxial elastic moduli of semiflexible biopolymer networks: Compression-softening and stretch-stiffening. *Scientific Reports,* 6**,** 1-9.

VAVKEN, P., JOSHI, S. & MURRAY, M. M. 2009. TRITON-X is most effective among three decellularization agents for ACL tissue engineering. *Journal of Orthopaedic Research,* 27**,** 1612-1618.

VEDADGHAVAMI, A., MINOOEI, F., MOHAMMADI, M. H., KHETANI, S., REZAEI KOLAHCHI, A., MASHAYEKHAN, S. & SANATI-NEZHAD, A. 2017. Manufacturing of hydrogel biomaterials with controlled mechanical properties for tissue engineering applications. *Acta Biomaterialia,* 62**,** 42-63.

VOGEL, K. G., PAULSSON, M. & HEINEGARD, D. 1984. Specific inhibition of type I and type II collagen fibrillogenesis by the small proteoglycan of tendon. *Biochem J,* 223**,** 587-97.

VOYTIK-HARBIN, S. L., BRIGHTMAN, A. O., KRAINE, M. R., WAISNER, B. & BADYLAK, S. F. 1997. Identification of extractable growth factors from small intestinal submucosa. *J Cell Biochem,* 67**,** 478-491.

VÝBORNÝ, K., VALLOVÁ, J., KOČÍ, Z., KEKULOVÁ, K., JIRÁKOVÁ, K., JENDELOVÁ, P., HODAN, J. & KUBINOVÁ, Š. 2019. Genipin and EDC crosslinking of extracellular matrix hydrogel derived from human umbilical cord for neural tissue repair. *Scientific Reports,* 9**,** 10674-10674.

WALL, P. D., DEVOR, M., INBAL, R., SCADDING, J. W., SCHONFELD, D., SELTZER, Z. & TOMKIEWICZ, M. M. 1979. Autotomy following peripheral nerve lesions: experimental anaesthesia dolorosa. *Pain,* 7**,** 103-113.

WALLES, T., HERDEN, T., HAVERICH, A. & MERTSCHING, H. 2003. Influence of scaffold thickness and scaffold composition on bioartificial graft survival. *Biomaterials,* 24**,** 1233-1239.

WANG, C., JIA, Y., YANG, W., ZHANG, C., ZHANG, K. & CHAI, Y. 2018. Silk fibroin enhances peripheral nerve regeneration by improving vascularization within nerve conduits. *Journal of Biomedical Materials Research - Part A,* 106**,** 2070-2077.

WANG, C. Y., ZHANG, K. H., FAN, C. Y., MO, X. M., RUAN, H. J. & LI, F. F. 2011. Aligned natural-synthetic polyblend nanofibers for peripheral nerve regeneration. *Acta Biomater,* 7**,** 634-43.

WANG, G. W., YANG, H., WU, W. F., ZHANG, P. & WANG, J. Y. 2017a. Design and optimization of a biodegradable porous zein conduit using microtubes as a guide for rat sciatic nerve defect repair. *Biomaterials,* 131**,** 145-159.

WANG, J., MUHEREMU, A., ZHANG, M., GONG, K., HUANG, C., JI, Y., WEI, Y. & AO, Q. 2016. MicroRNA-338 and microRNA-21 co-transfection for the treatment of rat sciatic nerve injury. *Neurological Sciences,* 37**,** 883-890.

WANG, J. Y., LIOU, A. K. F., REN, Z. H., ZHANG, L., BROWN, B. N., CUI, X. T., BADYLAK, S. F., CAI, Y. N., GUAN, Y. Q., LEAK, R. K., CHEN, J., JI, X. & CHEN, L. 2013. Neurorestorative Effect of Urinary Bladder Matrix-Mediated Neural Stem Cell Transplantation Following Traumatic Brain Injury in Rats. *CNS & Neurological Disorders - Drug Targets,* 12**,** 413-425.

WANG, R. M., JOHNSON, T. D., HE, J., RONG, Z., WONG, M., NIGAM, V., BEHFAR, A., XU, Y. & CHRISTMAN, K. L. 2017b. Humanized mouse model for assessing the human immune response to xenogeneic and allogeneic decellularized biomaterials. *Biomaterials,* 129**,** 98-110.

WANG, Z., HAN, N., WANG, J., ZHENG, H., PENG, J., KOU, Y., XU, C., AN, S., YIN, X., ZHANG, P. & JIANG, B. 2014. Improved peripheral nerve regeneration with sustained release nerve growth factor microspheres in small gap tubulization. *Am J Transl Res,* 6**,** 413-21.

WELLS, R. G. 2008. The role of matrix stiffness in regulating cell behavior. *Hepatology,* 47**,** 1394-1400.

WENSTRUP, R. J., FLORER, J. B., BRUNSKILL, E. W., BELL, S. M., CHERVONEVA, I. & BIRK, D. E. 2004. Type V collagen controls the initiation of collagen fibril assembly. *J Biol Chem,* 279**,** 53331-7.

WHITE, L. J., TAYLOR, A. J., FAULK, D. M., KEANE, T. J., SALDIN, L. T., REING, J. E., SWINEHART, I. T., TURNER, N. J., RATNER, B. D. & STEPHEN, F. 2017. The impact of detergents on the tissue decellularization process : a ToF-SIMS study. *Acta Biomaterialia,* 50**,** 207-219.

WHITLOCK, E. L., TUFFAHA, S. H., LUCIANO, J. P., YAN, Y., HUNTER, D. A., MAGILL, C. K., MOORE, A. M., TONG, A. Y., MACKINNON, S. E. & BORSCHEL, G. H. 2009. Processed allografts and type I collagen conduits for repair of peripheral nerve gaps. *Muscle and Nerve,* 39**,** 787-799.

WIGHT, T. N., KANG, I. & MERRILEES, M. J. 2014. Versican and the control of inflammation. *Matrix Biol,* 35**,** 152-61.

WILLEM, M., MIOSGE, N., HALFTER, W., SMYTH, N., JANNETTI, I., BURGHART, E., TIMPL, R. & MAYER, U. 2002. Specific ablation of the nidogen-binding site in the laminin gamma1 chain interferes with kidney and lung development. *Development,* 129**,** 2711-22.

WILLITS, R. K. & SKORNIA, S. L. 2004. Effect of collagen gel stiffness on neurite extension. *J Biomater Sci Polym Ed,* 15**,** 1521-31.

WOJTKIEWICZ, D. M., SAUNDERS, J., DOMESHEK, L., NOVAK, C. B., KASKUTAS, V. & MACKINNON, S. E. 2015. Social impact of peripheral nerve injuries. *Hand (N Y),* 10**,** 161-7.

WOLF, M. T., DALY, K. A., BRENNAN-PIERCE, E. P., JOHNSON, S. A., CARRUTHERS, C., AMORE, A. D., NAGARKAR, S. P., SACHIN, S. & BADYLAK, S. F. 2013. A Hydrogel Derived From Decellularized Dermal Extracellular Matrix. *Biomaterials,* 33**,** 7028-7038.

WOODHALL, E., WEST, A. K. & CHUAH, M. I. 2001. Cultured olfactory ensheathing cells express nerve growth factor, brain-derived neurotrophic factor, glia cell line-derived neurotrophic factor and their receptors. *Brain Res Mol Brain Res,* 88**,** 203-13.

WROBEL, M. R. & SUNDARARAGHAVAN, H. G. 2017. Positive and negative cues for modulating neurite dynamics and receptor expression. *Biomedical Materials (Bristol),* 12.

WROBEL, M. R. & SUNDARARAGHAVAN, H. G. 2018. Biomaterial Cues to Direct a Pro-regenerative Phenotype in Macrophages and Schwann Cells. *Neuroscience,* 376**,** 172-187.

WU, Y., WANG, J., SHI, Y., PU, H., LEAK, R. K., LIOU, A. K. F., BADYLAK, S. F., LIU, Z., ZHANG, J., CHEN, J. & CHEN, L. 2017. Implantation of brain-derived extracellular matrix enhances neurological recovery after traumatic brain injury. *Cell Transplantation,* 26**,** 1224-1234.

XU, H., XU, B., YANG, Q., LI, X., MA, X., XIA, Q., ZHANG, Y., ZHANG, C., WU, Y. & ZHANG, Y. 2014. Comparison of decellularization protocols for preparing a decellularized porcine annulus fibrosus scaffold. *PLoS ONE,* 9**,** 1-13.

XU, H. L., TIAN, F. R., LU, C. T., XU, J., FAN, Z. L., YANG, J. J., CHEN, P. P., HUANG, Y. D., XIAO, J. & ZHAO, Y. Z. 2016. Thermo-sensitive hydrogels combined with decellularised matrix deliver bFGF for the

functional recovery of rats after a spinal cord injury. *Scientific Reports,* 6**,** 1-15.

XU, H. L., TIAN, F. R., XIAO, J., CHEN, P. P., XU, J., FAN, Z. L., YANG, J. J., LU, C. T. & ZHAO, Y. Z. 2018. Sustained-release of FGF-2 from a hybrid hydrogel of heparin-poloxamer and decellular matrix promotes the neuroprotective effects of proteins after spinal injury. *International Journal of Nanomedicine,* 13**,** 681-694.

XU, Y., ZHOU, J., LIU, C., ZHANG, S., GAO, F., GUO, W., SUN, X., ZHANG, C., LI, H., RAO, Z., QIU, S., ZHU, Q., LIU, X., GUO, X., SHAO, Z., BAI, Y., ZHANG, X. & QUAN, D. 2021. Understanding the role of tissue-specific decellularized spinal cord matrix hydrogel for neural stem/progenitor cell microenvironment reconstruction and spinal cord injury. *Biomaterials,* 268**,** 120596.

XU, Z., ORKWIS, J. A., DEVINE, B. M. & HARRIS, G. M. 2020. Extracellular matrix cues modulate Schwann cell morphology, proliferation, and protein expression. *Journal of Tissue Engineering and Regenerative Medicine,* 14**,** 229-242.

YAMADA, S., SUGAHARA, K. & ÖZBEK, S. 2011. Evolution of glycosaminoglycans: Comparative biochemical study. *Communicative and Integrative Biology,* 4**,** 150-158.

YAMADA, Y., AVVEDIMENTO, V. E., MUDRYJ, M., OHKUBO, H., VOGELI, G., IRANI, M., PASTAN, I. & DE CROMBRUGGHE, B. 1980. The collagen gene: evidence for its evolutinary assembly by amplification of a DNA segment containing an exon of 54 bp. *Cell,* 22**,** 887-92.

YAMANAKA, H., MORIMOTO, N. & YAMAOKA, T. 2020. Decellularization of submillimeter-diameter vascular scaffolds using peracetic acid. *J Artif Organs,* 23**,** 156-162.

YAN, C. & POCHAN, D. J. 2010. Rheological properties of peptide-based hydrogels for biomedical and other applications. *Chem Soc Rev2,* 39**,** 3528-3540.

YANG, F., WILLIAMS, C. G., WANG, D. A., LEE, H., MANSON, P. N. & ELISSEEFF, J. 2005a. The effect of incorporating RGD adhesive peptide in polyethylene glycol diacrylate hydrogel on osteogenesis of bone marrow stromal cells. *Biomaterials,* 26**,** 5991-5998.

YANG, K.-J., PARK, K. C., CHOI, H., CHOI, J.-H., PARK, S.-R., LEE, I.-W. & LEE, H.-J. 2014. Identification and characterization of neurotrophic factors in porcine small intestinal submucosa. *Tissue Engineering and Regenerative Medicine,* 11**,** 372-378.

YANG, Y., DE LAPORTE, L., RIVES, C. B., JANG, J. H., LIN, W. C., SHULL, K. R. & SHEA, L. D. 2005b. Neurotrophin releasing single and multiple lumen nerve conduits. *Journal of Controlled Release,* 104**,** 433-446.

YAO, S., LIU, X., YU, S., WANG, X., ZHANG, S., WU, Q., SUN, X. & MAO, H. 2016. Co-effects of matrix low elasticity and aligned topography on stem cell neurogenic differentiation and rapid neurite outgrowth. *Nanoscale,* 8**,** 10252-10265.

YEAGLE, P. L. 2016. Detergents. Elsevier.

YEN, C. M., SHEN, C. C., YANG, Y. C., LIU, B. S., LEE, H. T., SHEU, M. L., TSAI, M. H. & CHENG, W. Y. 2019. Novel electrospun poly(ϵ-caprolactone)/type i collagen nanofiber conduits for repair of peripheral nerve injury. *Neural Regeneration Research,* 14**,** 1617-1625.

233

YI, J.-S., LEE, H.-J., LEE, H.-J., LEE, I.-W. & YANG, J.-H. 2013. Rat peripheral nerve regeneration using nerve guidance channel by porcine small intestinal submucosa. *Journal of Korean Neurosurgical Society,* 53**,** 65-71.

YI, S., XU, L. & GU, X. 2019. Scaffolds for peripheral nerve repair and reconstruction. *Experimental Neurology,* 319**,** 112761-112761.

YIN, J., XIA, Y. & LU, M. 2012. Concentration profiles of collagen and proteoglycan in articular cartilage by Fourier transform infrared imaging and principal component regression. *Spectrochimica Acta Part A: Molecular and Biomolecular Spectroscopy,* 88**,** 90-96.

YIN, K., DIVAKAR, P., HONG, J., MOODIE, K. L., ROSEN, J. M., SUNDBACK, C. A., MATTHEW, M. K. & WEGST, U. G. K. 2018. Freeze-cast Porous Chitosan Conduit for Peripheral Nerve Repair. *MRS Advances,* 3**,** 1677-1683.

YOO, J., PARK, J. H., KWON, Y. W., CHUNG, J. J., CHOI, I. C., NAM, J. J., LEE, H. S., JEON, E. Y., LEE, K., KIM, S. H., JUNG, Y. & PARK, J. W. 2020. Augmented peripheral nerve regeneration through elastic nerve guidance conduits prepared using a porous PLCL membrane with a 3D printed collagen hydrogel. *Biomater Sci,* 8**,** 6261-6271.

YU, X. & BELLAMKONDA, R. V. 2001. Dorsal root ganglia neurite extension is inhibited by mechanical and chondroitin sulfate-rich interfaces. *Journal of Neuroscience Research,* 66**,** 303-310.

YUAN, X., WEI, Y., VILLASANTE, A., NG, J. J. D., ARKONAC, D. E., CHAO, P. H. G. & VUNJAK-NOVAKOVIC, G. 2017. Stem cell delivery in tissue-specific hydrogel enabled meniscal repair in an orthotopic rat model. *Biomaterials,* 132**,** 59-71.

YUAN, Y. M. & HE, C. 2013. The glial scar in spinal cord injury and repair. *Neurosci Bull,* 29**,** 421-35.

YURCHENCO, P. D. & RUBEN, G. C. 1987. Basement membrane structure in situ: evidence for lateral associations in the type IV collagen network. *J Cell Biol,* 105**,** 2559-68.

ZANDER, N. E., ORLICKI, J. A., RAWLETT, A. M. & BEEBE, T. P., JR. 2010. Surface-modified nanofibrous biomaterial bridge for the enhancement and control of neurite outgrowth. *Biointerphases,* 5**,** 149-58.

ZHANG, D., YANG, W., WANG, C., ZHENG, H., LIU, Z., CHEN, Z. & GAO, C. 2020a. Methylcobalamin-Loaded PLCL Conduits Facilitate the Peripheral Nerve Regeneration. *Macromolecular Bioscience,* 1900382**,** 1900382-1900382.

ZHANG, D., ZHANG, Y., ZHANG, Y., YI, H., WANG, Z., WU, R., HE, D., WEI, G., WEI, S., HU, Y., DENG, J., CRISWELL, T., YOO, J., ZHOU, Y. & ATALA, A. 2017. Tissue-Specific Extracellular Matrix Enhances Skeletal Muscle Precursor Cell Expansion and Differentiation for Potential Application in Cell Therapy. *Tissue Engineering - Part A,* 23**,** 784-794.

ZHANG, L., ZHANG, F., WENG, Z., BROWN, B. N., YAN, H., MA, X. M., VOSLER, P. S., BADYLAK, S. F., DIXON, C. E., CUI, X. T. & CHEN, J. 2013. Effect of an inductive hydrogel composed of urinary bladder matrix upon functional recovery following traumatic brain injury. *Tissue Engineering - Part A,* 19**,** 1909-1918.

ZHANG, Q., WU, P., CHEN, F., ZHAO, Y., LI, Y., HE, X., HUSELSTEIN, C., YE, Q., TONG, Z. & CHEN, Y. 2020b. Brain Derived Neurotrophic Factor and

Glial Cell Line-Derived Neurotrophic Factor-Transfected Bone Mesenchymal Stem Cells for the Repair of Periphery Nerve Injury. *Front Bioeng Biotechnol,* 8**,** 874.

ZHANG, Y., LUO, H., ZHANG, Z., LU, Y., HUANG, X., YANG, L., XU, J., YANG, W., FAN, X., DU, B., GAO, P., HU, G. & JIN, Y. 2010. A nerve graft constructed with xenogeneic acellular nerve matrix and autologous adipose-derived mesenchymal stem cells. *Biomaterials,* 31**,** 5312-24.

ZHANG, Z., ROUABHIA, M., WANG, Z., ROBERGE, C., SHI, G., ROCHE, P., LI, J. & DAO, L. H. 2007. Electrically conductive biodegradable polymer composite for nerve regeneration: electricity-stimulated neurite outgrowth and axon regeneration. *Artif Organs,* 31**,** 13-22.

ZHANG, Z., XU, H., MAZZA, G., ZHANG, M., FRENGUELLI, L., LIU, Q., AL-AKKAD, W., REN, J., ZHAO, R., REN, F., CHEN, X., HUANG, A. & CHEN, J. 2019. Decellularized human liver scaffold-based three-dimensional culture system facilitate hepatitis B virus infection. *J Biomed Mater Res A,* 107**,** 1744-1753.

ZHAO, Y., WANG, Y., GONG, J., YANG, L., NIU, C., NI, X., WANG, Y., PENG, S., GU, X., SUN, C. & YANG, Y. 2017a. Chitosan degradation products facilitate peripheral nerve regeneration by improving macrophage-constructed microenvironments. *Biomaterials,* 134**,** 64-77.

ZHAO, Y., ZHANG, Q., ZHAO, L., GAN, L., YI, L., ZHAO, Y., XUE, J., LUO, L., DU, Q., GENG, R., SUN, Z., BENKIRANE-JESSEL, N., CHEN, P., LI, Y. & CHEN, Y. 2017b. Enhanced Peripheral Nerve Regeneration by a High Surface Area to Volume Ratio of Nerve Conduits Fabricated from Hydroxyethyl Cellulose/Soy Protein Composite Sponges. *ACS Omega,* 2**,** 7471-7481.

ZHENG, C., YANG, Z., CHEN, S., ZHANG, F., RAO, Z., ZHAO, C., QUAN, D., BAI, Y. & SHEN, J. 2021. Nanofibrous nerve guidance conduits decorated with decellularized matrix hydrogel facilitate peripheral nerve injury repair. *Theranostics,* 11**,** 2917-2931.

ZHENG, C. H. & LEVENSTON, M. E. 2015. Fact versus artifact: avoiding erroneous estimates of sulfated glycosaminoglycan content using the dimethylmethylene blue colorimetric assay for tissue-engineered constructs. *Eur Cell Mater,* 29**,** 224-36; discussion 236.

ZHENG, M. H., CHEN, J., KIRILAK, Y., WILLERS, C., XU, J. & WOOD, D. 2005. Porcine small intestine submucosa (SIS) is not an acellular collagenous matrix and contains porcine DNA: Possible implications in human implantation. *Journal of Biomedical Materials Research - Part B Applied Biomaterials,* 73**,** 61-67.

ZHOU, C., LIU, B., HUANG, Y., ZENG, X., YOU, H., LI, J. & ZHANG, Y. 2017. The effect of four types of artificial nerve graft structures on the repair of 10-mm rat sciatic nerve gap. *Journal of Biomedical Materials Research - Part A,* 105**,** 3077-3085.

ZHOU, W., BLEWITT, M., HOBGOOD, A. & WILLITS, R. K. 2013. Comparison of neurite growth in three dimensional natural and synthetic hydrogels. *J Biomater Sci Polym Ed,* 24**,** 301-14.

ZHOU, X., WANG, J., HUANG, X., FANG, W., TAO, Y., ZHAO, T., LIANG, C., HUA, J., CHEN, Q. & LI, F. 2018. Injectable decellularized nucleus pulposus-based cell delivery system for differentiation of adipose-derived

stem cells and nucleus pulposus regeneration. *Acta Biomater,* 81**,** 115-128.

ZOU, J. L., LIU, S., SUN, J. H., YANG, W. H., XU, Y. W., RAO, Z. L., JIANG, B., ZHU, Q. T., LIU, X. L., WU, J. L., CHANG, C., MAO, H. Q., LING, E. A., QUAN, D. P. & ZENG, Y. S. 2018. Peripheral Nerve-Derived Matrix Hydrogel Promotes Remyelination and Inhibits Synapse Formation. *Advanced Functional Materials,* 28**,** 1-12.

ZUIDEMA, J. M., RIVET, C. J., GILBERT, R. J. & MORRISON, F. A. 2014. A protocol for rheological characterization of hydrogels for tissue engineering strategies. *Journal of Biomedical Materials Research - Part B Applied Biomaterials,* 102**,** 1063-1073.

ZUO, J., NEUBAUER, D., GRAHAM, J., KREKOSKI, C. A., FERGUSON, T. A. & MUIR, D. 2002. Regeneration of axons after nerve transection repair is enhanced by degradation of chondroitin sulfate proteoglycan. *Experimental Neurology,* 176**,** 221-228.

Appendices

Appendix A

Porcine peripheral nerve dissection

Figure A1 Pig leg dissection and sciatic nerve removal. Pig legs were dissected to expose sciatic nerves [A]. Sciatic nerves were removed [B] and cut into 5 mm pieces to be stored at -20 °C for decellularisation.
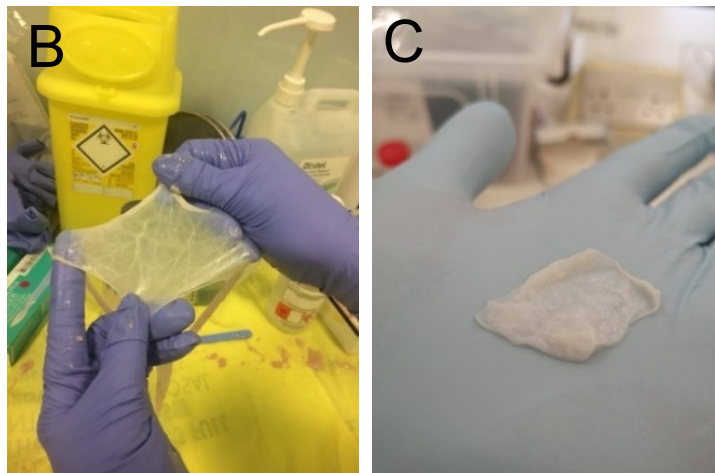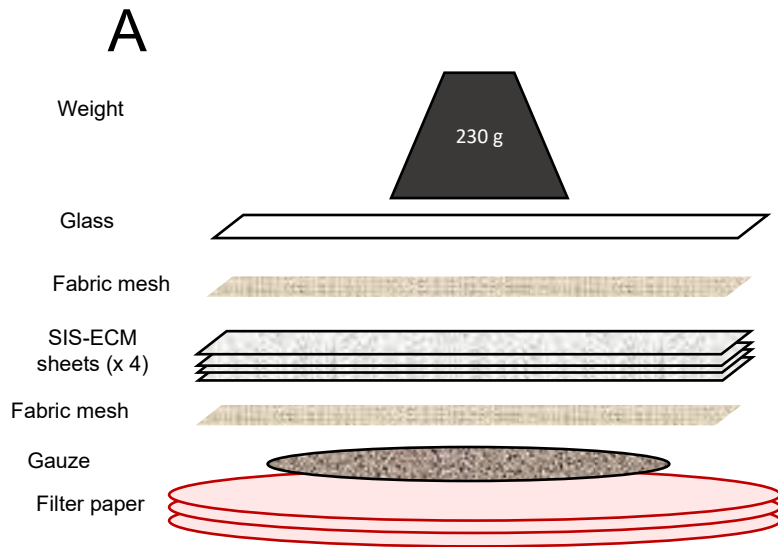
Appendix B

SIS-ECM sheet plastic compression

Figure B1 Production of multilamellar sheets composed of SIS-ECM.
Schematic for plastic compression method to produce multi-layered sheets [A].
Single SIS-ECM sheet [B] and resultant material comprised of 4 sheets of SIS-ECM [C].